ENGINEERING RESEARCH INSTITUTE
UNIVERSITY OF MICHIGAN
ANN ARBOR

DYNAMIC FREQUENCY CHARACTERISTICS OF THE MAGNETRON SPACE CHARGE; FREQUENCY PUSHING AND VOLTAGE TUNING

Technical Report No. 12
Electron Tube Laboratory
Department of Electrical Engineering

BY

H. W. WELCH, JR.

Approved by: W. G. DOW

G. HOK

Project M921

CONTRACT NO. DA-36-039 sc-5423
SIGNAL CORPS, DEPARTMENT OF THE ARMY
DEPARTMENT OF ARMY PROJECT NO. 3-99-13-022
SIGNAL CORPS PROJECT 27-112B-0

Submitted in partial fulfillment of the requirements for the Degree of Doctor of Philosophy in the University of Michigan.

November, 1951

ERRATA TO TECHNICAL REPORT NO. 12

Page	Location	Correction
20 and 21		For Ludi read Lüdi.
33	2d line from bottom	For capactive read capacitive.
38	Line 3	For test read tests.
38	Line 8	For indicates read indicate.
52	Footnote	For May 1938 read Mag. 38.
63	Line 13	For prescence read presence.
69	Lines 1 and 3	For energy read kinetic energy.
92	Line 8	For r-f read r-f + d-c.
103	Line 4	Replace period (.) with colon (:).
109	Line 6	This statement should be qualified "Except for frequencies near the cyclotron frequency $Be/2\pi m$."
121, 122, 123		Where r_1 occurs read r_n. Where r_2 occurs read r_a.
121	Equation following 3.26	Closing bracket should not include $rdrd\theta$.
122	Equation 3.10	For θ_1 read ω_n t.
149	Line 5	"Factor within the brackets" refers to Equation 3.47.
152	Left-hand scale	For ϕ_a ϕ_{at} read ϕ_a-ϕ_{at}.
163	Line 9	For Fig. 2.16 read Fig. 2.15.
175	Legend under figure	Squares representing synchronism potential should not be joined by a line.
194, 195, 196, 197, 202, 210, 211		f_o, as defined in connection with the data on the Model 7D magnetron, is given no other interpretation than that of representing the position of the 13-cm minimum in Fig. 4.24. It is not the resonance frequency of the circuit as it is defined elsewhere.
229	Line 4	For suudy read study.
229	Line 6	Comma after Laboratories, no comma after effect.

SUMMARY

Chapter 1: Introduction

Frequency pushing and voltage tuning, two fundamentally different frequency characteristics of magnetrons, are defined. An approximate picture of the space-charge behavior is presented with the purpose of acquainting the reader with the broad aspects of the problem before attention is given to details. Other work related to the present treatment is reviewed.

Chapter 2: Large-Signal Theory of Phase Focussing in the Travelling-Wave Magnetron

The magnetron is compared to other travelling-wave electronic devices. The basic assumptions and the differential equations describing the motion of the electron are stated. The anode potential required to bring an electron into synchronism with the travelling wave is derived. A threshold energy which is the minimum potential energy which must be given up by the electron to reach the anode is defined. A drift velocity condition is defined by analysis of the direction of drift motion of the electron in the crossed r-f electric field and d-c magnetic field. This condition combines with the threshold energy condition to focus the electrons into bunches or spokes maintaining a particular phase angle relative to the travelling r-f potential wave. A phase-focussing diagram which allows interpretation of magnetron behavior by graphical construction is described. The space-charge density in the spokes is estimated. The effect of limitation of the availability of d-c current is discussed and shown to be a condition favorable to voltage tuning.

Chapter 3: Theoretical Analysis Relating the Phase-Focussing Mechanism to the R-F Circuit Admittance Characteristic

The theory of induced current is reviewed briefly. This theory is applied to the magnetron using the picture of space-charge configuration developed in Chapter 2. Phase and admittance characteristics of equivalent circuits typical of magnetrons are analyzed. The results of this analysis are combined with the induced-current calculation and the theory of the space charge to compute the power generated and the operating anode potential as a function of frequency of oscillation. Curves illustrating the predicted form of frequency-pushing and voltage-tuning characteristics are plotted in dimensionless variables.

Chapter 4: Experimental Results

Measurements of the effect of the space charge on the resonance frequency of a 10-cm magnetron at various anode potentials and magnetic fields in the preoscillatory range are presented. Performance characteristics of several types, with emphasis on frequency pushing and the effects of cathode emission, are presented and, in some cases, compared with the theory for four different magnetrons in the 13-cm to 17-cm range. Typical voltage-tuning characteristics are reproduced and interpreted.

Chapter 5: Conclusions

The limitations inherent in the method of analysis which has been proposed are summarized. The most important points in the theory are reviewed. The practicability of the theory in its applications to design problem or analysis of experimental design is discussed. Topics for further study are suggested.

ACKNOWLEDGMENTS

The author wishes to express his appreciation to the several individuals who were helpful in the preparation of this work. Professor W. G. Dow, Mr. G. Hok, and Dr. J. S. Needle, of the Department of Electrical Engineering, and Mr. J. F. Hull, of Evans Signal Laboratory, offered many valuable suggestions, comments, and criticisms relative to the theoretical development. Mr. W. C. Brown and Mr. E. C. Dench, of Raytheon Manufacturing Company, and Dr. D. A. Wilbur and Mr. P. H. Peters, of General Electric Company, were very helpful in providing and discussing data and test information on magnetrons built in their laboratories. Dr. G. R. Brewer and Mr. S. R. Ruthberg assisted in the gathering of experimental data on the Model 7 magnetrons. The magnetrons and test equipment which were designed by the author were constructed, under supervision of Mr. J. R. Black, by the personnel of the University of Michigan Electron Tube Laboratory.

TABLE OF CONTENTS

LIST OF TABLES

LIST OF ILLUSTRATIONS

LIST OF ILLUSTRATIONS (Cont'd.)

LIST OF ILLUSTRATIONS (Cont'd.)

LIST OF ILLUSTRATIONS (Cont'd.)

LIST OF ILLUSTRATIONS (Cont'd.)

LIST OF ILLUSTRATIONS (Cont'd.)

INDEX OF SYMBOLS

*Starred symbols have more than one definition.

*Starred symbols have more than one definition.

Physical Constants

Symbol	Definition
c	velocity of radiation in free space = 2.99×10^8 m/sec
e	electronic charge = 1.6×10^{-19} coulombs
m	electronic mass = 9.1×10^{-31} kgm.
e/m	specific charge of electron = 1.759×10^{11} coulombs/kgm.
ε_o	dielectric constant of free space = $\frac{1}{36\pi} \times 10^{-9}$ farads/m

DYNAMIC FREQUENCY CHARACTERISTICS OF THE MAGNETRON SPACE CHARGE; FREQUENCY PUSHING AND VOLTAGE TUNING

I. INTRODUCTION

1.1 Statement of the Problem

The study of the magnetron problem has probably attracted the attention of more engineers and physicists as a subject for fundamental analysis than any other vacuum-tube problem in recent years. A number of the investigators who have been more or less briefly involved with the problem, particularly the physicists, have not been otherwise associated with vacuum-tube problems. Many of the men who have made very fundamental contributions to the theory of magnetron behavior are now otherwise involved.

Because of the complexity of the problem, in spite of the rather imposing amount of work that has been done, there are still many well known observable phenomena associated with magnetron behavior which have no satisfactory explanation in physical or mathematical terms. In fact, it is in many cases possible to demonstrate that even a semi-quantitative explanation is not practically feasible. It thus becomes necessary to supply qualitative interpretations which, although they cannot give the satisfaction of an exact solution, can

reduce the problem in its scope by indicating directions, if not exact magnitudes, and by placing magnitudes within boundaries.

The resulting more complete understanding of magnetron performance can be used as a basis for making engineering judgments in the improvement and application of the magnetron in its increasing number of uses.

The development of the magnetron was greatly accelerated by its use as a transmitter tube in the many radar installations used during World War II. The magnetron was particularly applicable to this use because, fundamentally, it works best as a generator of high powers (kilowatts or greater), at frequencies from 1000 to 10,000 megacycles. The limitations on production of power are, in general, those imposed by heat dissipation and cathode emission. Thus the high peak power, short pulses and relatively low average power desired from the radar magnetron were requirements suited to its capabilities.

Continuous-wave magnetrons received less attention than the pulsed variety in early development, but, as the possibility of their use in radio communication became more conceivable, this development was accelerated. It was immediately discovered that operation under these conditions interposed new problems as well as new possibilities. It is the purpose of this report to present an analysis of two aspects of c-w magnetron behavior which are very important to the use of magnetrons in radio communication; namely frequency pushing and voltage tuning. These terms require definition, and part of the

purpose of this report will be to provide basis for explicit definition. However, definitions more or less acceptable to those who are well acquainted with c-w magnetron behavior are the following.

Frequency pushing is defined as the variation of the frequency, generated by an oscillating magnetron, which is associated with the change in d-c anode current as anode voltage is raised for constant resonator temperature. A frequency-pushing characteristic would therefore be a plot of generated frequency versus d-c anode current for the conditions mentioned. Actually, to be complete, a three-dimensional plot,including anode voltage, current, and frequency, should be used.

A typical frequency-pushing characteristic is shown in Fig. 1.1.

Voltage tuning is defined as the variation in frequency generated by an oscillating magnetron which is associated with the change in d-c anode voltage when d-c anode current, load impedance, magnetic field, and resonator temperature are held constant. In order for d-c anode current to be held constant, the cathode emission must be limited by operation at a reduced temperature. Otherwise, increase in anode voltage will increase anode current. A voltage-tuning characteristic is therefore a plot of generated frequency versus anode voltage for the conditions mentioned.

A typical voltage-tuning characteristic is shown in Fig. 1.2.

In practice it is not always possible to make a complete distinction between frequency changes produced by pushing and voltage

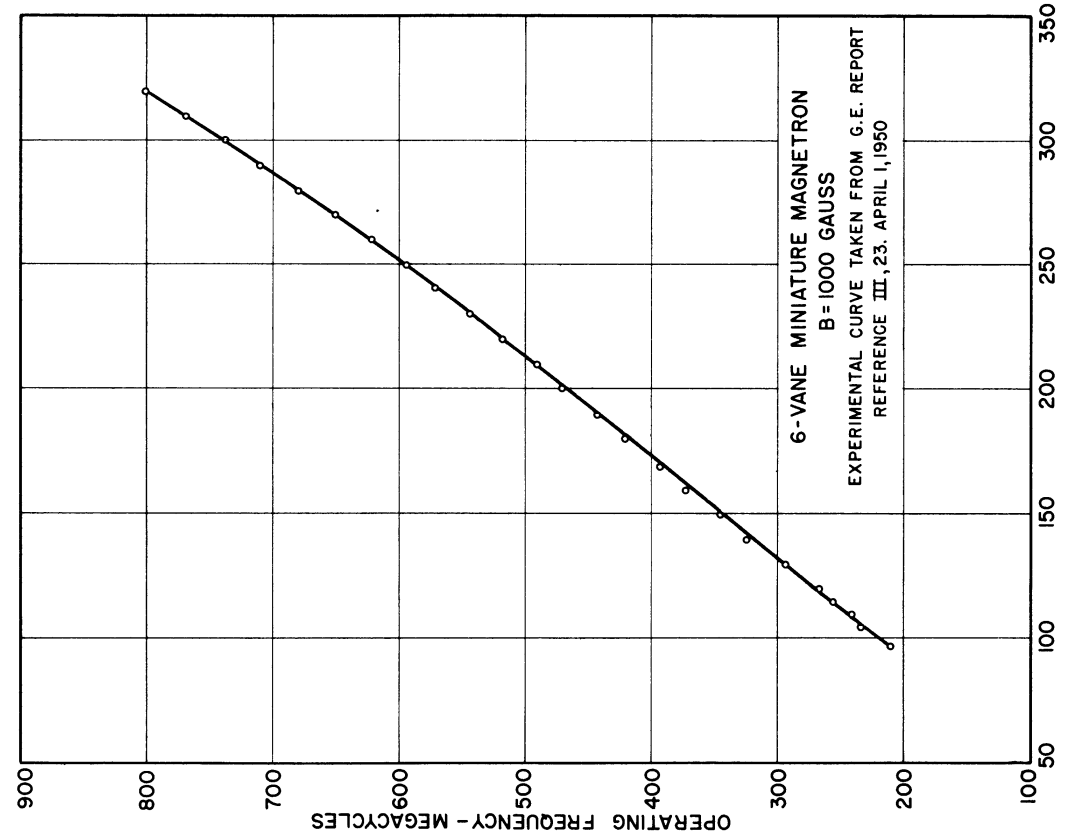

FIG. 1.2 TYPICAL VOLTAGE TUNING CHARACTERISTIC

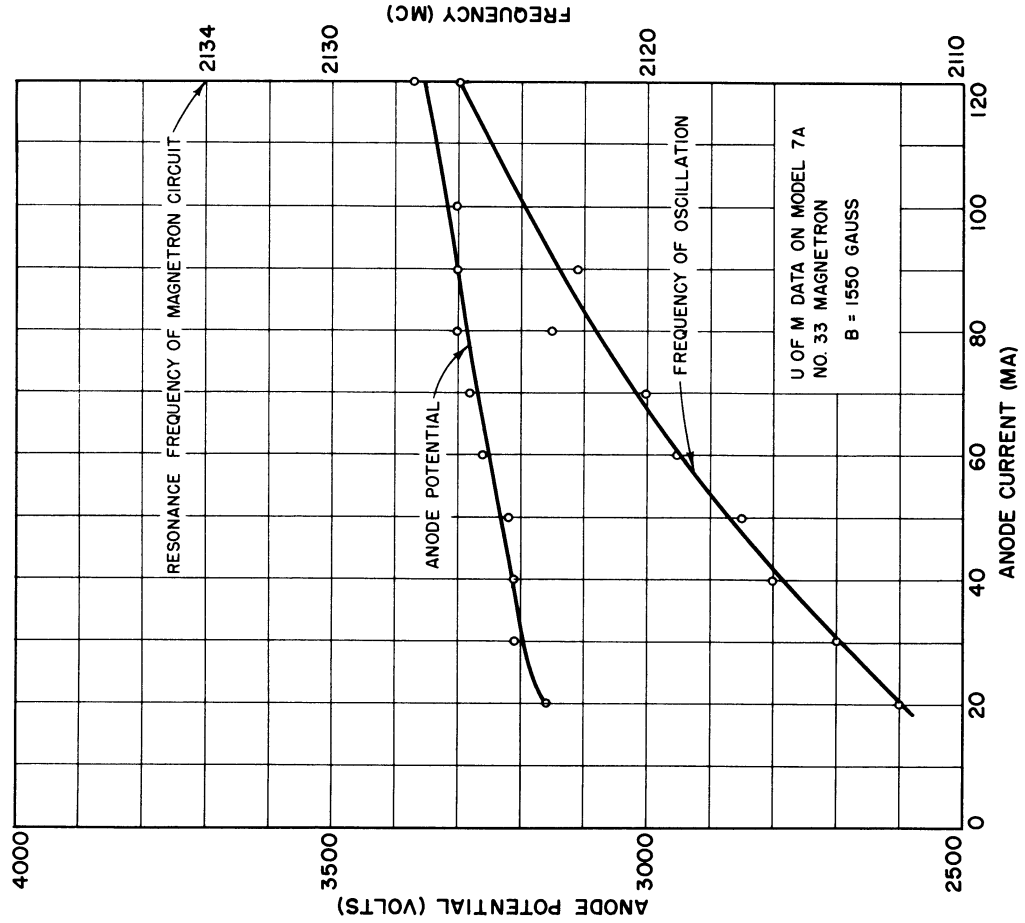

FIG. 1.1
TYPICAL FREQUENCY PUSHING CHARACTERISTIC

tuning. However, examination of a number of typical sets of data on c-w magnetrons will show that, in normal operation (when frequency pushing is observed), the frequency is relatively insensitive to the voltage change which is required to increase anode current compared to the large frequency shifts obtained under the conditions required for voltage-tuning operation. For example, in the figures shown, a change of 100 volts produces a frequency pushing of 10 megacycles, while a change of 5 volts produces a voltage tuning over the same frequency range. Typical frequency-pushing characteristics show a change of 3 to 50 megacycles per ampere. Typical voltage-tuning characteristics show a change of .1 to 2 megacycles per volt.

The term frequency pushing was coined in contrast to the term frequency pulling, which is defined as the variation in frequency generated by the magnetron with load at constant anode current, magnetic field, and resonator temperature. Frequency pulling is essentially a tuning of the magnetron through the external circuit and its interpretation requires no very complete understanding of the magnetron space-charge behavior. It is not the purpose of this report to present any complete discussion of frequency pulling but it will be shown that it is also not always possible to attribute observed frequency shifts entirely to frequency pulling or frequency pushing, and the relationships between the two phenomena will be discussed. In fact it will be necessary to bring into the discussion many related magnetron characteristics, some of which are not completely understood. The thread of the discussion will be limited to those directions which lead toward a better quantitative understanding of frequency pushing and voltage tuning.

The importance of an understanding of these phenomena to the use of the magnetron in radio communication arises in both amplitude-modulation and frequency-modulation systems. It is immediately evident that if one attempts to amplitude-modulate a magnetron, a substantial frequency modulation will also result due to the frequency-pushing effect. If, on the other hand, one wishes to make use of frequency pushing to obtain frequency modulation, amplitude modulation will also be a result. It is this latter fact which led to the discovery of voltage tuning in 1949 by Wilbur and Peters at General Electric Company. In attempting to reduce the amount of amplitude modulation associated with the frequency pushing, they were led to using the operating conditions which allow voltage tuning (heavily loaded, temperature-limited operation). The present major needs in voltage-tunable operations are for more power, higher frequencies, and less noise in the generated signal. Tubes operable at low power levels (of the order of milliwatts) and very wide tuning range have application as local oscillators in search receivers, spectrum analyzers, and signal generators. For higher power levels (of the order of hundreds of watts), relatively narrow tuning range, they have application as the transmitter tube in frequency-modulation systems.

Frequency pushing, since, by its very nature in our definition, it is obtained coincident with amplitude modulation, seems to have little possibility of use in the conventional f-m communication system. There is, however, a possibility of minimizing it for use in a-m systems and the possibility of development of new types of systems in which it would be usable. Most important, perhaps, is the fact that a complete

understanding of the underlying causes of frequency pushing is almost synonymous with a complete understanding of magnetron space-charge behavior. This means that it will be necessary to present a fairly thorough discussion of the magnetron space charge in order to develop the hypothesis necessary to the explanation of frequency pushing. Some of the results will be familiar to those well-versed in magnetron theory but it is believed that the method used in arriving at these results and the way they are used will give them a new interpretation which will be very useful in the understanding of magnetron behavior.

Before going through the theoretical development, a simplified picture of the magnetron space charge will be presented with a statement of the distinction which will be made in the physical picture between the mechanism of frequency pushing and voltage tuning. Then a historical summary of other work particularly related to the problem will be given which should place the results obtained in proper perspective. After the analysis is presented, experimental data will be given which substantiates the results. The analysis has led to some ideas which suggest further work. These will be mentioned in the conclusions.

1.2 Approximate Picture of Space-Charge Behavior

Before a detailed study of the magnetron space charge is presented, an approximate picture will be described which will acquaint the reader with broad aspects of the problem. In this way the relationship of the various parts of the succeeding development to the total problem can be realized.

A conceptual picture of the space charge in the multianode cylindrical magnetron under large-signal conditions is shown in Fig. 1.3.

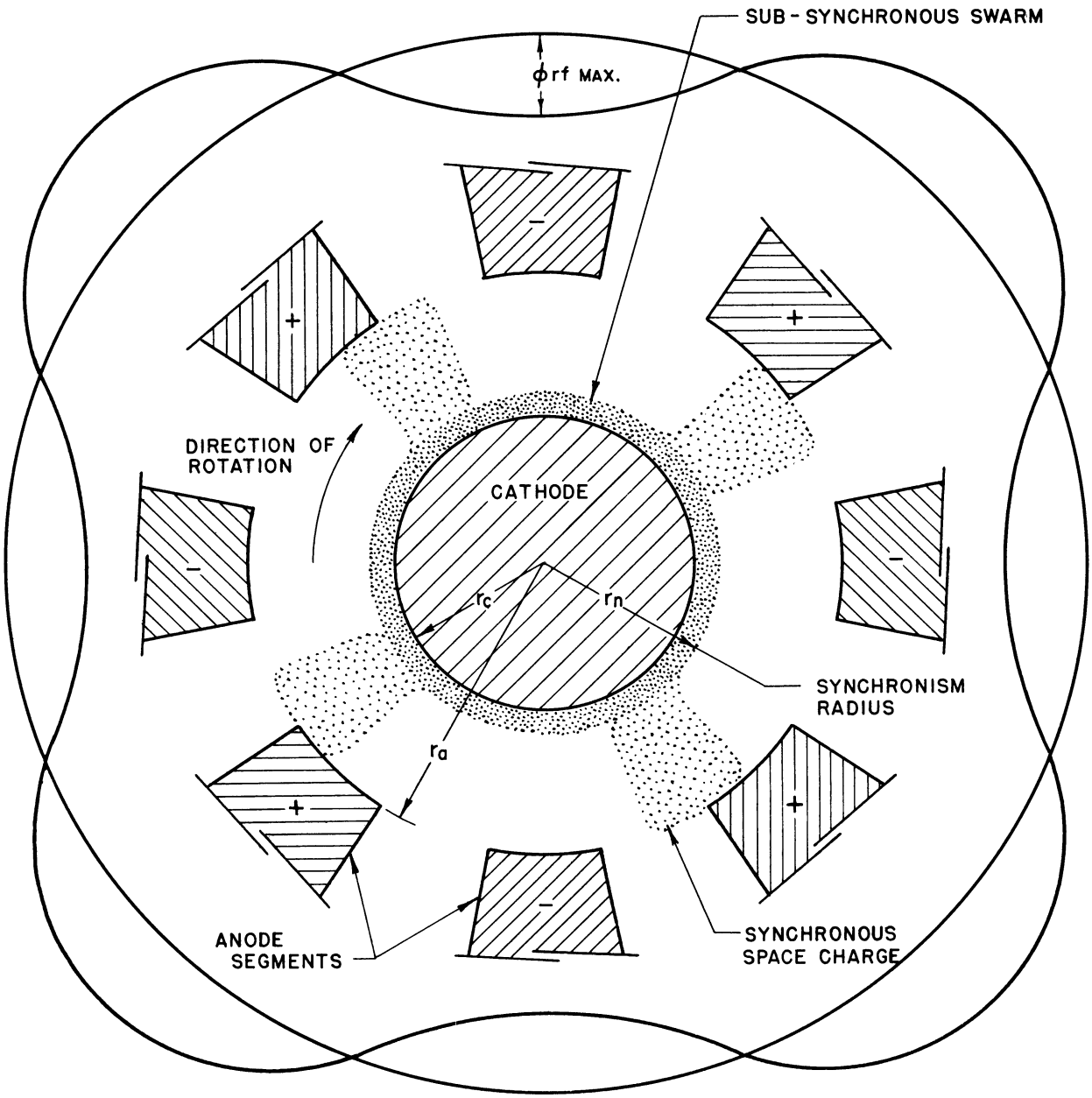

FIG. 1.3
BASIC PHYSICAL PICTURE OF THE MAGNETRON SPACE CHARGE WITH LARGE SIGNAL R-F POTENTIAL ON THE ANODE

That this picture is approximately correct has been well established and is generally accepted by the many investigators who have considered the problem. The anode segments which are shown in this picture are assumed attached to an external circuit which is not shown. The actual geometry of the circuit may assume any one of many forms in a particular case depending on the type of magnetron. In the conventional magnetron the circuit is always resonant; however, in magnetrons used for voltage tuning this may not be the case. In any case the electromagnetic field distribution seen by the electrons within the anode structure is independent of the circuit for a given radio-frequency voltage between the anode segments. The region for which this is true, that is, the region where there is mutual interaction between the electrons and the electromagnetic field, is known as the interaction region or interaction space. The swarm of electrons is caused to exist in the interaction region by applying a positive voltage to the anode, making electrons emitted from the cathode move toward the anode. This motion takes place in an axially directed magnetic field which produces a force perpendicular to the electron motion, thus causing a drift around the cathode as well as toward the anode. In the static magnetron the angular velocity of this drift increases as the electron proceeds from the cathode toward the anode and as the magnetic field is increased.

In the oscillating magnetron an r-f potential is caused to exist between the anode segments. The effect of the r-f potential is superimposed on the effect of the d-c field. The distribution shown in Fig. 1.3 is usually referred to as the π mode and is so named because there is a phase difference between the voltages on adjacent segments

of π radians or 180°. It is found to be convenient to represent this distribution, which is a stationary wave in space, as the Fourier sum of a number of travelling waves which proceed in opposite directions around the interaction space. In the π mode the electrons interact primarily with the fundamental wave of this sum which is moving in the same direction as the electron drift around the cathode with a velocity such that the maximum of the wave proceeds from one anode segment to the next in one-half cycle. For a given frequency f and a given number of anodes 2n the time of one-half cycle is 1/2f, the angular distance between adjacent anodes if $2\pi/2n$, thus the angular velocity corresponding to the fundamental wave is

$$\omega_n = \frac{2\pi f}{n} \tag{1.1}$$

Electrons moving in the direction of the fundamental wave will in some regions be accelerated and in other regions retarded. Where the radial velocity of the electron is increased, under a positive potential maximum, the force due to the magnetic field will encourage electrons to move into a region where the tangential electric field is opposing their motion, between a positive maximum and a negative maximum. The force due to the tangential field in this region will reduce the electron velocity parallel to the cathode, reducing the inward directed radial force due to the magnetic field, and encouraging electrons to drift toward the anode. Similar arguments will show that electrons under a negative potential maximum will be encouraged to drift backward into a region of retarding tangential field, and electrons in an accelerating tangential field will be encouraged to move toward the cathode. The net effect

results in a phase focussing of electrons into a region between the positive and negative maximum on the traveling wave where the tangential field is opposing the motion of the electrons and the electrons are drifting outward toward the anode. If the r-f voltage is sufficiently high this focussing will actually bunch the electrons into spokes as shown in Fig. 1.3. Fig. 1.3 may be thought of as showing the total anode potential and space-charge distribution at a given instant. The phase-focussing action just described will cause the bulk of the electrons in the spoke to be found somewhere between a positive anode and a negative anode moving toward the negative when the potential difference between the anodes is a maximum.

The transfer of energy from the electrons to the circuit is best analysed by using the theory of induced currents caused by moving charge densities.[1] It is obvious that the rotating spokes of charge will induce currents which will flow from the anode segments through the circuit to which they are attached. Theoretical and experimental evidence indicates that the r-f current is primarily that caused by the rotation of these spokes and that the effects of radial motion should be negligible. A spoke of negative charge moving away from an anode segment will cause positive current to flow away from that segment into the circuit. When the spoke is moving toward a segment positive current will flow from the circuit into the segment. The complete set of spokes, since they are symmetrically disposed between every other pair of anodes, will act as

---

[1] The arguments given in the following few paragraphs are given detailed treatment in the discussion of phase focussing in Chapter 2. Appropriate diagrams are also given there to clarify the meaning. (Figs. 2.8 and 2.9 in particular).

a current generator connected to the two sets of alternate anodes. When the spokes are half way between the anode sets the current generator output will be a maximum, positive current flowing into the circuit from the set of anodes away from which the spokes are moving and out of the circuit to the set of anodes toward which the spokes are moving. It is further evident that, if the spokes are in this position at the instant when the anode set from which positive current is being delivered is at maximum positive potential, power will be delivered to the circuit. If the angular velocity of the spoke is synchronous with the angular velocity of the fundamental wave of the r-f field around the interaction space the spokes will continue to bear this relationship to the field and continually deliver r-f power to the circuit. This power is acquired from the d-c field in the drift motion of the electrons toward the anode which will occur under this condition since the electrons are moving in a retarding phase.

Another situation can be imagined as follows: suppose the spokes are symmetrically disposed about a positive potential maximum in the fundamental travelling wave. In this case the maximum positive current from an anode set into the circuit will occur when potential of the anode set is going through zero from positive to negative values. The current into the circuit will, therefore, lag the voltage by 90° and a purely reactive effect will be induced into the circuit.

A positive current from an anode set into the circuit is equivalent to a negative current from the anode set into the space charge. The space-charge swarm, acting as an induced-current generator and inducing a current into the circuit which lags the voltage by 90°, can be thought of as a passive capacitance in the interaction region accepting

a current which leads the voltage by 90°. The magnitude of this capacitance is given by the ratio of the r-f voltage to the r-f current induced by the space charge, and will be a function of the several variables involved in the interaction space geometry and the static fields imposed on the circuit.

Two cases have been described which illustrate that under certain conditions the space-charge spokes can be contributing only real power to the circuit and under certain other conditions the spokes can be contributing only reactive power to the circuit. By the same qualitative arguments it can be shown that for intermediate positions of the spokes relative to the maximum potential between anode sets the spokes of space charge will contribute both an in-phase and an out-of-phase component of induced current. The in-phase component of current represents a delivery of energy from the electrons to the circuit. This energy is received by the electrons from the static field so anode current must flow as soon as there is an in-phase component of r-f current.

The effect of induced current due to radial motion, although not a first-order effect, may be significant in magnetrons operating at high anode currents and will be discussed briefly in a later section. The collection current into the circuit will always lead the induced current by approximately 90°.

We can see, that in order for the magnetron to act as a self-excited oscillator, the space-charge-spoke configuration must induce current into the circuit with a phase and magnitude required by the circuit. Thus the circuit will determine the static fields and interaction-space geometry required for a given frequency of operation. Or, to look

at the problem from another point of view, for a particular set of static field conditions and interaction-space geometry, there is a circuit impedance which will encourage the formation of spokes and thus the induction of currents and r-f voltages of the proper phase and magnitude.

When the circuit between anode sets is resonant the phase and magnitude of the impedance, looking out from the anode sets are, near resonance, rapidly varying functions of frequency. In the range which encourages the formation of spokes and thus the delivery of power from the magnetron space charge for the given interaction-space conditions, the magnetron will oscillate. In typical magnetrons with circuit Q's from twenty to three or four hundred it is generally observed that oscillations begin at frequencies below resonance by a factor of approximately the resonance frequency divided by $\frac{1}{2}Q$. As the anode voltage and anode current are raised and the power input increased the frequency moves toward resonance while power output is increased. This implies a phase change and is the behavior which would be expected from a constant-current generator with variable frequency output. The constant-current generator operating into a parallel-resonant circuit will, below resonance, be injecting a current into the circuit which lags the voltage by approximately 90°. The circuit will look like an inductance. As the frequency is raised the circuit accepts more power from the generator and the current is split into in-phase and out-of-phase components. At resonance the circuit looks like a pure resistance and all of the current output is in phase with the voltage developed across the circuit.

These arguments can be compared to those presented in the discussion above relative to the space-charge-spoke behavior. It is

seen that the effect produced by advancing the phase of the spokes relative to the r-f voltage maxima, starting from the position of the spokes symmetrically disposed around the r-f voltage maxima, is the same as the effect produced by increasing the output frequency of the constant-current generator if the velocity of rotation of the spokes is increased in the process. The frequency change accompanying a given phase change will depend on the Q of the circuit and will, in general, be of the order of $2/Q \times f_o$ where f_o is the resonance frequency of the circuit.

This qualitative discussion is sufficient to provide basis for a further clarification of the definitions of frequency pushing and voltage tuning as they will be developed in the following pages. It will be shown that in order to advance the phase and increase the velocity of the space-charge spokes to produce the effect just mentioned the anode voltage and current must be increased. The change in phase is associated with an increase in d-c collection current which is large compared to the increase in anode voltage. The velocity change, and therefore, the frequency change, is relatively small for a high-Q circuit. This small frequency change, associated with a large phase change, is what we describe as <u>frequency pushing</u>.

For a given phase relationship and r-f voltage amplitude the velocity of rotation of the spokes is determined by the d-c anode voltage. If a nonresonant circuit is used, i.e., one in which the phase angle and magnitude of the impedance are not rapidly varying functions of frequency, then the magnitude of the induced r-f voltage will be primarily a function of the induced current magnitude and the frequency a function of the d-c

anode voltage. This large frequency change associated with a small phase change is what we describe as voltage tuning.

If the collection current is held constant as anode voltage is raised (by limiting available current at the cathode) there is also a tendency to limit the amount of r-f current which can be induced by the spokes. Under these conditions, with the right kind of circuit, voltage tuning with constant power output will result. This is, of course, desirable in frequency modulation applications.

It should be quite obvious at this point that the distinction between voltage tuning and frequency pushing becomes arbitrary and, in fact, nonexistent for certain intermediate cases of low-Q resonant circuits. The extremes represent, nevertheless, definitely different types of behavior and the use of the terms is justified.

In order to establish more quantitatively the concepts discussed in this section it will be necessary to present theories which are based on more or less unrelated concepts. The results of these theoretical developments will then be brought together and used to interpret experimental information. Approximations will be continually necessary because of the nonlinearity of the differential equations involved even in the most ideal geometry. The variables in the problem are so many that it is impractical to obtain experimental evidence showing completely the effect of all parameters. Three quantities are essential to the complete interpretation of the results. These are the angular velocity of the spokes, the geometrical configuration of the spokes, and the space-charge density in the spokes. The angular velocity can be determined and a physical picture will be given which makes possible estimation

of the latter two quantities. Methods for applying the estimated results to the calculation of magnetron characteristics are developed. The results of application of these methods check reasonably well with experimentally observed characteristics. The experiments which have been chosen illustrate the most important points of the theory and show the effect of variation over a limited range of most of the parameters involved.

In the next section a brief historical survey of the work particularly related to the problem discussed here will be presented. Some of this work will be discussed in more detail as it is used in the following development.

1.3 Historical Survey of Related Work

It is not the purpose of this section, or the bibliography which will be found at the end of this report, to make reference to all of the important work which has been done on magnetrons. We do attempt to include fairly complete references of four general types. These are: I -- References to survey or general treatment of the magnetron problem, II -- References to the study of space charge in the static magnetron, III -- References to the study of the oscillating travelling-wave magnetron and to the effects of magnetron space charge on frequency, IV -- References to the study of related space-charge problems not specifically concerned with the magnetron. The references in the third category are the most closely related to the problem under discussion. We are omitting, except where it may become necessary to the development of the theory, reference to detailed treatments of the magnetron circuitry and problems of electrode design such as those connected with the cathode, heat

dissipation, fabrication,etc. All of these problems are mentioned and references made to more detailed treatments in the references of the first category. A rather complete reference to early work on magnetrons (prior to 1941) is given in High Frequency Thermionic Tubes by Harvey (Chapman and Hall, 1943).

The first mention of the magnetron principle is credited to A. W. Hull in 1921.[1] This was followed by rather extensive use of the magnetron principle in three different types of oscillation mechanism which, at first, were not clearly differentiated by the various investigators.[2] The three mechanisms which seem to be important and definitely observable are negative-resistance oscillations, "electronic" or cyclotron-frequency oscillations, and travelling-wave oscillations. The basis for this differentiation is adequately covered in the references.[3] A recent investigation has shown oscillations which this author believes may properly be placed in a fourth category.[4] These oscillations occur only at voltages near the critical anode voltage and magnetic field for which electrons are just synchronous at the anode radius. The understanding of this type may be helpful to the understanding of magnetron amplifier behavior and generation of higher frequencies. These are problems which have attracted considerable recent interest. The magnetron amplifier is being studied particularly by the French[5] and several groups in this country.

---

[1] II, 5.

[2] I, 8, a. p. 977.

[3] I, 4, pp. 177-182; I, 3, b. pp. 170-171; I, 2. pp. 3-7.

[4] III, 25.

[5] I, 3, c, d. and numerous other papers during the past year in Annales de Radioelectricite. In this country particularly by E. Dench at Raytheon Mfg. Co. and J. F. Hull at Evans Signal Laboratory.

The type of oscillation which is by far the most commonly used and which is the subject of this study is travelling-wave oscillation. The first interpretation of electron interaction with a travelling wave in a magnetron was given by Posthumus[1] in 1935. The ideas presented by Posthumus are quite correct including an expression for the maximum electronic efficiency of a magnetron which, although used by the British[2] (after a derivation by Hartree), was almost neglected in the wartime development of the magnetron which was carried on in this country. This maximum electronic efficiency is given by

$$\eta_{e\ max} = \frac{\phi_a\ e - 1/2\ m\ \omega_n^2\ r_a^2}{\phi_a\ e} \qquad (1.2)$$

where

e and m are the absolute charge and mass of the electron

$\omega_n = \frac{2\pi f}{n}$ the synchronous electron angular velocity

r_a = radius of the magnetron anode

ϕ_a = potential on the magnetron anode

This equation states that the maximum electronic efficiency is obtainable when the electron strikes the anode with no radial velocity and with an angular velocity equal to the angular velocity of the wave. The energy input is in this case ϕ_a e and the heat energy lost to the anode $1/2\ m\ \omega_n^2\ r_a^2$. It is also assumed in this expression that no energy is lost by back-bombardment of the cathode by electrons. A convenient

---

1 III, 13.

2 I, 12, a, p. 992.

definition, often used, is

$$\phi_o = \frac{1}{2} \frac{m}{e} \omega_n^2 r_a^2 \qquad (1.3)$$

representing the energy in electron volts of a synchronous electron at the anode. It is immediately obvious from examination of Equation 1.2 that a high ratio of ϕ/ϕ_o is a desirable design criterion if high electronic efficiency is the objective. This was indicated by Posthumus and by the British.

The most important feature of the magnetron space charge which makes possible the use of the magnetron as a large-signal microwave generator, is the mechanism of phase focussing as it occurs in crossed magnetic and alternating electric fields. This was discussed qualitatively in the last section. This feature is the basis of Posthumus' arguments as they were presented in 1935. Investigators in the klystron field, who are quite familiar with the term phase focussing, were quick to carry these concepts into the investigation of magnetrons. A paper by Ludi[1] is one of the first published to give a detailed discussion of the phase-focussing action. The effect of space charge is neglected in this paper but, with the use of some restricting approximations, the focussing action in the absence of space charge is quite clearly demonstrated. An important point made in Ludi's paper is that there must be a drift of electrons toward the anode in the region of retarding electric field where the electrons are giving up energy. This shows that d-c plate current will flow as is required if energy is absorbed

---

[1] III, 12, b.

by the system. Ludi's earlier papers[1] also deal with interaction between electrons and travelling waves in klystrons and other tubes and are interesting as background material to his work on magnetrons. He defines, for example, a compression factor which indicates the amount of increase in electron density in the electron bunches to be expected under various interaction-space conditions. He suggests using the compression factor in the treatment of the magnetron and presents some approximate relationships in his discussion. A more recent paper by Ludi[2] discusses the magnetron problem more completely with rather interesting experimental results on tubes constructed at Brown, Boveri and Company in Baden, Switzerland. The effect of cathode size on efficiency is discussed and data given for forty different combinations of number of anode segments and cathode size at approximately the same frequency.

The most important theories of space-charge behavior in the oscillating magnetron were developed in England by groups working on the radar magnetron in 1940 and the following years. This work was published only in wartime reports[3] until 1946 when articles appeared by H. A. H. Boot and J. T. Randall[4] the co-inventors of the multi-cavity magnetron, and W. E. Willshaw[5] with others which described the early work of D. R. Hartree, E. C. Stoner and O. Bunemann. Particularly

---

1 IV, 8, a, b, c.

2 I, 7.

3 Committee on Valve Development Magnetron Reports.

4 I, 1.

5 I, 12.

important results which were obtained by these three investigators have also been given detailed treatment by Walker[1].

Professor Hartree is responsible for a detailed discussion of electronic efficiency[2] (for which he gets the same maximum value given in Eq 1.2) and for the derivation of the Hartree equation[2] which gives the anode voltage for which oscillation should be possible at infinitesimal amplitudes of the r-f voltage. This equation is the following:

$$\phi_{at} = \frac{1}{2} B \omega_n (r_a^2 - r_c^2) - \frac{1}{2} \frac{m}{e} \omega_n^2 r_a^2 . \qquad (1.4)$$

ϕ_{at} = threshold voltage for oscillation

B = magnetic field strength

r_a = anode radius

r_c = cathode radius

ω_n = synchronous angular velocity.

This is the most important single equation governing oscillatory magnetron behavior. Since for the usual case of large B, the second term on the right is small compared to the first, we see that the frequency (contained in ω_n) is approximately a linear function of anode voltage. It is this functional relationship which, under very special conditions, determines the frequency in voltage tuning. It is quite obvious from the examination of frequency-pushing characteristics, that other factors are involved in the relationship between voltage and frequency normally encountered. It is hoped that the present report will serve to clarify this relationship.

---

1 III, 20.

2 I, 1; I, 9; I, 12; III, 20. Professor D. R. Hartree, "Estimates of Electron Energies, Oscillation Amplitude and Efficiencies in a Magnetron Operating under Rotating Space Charge Conditions" C.V.D. Report Ref. Mag. 11, Apr. 10, 1942.

Another very important contribution of Hartree and Stoner was the calculation of electron positions in the magnetron by the self-consistent field method. The method of self-consistent fields was originally used by Hartree in the calculation of electronic orbits in the atomic problem. It applies to any problem where space-charge is involved, i.e., where the motion and position of electrons is determined by the field and where, through Poisson's equation, the field must in turn be consistent with the presence of the electrons. The problem is simplified by the proper initial choice of fields consistent with the boundary conditions such that small revision is necessary to arrive at the field and charge distribution which represent good approximations to the solution of the problem. Once a solution is obtained it is known that for the given distribution of charge density it is the only possible solution of Poisson's equation if it satisfies the boundary conditions.[1]

A typical result of the self-consistent field method is shown in Fig. 1.4. This picture shows electron trajectories in a reference frame moving with the synchronous angular velocity for an assumed field. By rather involved calculation the approximate required cathode emission and the density of electrons at various points throughout the "spoke" region can be calculated from knowledge of these orbits. If this result gives the assumed field with reasonable accuracy the calculation is considered complete. The particular trajectories in Fig. 1.4 are the result of several trials and still do not give a self-consistent result.

---

[1] S. Ramo and J. R. Whinnery, Fields and Waves in Modern Radio, New York, John Wiley and Sons, Inc., 1944, p. 96.

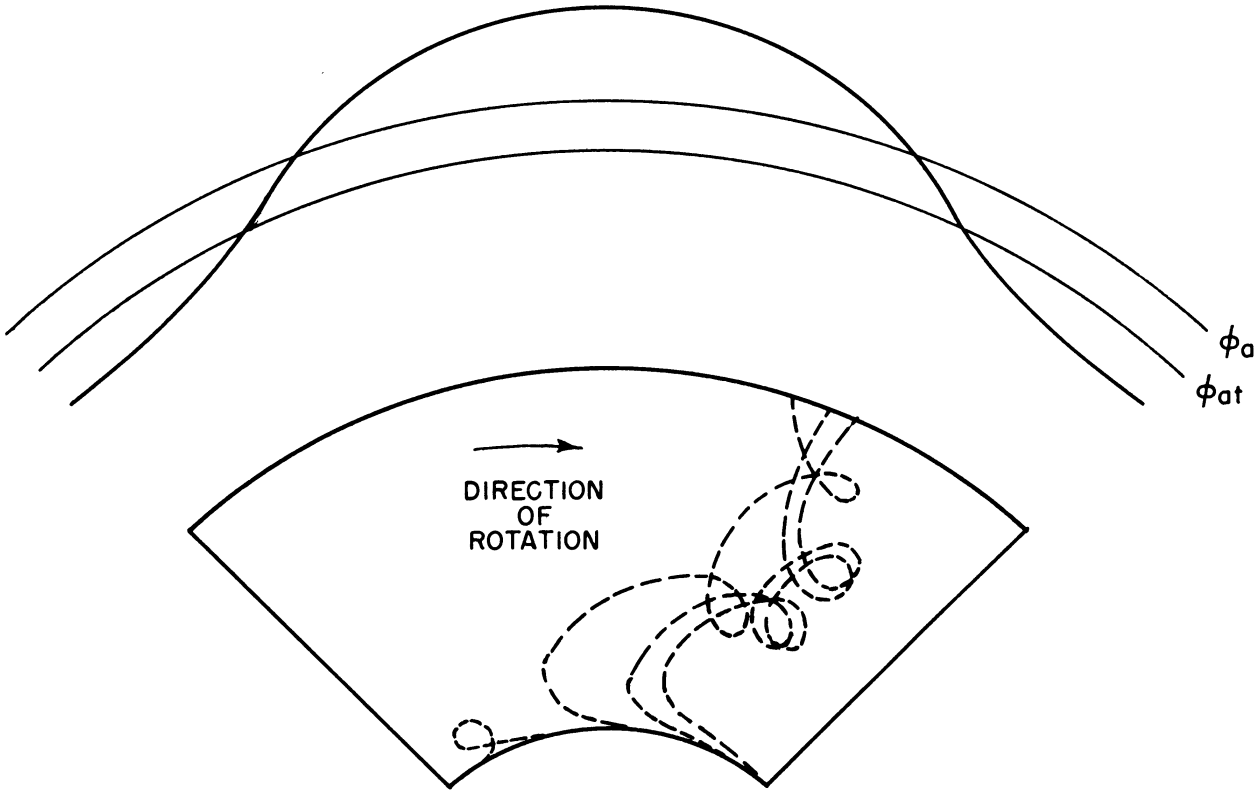

FIG. 1.4

ELECTRON TRAJECTORIES IN A MOVING FRAME OF REFERENCE FROM CALCULATIONS MADE BY TIBBS AND WRIGHT.[1] POTENTIAL DISTRIBUTION IS FOR THE FUNDAMENTAL WAVE STATIONARY IN THE MOVING FRAME.

REPRODUCED FROM I,2 P. 270 FIG. 6.15. TIBBS AND WRIGHT WORKED WITH STONER'S GROUP AT LEEDS

An obvious disadvantage exists in this method. The calculations are much too involved to use in the prediction of operating conditions for a magnetron of new design. A particular calculation if carried out carefully, gives much more detailed information about the magnetron behavior at a particular operating point than any other method. The geometry, density and current flow through the spokes is given for a particular anode voltage and r-f voltage. With knowledge of the geometry, density and angular velocity of the spokes the magnitude of induced r-f current can be calculated with its phase relationship to the r-f voltage[1]. The ratio of these two quantities gives the impedance which, at the particular frequency involved, must be placed between the anode sets. In order to make another calculation at a new anode voltage and r-f voltage and, in addition, to specify the load conditions, we find that we have extended our analysis to a new kind of self-consistent calculation. We assume an r-f voltage and d-c anode voltage, then try it to see if the required ratio of r-f voltage to induced current, in both magnitude and phase, is produced. If the result is not consistent a correction must be applied, after the self consistency of the Poisson field is satisfied. We will become even more discouraged when we attempt to interpret an effect such as frequency pushing which is usually a one or two per cent change in frequency.

Another interesting treatment of the space charge problem was carried out by Bunemann.[2] Bunemann calculated the impedance of the

---

[1] Methods for making induced-current calculations in the magnetron have been described by H. W. Batten, W. Peterson, S. Ruthberg and the author in III, 22, c.

[2] III, 20. O. Bunemann, "A Small Amplitude Theory for Magnetrons", C.V.D. Report, May, 1944, P. 37.

magnetron type space charge by assuming small amplitude perturbation of the steady-state (static) magnetron solution. These calculations have an advantage over the self-consistent-field calculations in that they give directly an impedance as a function of frequency (and would therefore give some interpretation to the frequency-pushing or voltage-tuning phenomena). They have a very serious disadvantage in that the results are definitely restricted to small-signal behavior, whereas the magnetron in its useful form is definitely a large-signal device.

Impedance calculations have also been made by Doehler[1] for the special case of a small cathode and narrow gaps between anodes. Doehler's approach is based on experimental evidence that the time-average space-charge density is approximately constant in the interaction space. The work which has been done at Michigan indicates that this assumption is correct but probably not correctly based on the static magnetron experimental evidence.[2]

Both the method of self-consistent fields and the small-amplitude theory require an initial choice of potential or space-charge distribution. In making this choice most of the investigators have been guided by the study of the static magnetron. The static, or symmetrical, state has been the subject of extensive theoretical investigation with very little revealing experimental work. Corresponding to the Hartree threshold

---

1 I, 3, b. This work is summarized by the author in III, 22, e.

2 III, 22, b.

equation is the Hull cutoff equation

$$\phi_{aH} = \frac{B^2 e}{8m} r_a^2 \left[1 - \left(\frac{r_c^2}{r_a^2}\right)\right]^2 \qquad (1.5)$$

ϕ_{aH} = cutoff anode potential

Other symbols defined with Eq 1.4.

The potential is given by this equation above which electrons should reach r_a, below which no electrons should be found at r_a. Thus, if r_a is the anode radius, anode current should exist for potentials greater than ϕ_{aH}, whereas, for potentials less than ϕ_{aH} no anode current should exist. The current for potentials greater than the cutoff potential has been calculated by Bethenod[1] and Brillouin[2] for the plane magnetron, by Hartree, Allis, Brillouin and Bloch[3] for the cylindrical magnetron and by others. The solution to the plane-magnetron problem is straightforward but the problem of the cylindrical case becomes quite involved and requires lengthy numerical calculations. The method used by Brillouin has advantages in simplicity in that analytical solutions are obtainable whereas the work of Hartree and Allis requires numerical integration or approximation. Brillouin uses the Llewellyn method in which the anode voltage is found as a function of the assumed current. This method proves to be much simpler than the inverse problem. Brillouin also emphasizes the importance of using the plane-magnetron solution as an approximation of the large-cathode cylindrical magnetron. The ratio of the current at

---

1 II, 1.

2 II, 2, a.

3 II, 8, p. 345-353. Slater reviews the work of Allis. II, 2, b.

cutoff to the nonmagnetic diode current at cutoff is a good measure of this approximation. This ratio is plotted in Fig. 1.5. In Fig. 1.6 the current is plotted as a function of magnetic field for the plane case and for a very large ratio of anode radius to cathode radius.

The behavior of the space charge in the static magnetron becomes a matter of conjecture when ϕ_a is below the cutoff value ϕ_{aH}.[1] In general, two types of solution are possible below the cutoff voltage. These are: a double-stream solution, in which electrons are steadily flowing to and from the cathode, and a single-stream solution, for which all electrons are moving parallel to the surface. In the latter case the potential distribution within the space-charge swarm is that given by Equation 1.5 since the radial velocity is everywhere zero and this is the condition for cutoff. A useful fact to have in mind is that the potential distribution for the double-stream solutions differs very slightly from the value given by Eq 1.5. This is equivalent to saying that the radial velocities of the electrons are small compared to the tangential velocities.

Slater has shown that several double-stream solutions are possible for which there may be one or many swarms or layers of electrons, one within the other, running tangentially around the cathode. Within each swarm or layer there is a double-stream solution. The current which streams in and out is greatest in the single-swarm double-stream solution. Slater points out that the type of solution which will exist is not determinate from the initial conditions (zero velocity and zero field at

---

[1] Mr. G. Hok has very recently discussed this problem in "Space-Charge Equilibrium in a Magnetron; A Statistical Approach", Technical Report No. 10, University of Michigan, Department of Electrical Engineering, Electron Tube Laboratory, July 13, 1951.

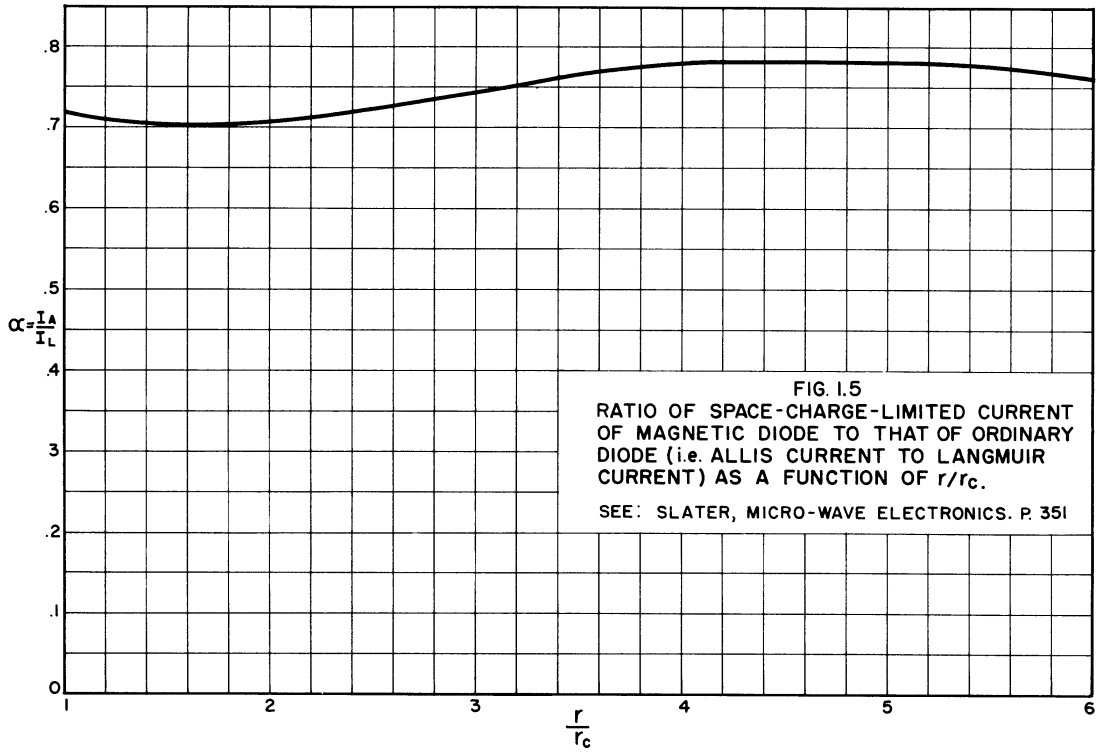

FIG. I.5
RATIO OF SPACE-CHARGE-LIMITED CURRENT OF MAGNETIC DIODE TO THAT OF ORDINARY DIODE (i.e. ALLIS CURRENT TO LANGMUIR CURRENT) AS A FUNCTION OF r/r_c.
SEE: SLATER, MICRO-WAVE ELECTRONICS. P. 351

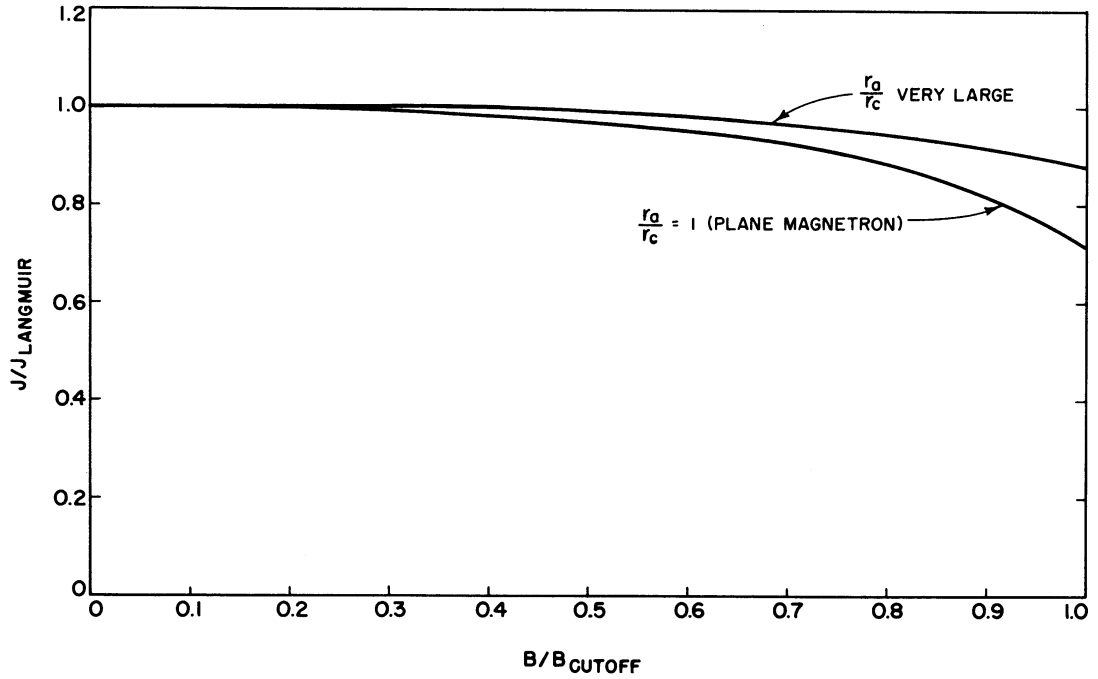

FIG. I.6
RATIO OF SPACE-CHARGE-LIMITED CURRENT OF MAGNETIC DIODE TO THAT OF ORDINARY DIODE AS FUNCTION OF MAGNETIC FIELD. FROM PAGE AND ADAMS, II, 6, p. 493 AND p. 499.

the cathode). A recent study of the problem by Twiss,[1] which discusses the effect of randomly distributed initial velocities, indicates the following: when initial velocities are assumed entirely normal to the cathode surface, and the cathode absolute temperature allowed to go to zero, the limiting solution is the single-stream solution (Brillouin steady-state solution); when initial velocities are assumed entirely tangential to the cathode surface, and the cathode absolute temperature is allowed to go to zero, the limiting solution is the double-stream solution; multiple-layer, double-stream solutions are possible, but only in a very small range of voltages near cutoff (of the order of one to three per cent of the anode potential).

A more detailed discussion of these theories has been given by the author in a recent technical report of the University of Michigan Electron Tube Laboratory.[2] The importance of the static magnetron theories lies in the assumption that they approximately describe conditions in the hub of the space charge wheel which exists in the oscillating magnetron. The space charge can be divided into two regions, the hub region and the spoke region. At the boundary of the hub the variations in potential and field due to the r-f anode potential are small compared to the variations nearer the anode. The diameter of the hub has been calculated by the author[3] and is in conventional magnetrons

---

1 II, 10, M.I.T. Doctoral Thesis.

2 III, 22, e.

3 III, 22, b.

of the order of 10 per cent greater than the cathode diameter. The space-charge-limited current through the hub should be a measure of the upper limit of current possible in oscillatory operation. This has been calculated by the author and W. W. Peterson.[1] Actually a more conservative estimate of the upper limit of current should be made since the small variations in potential and field in this region play a very important role in phase sorting of the electrons which are moving from the cathode through the hub. Some of the electrons, probably half or more, are emitted in an unfavorable phase relative to the r-f field and are sent back to the cathode. Some of these electrons extract energy from the r-f field and produce the back-bombardment power which makes difficult the design of cathodes for c-w magnetrons and which makes possible the design of cathodes for pulsed magnetrons. Ordinarily this power is from 3 to 6 per cent of the total input power.[2]

This division of the space-charge swarm into two regions is quite important to the understanding of the detailed behavior of the magnetron and has been used, whether specifically indicated or not, by almost all investigators. These regions may be called by various appropriate names including: hub and spoke region, sub-synchronous and synchronous swarms, or phase-sorting and phase-focussing regions. Frequency pushing and voltage tuning are explained chiefly by discussion of behavior in the spoke region. The importance of the hub region cannot be ignored, however, since it must have a very definite bearing on the volt-ampere characteristic, maximum current boundary, effects of

---

[1] III, 22, e.

[2] I, 12, a., p. 1002

temperature and in a second-order way, on frequency. No really firm statements of these relationships have been made but we will attempt to show as clearly as possible through qualitative discussion their position in the solution of the problem at hand.

There have been few papers specifically treating the frequency characteristics of the magnetron space charge. Blewett and Ramo[1] discussed these properties in 1940 using as a basis the perturbation of the static magnetron swarm. The results of this treatment are not very revealing, however, since the effect of the cross product of the perturbed velocity and the magnetic field was neglected. It is this term which leads to resonance effects. Lamb and Phillips[2] presented a treatment of this problem in 1947 which, quantitatively, applies only to very small thickness sheaths of space charge around the magnetron cathode. Fechner[3] has treated the resonance behavior of the space charge in two very short articles, one dealing with theoretical analysis and the other with experimental measurements. The general problem, with emphasis on effects in the preoscillating magnetron has been treated by the author in recent publications[4] and in numerous reports of the Michigan Electron Tube Laboratory.

The conclusions resulting from this study[5] are the following:

---

1 III, 1.

2 III, 11.

3 III,22, a, b.

4 III, 7, a, b.

5 Op. cit., p. 1447

a. Resonance-frequency shifts can be caused by the hub or sub-synchronous swarm by an effective change in the capacitance between the cathode and the anode sets. This frequency shift can be positive or negative depending on the electron density and the frequency. The results are conveniently expressed in terms of the ratio $\omega_f/\omega_c = 2\pi f/\frac{Be}{m}$. Generally speaking, for values of ω_f/ω_c slightly greater than unity, the electronic space charge is equivalent to a medium with dielectric constant between zero and one. In this region the capacitance will be decreased by the presence of the space charge so that the resonance frequency increases as the hub expands. For values of ω_f/ω_c slightly less than unity the electronic space charge is equivalent to a medium with negative dielectric constant. In this region the capacitance will be effectively increased by the presence of the space charge so that the resonance frequency decreases as the hub expands.

b. For values of ω_f/ω_c near unity the natural resonance of the individual electron motions in the space charge causes relatively large perturbations of the resonance frequency. This is what is usually called the cyclotron resonance.

c. When r-f voltages of appreciable magnitudes are imposed upon the anode sets spoke formation can begin as soon as the anode voltage is reached for which the swarm has expanded to the synchronous radius. The action of the phase-focussing fields will cause these spokes to expand in radial extent as the anode voltage is raised. The spokes will be roughly symmetrically disposed about r-f voltage maxima so that they will contribute capactive reactance to the system, thus decreasing the resonance frequency.

d. Frequency pushing, which has already been discussed qualitatively, is the increase in frequency with current which occurs after oscillations start due to the increase in angular velocity of the spokes of the space charge wheel which is associated with their advance in phase relative to the r-f voltage maxima.

e. Frequency pulling is primarily a tuning of the magnetron resonance frequency through the load circuit. Deviations from the values predicted on the basis of circuit concepts are due to interrelation of the in-phase and out-of-phase components of the induced current produced by the spokes of space charge. They are therefore related to frequency pushing.

Two areas of investigation which are directly related to the problem remain to be discussed. These are experimental studies of frequency pushing and voltage tuning. Except for a few cases, where typical curves etc., are given, this type of data has not been published.

The importance of frequency-pushing data as an indication of magnetron performance under modulated conditions was suggested by the author[1] early in 1945 during research on the modulation of the 6J21 magnetron. This was followed by extensive measurements on several tubes by the research group at Harvard and the engineering group at the Litton Engineering Laboratories.

In earlier work on pulsed radar magnetrons the pushing was not so important (although the fact that the magnetron oscillates at frequencies below the tank resonance was utilized.[2]) The 6J21 magnetron

---

1 Internal Memorandum, Radio Research Laboratory, Harvard University, April 2, 1945.

2 I, 4, p. 252.

is a 1000 watt c-w tube tunable from about 8.5 cm to 12.5 cm.[1] The pushing test made on these tubes were found to correlate quite well with modulation data but not with controllable design parameters such as loaded Q. Some of the results of these tests are shown in Figs. 1.7 to 1.9.[2] Fig. 1.7 shows correlation between pushing figure and pulling figure at three points in the tuning range. Pushing figure in this case was defined as the frequency shift in megacycles between .25 amperes and 1 ampere anode current. Pulling figure is standardly defined as the maximum change in frequency obtained at 1.5 to 1 standing ratio in the load line when the load is allowed to assume all phases. It is an approximate measure of the loaded Q through the following formula:

$$Q_L = .41 \frac{f_o \ \eta_c}{P.F.} \ \frac{1}{\cos \alpha} \qquad (1.6)^3$$

f_o = resonance frequency of the circuit

Q_L = loaded Q at matched load

η_c = circuit efficiency

P.F. = pulling figure in megacycles

α = angle between constant frequency contours and constant susceptance contours in a load diagram. Actually α is usually small and always an approximate quantity because the constant frequency contours are not exactly straight lines.[4]

---

1 III, 19.

2 III, 17.

3 I, 4, p. 244.

4 I, 4, p. 240. Also, H. W. Welch, Jr., "Space Charge Effects and Frequency Characteristics of C-W Magnetrons Relative to the Problem of Frequency Modulation", Technical Report No. 1, Electron Tube Laboratory, Dept. of Elec. Eng., Univ. of Mich., Nov. 15, 1948, pp. 7-11.

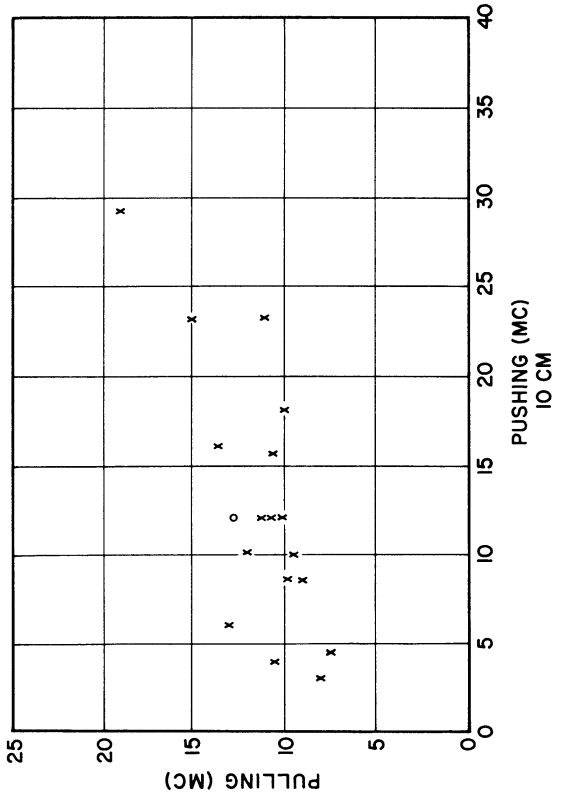

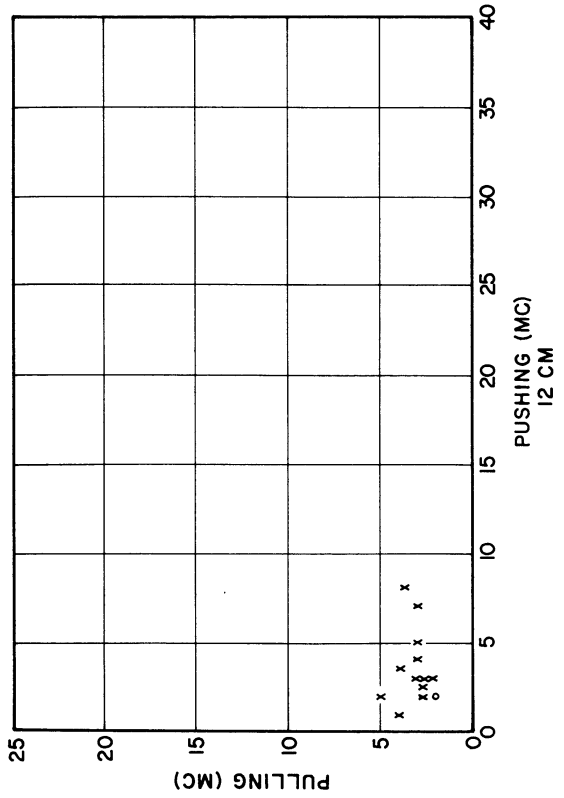

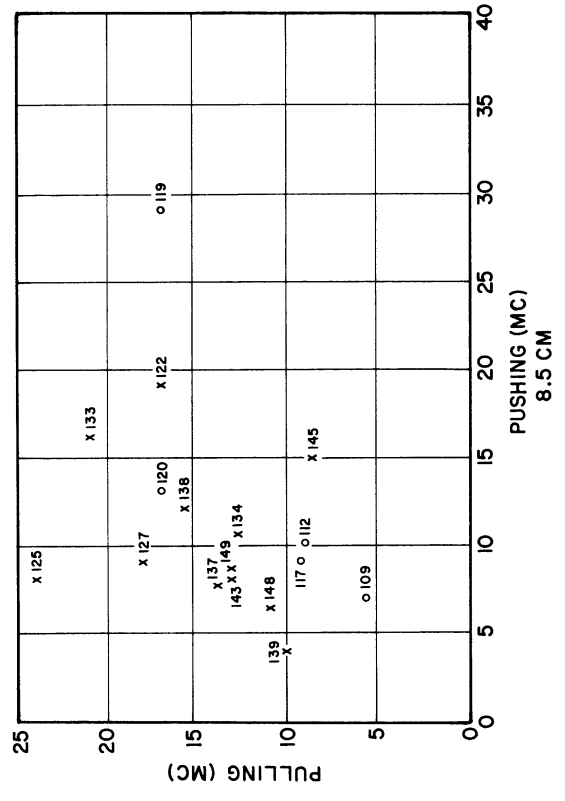

FIG. 1.7
CORRELATION BETWEEN PUSHING FIGURE AND PULLING FIGURE FOR THREE POINTS IN THE TUNING RANGE OF THE 6J21 MAGNETRON.
REPRODUCED FROM III, 17.
EACH POINT IS FOR A DIFFERENT MAGNETRON.
SERIAL NUMBERS OF TUBES ARE GIVEN FOR 8.5 CM CASE.

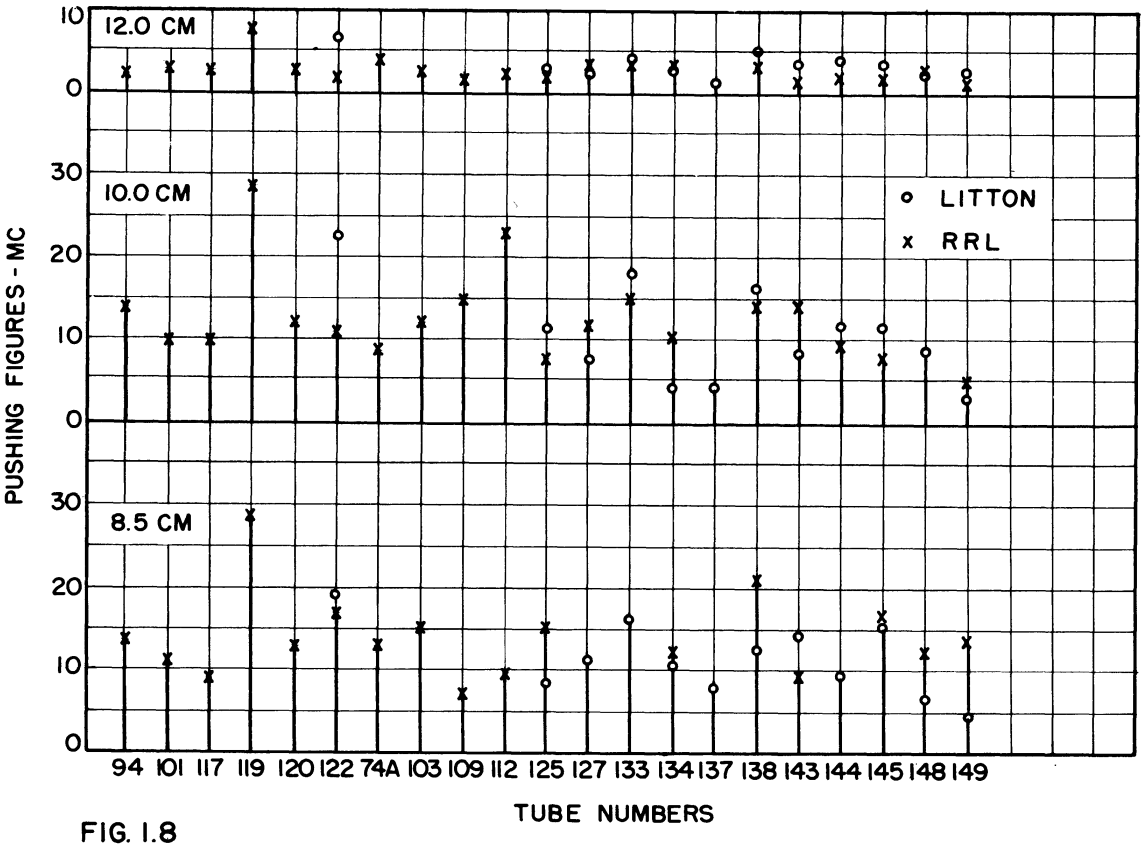

FIG. 1.8

PUSHING DATA TAKEN AT LITTON ENGINEERING LABORATORIES AND RADIO RESEARCH LABORATORY ON SEVERAL 6J21 MAGNETRONS. REPRODUCED FROM III, 17

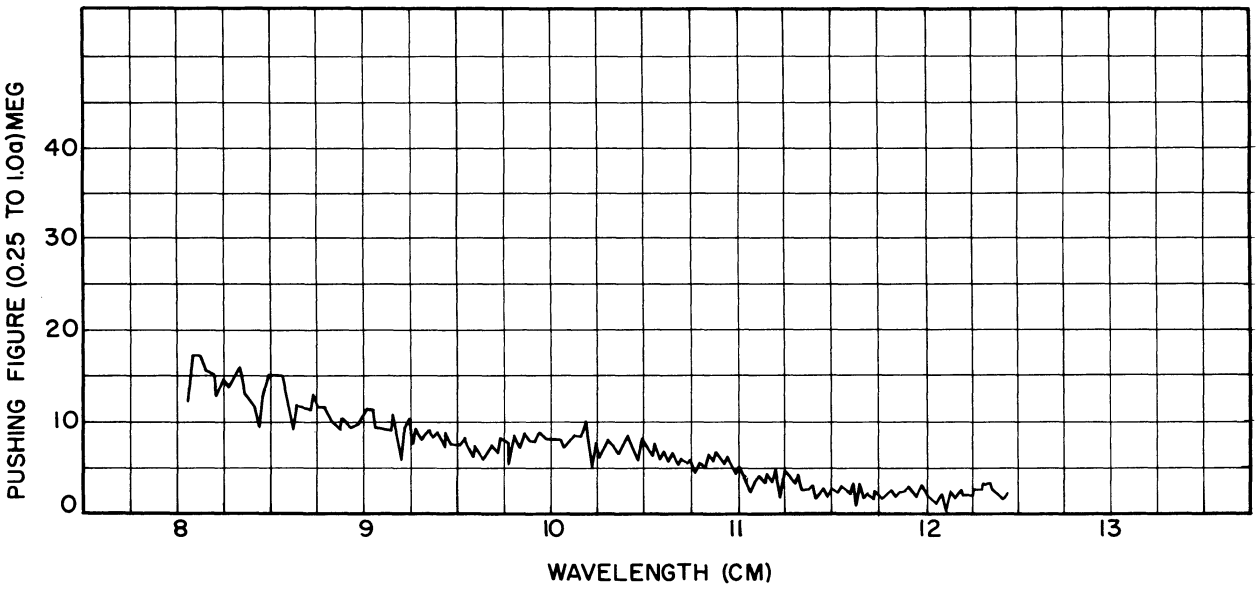

FIG. 1.9

PUSHING DATA TAKEN AT SEVERAL POINTS IN TUNING RANGE OF 6J21 MAGNETRON. REPRODUCED FROM III, 17

At 3000 mc, for example, a pulling figure of 10 mc represents typically a Q_L of 100. The correlation of pushing figures and pulling figures in the test recorded here for almost 20 tubes of the 6J21 type is seen to be very poor for each particular wavelength. However, it is evident that both pushing and pulling tend to be high at 8.5 centimeters wavelength and low at 12 centimeters wavelength. The tests at 10 centimeters wavelength are extremely inconclusive.

The data shown in Fig. 1.8 indicates the variability in a number of tubes but again a definitely higher pushing at 8.5 centimeters than at 12 centimeters. Another series of tests which indicates some of the source of discrepancy, is shown in Fig. 1.9. Pushing figures were measured at a very large number of points of the tuning range of a single tube. Wide local variations are indicated with a definite trend from high to low pushing as the tube is tuned from 8.5 to 12 centimeters. Part of the reason for poor correlation in these data is probably in the definition of pushing "figure" between .25 and 1 ampere. The complete pushing curve is a much more accurate index. The curve given in Fig. 1.1 is typical. Others are given in Chapter 4.

Recent developments in the Litton Laboratories are resulting in a much better control over the magnitude of pushing in production. Changes in the method of loading the magnetron and incorporation of adjustable loading are two steps which have helped in this direction.[1]

Frequency pushing is, quite obviously, a phenomenon observable and necessarily considered in almost any magnetron development or application. Voltage tuning, on the other hand, is in an entirely separate

---

[1] Privately communicated by C. V. Litton.

category in that it is only possible under very special conditions which may not be easily established. These conditions were first achieved in the 500 to 1000 mc range by W. H. Wilbur and P. H. Peters at General Electric Company in 1949.[1] The first experiments were made with existing power magnetrons of the tropotron variety. Power outputs between 10 and 200 watts were obtained with voltage tuning ranges of the order of two to one in ratio. The magnetrons had four to six anodes. Later experiments were carried out with specially designed magnetrons at low power levels. The load conditions varied from very low Q resonant circuits (less than 10) to circuits which were essentially non-resonant. Typical curves are given in Figs. 1.2, 1.10 and 1.11. The curve of Fig. 1.2 represents data on a specially designed tube at very low power levels with a non-resonant circuit. The curve in Fig. 1.10 is for a low Q resonant load and shows appreciable power output. The curve in Fig. 1.11 illustrates operation at appreciable power levels into a circuit which appears to be non-resonant over the range of the experiment. The erratic behavior of the power output is not explained in the General Electric report. The length of line used does not seem to be great enough to interpret this picture as the result of long-line effect. A long line is resonant at several frequencies which are spaced more closely together as the length of the line is made greater. The Q of the long line circuit is proportional to the amount of energy stored in the line or the amount of power reflected from the termination and inversely proportional to the power dissipated or the power transmitted through the

---

[1] III, 23, p. 19-25.

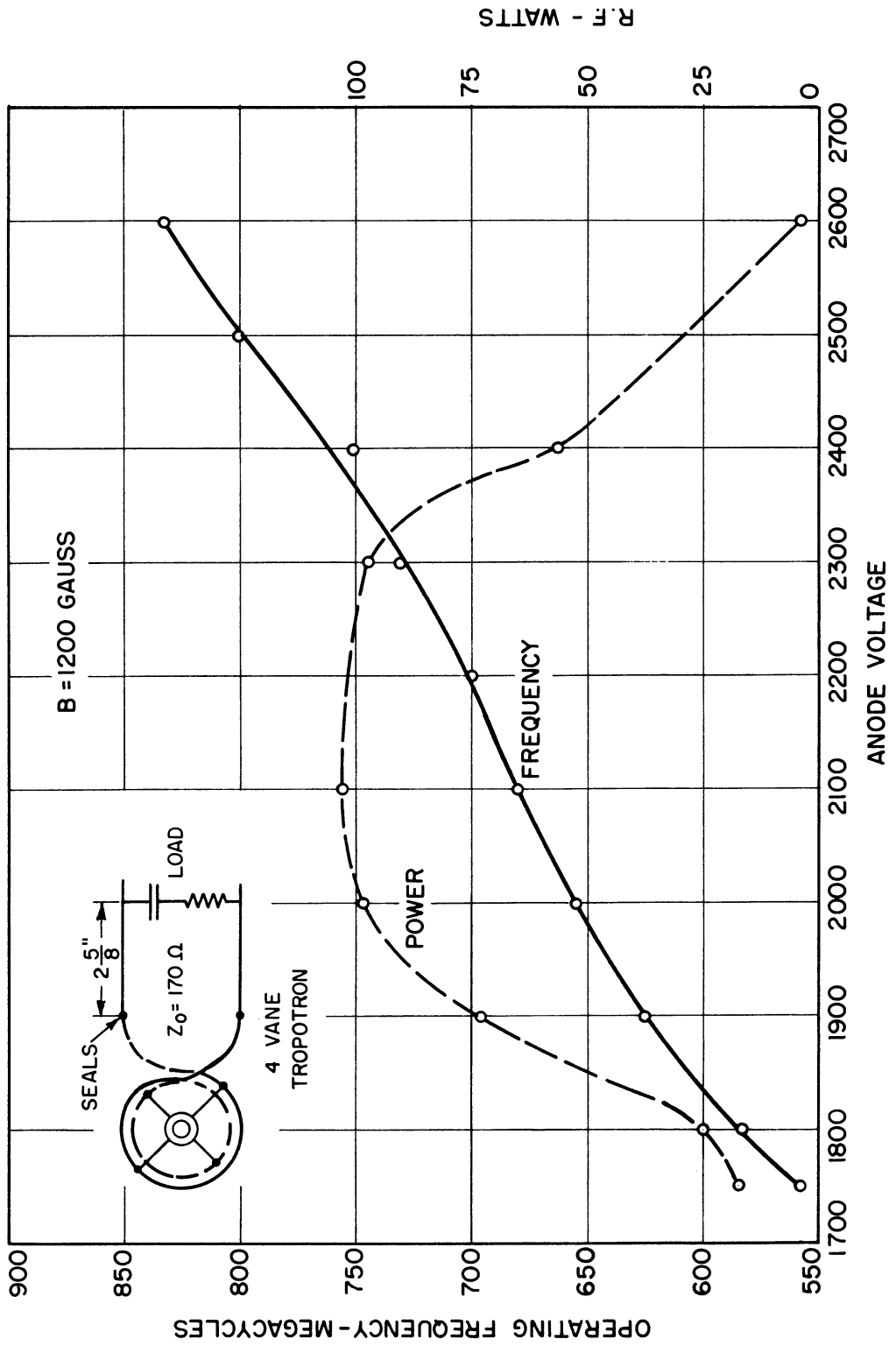

FIG. 1.10
VOLTAGE TUNING DATA FOR MODERATELY LOW Q OPERATION. FROM GENERAL ELECTRIC REPORT REFERENCE III, 23

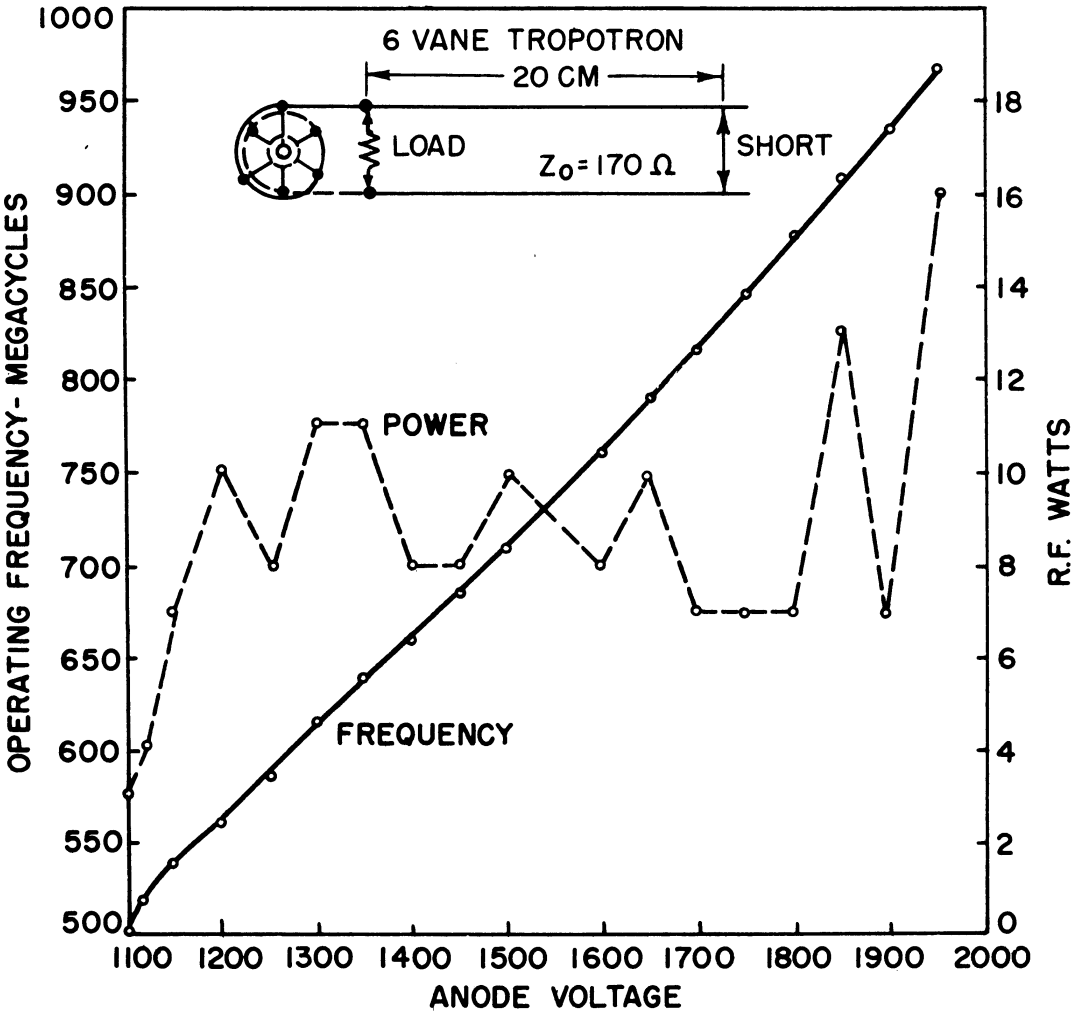

FIG. I.II

VOLTAGE-TUNING DATA FOR OPERATION INTO NON-RESONANT CIRCUIT. FROM GENERAL ELECTRIC REPORT REFERENCE III, 23.

termination plus power dissipated in the line. The power output of an electronic generator (with a low internal Q) into such a line will display peaks over the frequency range similar to those indicated by the data in Fig. 1.11. Recent measurements by J. S. Needle[1] in the University of Michigan Laboratory display these characteristics without any doubt.

The most apparent features of the operation obtained at General Electric Company are the following:

a) The Q_L is undoubtedly very low. Although no direct measurements of Q are available, it is probable that Q_L's of the order of 10 or less are being used.

b) The voltage-tuning phenomenon is similar to the usually observed frequency pushing, but is much more pronounced because of the low Q_L.

c) The low current dropout usually experienced when a magnetron is loaded heavily is conspicuously absent.

d) The temperature of the cathode must be limited to achieve satisfactory operation. This requires use of a tungsten cathode giving a definite emission boundary. This limitation of emission seems to be intimately related to the maximum-current boundary and a required criterion for obtaining oscillation.

e) Efficiency is reduced as band width is increased. This must be due to decreased electronic efficiency, since circuit efficiency is obviously high.

f) Loading is accomplished right at the tube anode terminals (i.e., almost directly across the capacitive portion of the resonant circuit). Loads farther from the tube may cause trouble with the long-line effect.

In the experiments being carried on currently in the University

---

[1] See Quarterly Report No. 2 for 1951. Project M921, University of Michigan, Department of Electrical Engineering, Electron Tube Laboratory and "The Insertion Magnetron", Technical Report No. 11 by J. S. Needle.

of Michigan laboratory by Dr. J. S. Needle, voltage tuning at very low powers has been accomplished at higher frequencies (near 3000 megacycles). Some of these measurements will be discussed in later sections after the theoretical analysis of magnetron performance which follows immediately.

2. LARGE-SIGNAL THEORY OF PHASE FOCUSSING IN THE TRAVELLING-WAVE MAGNETRON

2.1 Comparison of the Magnetron to Other Travelling-Wave Electronic Structures

Before presenting a detailed analysis of phase focussing in the magnetron, it is in order to compare briefly the focussing mechanism in the magnetron to the focussing mechanism in other structures in which electrons and waves travel together. It will be evident that there are certain features which clearly distinguish the magnetron from the other structures. The distinction made here, which has not been emphasized in other treatments of the subject, is extremely useful in the evaluation of the various methods of approach to the magnetron problem.

It is proposed that travelling-wave electronic structures may be placed into three general categories determined by the following characteristics:

(a) The electrons in the beam are weakly bunched, without trapping, in proper phase to give energy to the wave. Bunches travel with the phase velocity of the wave in the interaction region. Electrons travel slightly faster than the bunches. Example, travelling-wave amplifier.

(b) The electrons in the beam are strongly bunched and trapped in proper phase to accept energy from the wave. Bunches and electrons

travel with the phase velocity of the wave in the interaction region. Example, electron accelerator.

(c) The electrons in the beam are strongly bunched and trapped in the proper phase to deliver energy to the wave. Bunches and electrons travel with the phase velocity of the wave in the interaction region. Example, magnetron.

Travelling-wave electronic devices may also be distinguished on the basis of the space-charge density in the beam, the number of dimensions which must be considered in determining the beam cross section, and the number of dimensions which must be considered in the discussion of the beam flow. Various combinations of these distinctions can be applied to the three categories of (a), (b), and (c) with the result that mathematical problems of varying degrees of difficulty will be formulated.

The first two categories, (a) and (b), have been discussed in a brief paper by Brillouin.[1] This division is a convenient mathematical one since the two extremes of (a) and (b) lead to approximations which reduce the equations to linear form. The extremes are given when, in (a), a small signal with high space charge is assumed and, in (b), large signal with small space charge. Brillouin suggests that the travelling-wave magnetron belongs in the category (a). This, however, is not the case except under the very special conditions of small-signal analysis.

The statements (a), (b), and (c) imply that a set of boundary conditions exists which will cause phase focussing of the type described. In all cases a periodic structure is assumed which determines the phase

---

[1] IV, 1, a.

velocity of the wave in the direction of the beam. Standing-wave or travelling-wave structures may be used depending on the existence or non-existence of a reflecting termination at the end of the structure. The standing wave may always be resolved into components, some of which have a velocity in the direction of flow of the electron beam. The beam then interacts, primarily, with the component which has a phase velocity nearest to the bunch velocity in the beam. The structure may be re-entrant, as in the magnetron. The problem of the electronic analyst is to invent a soluble mathematical fiction which offers the closest approximation to the actual physical environment. Some of the difficulties of the various approaches to the magnetron problem have been discussed in the last section.

In order to add meaning to the statements which have been made above schematic pictures of the phase-focussing action in a travelling-wave tube, linear electron accelerator and magnetron are presented in Fig. 2.1. These structures are examples of the three categories mentioned above. Other distinguishing features which are worth noting are the following.

The travelling-wave tube has, essentially, a one-dimensional flow of electrons. Approximate analyses have been made considering beams of negligible cross section and of finite cross section. Small signal is usually assumed in the mathematical problem although this assumption is definitely not valid in some of the higher-power travelling-wave tubes. The phase velocity of the wave is of the order of one-tenth of the velocity of light. Aside from a focussing[1] magnetic field

---

[1] The reader should take care to distinguish between "focussing" or concentration of the beam cross section and "phase focussing" or bunching of the beam.

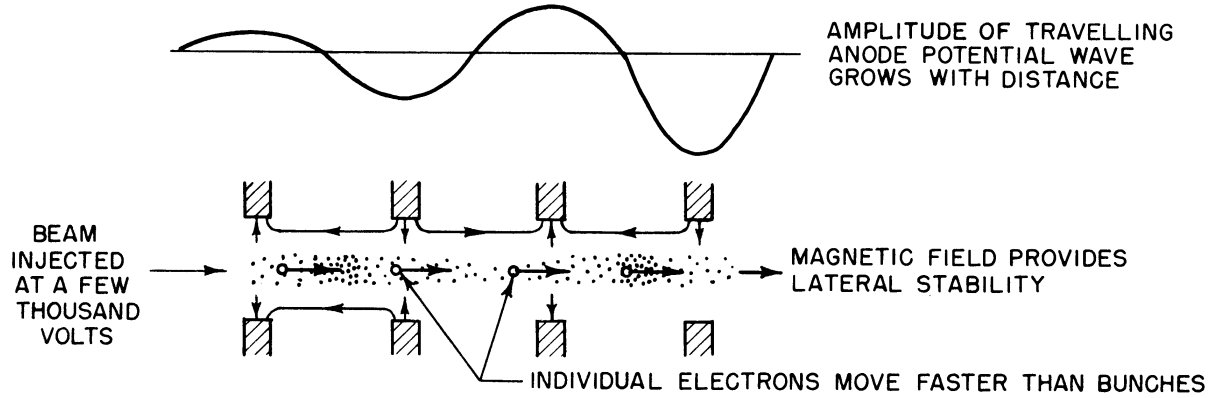

FIG. 2.1a
PHASE FOCUSSING IN TRAVELLING WAVE TUBE

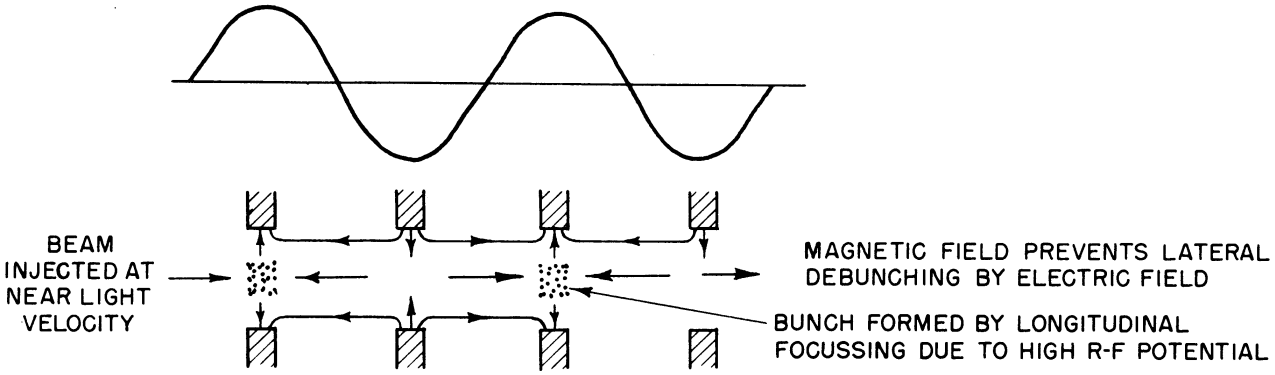

FIG. 2.1b
PHASE FOCUSSING IN ELECTRON ACCELERATOR

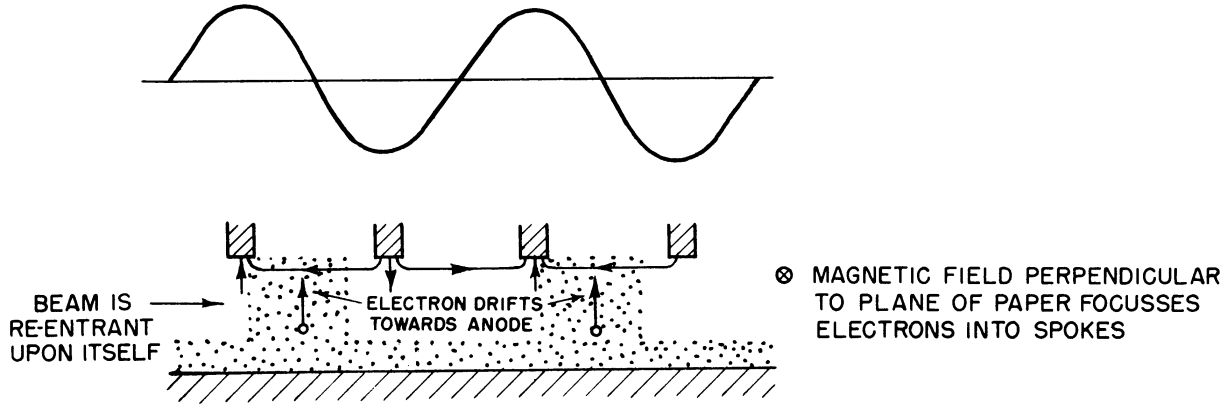

FIG. 2.1c
PHASE FOCUSSING IN MAGNETRON

FIG. 2.1
SCHEMATIC REPRESENTATION OF PHASE FOCUSSING IN TRAVELLING WAVE STRUCTURES

in the direction of the beam, the r-f field is the only field acting in the interaction space. The phase-focussing action is completely supplied by the r-f field.

Electron accelerators are also essentially one-dimensional in electron flow. As is indicated in the sketch in Fig. 2.1b, a focussing magnetic field is necessary to provide transverse stability. The linear electron accelerator is non-re-entrant; other types, variations of the synchrotron, are re-entrant. All accelerators are large-signal devices and, except for de-focussing of the beam, the effects of space charge can be neglected in the analysis. The phase-focussing action is supplied by the r-f field. In the circular, re-entrant structures magnetic field is supplied to constrain the beam to a circular path. The phase velocity of the wave is essentially the velocity of light.

The magnetron uses a two-dimensional electron flow. The bunches of electrons move in the direction of the wave propagation. A drift motion perpendicular to the direction of wave propagation allows for acceptance of energy from the d-c power supply. The d-c electric and magnetic fields, in addition to the r-f field, are essential to the phase focussing in the large-signal problem. The electron drift velocity is not the same in all parts of the beam but, for large signals, is usually less than or equal to the phase velocity of the wave in the direction of the wave propagation. The velocity of the bunches is equal to (synchronous with) the phase velocity of the wave. For small-signal operation, as might be observed in the magnetron just starting to oscillate, or in the magnetron amplifier, the velocity of electrons in the beam may exceed the synchronous velocity of the bunches.

The use of phase space[1] and Hamiltonian mechanics has frequently been suggested and applied to problems in electron dynamics. A very concise general discussion of the problem has been given by Gabor[2] with some interesting conclusions. Slater[3] demonstrates the usefulness of the phase-space representation in the discussion of the linear accelerator. The merit of these methods is diminished in the large-signal magnetron analysis for two reasons: effects of space charge are not easily accounted for; the two-dimensional beam flow leads to four-dimensional phase space. The complexities introduced by the use of four-dimensional phase space are not unsurmountable but they make the method appear less attractive. The possibility of the use of these techniques needs further investigation.

2.2 General Discussion of the Problem and the Boundary Conditions

There are several basic assumptions which are standard in the discussion of the magnetron. These will be stated briefly. For a complete discussion and justification of certain of these assumptions the reader is referred to the treatment by Walker in the book on magnetrons of the M.I.T. Radiation Laboratory Series.[4]

It is assumed that the problem can be reduced to a two-dimensional one insofar as the electric fields and the electron motion are concerned. The magnetic field is considered uniform and everywhere parallel to the axis of the third dimension. The coordinate arrangement

---

1 Position and momentum are the coordinates.

2 IV, 4, b.

3 I, 9. Chapt. XI.

4 II, 11. Chapt. VI.

is shown in Fig. 2.2. It is true that, in some magnetron structures, end effects cannot be neglected, but it can be said that it is usually very desirable that they are negligible for practical reasons as well as for the purpose of simplifying the analysis.

Relativistic corrections and other corrections which depend on the finite velocity of the propagation of radio waves are assumed negligible.[1] It has been shown by Walker[2] that effects due to the vector potential of the circulating currents and the r-f field are negligible if all voltages are small compared to $\frac{mc^2}{e}$ = 506 KV, where e/m is the charge-mass ratio of the electron and c is the velocity of light.

It will be assumed that the effect of initial velocities of the electrons may be neglected. In normal high-power operation this is justifiable on the basis that the mean thermal energy is small compared to the energy obtained by the electrons from the field. However, it is not clearly justified when the effects at extremely low anode currents or the noise problem are under consideration.

The assumption usually made which is not justified in this discussion is that the behavior at the cathode is space-charge limited. Space-charge-limited conditions imply zero gradient at the cathode. Under temperature-limited conditions a gradient will exist at the cathode and consequently the electron behavior in the interaction space must be entirely different for the same boundary conditions at the anode. In order to compare the two cases approximately the space-charge-limited

---

1 The complete relativistic equations are given by Walker. I, 2, pp. 217-231.

2 Ibid., p. 230.

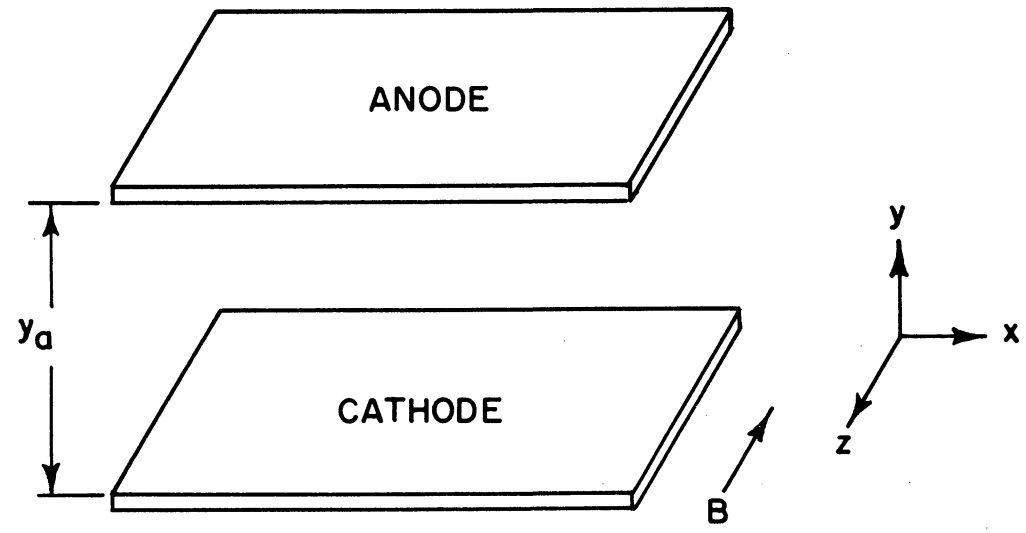

FIG. 2.2 a
COORDINATE ARRANGEMENT USED IN THE DISCUSSION OF THE PLANE MAGNETRON

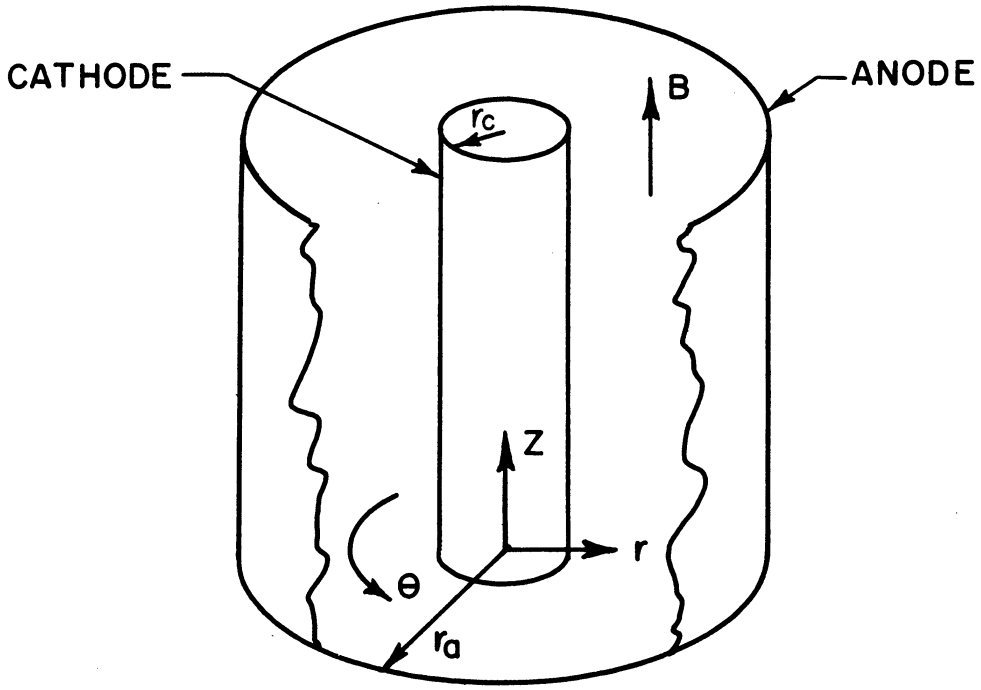

FIG. 2.2b
COORDINATE ARRANGEMENT USED IN THE DISCUSSION OF THE CYLINDRICAL MAGNETRON

behavior of the electron will be compared to the space-charge-free behavior. The behavior of a magnetron under temperature-limited conditions is much more important than generally realized. For example, in very-short-wavelength magnetrons it has been shown to be impractical that the cathode supply the current required for space-charge-limited operation.[1] The procedure of neglecting, in analysis, temperature-limited operation in favor of space-charge-limited operation is more based on habit than scientific judgment and in many cases should be discarded in the detailed analysis of high-frequency power tubes. Experimental evidence in the magnetron forcefully indicates that the conditions at the cathode can completely alter the details of operational behavior.

In this treatment the problem will be approached by, first, deriving relationships for the energy of the electron as a function of position in the interaction space with various assumed boundary conditions and, second, determining the direction of drift motion of the electrons as a function of position. The result will be a definition of threshold energy required for the existence of the electron at a point in the interaction space and the elimination of certain portions of the volume as inaccessible because no electrons are emitted from the anode. Both plane and cylindrical geometry will be considered. The plane case will be emphasized because it is considerably simpler and a reasonably good approximation to the large cathode magnetron. The exact calculation of anode-current is considered beyond the scope of

---

[1] Dr. S. R. Tibbs and Mr. F. I. Wright, "Temperature and Space-Charge-Limited Emission in Magnetrons," C.V.D. Report, May 1938.

this treatment since, for even the most ideal cases in the non-magnetic diode and the static magnetron, the results are quite involved and they cannot be used in the discussion of the oscillating magnetron without extensive modification.

It is convenient to begin the mathematical analysis of space-charge behavior in a magnetron with the force equation for an electron in an electromagnetic field. This equation in vector form is the following:

$$\frac{d\vec{v}}{dt} = -\frac{e}{m}\left(\vec{E} + \vec{v} \times \vec{B}\right) . \qquad (2.1)$$

e = absolute value of electronic charge,

m = mass of the electron,

$\vec{v}$ = velocity of the electron,

$\vec{E}$ = vector value of the electric field,

$\vec{B}$ = vector value of the magnetic field.

In the rectangular coordinate system, the component equations become

$$\frac{dv_y}{dt} = -\frac{e}{m} E_y - B\frac{e}{m} v_x , \qquad (2.2)$$

$$\frac{dv_x}{dt} = -\frac{e}{m} E_x + \frac{Be}{m} v_y , \qquad (2.3)$$

Here B is arbitrarily assumed to be directed in the negative z-direction.

In cylindrical coordinates the equations become

$$\frac{dv_r}{dt} = -\frac{e}{m} E_r - r\omega\frac{Be}{m} + \omega^2 r , \qquad (2.4)$$

$$2 v_r\omega + \frac{r d\omega}{dt} = - \frac{e}{m} E_\theta + v_r \frac{Be}{m} \quad . \tag{2.5}$$

Here B is arbitrarily assumed to be in the positive z-direction.

The field components are derivable from a scalar potential (the contribution of the vector potential is not significant).

$$E_x = - \frac{\partial \phi}{\partial x} \quad , \tag{2.6}$$

$$E_y = - \frac{\partial \phi}{\partial y} \quad ,$$

in rectangular coordinates.

$$E_r = - \frac{\partial \phi}{\partial r} \quad , \tag{2.7}$$

$$E_\theta = - \frac{1}{r} \frac{\partial \phi}{\partial \theta} \quad ,$$

in cylindrical coordinates.

In general the scalar potential ϕ is assumed to be a function of time as well as position. However, the assumption is made that the electron interaction is predominantly with the fundamental travelling-wave component of potential which moves in the direction of electron drift motion parallel to the cathode surface. A suitable choice of moving coordinate system will cause the effects of this travelling-potential wave to appear stationary. The effects of other wave components can be neglected in the first approximation since, in the moving system, they are rapidly varying compared to the stationary fundamental, and the total effect of interaction with the electron during transit, therefore, is small in comparison.

The change of variables is made by substituting in the planar system

$$v_x = v_x' + v_n \quad , \tag{2.8}$$

and in the cylindrical system

$$\omega = \omega' + \omega_n \quad . \tag{2.9}$$

v_x' = x-component of velocity in planar-moving coordinate system,

v_n = constant velocity of moving-planar-coordinate system in positive x-direction.

ω' = angular velocity in rotating cylindrical coordinate system,

ω_n = constant angular velocity of rotation of cylindrical coordinate system in positive θ-direction.

Before making the transformation into the moving coordinate system, it is convenient to write the equations of motion in a different form. When Eq 2.2 is multiplied by v_y it can be written

$$\frac{d}{dt}\left(\frac{1}{2} m v_y^2\right) = - e E_y \frac{dy}{dt} - B e v_x \frac{dy}{dt} \quad . \tag{2.10}$$

Eq 2.3 will be left in approximately the same form

$$\frac{dv_x}{dt} = - \frac{e}{m} E_x + \frac{Be}{m} \frac{dy}{dt} \quad . \tag{2.11}$$

Eq 2.4 is multiplied by v_r and rewritten

$$\frac{d}{dt}\left(\frac{1}{2} m v_r^2\right) = - e E_r \frac{dr}{dt} - (B e \omega r - m\omega^2 r) \frac{dr}{dt} \quad . \tag{2.12}$$

Reorganization of the terms in Eq 2.5 yields

$$\frac{d(\omega r)}{dt} = -\frac{e}{m} E_\theta + \left[\frac{Be}{m} - \omega\right] \frac{dr}{dt} \quad . \tag{2.13}$$

By making the substitutions 2.6 through 2.9 in Eqs 2.10 through 2.13, we finally have:

$$\frac{d}{dt}\left(\frac{1}{2} m v_y^2\right) = e \frac{\partial \phi}{\partial y} \frac{dy}{dt} - Be\,(v_x' + v_n) \frac{dy}{dt} \quad , \tag{2.14}$$

$$\frac{dv_x'}{dt} = \frac{e}{m} \frac{\partial \phi}{\partial x} + \frac{Be}{m} \frac{dy}{dt} \quad , \tag{2.15}$$

in the planar system, and

$$\frac{d}{dt}\left(\frac{1}{2} m v_r^2\right) = e \frac{\partial \phi}{\partial r} \frac{dr}{dt} - \left[Be(\omega' + \omega_n)\, r - m(\omega' + \omega_n)^2 r\right] \frac{dr}{dt} \tag{2.16}$$

$$\frac{d(\omega' + \omega_n) r}{dt} = \frac{e}{m} \frac{\partial \phi}{\partial \theta} + \left[\frac{Be}{m} - (\omega' + \omega_n)\right] \frac{dr}{dt} \quad , \tag{2.17}$$

in the cylindrical system.

The convenience of writing these equations in the form just given will be more evident as they are studied under various boundary conditions in the following sections. Eqs 2.14 and 2.16 are energy equations expressing the equality of the rate of increase of kinetic energy of velocity directed normally to the cathode to the rate that normally directed forces act on the particle. The normally directed forces are the forces due to the electric and magnetic fields and, in the case of the cylindrical magnetron, the centrifugal force. Eqs 2.15 and 2.17 express the relationship between tangentially directed velocity and tangentially directed forces. In these equations the variables v_x' and ω' are still, in general, functions of t. The

potential ϕ, however, is now stationary. It is only necessary therefore to be able to express v_x' and ω' as functions of x and r, respectively, to make Eqs 2.14 and 2.16 integrable. Complete calculation of this functional relationship involves computation of trajectories of all electrons, which depend on the phase of emission from the cathode and on the spatial potential distribution. Attempts at this type of calculation have been described in the last section. The express purpose of the development of the next few sections is to make an estimate of the gross space-charge behavior on the basis of an approximate choice of values for v_x' and ω'.

2.3 Synchronism Energy and Synchronism Potential

It will be assumed in this section that there exists a wave phase velocity characteristic of the magnetron anode structure, given by v_n or ω_n, which depends on the frequency and the geometry of the structure. No r-f potential between anode segments will be assumed. A d-c potential will be applied between cathode and anode. The relationships between anode potential, magnetic-field intensity, swarm extent, and electron energy at the edge of the swarm will be computed for electron velocity just synchronous with the velocity characteristic of the anode structure.

Case I - Planar Magnetron. The velocity of the electron as a function of distance from the cathode is obtained by solution of Eq 2.15. All anode segments are assumed to be at the same potential so that

$$\frac{\partial \phi}{\partial x} = 0 \quad .$$

The integral equation to be solved is

$$\int dv_x' = \int \frac{Be}{m}\, dy \quad , \tag{2.18}$$

with the boundary conditions

$$y = 0, \quad v_x' = - v_n \quad .$$

The solution is

$$v_x' + v_n = \frac{Be}{m}\, y \quad . \tag{2.19}$$

Thus the tangential electron velocity in stationary coordinates is linearly related to the distance from the cathode. The distance y_n will be defined such that $v_x' = 0$. That is, in the moving reference frame, the electron is stationary. In the stationary reference frame the electron moves with synchronism velocity,

$$y_n = \frac{m}{e}\frac{v_n}{B} \quad . \tag{2.20}$$

If the value from Eq 2.19 is substituted into 2.14, the energy equation becomes integrable.

$$\int d\left(\frac{1}{2}\, mv_y^2\right) = e\int d\phi - \int \frac{B^2e^2}{m}\, y\, dy \quad , \tag{2.21}$$

with boundary conditions

$$y = 0 , \quad v_y = 0 , \quad \phi = 0 .$$

The result is

$$e\phi = \frac{1}{2}\, mv_y^2 + \frac{B^2e^2}{2m}\, y^2 \quad . \tag{2.22}$$

The second term on the right can be written

$$\frac{1}{2} m \left(\frac{Be}{m} y\right)^2 = \frac{1}{2} m v_x^2 \quad .$$

This shows that Eq 2.21 is simply a statement of the conservation of energy. The significance of this statement is that, even with no energy of y-directed motion, a swarm of electrons will be established between the anode and cathode. The energy received by the electrons from the static field goes into kinetic energy of drift motion with velocity parallel to the cathode given by Eq 2.19. If it is assumed that the swarm is bounded between cathode and anode, the y-directed velocity must be zero at the boundary. For electrons to be synchronous at this boundary they must have acquired a certain synchronism energy given by

$$e \phi_n = \frac{1}{2} m v_n^2 \quad . \tag{2.23}$$

If the y-directed velocites are zero throughout the swarm of electrons, the potential energy of the electrons will be decreased by

$$e\phi = \frac{B^2e^2}{2m} y^2 \quad . \tag{2.24}$$

All of this energy, in this case, will appear as kinetic energy of the electron. This energy will be referred to as the cutoff energy parabola. In Fig. 2.3 this parabola is plotted with the synchronism energy level which is a constant determined by v_n in the planar magnetron. The distance y_n at which the electrons become synchronous, determined by the intersection of the two curves, is a function of v_n and B.

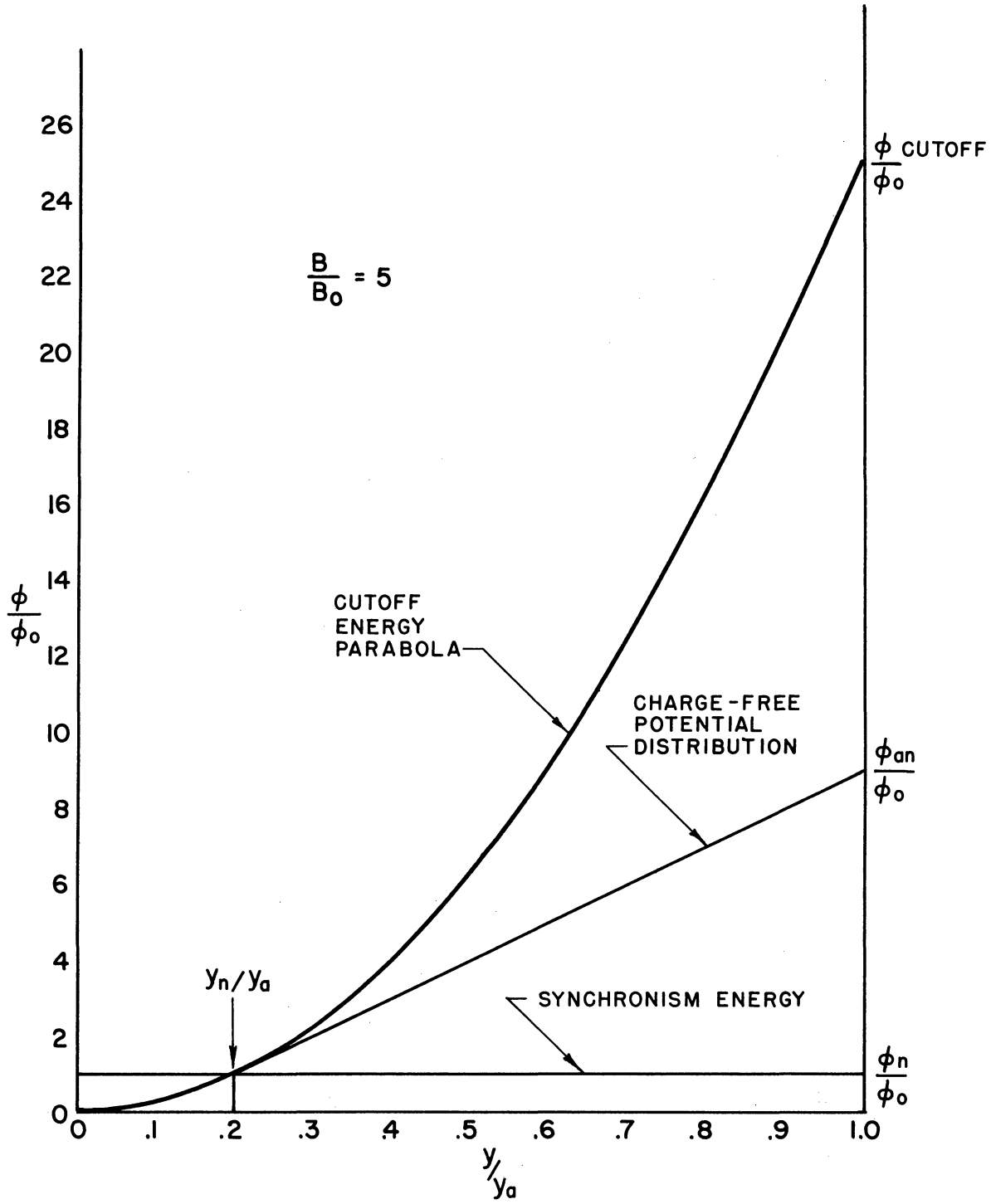

FIG. 2.3
ENERGY DISTRIBUTIONS RELATED TO SYNCHRONISM CONDITIONS IN THE PLANAR MAGNETRON

If there is an ample supply of electrons at the cathode and initial velocities are neglected, the space charge in the swarm within y_n will build up until the gradient at the cathode is zero. The potential within the swarm may exceed that given by Eq 2.24 if electrons are streaming inward and outward through the swarm because of the energy of y-directed velocities. At the boundary the cutoff energy parabola must give the electron energy since it is assumed that the electrons do not cross the boundary. It has been shown by Slater[1] that for the case of zero electric-field gradient at the cathode the actual potential distribution curve is tangent to the cutoff parabola at the swarm boundary. Thus the field gradients are equal at the cathode and at the outer boundary of the swarm, which is equivalent to stating that the total amount of charge within the swarm is independent of the potential or charge distribution within the swarm. If the total charge within a given boundary is determined and no charge exists on the cathode (zero gradient at the cathode) the anode potential must be determined. The anode potential required for establishment of a swarm within the synchronism boundary y_n is determined in Fig. 2.3 by drawing a straight line tangent to the synchronism energy parabola at the intersection with the synchronism energy level. The straight line is the linear distribution of potential which exists in charge-free space between parallel planes. The field gradient and the potential are matched at the space-charge boundary. This equality is expressed by the following:

---

[1] I, 9, p. 340.

$$\frac{\phi_{an} - \phi_n}{y_a - y_n} = \left.\frac{\partial \phi}{\partial y}\right|_{y = y_n} = - \frac{B^2 e}{m} y_n \quad .$$

By making the proper substitutions this relationship reduces to the following form:

$$\phi_{an} = B v_n y_a - \frac{1}{2} \frac{m}{e} v_n^2 \quad . \tag{2.25}$$

This potential, which will be called the synchronism potential for the anode, must be exceeded before any electrons which are moving fast enough to deliver energy to the travelling wave exist in the interaction space. Above this potential, if such a wave exists and if there is a mechanism for collecting the electrons which have expended energy, a net energy can be transferred from the d-c field to the wave through the medium of the space charge. This mechanism will be discussed further in the following two sections.

Before closing this discussion of synchronism in the plane magnetron, the significant equations will be written in a dimensionless form. For this purpose the following will be defined:

$$\phi_o = \frac{1}{2} \frac{m}{e} v_n^2 \quad ,$$

$$B_o = \frac{m}{e} \frac{v_n}{y_a} \quad .$$

In terms of these variables the various equations become:

Synchronism boundary equation

$$\frac{y_n}{y_a} = \frac{B_o}{B} \quad . \tag{2.20a}$$

Synchronism energy equation

$$\frac{\phi_n}{\phi_o} = 1 \quad . \tag{2.23a}$$

Cutoff energy parabola

$$\frac{\phi}{\phi_o} = \left(\frac{B}{B_o}\right)^2 \left(\frac{y}{y_a}\right)^2 . \tag{2.24a}$$

Synchronism anode potential

$$\frac{\phi_{an}}{\phi_o} = 2\frac{B}{B_o} - 1 \quad . \tag{2.25a}$$

These dimensionless variables were used in the plotting of curves in Fig. 2.3.

Case II - Cylindrical Magnetron. The discussion of the planar magnetron case was made fairly complete in order to present a physical picture of the meaning of synchronism energy and synchronism potential. The mathematics of the cylindrical case is slightly more involved because of the prescence of the centrifugal force term and because of the linear dependence of the tangential velocity on radius for a contant angular velocity. The resulting relationship will, nevertheless, have similar significance.

In this case the angular velocity as a function of radial distance from the cathode is obtained by solution of Eq 2.17. Again all anode segments are assumed to be at the same potential so that

$$\frac{\partial \phi}{\partial \theta} = 0 \quad .$$

The integration to be carried out is

$$\int \frac{d\,(\omega' + \omega_n)}{\frac{Be}{2m} - (\omega' + \omega_n)} = 2\int \frac{dr}{r} \quad , \tag{2.26}$$

with the boundary conditions

$$\omega' = -\omega_n \, , \quad r = r_c \, .$$

After integration and reorganization of terms, the result is

$$\omega' + \omega_n = \frac{Be}{2m}\left(1 - \frac{r_c^2}{r^2}\right) . \tag{2.27}$$

If ω' is set equal to zero the synchronism radius is determined.

$$\omega_n = \frac{Be}{2m}\left(1 - \frac{r_c^2}{r_n^2}\right),$$

or

$$\frac{r_n}{r_c} = \sqrt{\frac{Be/2m}{\frac{Be}{2m} - \omega_n}} \, . \tag{2.28}$$

At the value r_n/r_c given by this relationship the electron is stationary in the moving reference frame.

The energy Eq, 2.16, becomes integrable upon substitution of the angular velocity from Eq 2.27. After algebraic simplification, the integration to be performed is

$$\int d\left(\tfrac{1}{2} m v_r^2\right) = \int e\,d\phi - \int \frac{B^2e^2}{4m} r\left(1 - \frac{r_c^4}{r^4}\right)dr \, . \tag{2.29}$$

with the boundary conditions

$$r = r_c \, , \quad \phi = 0 \, , \quad v_r = 0 \, .$$

r_c = radius of the cathode.

The result is

$$e\phi = \frac{1}{2} m v_r^2 + \frac{B^2e^2}{8m} r^2 \left(1 - \frac{r_c^2}{r^2}\right)^2 , \qquad (2.30)$$

the second term on the right can be written

$$\frac{1}{2} m \left[\frac{Be}{2m}\left(1 - \frac{r_c^2}{r^2}\right)\right]^2 r^2 = \frac{1}{2} m \omega^2 r^2 ,$$

again showing that this term represents energy of motion parallel to the cathode surface. If the swarm is bounded at the synchronism radius the electron must have the synchronism energy.

$$e \phi_n = \frac{1}{2} m \omega_n^2 r_n^2 . \qquad (2.31)$$

The cutoff energy parabola is

$$e \phi = \frac{B^2e^2}{8m} r^2 \left(1 - \frac{r_c^2}{r^2}\right)^2 . \qquad (2.32)$$

The anode potential for which electrons just reach the synchronism boundary is again obtained by matching fields and potential at the boundary. In the cylindrical case the potential distribution in the charge-free space is logarithmic rather than linear.

$$\phi_{an} - \phi_n = - \frac{\tau}{2\pi \epsilon_o} \ln \frac{r_a}{r_n} , \qquad (2.33)$$

τ = total charge/unit length within synchronism boundary,

ϵ_o = dielectric constant of free space = $\frac{1}{36\pi} \times 10^{-9}$ farads/meter, and

r_a = radius of the anode.

Using Eq 2.32 and the gaussian theorem

$$\tau = -2\pi \epsilon_o r_n \frac{\partial \phi}{\partial r}$$

$$= -\frac{\pi}{2} \epsilon_o \frac{B^2 e}{m} r_n^2 \left(1 - \frac{r_c^4}{r^4}\right) \quad . \qquad (2.34)$$

Combining 2.33 and 2.34

$$\phi_{an} - \phi_n = \frac{B^2 e}{4m} r_n^2 \left[\left(1 - \left(\frac{r_c}{r_n}\right)^4\right)\right] \ln \frac{r_a}{r_n} \quad .$$

Substituting from Eq 2.27 (with $\omega' = 0$) and 2.28 and 2.31, an intermediate result is

$$\phi_{an} = B \omega_n (r_n^2 + r_c^2) \ln \frac{r_c}{r_n} + \frac{1}{2} \frac{m}{e} \omega_n r_n^2 \quad . \qquad (2.35)$$

Final elimination of r_n by Eq 2.28 yields

$$\phi_{an} = \frac{r_c^2}{r_a^2} \frac{1}{1 - \frac{2m}{Be} \omega_n} \left[\frac{Be}{m} \omega_n r_a^2 \left(1 - \frac{m}{Be} \omega_n\right) \ln\left(\frac{r_a}{r_c} \times \sqrt{1 - \frac{2m}{Be} \cdot \omega_n}\right)\right.$$

$$\left. + \frac{1}{2} \frac{m}{e} \omega_n^2 r_a^2 \right] \quad . \qquad (2.36)$$

for the synchronism anode potential.

In cylindrical coordinates the definitions of ϕ_o and B_o corresponding to those given for planar coordinates on page 62 are

$$\phi_o = \frac{1}{2} \frac{m}{e} \omega_n^2 r_a^2$$

$$B_o = \frac{2 \frac{m}{e} \omega_n}{1 - \frac{r_c^2}{r_a^2}} \quad .$$

The important equations for the synchronism conditions in the

cylindrical system become:

Synchronism boundary equation

$$\frac{1 - \frac{r_c^2}{r_n^2}}{1 - \frac{r_c^2}{r_a^2}} = \frac{B_o}{B} \quad . \tag{2.28a}$$

Synchronism energy equation

$$\frac{\phi_n}{\phi_o} = \frac{r_n^2}{r_a^2} \quad . \tag{2.31a}$$

Cutoff energy parabola

$$\frac{\phi}{\phi_o} = \left(\frac{B}{B_o}\right)^2 \left[\frac{r}{r_a} \frac{1 - \frac{r_c^2}{r^2}}{1 - \frac{r_c^2}{r_a^2}}\right]^2 \quad . \tag{2.32a}$$

Synchronism anode potential

$$\frac{\phi_{an}}{\phi_o} = \frac{\frac{B}{B_o} \frac{r_c^2/r_a^2}{\frac{B}{B_o} - \left[1 - \frac{r_c^2}{r_a^2}\right]}}{\left[2\left[\frac{B}{B_o} \frac{2}{1 - \frac{r_c^2}{r_a^2}} - 1\right] \ln \frac{r_a}{r_c} \frac{\sqrt{\frac{B}{B_o} - \left(1 - \frac{r_c^2}{r_a^2}\right)}}{\sqrt{\frac{B}{B_o}}} + 1\right]} \quad . \tag{2.36a}$$

The relative energy distributions in the interaction space are plotted in Fig. 2.4. The important differences from the planar case are that the synchronism energy is no longer constant but increases with the square of the radius and the potential distribution in charge-free space is now logarithmic rather than linear.

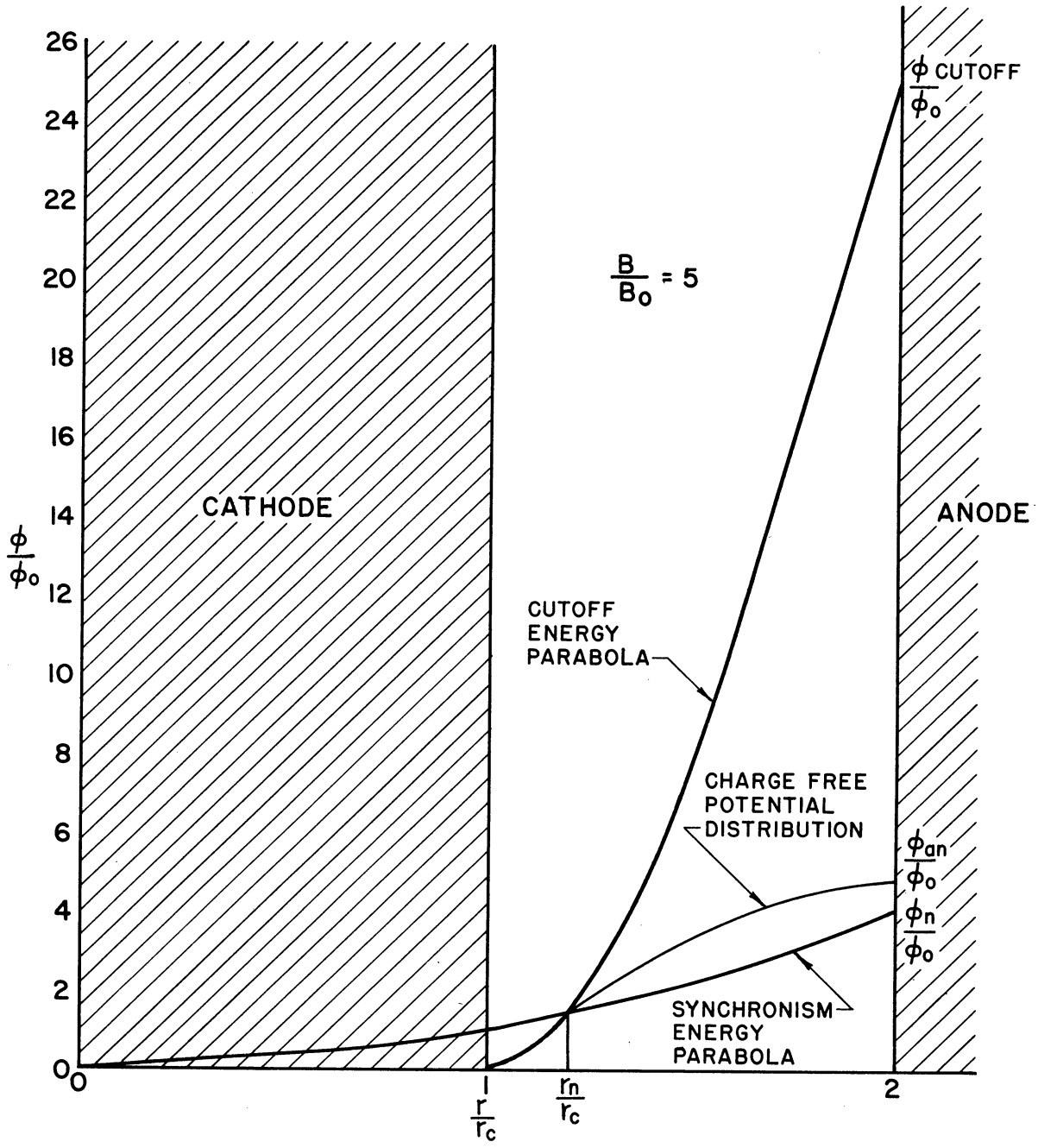

FIG. 2.4
ENERGY DISTRIBUTIONS RELATED TO SYNCHRONISM CONDITIONS IN THE CYLINDRICAL MAGNETRON

The fact that electrons in synchronism at the anode have more energy than electrons just reaching the synchronism boundary in the case of the cylindrical magnetron, and the same energy in the planar magnetron, is significant, and will be discussed further in the following sections.

2.4 Drift Velocity and Threshold Energy Conditions

In this section it will be assumed that an r-f voltage exists between the anode segments so that the field due to the fundamental travelling-wave component is actually present. This potential is superimposed on the d-c potential which is still applied between anode and cathode. The field component parallel to the cathode surface is now non-vanishing. The presence of this component makes possible the drift of electrons from the cathode toward the anode at potentials lower than the static-cutoff anode potential which is given by substitution of the anode-cathode distance in Eqs 2.24 and 2.32. The region of the interaction space which is accessible to the electrons will be determined by an approximate method. This method involves estimation of the minimum energy required for an electron to reach the anode, and the boundaries of the region through which electrons drift toward the anode.

A semi-graphical illustration of the travelling-wave potential and field distributions along the anode surface is shown in Fig. 2.5. The lower potential graph is in the moving reference frame so that the electrode system and upper potential graph are moving toward the left with the synchronism velocity. The illustration is made for the instant that the maximum potential difference exists

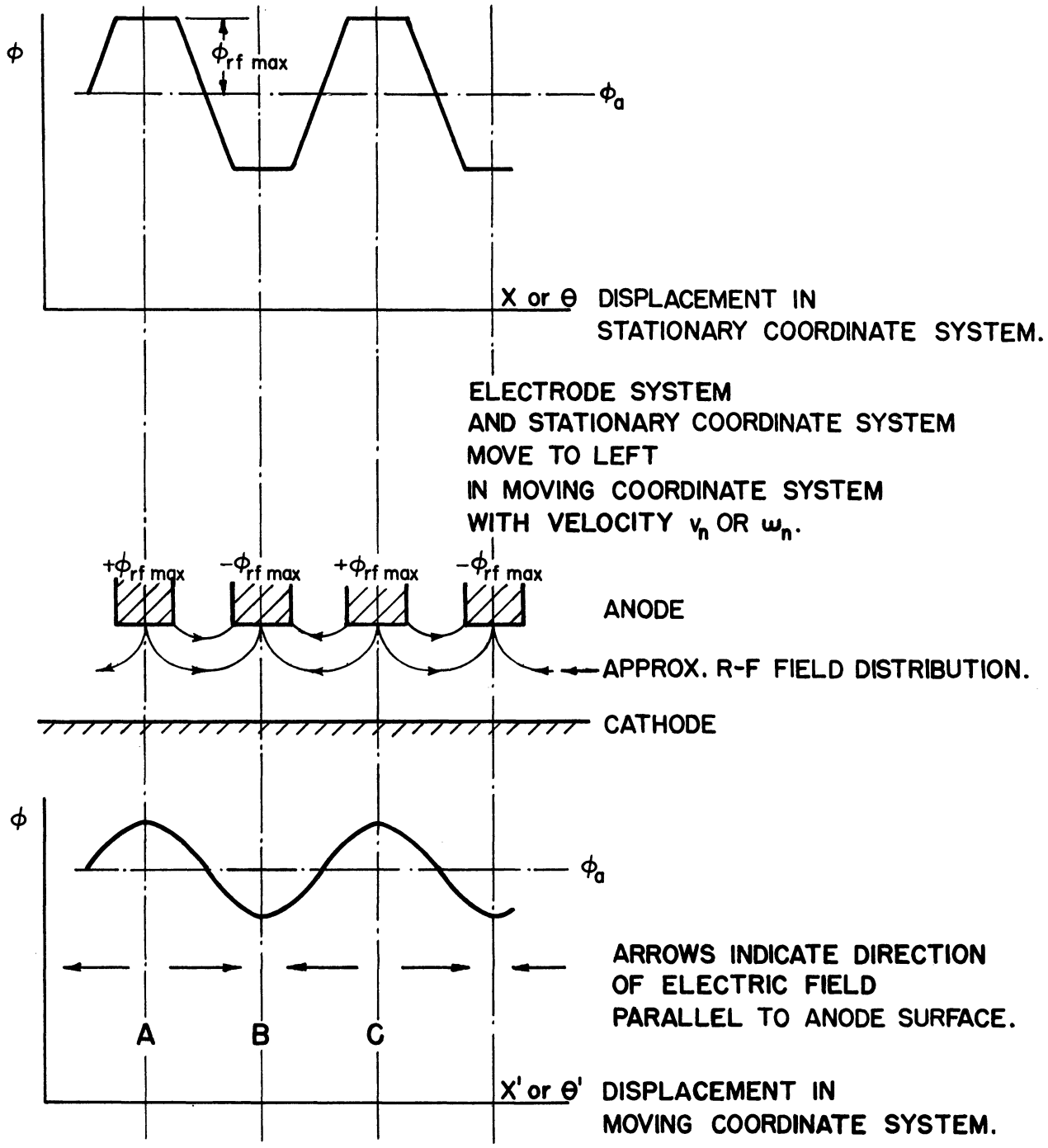

FIG. 2.5
FUNDAMENTAL TRAVELLING WAVE COMPONENT OF ANODE POTENTIAL AND APPROXIMATE R-F FIELD DISTRIBUTION IN THE MAGNETRON INTERACTION SPACE AT THE INSTANT FOR MAXIMUM POTENTIAL BETWEEN ANODE SEGMENTS.

between anode segments. The following symbols are defined with reference to this picture.

$\phi_{rf\ max}$ = maximum value of r-f potential difference between anode segments,

ϕ_f = maximum value of fundamental travelling-wave component of anode r-f potential, and

ϕ_a = average d-c anode potential.

The relationship between ϕ_f and ϕ_{rf} can only be determined as a result of analysis of the particular electrode system.

The synchronism anode potential derived in the last section was sufficient to bring electrons to the synchronism boundary. In typical practical cases calculations show that this boundary is very close to the cathode. Variation in the potential distribution due to the r-f field become relatively small very rapidly with increasing distance from the anode in conventional anode structures. It is, therefore, reasonable to assume that the velocity distribution within the subsynchronous swarm is the same as was obtained for the static case. Electrons which have reached the synchronism boundary are stationary in the moving reference frame so that the action of the tangential field, even though small, will begin to be significant as this boundary is exceeded. Both the plane and the cylindrical magnetrons will be discussed to describe the behavior in the synchronism region.

Case I - Planar Magnetron. If it is assumed that v_x' is expressed as a function of y, Eq 2.14, derived in Section 2.2, may be written

$$\int e \, d\phi = \int Be \, v_n \, dy + \int Be \, v_x' \, dy + \int d\left(\frac{1}{2} m \, v_y^2\right) \quad . \quad (2.37)$$

For the purposes of this discussion, Eq 2.15 is conveniently rewritten

$$v_y = \frac{E_x}{B} + \frac{m}{Be} \frac{dv_x'}{dt} \quad . \quad (2.15a)$$

Let us assume that the d-c voltage ϕ_a is greater than the synchronism potential ϕ_{an}. Without the presence of the r-f potential v_x' would have a positive value. With the r-f present E_x may be positive or negative. In Fig. 2.5 this sign is indicated by the arrows in the lower diagram. Let us examine the behavior of an electron in the region A-B and then in the region B-C.

In the region A-B E_x has a positive direction. The force on the electron is opposite to the direction of the field so that the electron will be forced to the left, or be decelerated, making v_x' smaller and dv_x'/dt negative. A reduction of the velocity v_x' will cause a reduction in the term $Be \, v_x'$ in Eq 2.37 which represents a force on the electron directed toward the cathode. The force due to the y-component of electric field is still the same so that the electron tends to move toward the anode giving v_y a positive value. In the region A-B, therefore,

$$v_y = \frac{E_x}{B} + \frac{m}{Be} \frac{dv_x'}{dt} > 0 \quad ,$$

and since

$$\frac{E_x}{B} \quad \text{is positive,}$$

$$\frac{m}{Be}\frac{dv_x'}{dt} \quad \text{is negative,}$$

we have

$$\left|\frac{E_x}{B}\right| > \left|\frac{m}{Be}\frac{dv_x'}{dt}\right| \quad .$$

As long as v_x' is positive the electron is moving to the right in the moving reference frame. While dv_x'/dt is negative v_x' is becoming smaller, the electron is drifting outward, and the maximum of E_x is becoming larger. Since v_y is positive the force due to v_y (Be v_y) is tending to balance the force due to the tangential field component (e E_x).

In the region B-C E_x has a negative direction. The electron will be accelerated making v_x' larger and dv_x'/dt positive. The term Be v_x' is increased, tending to force the electron toward the cathode. In the region B-C, therefore

$$v_y = \frac{E_x}{B} + \frac{m}{Be}\frac{dv_x'}{dt} < 0 \quad ,$$

$$\frac{E_x}{B} \text{ is negative,}$$

$$\frac{m}{Be}\frac{dv_x'}{dt} \text{ is positive,}$$

therefore,

$$\left|\frac{E_x}{B}\right| > \left|\frac{m}{Be}\frac{dv_x'}{dt}\right| \quad .$$

The conclusions to be derived from these arguments are:

a. In the region A-B where a decelerating tangential field exists, v_y is directed toward the anode.

b. In the region B-C where an accelerating field exists, v_y is directed toward the cathode.

c. The term E_x/B dominates over the term $\frac{m}{Be}\frac{dvx'}{dt}$ in Eq 2.15a.

d. The sign of dv_x'/dt is such that v_x' tends toward zero.

Actually, more elaborate calculations would show that the electron executes a cycloidal-like motion around a path of drift which tends to follow constant potential contours. The term E_x/B is recognized as the translation velocity of the rolling circle which generates a cycloid in the case of uniform crossed electric and magnetic fields.

The preceding discussion makes reasonable the following choice of v_x' in integrating Eq 2.37 to obtain the anode potential which must be approximated if electrons are to reach the anode.

In the subsynchronous region

$$v_x' = \frac{Be}{m} y - v_n \quad ,$$

the value which it has in the static magnetron.

In the synchronous region

$$v_x' = 0$$

or

$$v_x = v_n \text{ , the synchronism velocity.}$$

The boundary conditions are

$$y = 0, \quad \phi = 0, \quad v_y = 0,$$

$$y = y_a, \quad \phi = \phi_a .$$

Eq 2.36 becomes

$$e\phi_a = \frac{1}{2} m v_y^2 \Big|_{y = y_a} + \int_{y_n}^{y_a} Be\, v_n\, dy + \int_{o}^{y_n} \frac{B^2e^2}{m} y\, dy$$

$$= \frac{1}{2} m v_y^2 \Big|_{y = y_a} + Be\, v_n\, y_a - Be\, v_n\, y_n + \frac{B^2e^2}{2m} y_n^2 ,$$

but

$$\frac{Be}{m} y_n = v_n ,$$

so that the last two terms can be combined and the equation re-written

$$e\phi_a = \frac{1}{2} m v_y^2 \Big|_{y = y_a} + Be\, v_n\, y_a - \frac{1}{2} m v_n^2 \qquad (2.38)$$

The <u>threshold anode potential</u> ϕ_{at} will be defined as the anode potential given by Eq 2.38, for which the y-component of velocity is just zero. The term $\frac{1}{2} m v_y^2$ represents kinetic energy in excess of the minimum energy which the electron must accept from the d-c field in order to exist at the anode.

$$e\phi_{at} = Be\, v_n\, y_a - \frac{1}{2} m v_n^2 , \qquad (2.39)$$

or in dimensionless variables

$$\frac{\phi_{at}}{\phi_o} = 2\frac{B}{B_o} - 1 \quad . \tag{2.39a}$$

It is interesting to note that this anode potential is the same as the synchronism anode potential defined in the last section. This is a consequence of the fact that no kinetic energy, in addition to the synchronism energy, is retained by the electron in its passage from the synchronism boundary to the anode. Work is done on the electron by the radial field, represented by the term

$$\int_{y_n}^{y_a} Be\, v_n\, dy \quad . \tag{2.40}$$

However, this energy is immediately transferred from the electron to the r-f field so that the electron reaches the anode retaining only the kinetic energy represented by

$$\int_{o}^{y_n} \frac{B^2e^2}{m}\, y\, dy \quad , \tag{2.41}$$

$$= \frac{1}{2} m v_n^2 \quad .$$

The two terms of Eqs 2.40 and 2.41 have an interesting interpretation. They represent the work done on an element of current in moving it from 0 to y_a through the magnetic field B. This element of current is that due to a single charge moving with a velocity given by $\frac{Be}{m}$ y between 0 and y_n and a velocity v_n between y_n and y_a.

This problem is typical of many physical problems where the energy required to perform an operation can be determined from a force-distance integral but the disposition of the energy can only be determined by more detailed examination of the physical system. In this particular case the energy given by Eq 2.41 is dissipated into heat in the anode. It is concluded that the rest of the energy must be transferred to the r-f field. Some of this energy is in turn transmitted to the cathode in back-bombardment power by the electrons which have negative y-directed velocities.

Case II - Cylindrical Magnetron. The discussion of the cylindrical magnetron proceeds with exactly the same basic assumptions which were used in the treatment of the planar magnetron problem. The angular velocity of the electron is assumed to have the following distribution:

In the subsynchronous region

$$\omega' = \frac{Be}{2m}\left(1 - \frac{r_c^2}{r^2}\right) - \omega_n \quad .$$

In the synchronous region

$$\omega' = 0 \quad \text{or} \quad \omega = \omega_n \quad .$$

The boundary conditions are

$$r = r_c \,, \quad \phi = 0 \,, \quad v_r = 0 \,,$$

$$y = y_a \,, \quad \phi = \phi_a \,.$$

Eq 2.16 becomes

$$e\,\phi_a = \tfrac{1}{2}\,m\,v_r^2\Big|_{r=r_a} + \int_{r_n}^{r_a} (Be\,\omega_n\,r - m\,\omega_n^2\,r)\,dr$$

$$+ \int_{r_c}^{r_n} \left[\frac{B^2e^2}{2m}\left(1 - \frac{r_c^2}{r^2}\right) r - \frac{B^2e^2}{4m^2}\left(1 - \frac{r_c^2}{r^2}\right)^2\right] dr \quad .$$

After integration and simplification, this yields

$$e\,\phi_a = \tfrac{1}{2}\,m\,v_r^2\Big|_{r=r_a} + (Be\,\omega_n - m\,\omega_n^2)\frac{r_a^2 - r_n^2}{2}$$

$$+ \tfrac{1}{2}\,m\,\omega_n^2\,r_n^2 \quad .$$

To eliminate r_n, we write

$$e\,\phi_a = \tfrac{1}{2}\,m\,v_r^2\Big|_{r=r_a} + \tfrac{1}{2}\,Be\,\omega_n\,(r_a^2 - r_c^2) - \tfrac{1}{2}\,m\,\omega_n^2\,r_a^2$$

$$- \tfrac{1}{2}\,Be\,\omega_n\,(r_n^2 - r_c^2) + m\,\omega_n^2\,r_n^2 \, .$$

Substituting for one of the ω_n's in the last term, the last two terms become

$$-\tfrac{1}{2}\,Be\,\omega_n\,(r_n^2 - r_c^2) + \tfrac{1}{2}\,Be\,\omega_n\,(r_n^2 - r_c^2) = 0$$

We have, finally, for the threshold anode potential in the cylindrical system

$$e\,\phi_{at} = \frac{1}{2} Be\,\omega_n\,(r_a^2 - r_c^2) - \frac{1}{2} m\,\omega_n^2\,r_a^2 \quad , \qquad (2.42)$$

or, in dimensionless variables,

$$\frac{\phi_{at}}{\phi_o} = 2\,\frac{B}{B_o} - 1 \quad . \qquad (2.42a)$$

Comparison of this result with the synchronism anode potential of Eq 2.36a will show that the threshold anode potential is greater. This difference results from the additional energy which must be given to the electron to maintain the angular velocity synchronism as the radial distance to the position of the electron is increased. We must conclude that, if the gradient at the cathode is still zero, the total space charge in the interaction space must be greater than it was at the synchronism potential. The potential which will just maintain this synchronism between $r = r_n$ and $r = r_a$ is the following

$$\frac{\phi}{\phi_o} = 2\,\frac{B}{B_o}\,\frac{r^2 - r_c^2}{r_a^2 - r_c^2} - \frac{r^2}{r_a^2} \quad , \qquad (2.43)^1$$

$$r_n < r < r_a \quad .$$

Eq 2.43 reduces to Eq 2.42 at the anode radius. Application of Poisson's equation to Eq 2.43 will determine the distribution of space-charge density, which would give rise to the potential distribution. This is found to be a constant independent of radius, given by

---

[1] See III, 22, b, p. 436, for derivation.

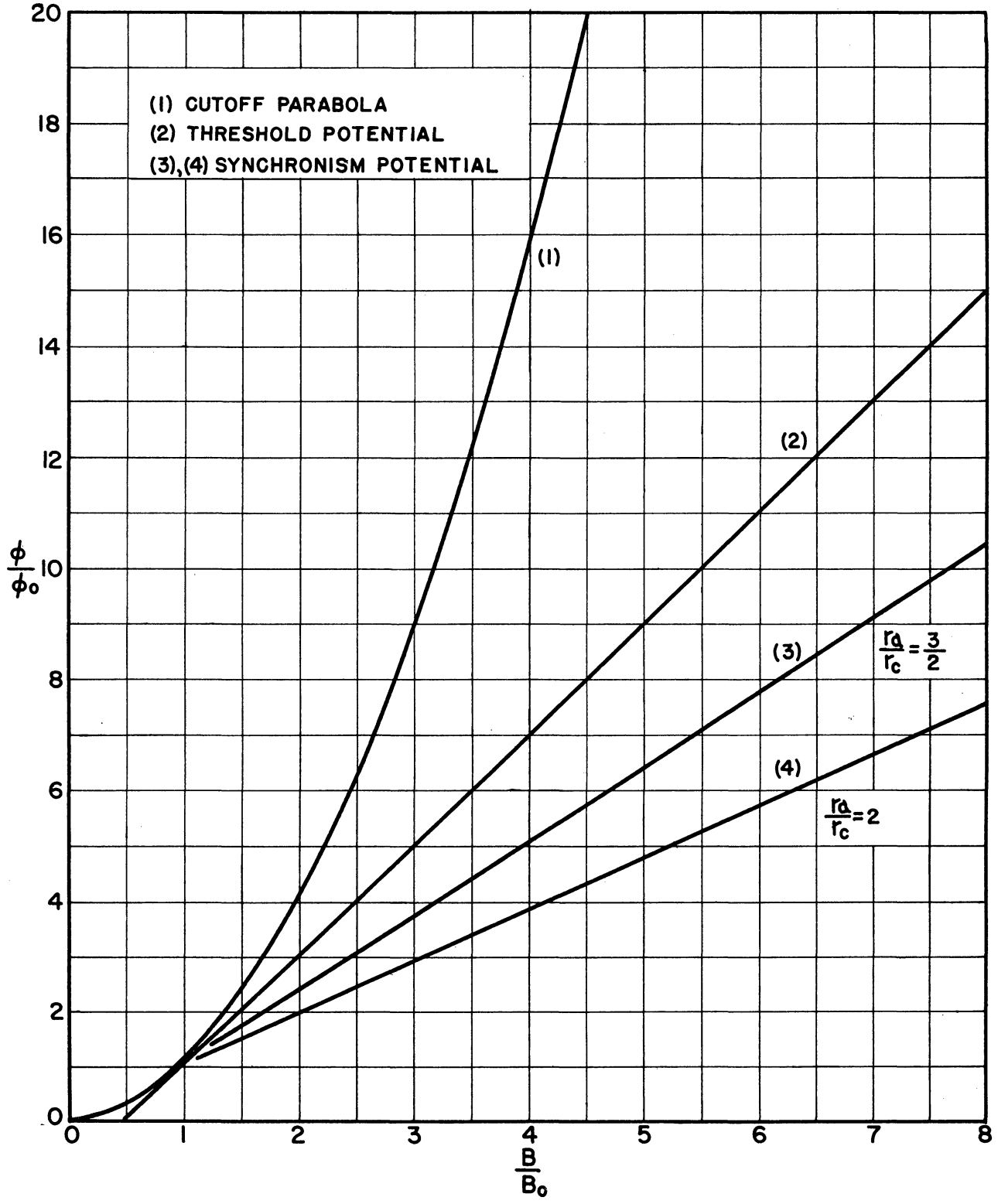

FIG. 2.6

ANODE POTENTIAL FOR CUTOFF, THRESHOLD AND SYNCHRONISM CONDITIONS AS A FUNCTION OF MAGNETIC FIELD

$$\rho_o = -2\varepsilon_o \frac{m}{e}\omega_n\left(\frac{Be}{m} - \omega_n\right) \quad . \qquad (2.44)^1$$

This value will be used later in calculation of induced currents in the magnetron.

The cutoff potential, threshold potential, and synchronism potential as functions of magnetic field, in dimensionless variables, are plotted in Fig. 2.6. These curves apply to either the planar or cylindrical magnetron. The synchronism potential curve for $r_a/r_c = 1$ coincides with the threshold potential line.

2.5 Phase Focussing; Formation of Space-Charge Spokes

The threshold potential derived in the last section is well known to workers in the magnetron field as the Hartree equation. The purpose of presenting a detailed discussion was to point out the exact nature of the assumptions necessary in its derivation in order to justify the physical picture of the space-charge distribution, which will be used as a basis for the prediction of large-signal phase focussing in the magnetron. This picture is presented graphically, in the moving reference frame, in Fig. 2.7.

The threshold energy level is represented by the line labeled ϕ_{at}, the actual anode voltage by the line ϕ_a. An r-f potential is represented with peak amplitude ϕ_f. This is the peak value of the fundamental travelling-wave component which appears stationary in the moving reference frame. Fig. 2.7a illustrates the possibility that, even though the threshold potential is not exceeded by ϕ_a, if an r-f

---

1 Ibid.

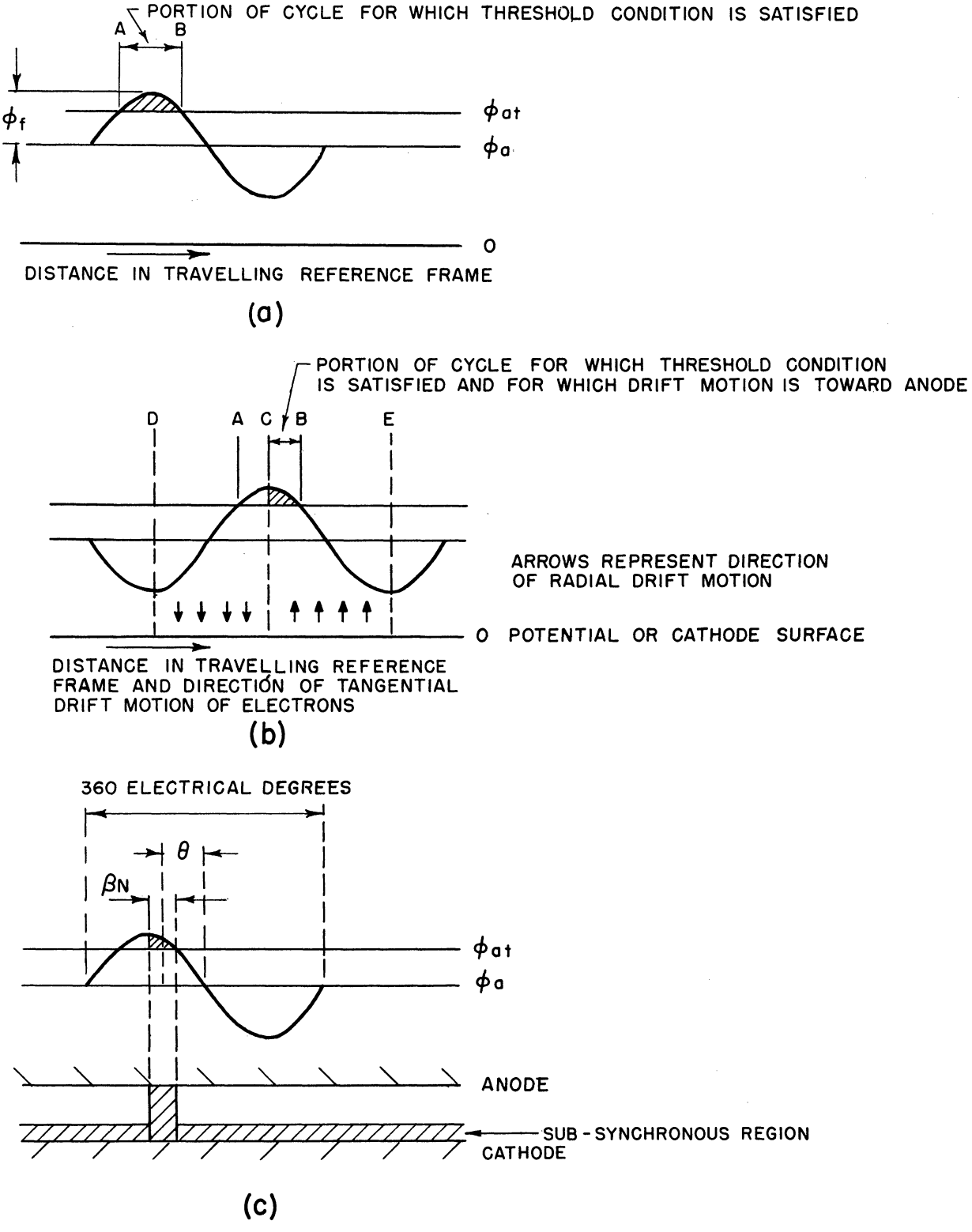

FIG. 2.7
ILLUSTRATION OF GRAPHICAL METHOD FOR DETERMINING SPOKE WIDTH AND PHASE ANGLE

potential exists, the threshold may be exceeded during part of the cycle designated by the interval A-B. In Fig. 2.7b the effect of the drift-velocity condition is illustrated. The drift motion of the electrons is toward the anode in the region C-E and away from the anode in the region D-C. Therefore, although the threshold energy is exceeded in the entire region A-B, electrons can only drift toward the anode in half of this region bounded by C-B. In the region A-C electrons can only exist if they come from the anode, and the assumption is that all electrons are emitted from the cathode. The final picture to be derived from this line of argument is shown in Fig. 2.7c. Here the potential distribution is plotted over a diagram of the interaction region. The width of the spoke and its phase angle relative to the r-f potential are approximately determined. These quantities are defined by the following symbols which will be used later when the current induced into the circuit is to be calculated.

θ = phase angle between center of spoke and zero of r-f potential in electrical degrees, negative as shown.

βN = width of spoke in electrical degrees.

β = half the actual space angle width of the spoke.

N = number of anodes.

There are N/2 full wavelengths (each 360 electrical degrees) around the cylindrical magnetron structure. The width of a spoke in electrical degrees, therefore is

$$\frac{N}{2} \cdot 2\beta = \beta N \quad .$$

The reference for the angle θ is chosen so that θ represents the phase angle between the current induced in the circuit by the

motion of the spoke parallel to the anode surface and the r-f potential which is developed between the anode sets. The way in which θ depends upon d-c anode voltage is illustrated by the development of the graphs in Fig. 2.8 and Fig. 2.9. In these graphs the r-f potential and the frequency are assumed constant. This would place a very special requirement on the circuit-operating parameters but is a convenient choice for the purpose of discussion.

In Fig. 2.8a, a case is illustrated which cannot occur in the oscillating magnetron, but is observable experimentally if an external source of r-f is imposed on the magnetron circuit. If the anode potential is above the synchronism potential but below the threshold potential and an r-f potential superimposed, the electrons will tend to drift toward the anode, but, because the threshold energy is not exceeded, will be forced to drift back again toward the cathode. However, the bunching effect of the radial component of the r-f will take effect to the extent that a greater density of electrons will circulate under a positive potential maximum than under a negative potential maximum. The bunching will be symmetrically disposed about the positive maximum. In this case, the induced current into the circuit due to the motion of the electrons parallel to the cathode will go through zero from negative to positive as the spoke passes under the anode segment at the same instant the anode segment reaches its maximum positive value. This is illustrated in Fig. 2.9a where the current and voltage are plotted on a time scale. The maximum current into the circuit, in this instance, lags the r-f potential maximum by 90°. This is equivalent to a current into the electron swarm which leads by 90° or to the addition of a capacitance

$$\phi_a = \phi_{at} + \phi_f \qquad (2.45)$$

is just satisfied. The entire region for which drift velocity is toward the anode is filled. The spokes have reached a width just half filling the interaction space. The phase angle θ is zero degrees so that the circuit must be on resonance to present a real admittance to the induced current. At a higher anode potential, represented by Fig. 2.8e, the threshold potential is exceeded everywhere and the only focussing mechanism left is that due to the tangential component of the r-f field. The electrons are, therefore, not in well defined bunches but continuously distributed with periodic condensations and rarefactions. Moreover, as the circuit passes through resonance, the admittance of the circuit goes through a minimum; raising the anode potential will result, in general, in greater power input; a smaller r-f potential (therefore smaller power output) will tend to be the result of the induced current; and the focussing forces will tend to be reduced. These factors result in inconsistency which leads one to expect that the magnetron will cease oscillating or oscillate in another mode. The conclusion is that Eq 2.45 represents a critical condition defining an upper-mode boundary on magnetron oscillation.

There is a similarity between the cases represented by Fig. 2.8a and Fig. 2.8e. Let us assume that the synchronous swarm of Fig. 2.8a <u>just</u> reaches the anode and is produced by a very small r-f voltage which is the initial oscillation. The anode potential is very slightly below the threshold potential but the r-f potential is so small that the phase angle is practically 90°. Under these conditions, the

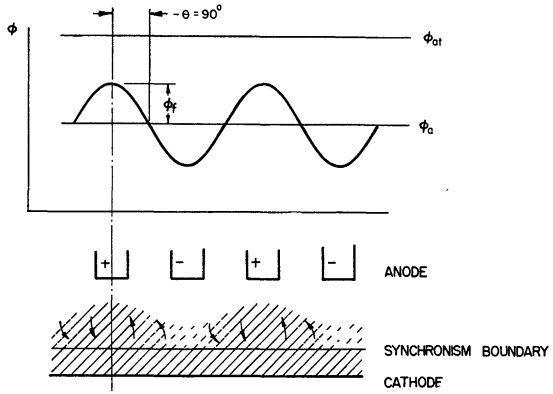

FIG. 2.8a

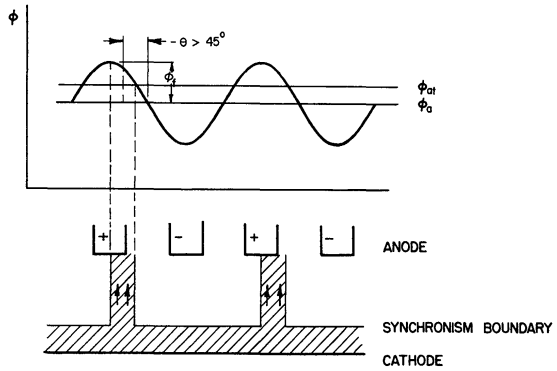

FIG. 2.8b

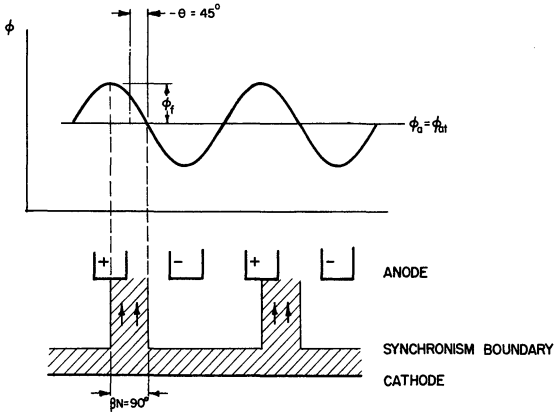

FIG. 2.8c

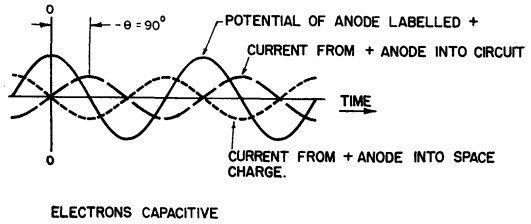

ELECTRONS CAPACITIVE

FIG. 2.9a

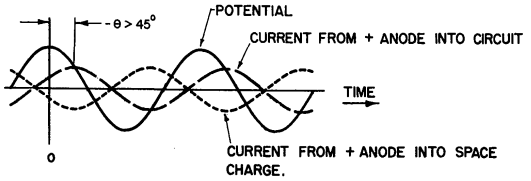

CIRCUIT INDUCTIVE

FIG. 2.9b

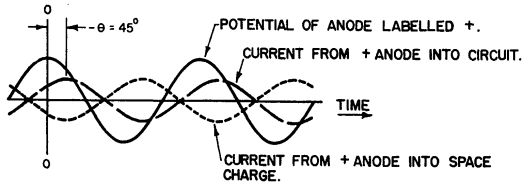

CIRCUIT INDUCTIVE AT HALF POWER POINT.

FIG. 2.9c

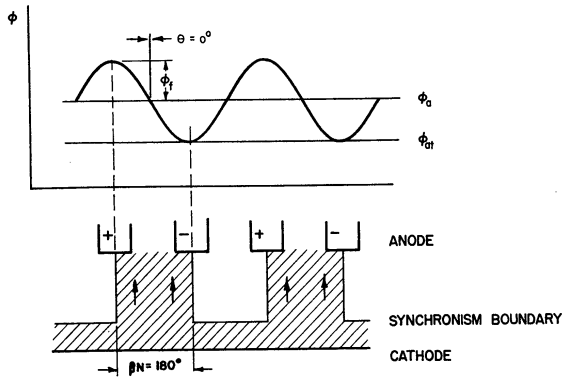

FIG. 2.8 d

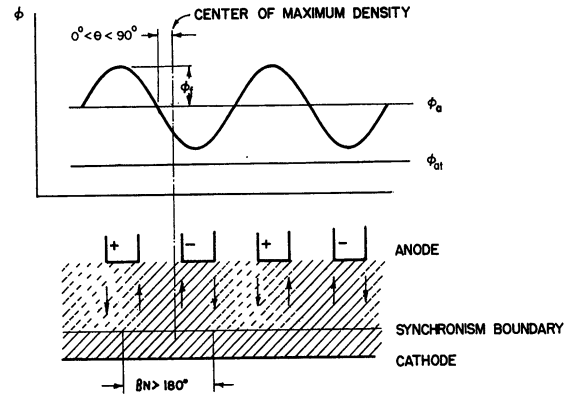

FIG. 2.8e

FIG. 2.8

PHASE FOCUSSING DIAGRAM. GRAPHICAL DEVELOPMENT OF RELATIONSHIP BETWEEN PHASE ANGLE θ AND ANODE POTENTIAL. CONSTANT R-F POTENTIAL AND FREQUENCY ARE ASSUMED. ARROWS INDICATE DIRECTION OF ELECTRON DRIFT BETWEEN ANODE AND CATHODE.

THIS FIGURE SHOULD BE STUDIED WITH FIG. 2.9

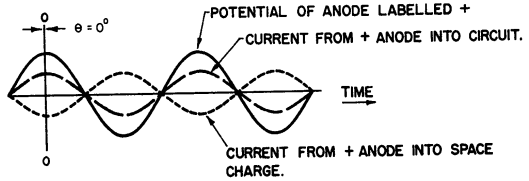

CIRCUIT RESISTIVE ON RESONANCE.

FIG. 2.9d

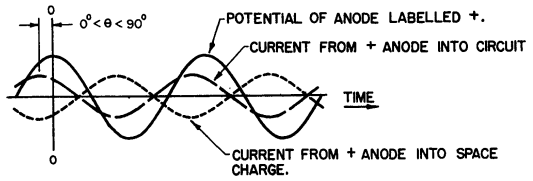

CIRCUIT CAPACITIVE

FIG. 2.9e

FIG. 2.9

CURRENT INDUCED BY SPOKE INTO CIRCUIT ON TIME SCALE. TIME 0-0 MARKS THE INSTANT OBSERVED IN ILLUSTRATION LABELLED BY THE SAME LETTER IN FIG. 2.8.

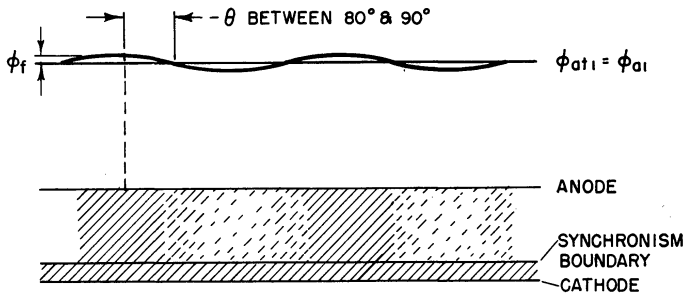

FIG. 2.10a

MAGNETRON JUST STARTING. ϕ_f IS VERY SMALL.
FREQUENCY IS 5 OR 10 % OFF RESONANCE.
BUNCHING NOT COMPLETE, POSSIBLY NOISY OPERATION

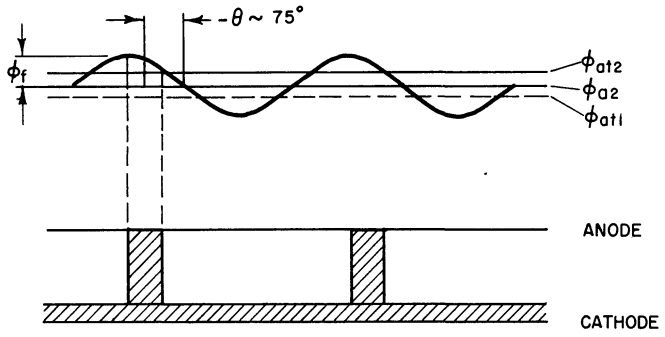

FIG. 2.10b

MAGNETRON IS OSCILLATING STRONGLY.
ϕ_f IS GREATER THAN 10% OF ϕ_a.
FREQUENCY IS 1 TO 3 % OFF RESONANCE.
BUNCHING IS COMPLETE BUT BUNCHES AND
INDUCED CURRENT ARE MUCH LESS THAN
MAXIMUM.

FIG. 2.10
PHASE FOCUSSING DIAGRAMS FOR A TYPICAL
MAGNETRON VOLT-AMPERE CHARACTERISTIC

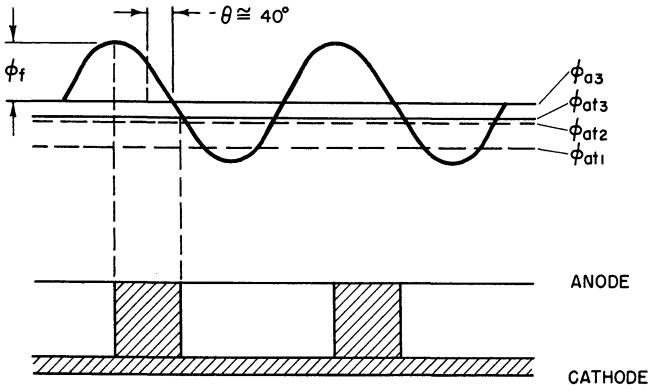

FIG. 2.10 c

MAGNETRON IS OSCILLATING AT A MEDIUM POWER LEVEL
ϕ_f IS 30 OR 40% OF ϕ_a FREQUENCY IS LESS THAN 1%
OFF RESONANCE. BUNCH HAS INCREASED IN SIZE AND
INDUCED CURRENT IS GREATER THAN IN LAST PICTURE

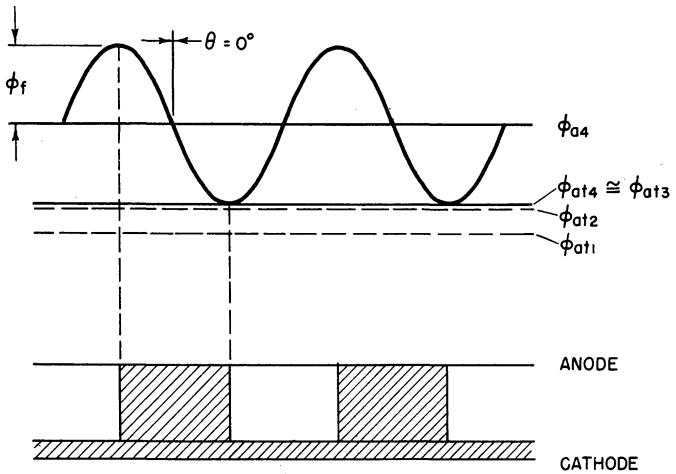

FIG. 2.10 d

MAGNETRON IS OSCILLATING AT HIGHEST POSSIBLE LEVEL
ϕ_f IS OF THE ORDER OF HALF ϕ_a. FREQUENCY IS ON RESONANCE
BUNCHES OCCUPY HALF OF THE SPACE. INDUCED CURRENT
IS MAXIMUM.

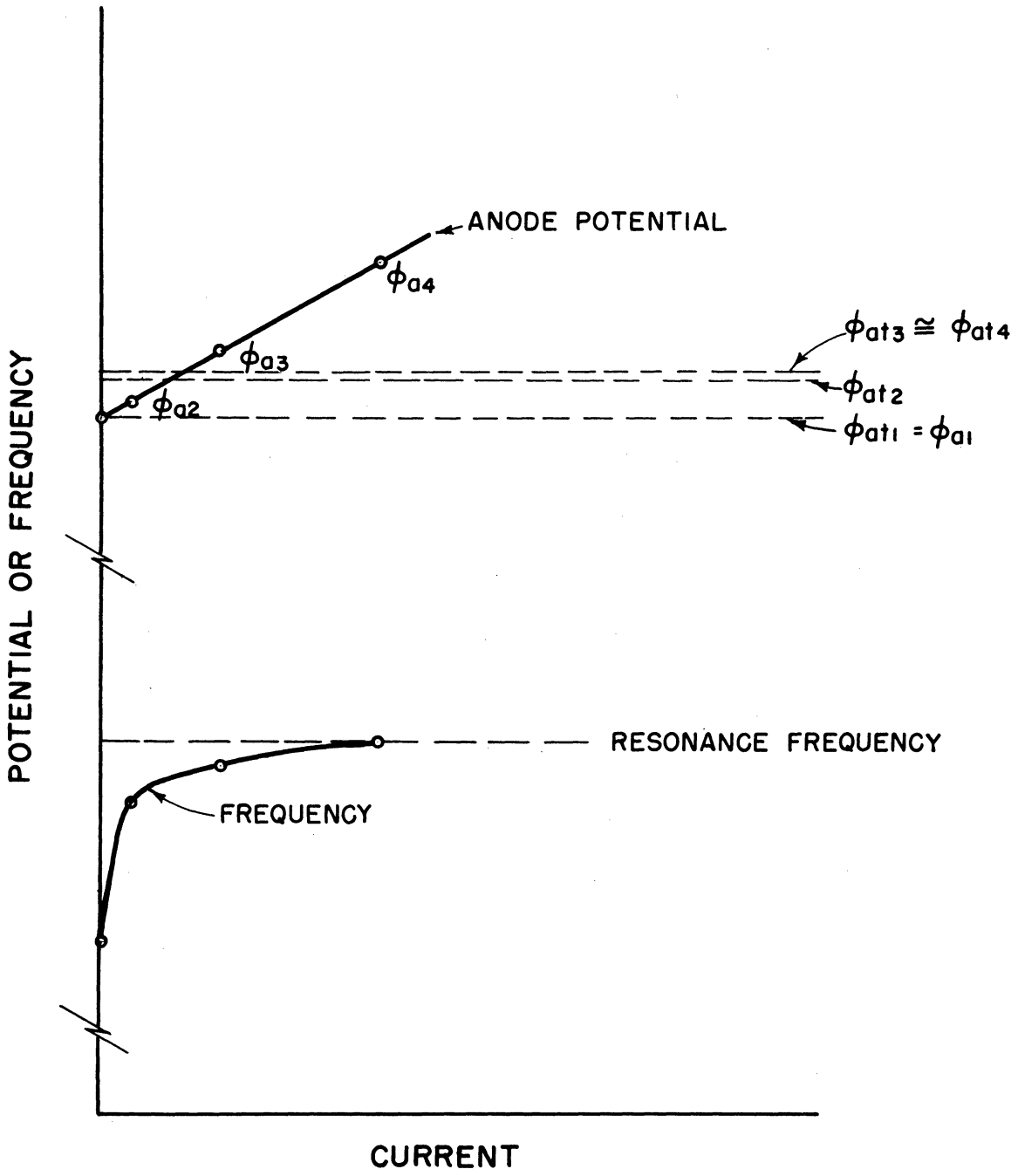

FIG. 2.11
TYPICAL VOLT-AMPERE CHARACTERISTIC USED IN MAKING PHASE-FOCUSSING DIAGRAMS OF FIG. 2.10

focussing effects on the electrons due to their radial motion would be relatively weak and the electrons would maintain a positively directed velocity (ω') in the moving reference frame. In other words, they would be moving slightly faster than the synchronism velocity but spending more time, or piling up, in the decelerating field region.

In the case of Fig. 2.8e, a substantial r-f potential exists but the average potential is high enough to make the forces due to the radial motion overbalance the forces of the tangential field. The electrons tend to drift forward and outward in the moving reference frame. Those which miss the anode are circulated back into the accelerating tangential field region, as in the case of Fig. 2.8a.

In Fig. 2.10 a series of phase-focussing diagrams illustrates the behavior to be expected over the range of a typical volt-ampere characteristic when the magnetron is operating into a resonant load. The characteristic corresponding to the diagrams is shown in Fig. 2.11. Through the threshold energy equation (Eq 2.42), there is a threshold potential, characteristic of any synchronism angular velocity, that is, frequency. When the anode potential reaches a threshold potential ϕ_{at}, characteristic of a frequency for which the circuit presents an impedance sufficient to start the phase focussing, the magnetron will start oscillating. This potential may, in general, be as much as 10 or 20 per cent below the threshold potential which is characteristic of the resonance frequency. This condition is represented by the diagram of Fig. 2.10a. The r-f potential is very small and the synchronism velocity is not definitely determined; bunching is weak so that noisy operation may be expected. As the anode potential is raised further

to a value ϕ_{a2}, the frequency increases substantially to a value two or three percent off resonance. The characteristic threshold potential ϕ_{at2} is proportionally higher than ϕ_{at}. The r-f is now strong enough to produce a well-focussed spoke. As the anode potential is increased further, the threshold potential remains substantially constant since the frequency is a very slowly varying function of phase angle near resonance. The separation between ϕ_a and ϕ_{at} increases with increased power input and the r-f amplitude builds up, because of the decreasing total circuit admittance, until finally the critical condition of Eq 2.45 is reached and oscillation ceases.

The quantity $\phi_a - \phi_{at}$ can be analytically related to βN by use of the phase-focussing diagram. Referring to Fig. 2.7c,

$$\frac{\phi_a - \phi_{at}}{\phi_f} = - \cos \beta N \quad . \tag{2.46}$$

The phase angle θ is given by

$$\pi + 2\theta = \beta N \quad . \tag{2.47}$$

Note that θ, in normal operation, is a **lagging** phase angle and, therefore, negative as conventionally defined. Thus βN is less than π. The phase angle may also be related to $\phi_a - \phi_{at}$.

$$- \cos \beta N = \cos 2\theta = \frac{\phi_a - \phi_{at}}{\phi_f} \quad . \tag{2.48}$$

ϕ_f, the peak value of the fundamental travelling-wave, is related to the actual peak r-f potential between anode segments by a constant which depends only on the electrode geometry.

between the anode segments in the interaction space. This capacitance is entirely due to the synchronous bunching of the electrons and not related to the capacitance effect which can be introduced by an evenly distributed swarm of electrons. Experimental evidence of this effect will be presented in Chapter 4.

In Fig. 2.8b, the situation is illustrated just after the anode potential has been increased to the point where, during part of the cycle, the r-f exceeds the threshold potential. Electrons in the spoke now drift toward the anode and are collected so that power can be delivered to the system. As one would expect, there is now an in-phase component of current as illustrated in Fig. 2.9b. The zero of the current slightly precedes the r-f potential maximum in time. The space-charge swarm as an induced-current generator is delivering energy into a highly inductive load. Oscillations, in this case, can be supported if they have been initiated. At the potential, ϕ_a, however, an infinitesimal r-f potential would not exceed the threshold potential. One must assume, therefore, that the threshold potential must have been exceeded by ϕ_a in order to initiate the oscillation and that ϕ_a subsequently dropped (i.e., by power supply regulation), or that a pulse of noise or external r-f source set the tube into oscillation.

In Fig. 2.8c, the case for ϕ_a exactly equal to the threshold potential, ϕ_{at}, is illustrated. The phase angle is -45° so that, for operation into a resonant circuit, the frequency would be such that the point of operation would be at the "half-power points."

Fig. 2.8d represents a case of particular importance. The anode potential is raised above the threshold potential so that the condition

$$\phi_f = K \phi_{rf\ max} \tag{2.49}$$

where $K < 1$.

The final condition on ϕ_{rf} is that it be produced as the result of the flow of the induced current through the external circuit, i.e.,

$$\phi_{rf\ max} |Y_T| \angle\theta = I_1$$

$|Y_T|$ = absolute value of the circuit admittance.

I_1 = amplitude of the fundamental component of the current induced in the circuit by the rotation of the space-charge spokes in the interaction space. It is given by Eq 3.19 developed in the next chapter.

θ = the phase angle determined by the circuit. θ must be equal to the value determined by Eq 2.48 and defined in Fig. 2.7.

This discussion of the phase-focussing diagram shows that the circuit phase characteristic, as well as the induced current due to the particular spoke configuration involved, must be known in order to make a more detailed analysis. Further discussion of the phase-focussing diagram will, therefore, be reserved until after these concepts are given some attention in the next chapter. In order to calculate the induced current, it will be necessary to estimate the space-charge density in the spokes. This problem is discussed in the following section.

2.6 Estimation of Space-Charge Density in the Interaction Region

It was pointed out in Section 2.4 that the potential

distribution which will just maintain synchronism with the r-f wave can be written in the form

$$\phi = a r^2 + b \quad . \tag{2.51}$$

See Eq 2.43. The potential distribution of Eq 2.43 yields the threshold potential at the anode surface, and through application of Poisson's equation a constant average space-charge density in the spoke region. This density is given by Eq 2.44. The phase-focussing diagrams of Section 2.5 predict that the angle 2β representing the angular width will be given by

$$2\beta = \frac{\pi}{N} \text{ radians or } \frac{180°}{N}$$

when the anode potential is equal to the threshold potential.

$$\phi_a = \phi_{at} \quad .$$

The maximum width of a spoke for the condition represented by Fig. 2.8d is

$$2\beta = \frac{2\pi}{N} \text{ radians or } \frac{360°}{N} .$$

This width will occur for

$$\phi_a = \phi_{at} + \phi_f \quad . \tag{2.45}$$

The minimum width of the spoke, if the phase-focussing diagram is used to this lower extreme, would, of course, be

$$2\beta = 0° \quad .$$

Actually the spoke is probably no longer well defined at this extreme, but more like the picture of Fig. 2.10a or 2.8a. If the hypothesis of zero spoke width were assumed, then the anode potential would be given by

$$\phi_a = \phi_{at} - \phi_{fo} \tag{2.52}$$

where ϕ_{fo} is the peak value of the fundamental travelling r-f wave as zero spoke width is approached. The point of this discussion is that the anode potential must lie somewhere between the extremes given by Eqs 2.45 and 2.52. If finite current is to be induced into the anodes as zero width is approached the space-charge density must, of course, approach an infinite value.

The condition $2\beta = 0°$ corresponds to the phase angle $\theta = -90°$. For $2\beta = \frac{360°}{N}$, the other extreme, $\theta = 0°$. Thus if it is desired to calculate the induced current over the range of operation indicated as feasible in the discussion of the phase-focussing diagrams from $\theta = -90°$ to $\theta = 0°$, it is necessary to estimate the space-charge density in the spokes over this range. The estimate given in Eq 2.44 applies only to the condition

$$\phi = \phi_{at}$$

or

$$\theta = -45° .$$

Actual calculation of the space-charge-density distribution is prohibitively laborious and only possible by a self-consistent field calculation. For the purposes of this treatment, therefore, it will be assumed that the average space-charge density is a constant independent of radius at all anode potentials within the range of interest as it is at the threshold

potential. This means that, whether the anode potential is below or above the threshold potential, a distribution of the form of Eq 2.51 is assumed to exist.

Application of Poisson's equation to Eq 2.51 yields

$$\frac{\rho}{\varepsilon_o} = -\frac{1}{r}\frac{\partial}{\partial r}\left(r\frac{\partial \phi}{\partial r}\right)$$

$$= -\frac{1}{r}\frac{\partial}{\partial r} 2 a r^2$$

$$\rho = -4 \varepsilon_o a \qquad (2.53)$$

The constant, a, in Eq 2.51 can be evaluated by substituting the boundary conditions

$$r = r_n, \quad \phi = \phi_n ,$$
$$r = r_a, \quad \phi = \phi_a .$$

Thus

$$\phi_a = a r_a^2 + b ,$$

$$\phi_n = a r_n^2 + b ,$$

and

$$\frac{\phi_a - \phi_n}{r_a^2 - r_n^2} = a . \qquad (2.54)$$

The constant average space-charge density is, therefore, given by

$$\rho = -4 \varepsilon_o \frac{\phi_a - \phi_n}{r_a^2 - r_n^2} . \qquad (2.55)$$

A convenient form for this expression is obtained by substitution for $\phi_n = \frac{1}{2}\frac{m}{e}\omega_n^2 r_n^2$ from the equation on page 78 preliminary to the threshold

potential eq., 2.42. The term $\frac{1}{2} m v_r^2$ is assumed negligible.

$$\frac{1}{2} \frac{m}{e} \omega_n^2 r_n^2 = \phi_n = \phi_{at} - \frac{\omega_n}{2} \frac{m}{e} \left(\frac{Be}{m} - \omega_n\right) (r_a^2 - r_n^2) \quad (2.56)$$

Substituting into Eq 2.55 yields

$$\rho = - \left[2 \varepsilon_o \frac{m}{e} \omega_n \left(\frac{Be}{m} - \omega_n\right) + 4 \varepsilon_o \frac{\phi_a - \phi_{at}}{r_a^2 - r_n^2} \right] . \quad (2.57)$$

The first term of this expression is identical with the value given by Eq 2.44. If we define

$$R_n = \frac{r_n}{r_c} ,$$

$$R_a = \frac{r_a}{r_c} ,$$

Eq 2.57 may be written

$$\rho = \rho_o \left(1 + \frac{4\varepsilon_o}{\rho_o r_c^2} \frac{\phi_a - \phi_{at}}{R_a^2 - R_n^2}\right) . \quad (2.58)$$

The effect of deviation of the anode potential from the threshold potential is now contained in the second term. Eq 2.58 is plotted in Fig. 2.12. In typical magnetrons the range of d-c anode voltage is well within the range covered by the graph. The theory of phase focussing presented here applies only to large-signal analysis and large-signal operation is seldom observed at ϕ_a less than 90 per cent of ϕ_{at}. ϕ_n is usually of the order of 10 per cent or less of ϕ_{at}. ϕ_a is seldom more than 20 or 30 per cent greater than ϕ_{at}. This range is indicated on the graph.

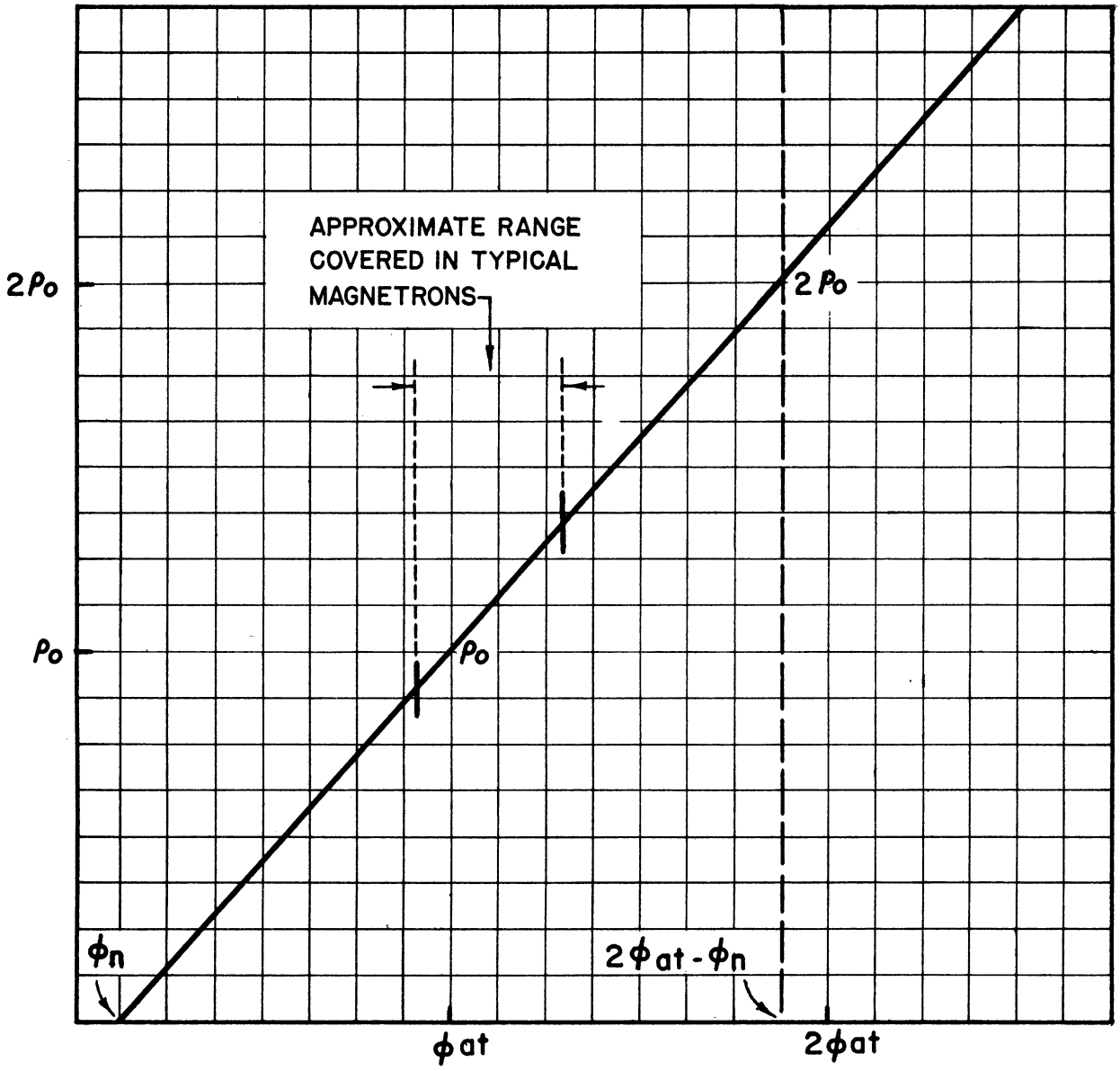

FIG. 2.12

AVERAGE SPACE-CHARGE DENSITY AS
A FUNCTION OF ANODE POTENTIAL

2.7 Electron Behavior in the Space-Charge-Free Magnetron. Temperature-Limited Operation

In all of the material which has just been presented, it has been assumed that zero field gradient existed at the cathode, or that the magnetron was operating under space-charge-limited conditions. This is not completely realistic in the analysis of many experimental results since, because of frequent necessity for compromise in design, cathodes for c-w magnetrons are frequently marginal in their emission capabilities. The enhanced emission which provides the very large currents in pulsed magnetrons does not exist when tungsten or other pure metal cathodes are used in c-w tubes. It can easily be shown that the subsynchronous space-charge swarm does not act as a reservoir[1] as has sometimes been proposed. Experimental evidence of the fact that cathode emission, and cathode properties other than straightforward emission-density capabilities, may have strange effects on oscillatory behavior is plentiful and, for the most part, uninterpreted. Attempts to derive complete relationships for field gradient at the cathode and energy distribution in the swarm, for various emission currents, result in discouragingly complex relationships even for the planar static magnetron. For the cylindrical static magnetron the information to be derived from the analytical solution assuming zero gradient at the cathode is questionably commensurate with the difficulty involved. The problem with a gradient at the cathode has received attention for the non-magnetic diode as recently as October, 1950,[2] although earlier papers[3] give fairly

---

1 III, 22, c, pp 63-64.

2 IV, 2.

3 IV, 3, 6, 9.

comprehensive treatments. If it is assumed that the solution to the static magnetron exists, there is no known method of extending the ideas to calculation of d-c current in the oscillating magnetron.

In order to get some idea of the effect of a positive field gradient at the cathode on the behavior of the oscillating magnetron, the various results involving anode potential and synchronism conditions which were discussed in Sections 2.3 and 2.4 will be compared with similar results of the analysis of the completely space-charge-free magnetron. The initial differential equations of Eqs 2.14, 2.15, 2.16 and 2.17 are the same. The problem, however, becomes simpler, since not only are the boundary conditions known, but the complete potential distribution within the interaction space is known. On paper, at least, it becomes conceivable to calculate the position and velocity of an electron at every instant. It is discouraging to discover that even this relatively simple physical problem leads to non-linear differential equations which have not been solved except for very simplified boundary conditions in the large-signal, travelling-reference-frame problem. The following result obtained by Lüdi[1] is such a special case.

$$y = -K\frac{k}{\omega_c^2}\cosh\frac{k}{\omega_c}t + \frac{v_o}{\omega_c}e^{-\frac{k}{\omega_c}t} + \frac{K\,k}{\omega_c^2}\cos\omega_c t - \frac{v_o}{\omega_c}\cos\omega_c t\,, \tag{2.59}$$

$$x' = K\left(1 - e^{\frac{k}{\omega_c}t}\right) + v_o\,t + x_o + \frac{K\,k}{\omega_c^2}\sin\omega_c t - \frac{v_o}{\omega_c}\sin\omega_c t\,. \tag{2.60}$$

---

[1] III, 12, b, p 64.

$\omega_c = B\frac{e}{m}$,

$v_o = \frac{\phi_a}{y_a}\frac{1}{B}$ = rolling circle velocity in static magnetron,

$K = \frac{x_n}{2\pi}\tan 2\pi\frac{x_o}{x_n}$,

$k = \gamma\frac{e}{m}\frac{\phi_a}{y_a}\frac{2\pi}{x_n}\cos 2\pi\frac{x_o}{x_n}$,

γ = ratio of r-f to d-c having algebraic sign of the x-directed field component,

$\frac{x_n}{2}$ = spacing between centers of adjacent anode segments,

x_o = position of emission of electron measured from position of maximum positively directed E_x, i.e., half the distance from A to B in Fig. 2.5, t = 0 at the time the electron left the cathode.

In this treatment it is assumed that

$$\frac{x_n}{y_a} \gg 1$$

$$v_n = v_o .$$

This latter assumption is only valid for large magnetic fields. It is, however, interesting to examine these results to this extent. The position and velocity are found to contain, in addition to oscillatory terms, terms which indicate steady drift of the electrons.

$$y = \frac{v_o}{\omega_c} e^{-\frac{k}{\omega_c}t} \qquad (2.61)$$

$$x' = K\left(1 - e^{\frac{k}{\omega_c}t}\right) + vt + x_o . \qquad (2.62)$$

Since the first unperiodic term in y of Eq 2.59 is small compared to the term given in 2.61, it is omitted. Examination of the sign of these terms shows that the drift motion toward the anode and away from the anode and

toward the decelerating field region is confined within the boundaries indicated by the analysis of the differential equations in Section 2.4. The arguments presented there were not related to the presence of space charge and need not be changed for the case of the space-charge-free magnetron. The important difference will be found in the anode potential required for synchronism and in the division of energy between energy due to motion directed perpendicular to the anode and energy due to motion directed parallel to the anode.

Case I - Planar Magnetron. The solution for the x-component of velocity in the static planar magnetron is, regardless of the field gradient at the cathode, the result given in Eq 2.19.

$$v_x' + v_n = \frac{Be}{m} y . \qquad (2.19)$$

This means that the electron reaches the synchronism velocity at the same distance from the cathode regardless of the potential distribution in the static magnetron.

$$y_n = \frac{m}{e} \frac{v_n}{B} . \qquad (2.20)$$

However, since it is assumed that the space charge present is having a negligible effect on the field and potential distribution, the anode potential required to bring electrons to this boundary is now changed. The potential of a given point in the interaction space will be linearly related to the distance from the cathode. We have, therefore

$$\phi_{an} = \phi_n \frac{y_a}{y_n} = \frac{1}{2} \frac{m}{e} v_n^2 \left(y_a \frac{e}{m} \frac{B}{v_n}\right) .$$

Finally

$$\phi_{an} = B v_n y_a . \qquad (2.63)$$

In dimensionless variables

$$\frac{\phi_{an}}{\phi_o} = \frac{B}{B_o} . \qquad (2.63a)$$

For large B/B_o this synchronism potential is approximately one-half the synchronism potential for the space-charge-limited case.

$$\frac{\phi_{an}}{\phi_o} = 2\frac{B}{B_o} - 1 . \qquad (2.25a)$$

There is nothing in the space-charge-free problem which gives reason to change the choice of v_x' used in the integration of the energy equation which yielded the threshold energy condition and the threshold anode potential. The cutoff anode potential also has the same value. The various energy distributions are plotted for comparison in Fig. 2.13. The curve for the space-charge-limited energy distribution displays a slight upward flexion in the synchronism region due to the presence of space charge in the spokes. If, for the same anode potential, the emission current were reduced gradually to zero, the flexion would gradually disappear and the energy distribution gradually approach the straight line of the space-charge-free energy distribution. The difference between the actual energy distribution curve and the threshold-energy curve is the energy of y-directed motion. The energy of the x-directed motion is represented by the shaded area under the synchronism-energy level outside the synchronism boundary and the cutoff-energy parabola inside the synchronism boundary. The remaining energy must be delivered to the r-f field.

In Fig. 2.14 the phase-focussing diagram is placed beside a potential diagram to illustrate behavior of the magnetron under temperature-limited conditions. Two conditions are shown, indicated by 1 and 2. In

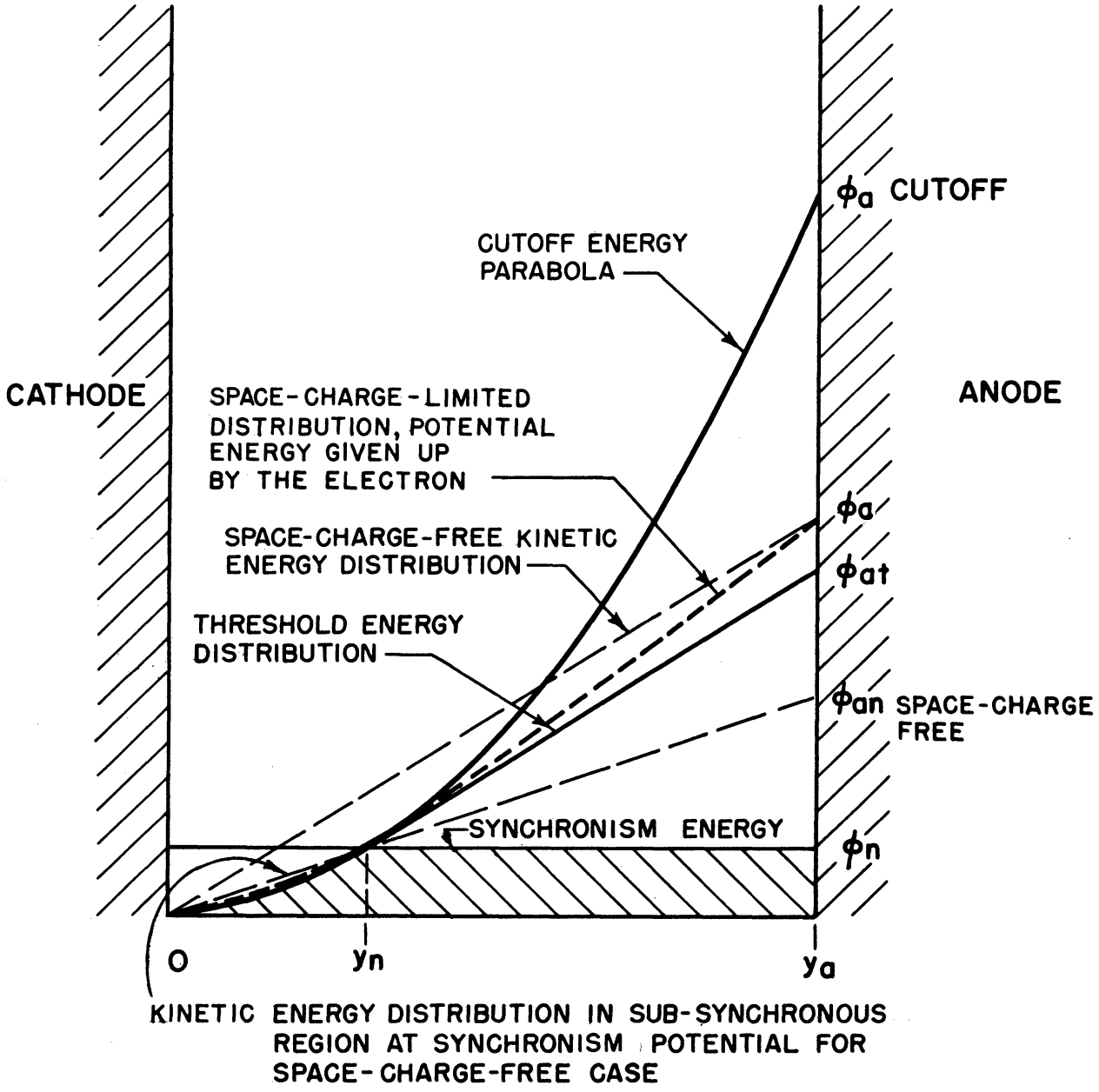

FIG. 2.13
ENERGY DISTRIBUTIONS IN THE PLANE MAGNETRON
(IN RELATIVE ELECTRON VOLTS)

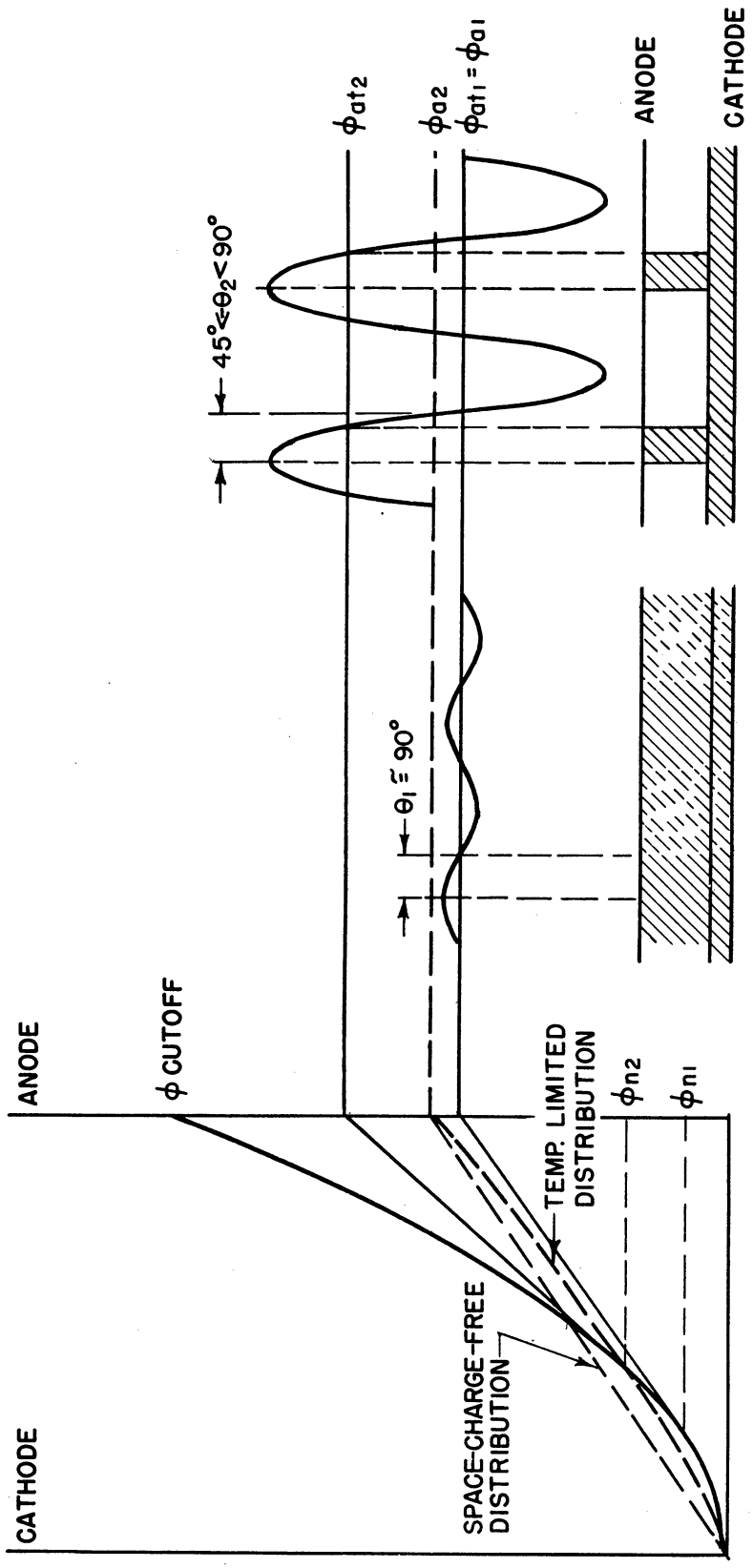

FIG. 2.14
PHASE-FOCUSSING DIAGRAM AND ENERGY-DISTRIBUTION DIAGRAM FOR TEMPERATURE-LIMITED OPERATION

condition 1 the anode current is sufficiently small that the operation is space-charge-limited. The anode potential, ϕ_{a1}, is equal to the threshold potential, ϕ_{at1}, corresponding to the frequency, f_1. The phase angle, θ_1, is represented as almost 90° since the space-charge swarm is assumed to be very weakly bunched. As the anode potential is raised a relatively small amount, the anode current rises rapidly to the saturation value. The reduction of space-charge density inside the magnetron causes a positive gradient to exist at the cathode and the potential required to produce synchronous electrons approaches the value given by Eq 2.63. For a given anode potential, ϕ_{a2}, therefore, the synchronism velocity tends to be higher than in the space-charge-limited case. This means that, if circuit conditions permit, a situation like that of condition 2 would be the expected result. The increase in threshold potential associated with the increase in synchronism velocity is considerably greater than the increase in the actual anode potential. The frequency is, of course, directly proportional to the synchronism velocity since

$$v_n = x_n f , \qquad (2.64)$$

where $x_n/2$ is the distance between centers of adjacent anode segments. We have, therefore,

$$\frac{f_2}{f_1} = \frac{v_{n2}}{v_{n1}} = \frac{\phi_{n2}}{\phi_{n1}} .$$

For the case illustrated it is implied that the difference between f_2 and f_1 is rather substantial, but that the phase angle, θ_2, is still large and not greatly different from θ_1. The question arises as to what factors determine the particular operating point which is established in condition 2.

Suppose that, in making the diagram, some other point of tangency to the cutoff-energy parabola had been chosen in the plotting of the threshold energy distribution. This would mean a different frequency; presumably as a consequence of the frequency change, a new circuit impedance; and a change in the r-f potential or spoke width. It is reasonable to assume that the d-c collection current is proportional to the spoke width. Thus if the particular operating anode potential and current are assumed constant, it becomes difficult to argue a change in any of the other parameters in the phase-focussing diagram without a change in the circuit. It is concluded that the operating conditions as specified by diagram 2 are unique. This leads to an interesting conclusion about temperature-limited operation. Suppose the anode potential is now raised above the value, ϕ_{a2}, and that, in addition to keeping the d-c current constant at the saturation level, the circuit impedance is kept constant. The first consequence to be expected of the increase in anode potential would be an increase in the synchronism velocity, v_n. One would also expect the power output to increase as the result of an increased induced current and r-f potential. However, since the d-c current is limited by saturation, any change in spoke width which would produce a change in induced current would tend to be suppressed. Since the circuit impedance has been maintained constant the phase angle and r-f voltage remain the same and we are led to the conclusion that the threshold potential and, consequently the frequency, must increase in the same proportion as the anode potential. This is illustrated by the phase-focussing diagrams of Fig. 2.15. The unique balance between all of the parameters at the saturation current level is approximately maintained if the whole phase-focussing diagram is raised with the anode

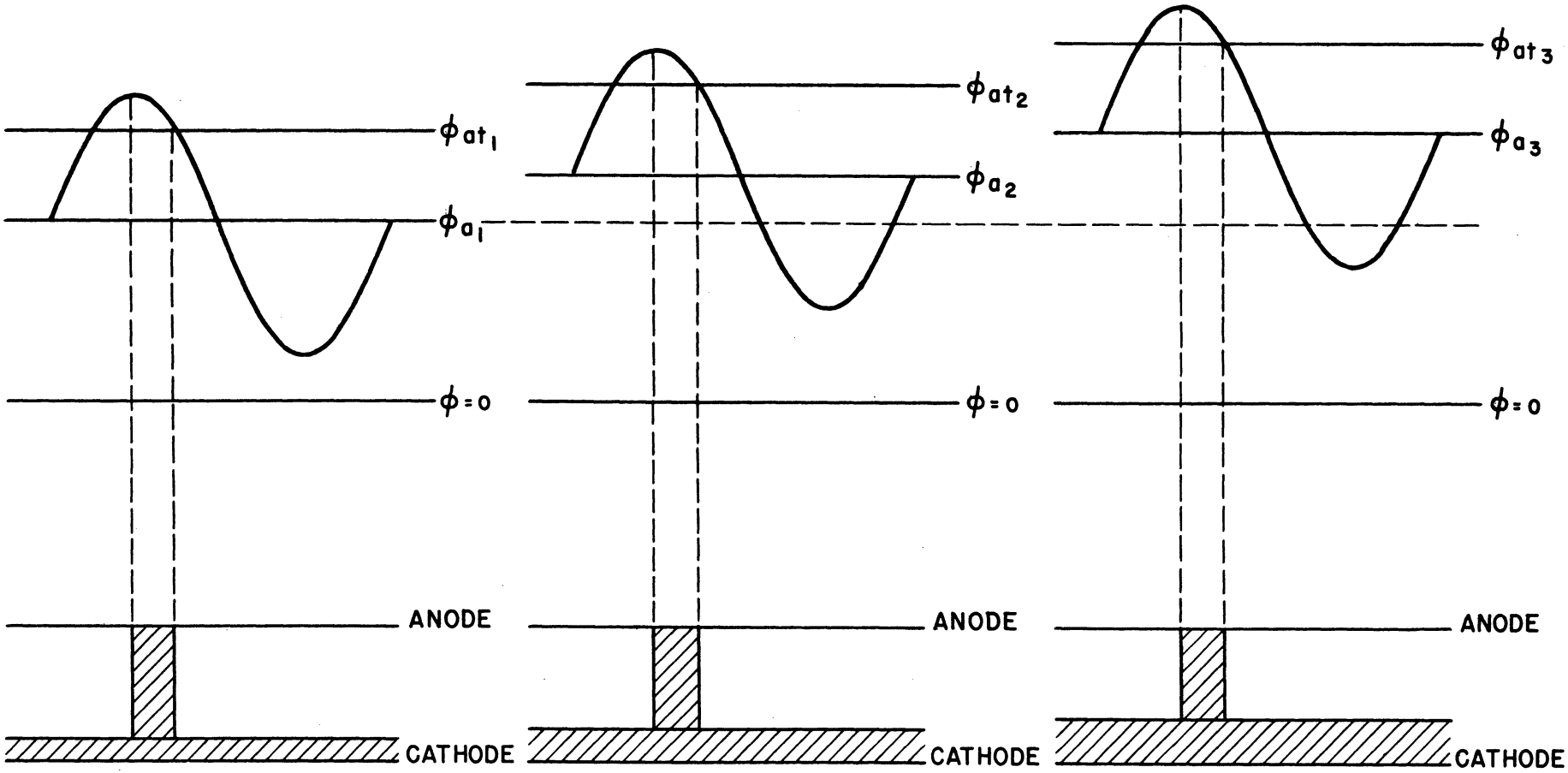

FIG. 2.15

PHASE-FOCUSSING DIAGRAMS FOR VARIOUS ANODE POTENTIALS. MAGNETIC FIELD, CIRCUIT IMPEDANCE, AND ANODE CURRENT MAINTAINED CONSTANT

potential. The frequency is therefore determined by the anode potential under these particular conditions.

An important assumption underlying these remarks is that the gross behavior of the space charge in response to given imposed voltages and boundary conditions is not a critical function of frequency. This is certainly true[1] and is an extremely important characteristic of magnetron behavior. The ability of the magnetron to operate over a wide range of voltages and magnetic fields and relatively large tuning ranges is a direct consequence of this property.

It becomes increasingly evident that, in order to complete the picture of magnetron response to various operating conditions, at least two more problems must be discussed. It is necessary to be able to calculate the current which will be induced in a circuit by a given spoke configuration. The spoke configuration is determined by the r-f potential which the current induces in the circuit. Therefore, certain specific circuit properties must be achieved in order to produce particular types of behavior in the phase-focussing diagram illustrated by the examples in this section. The induced current and circuit problems are treated in the next chapter, with particular reference to the final definition of frequency pushing and voltage tuning. It is evident that the conditions just described are those required for voltage tuning and that the conditions described in Section 2.5 in connection with Figs. 2.10 and 2.11 are those required for frequency pushing. Before discussing these phenomena in detail, however, the present analysis will be completed by a brief discussion of the space-charge-free energy distribution of the cylindrical magnetron.

---

[1] I, 2, p 217.

Case II - Cylindrical Magnetron. The dependence of the angular velocity of the electron on radius and, therefore, the radius for which this velocity is achieved is not affected by the presence of a field gradient at the cathode if it is assumed that initial velocities are zero. Eqs 2.27 and 2.28 are still valid in the space-charge-free case. The equation for the synchronism anode potential, however, must be modified to account for the logarithmic potential distribution which must now exist between anode and cathode. Making use of this fact, we may write,

$$\phi_{an} = \phi_n \frac{\ln \frac{r_a}{r_c}}{\ln \frac{r_n}{r_c}} .$$

But

$$\phi_n = \frac{1}{2} m \omega_n^2 r_n^2 = \frac{1}{2} m \omega_n^2 r_a^2 \frac{r_n^2}{r_c^2} \cdot \frac{r_c^2}{r_a^2} = \phi_o \frac{r_n^2}{r_c^2} \cdot \frac{r_c^2}{r_a^2} .$$

r_n/r_c can be written in terms of magnetic field by reference to Eq 2.28. Making this substitution, the following results.

$$\phi_{an} = \frac{r_c^2}{r_a^2} \frac{\frac{1}{2} m \omega_n^2 r_a^2}{1 - \frac{2m}{Be} \omega_n} \frac{\ln r_a/r_c}{\ln \sqrt{\frac{1}{1 - \frac{2m}{Be} \omega_n}}} . \qquad (2.65)$$

In dimensionless variables

$$\frac{\phi_{an}}{\phi_o} = \frac{r_c^2}{r_a^2} \frac{B/B_o}{\frac{B}{B_o} - \left(1 - \frac{r_c^2}{r_a^2}\right)} \frac{\ln \frac{r_a}{r_c}}{\ln \sqrt{\frac{B/B_o}{B/B_o - \left(1 - \frac{r_c^2}{r_a^2}\right)}}} \qquad (2.65a)$$

Typical energy distribution curves are plotted in Fig. 2.16. The discussion of these curves would follow very closely the line of discussion of the

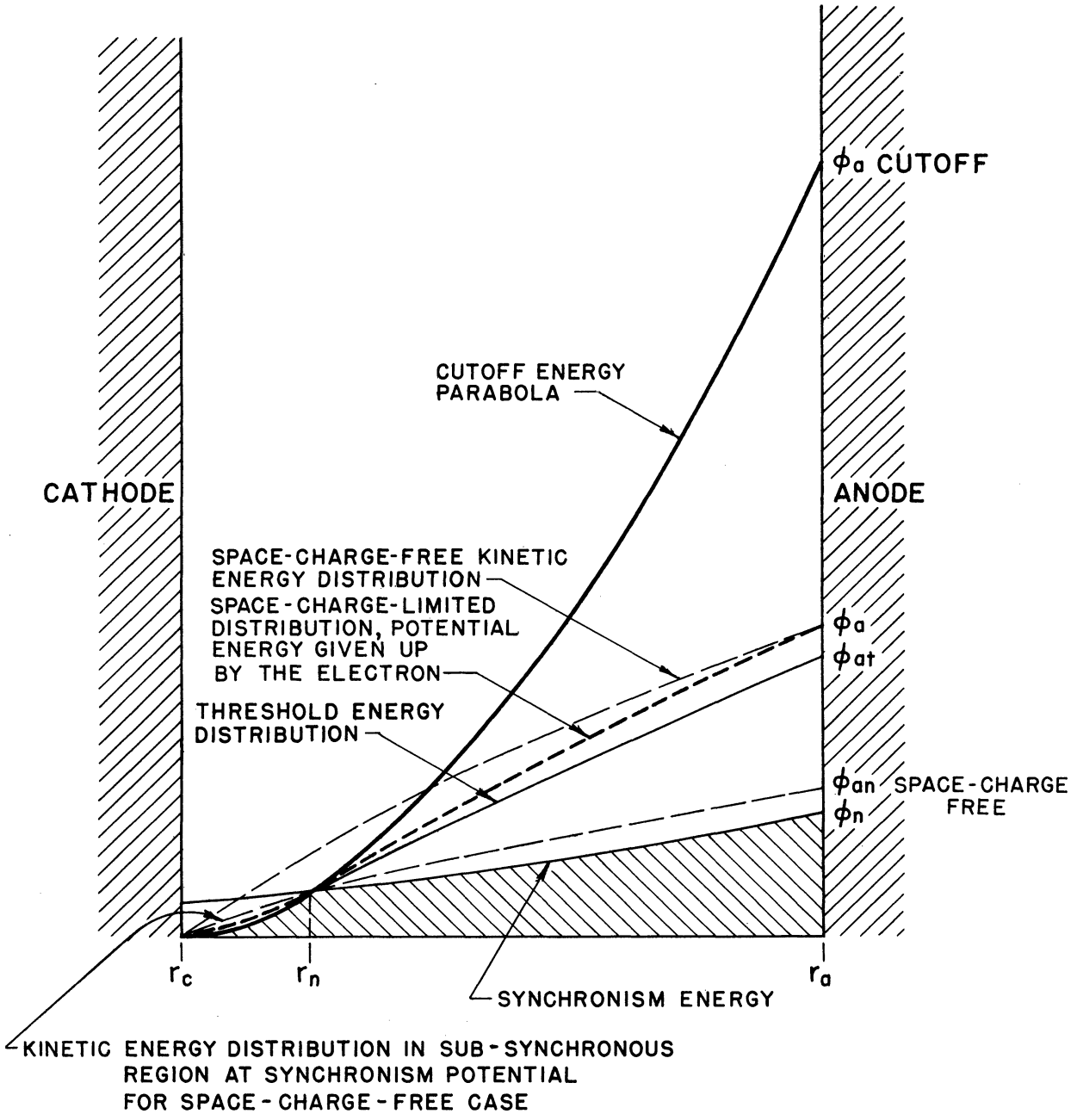

FIG. 2.16
ENERGY DISTRIBUTIONS IN THE CYLINDRICAL MAGNETRON
(IN RELATIVE ELECTRON VOLTS)

planar case. The major physical difference is in the necessity for the presence of a finite space-charge density in the spokes in the cylindrical magnetron. This is necessary even as the magnetron is just starting, since the energy of the electron corresponding to its position increases as the square of the radius in order to maintain synchronism. The potential distribution curve will have a smaller slope than the logarithmic curve at any position. This must be accounted for by the presence of the space charge. The difference in potential required to maintain synchronism energy and the space-charge-free potential distribution is accented by the downward flexion of the logarithmic distribution. In order for the average potential throughout the space to be as great as the potential corresponding to the synchronism energy, it is necessary for the anode to exceed the synchronism anode potential. The potential must be raised still further to meet the threshold condition. As a consequence, there will be a relatively large proportion of the electrons travelling at super-synchronous velocities just before the threshold is reached and the magnetron takes off. Immediately after the takeoff the distribution inside is altered completely, particularly so under temperature-limited conditions. A quite appreciable space-charge density must exist in the spokes so that the induced current and consequently the r-f potential must immediately assume appreciable values. The overall conclusion is that the cylindrical magnetron will be expected to "jump" into oscillation, whereas the planar magnetron may go through a quite smooth transition. This conclusion can be extended to say that a magnetron with relatively large ratio of anode-to-cathode radius, say greater than 1.5 to 1, will be expected to jump into oscillation at finite anode current,

whereas a magnetron which physically approaches the planar case, say $r_a/r_c < 1.5$ to 1, will experience a smooth transition with oscillation at very low anode currents.

Once the magnetron has started oscillating, the remarks relating to the phase-focussing diagrams of Fig. 2.15 still apply. The description of starting given in connection with Fig. 2.14 is, however, no longer accurate.

This concludes the discussion of the phase-focussing mechanism and the effects of limiting the available current. In the next chapter, the methods and concepts developed here will be applied to the examination of magnetron behavior under various circuit conditions.

3. THEORETICAL ANALYSIS RELATING THE PHASE-FOCUSSING MECHANISM TO THE R-F CIRCUIT ADMITTANCE CHARACTERISTIC

3.1 Basic Theory for Induced-Current Calculations

When the transit time of the electron in a vacuum tube begins to occupy an appreciable fraction of the r-f cycle it becomes necessary to apply techniques to the analysis of the electron behavior which are not necessary at low frequencies. The development of these techniques of analysis has gone hand in hand with the development of new tube types and the generation of higher frequencies by older tube types during the past twenty years. As a result several papers have appeared which treat the theory of induced currents due to moving charge distributions. At the suggestion of the author, this theory has recently been applied to the magnetron by Mr. H. W. Batten, Mr. W. Peterson, and Mr. S. Ruthberg of the University of Michigan laboratory.[1]

It should be stated at the outset that if the space-charge distribution is known the theory of induced currents permits an exact calculation of the effect of the electrons on the circuit. The accuracy of the results, therefore, is limited by the accuracy of prediction possible in the theory of phase focussing and not by the results of application of induced-current theory.

---

[1] III, 22, c. Sections 11 and 12, pp 73-93.

For the general treatment of induced-current theory the reader is referred to a comprehensive article by Gabor[1] and to articles by S. Ramo,[2] W. Shockley,[3] and C. K. Jen.[4] A brief but complete derivation of a formula applicable to an arbitrary geometry has been developed by H. W. Batten and W. Peterson.[5] Their results will be used in the following discussion. The results of all treatments must be basically the same. However, the choice of the most convenient form may greatly simplify the actual calculations. An excellent treatment by Chao-Chen Wang[6] applicable to tubes containing grids in parallel plane geometry is an example. In this treatment the choice of an integration over time, rather than the conventional integration over space, makes a substantial simplification in the problem. In contrast, the magnetron problem lends itself more readily to an integration over space.

Let us consider an arbitrary system of electrodes, as shown in Fig. 3.1. These electrodes are represented as connected together by a circuit. The circuit may consist only of the capacitance between electrodes, but in the system of Fig. 3.1, it is assumed to be entirely included in the impedances Z_{12}, Z_{13}, and Z_{23}. Once the currents are known, the relative electrode potentials can be calculated by computing the drop through the impedances.

---

1 IV, 4, b.

2 IV, 10.

3 IV, 11.

4 IV, 12.

5 III, 22, c. Section 10, pp 65-73.

6 IV, 12.

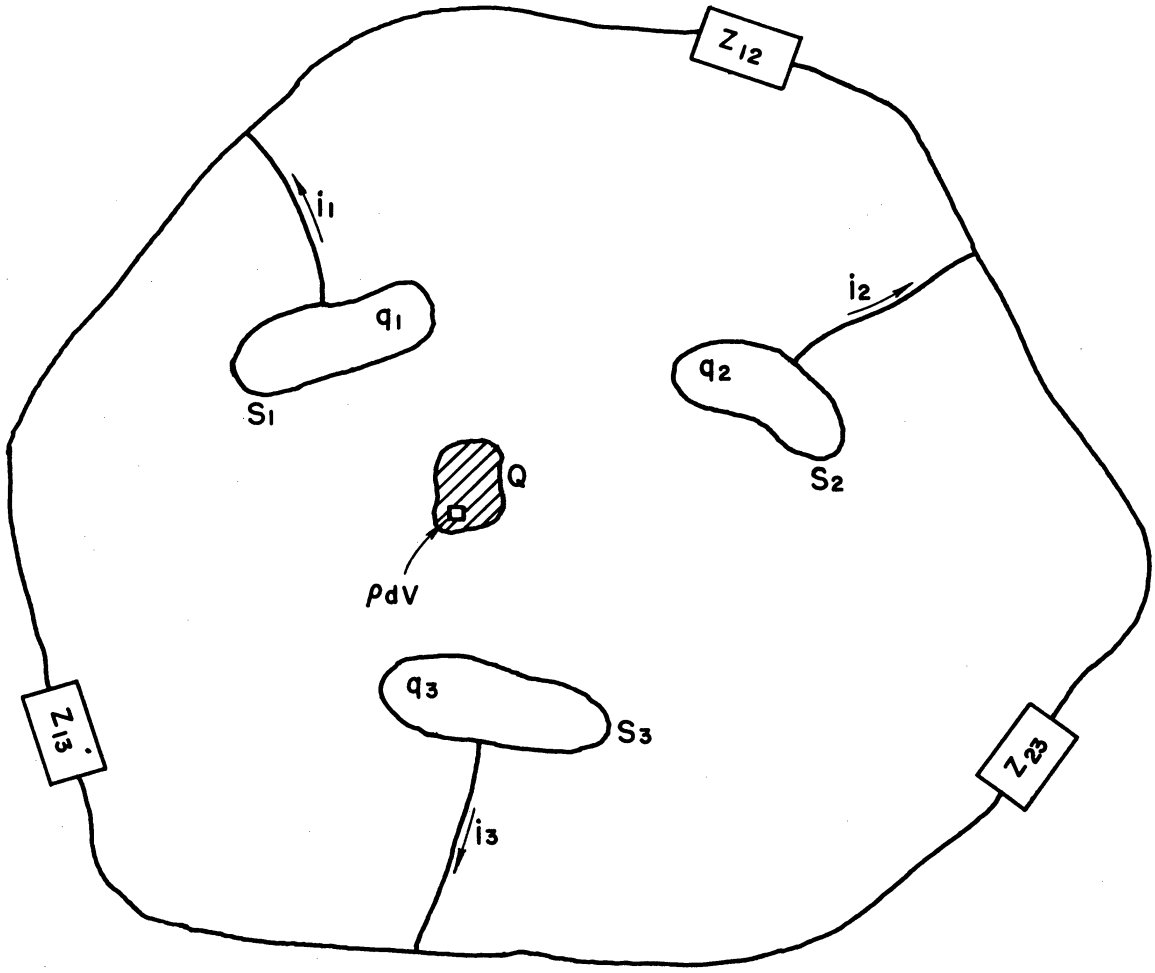

FIG. 3.1
ARBITRARY SYSTEM OF ELECTRODES USED IN THE DEVELOPMENT OF THE INDUCED CURRENT EQUATION

In order to compute the induced current, the field due to the charge distribution and the field due to the potentials on the electrodes, are considered quite separately. The flux through a given electrode surface S_k must be equal to the charge on that surface.

$$q_k = -\int_{S_k} D_n \, dS_k \, , \tag{3.1}$$

where D_n is the component of the displacement vector normal to the surface S_k and directed inward. The integration can be made over all space by the introduction of a potential function ψ_k which has the following properties

ψ_k = unity on S_k

= 0 on all other electrodes, and satisfies the Laplace equation throughout the interaction region.

ψ_k is <u>not</u> an electrical potential.

Eq 3.1 becomes

$$q_k = -\int_{S_k} D_n \, dS_k = -\int_{S} \psi_k \, D_n \, dS \, ,$$

where the integration is now over the entire surface, including the surface at infinity. By Gauss' theorem

$$q_k = -\int_{V} \mathrm{div}(\psi_k \vec{D}) \, dV \, .$$

Using a vector identity,

$$q_k = -\int_V \vec{D} \text{ grad } \psi_k \, dV - \int_V \psi_k \text{ div } \vec{D} \, dV .$$

The first term on the right can be shown to vanish if both $\vec{D}$ and ψ_k vanish at infinity.[1] We have also

$$\text{div } \vec{D} = \rho .$$

Therefore,

$$q_k = -\int_V \psi_k \rho \, dV .$$

where ρ is the charge density at a point in the interaction region. The induced current i_k leaving S_k is given by

$$i_k = -\frac{dq_k}{dt} = \frac{d}{dt}\int_V \psi_k \rho \, dV . \qquad (3.2)$$

The electrode will also gain charge by the collection of electrons from the interaction space. The total current will, therefore, be given by

$$i_k = \int_{S_k} (\rho v)_n \, dS_k + \frac{\partial}{\partial t}\int_V \psi_k \rho \, dV . \qquad (3.3)$$

3.2 Application of the Theory of Induced Currents to the Magnetron

The picture of the space-charge distribution which was developed in Chapter 2 is shown in the cylindrical multianode geometry in Fig. 3.2.

---

[1] II, 22, c, p 70.

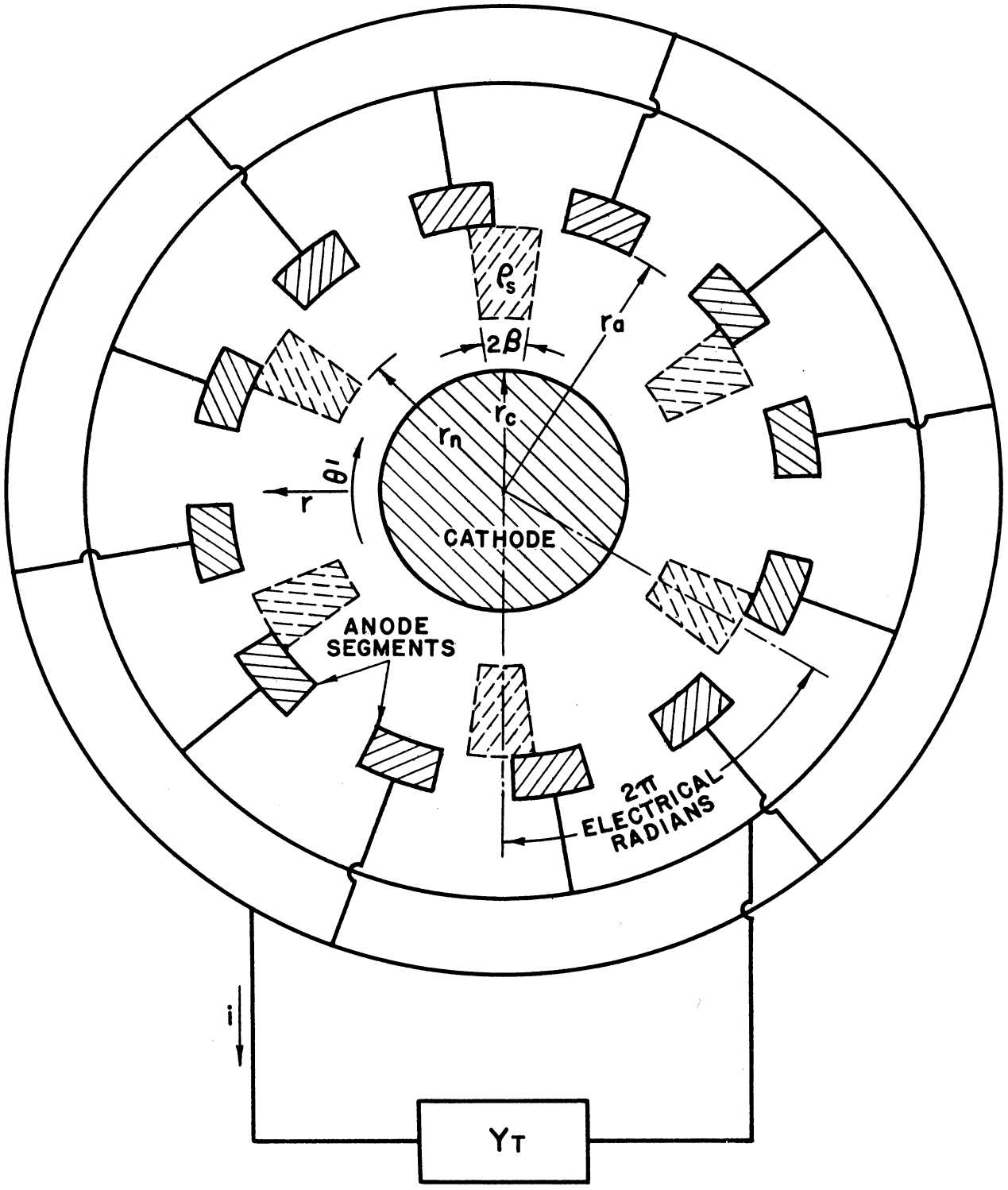

FIG. 3.2
SPACE-CHARGE SPOKE CONFIGURATION, ELECTRODE GEOMETRY, AND CIRCUIT ASSUMED IN SECTIONS 3.2 AND 3.3

It is assumed that the discharge is a steady-state process; i.e., the charge distribution in the spokes is constant, although there is a relatively slow transport of charge through the spokes to the anodes, contributing to the d-c current. Thus the time rate of change of the displacement vector on the anode, hence the induced current, is caused by the rotation of the spokes. The magnetron is assumed to be operating in the π mode, so that the circuit admittance can be correctly represented as connected between alternate anodes, connected in parallel. In this mode of operation it is therefore convenient to choose ψ_k as unity on one set of anode segments consisting of every other anode segment and zero on the others. Thus ψ_k and ρ are both periodic and can be given as Fourier expansions in a two-dimensional problem. At each value of the radius r in the interaction space

$$\psi_k = \sum_n A_n \cos n \frac{N}{2} \theta \, . \tag{3.4}$$

The A's are functions of r only; the angular measure is chosen so that ψ_k is symmetric around $\theta = 0$. The charge distribution at a particular value of r in the interaction space will be given by

$$\rho = \sum_a B_a \cos a \frac{N}{2} \theta' + \sum_a C_a \sin a \frac{N}{2} \theta' \, , \tag{3.5}$$

in the moving reference frame.

$$\theta' = \theta - \omega_n t$$

$$= \theta \text{ when } t = 0.$$

Note that ρ is not necessarily symmetric, and that the B_a's and C_a's may be functions of r. It is assumed that there is no variation in the axial

direction. Thus, if L is the axial length of the magnetron interaction space, we have for the induced current, from Eq 3.2

$$i = \frac{\partial}{\partial t} \int_{-\pi}^{\pi} \int_{r_n}^{r_a} \psi_k \rho L \, r dr d\theta \, . \tag{3.6}$$

Substitution of the Fourier expansions into this expression gives

$$i = L \frac{\partial}{\partial t} \sum_{na} \int_{-\pi}^{\pi} \int_{r_1}^{r_2} A_n \cos n \frac{N}{2} \theta \left[B_a \cos a \frac{N}{2} \theta' + C_a \sin a \frac{N}{2} \theta' \right] r dr d\theta \, .$$

Since the coefficients A's, B's and C's are independent of θ' all terms vanish for $a \neq n$ by orthogonality conditions. Therefore,

$$i = L \frac{\partial}{\partial t} \sum_{n} \left[\int_{-\pi}^{\pi} \cos n \frac{N}{2} \theta \cos n \frac{N}{2} \theta' \int_{r_1}^{r_2} A_n B_n \, r dr + \int_{-\pi}^{\pi} \cos n \frac{N}{2} \theta \sin n \frac{N}{2} \theta' \int_{r_1}^{r_2} A_n C_n \, r dr \right] .$$

This may be simplified to

$$i = L \pi \frac{\partial}{\partial t} \sum_{n} \left[\cos n \frac{N}{2} \omega_n t \int_{r_1}^{r_2} A_n B_n \, r dr - \sin n \frac{N}{2} \omega_n t \int_{r_1}^{r_2} A_n C_n \, r dr \right] . \tag{3.7}$$

The coefficients B_n and C_n are:

$$B_n = \frac{N}{2\pi} \int_{-\frac{2\pi}{N}}^{\frac{2\pi}{N}} \rho(r\theta') \cos n \frac{N}{2} \theta' \, d\theta' \qquad (3.8)$$

$$C_n = \frac{N}{2\pi} \int_{-\frac{2\pi}{N}}^{\frac{2\pi}{N}} \rho(r\theta') \sin n \frac{N}{2} \theta' \, d\theta' \, . \qquad (3.9)$$

The A_n's are determined by solution of Laplace's equation for ϕ_k.

The important component of the induced current is the fundamental

$$i_1 = - L \pi \frac{N}{2} \omega_n \left[\sin \frac{N}{2} \theta_1 \int_{r_1}^{r_2} A_1 B_1 \, r dr \right.$$

$$\left. + \cos \frac{N}{2} \theta_1 \int_{r_1}^{r_2} A_1 C_1 \, r dr \right] . \qquad (3.10)$$

The amplitude coefficient for the sine term is

$$I_1 = L \pi \frac{N}{2} \omega_n \int_{r_1}^{r_2} A_1 B_1 \, r dr \, . \qquad (3.11)$$

The amplitude coefficient for the cosine term is exactly the same with the substitution of C_1 for B_1.

By introduction of the total charge in the spokes Q and the relationship $2\pi f = \frac{N}{2} \omega_n$ the amplitude of the fundamental component of the induced current can be expressed in the following simple form.

$$I_1 = 4\,Qf\left[\left(\int_{r_1}^{r_2}\frac{\pi A_1}{2}\frac{\pi B_1}{Q}\,L\,rdr\right)^2 + \left(\int_{r_1}^{r_2}\frac{\pi A_1}{2}\cdot\frac{\pi C_1}{Q}\,L\,rdr\right)^2\right]^{1/2}. \qquad (3.12)$$

The factor in the brackets has been shown by Peterson[1] to be always less than unity. Thus 4 Qf is the maximum r-f induced current available and the factor in the brackets represents a sort of figure of merit for the induced current in a particular set of circumstances.

Approximate form for A_n. The coefficient A_n in the expansion for ψ_k can be approximated if ψ_k is presumed to have the distribution shown in Fig. 3.3 at the anode radius. The assumed linear variation in potential between anodes is substantiated by field maps of the magnetron interaction space.[2] A_n is determined by the solution of the equation $\nabla^2 \psi_k = 0$ with the boundary conditions of Fig. 3.3 and $\psi_k = 0$ in the cathode. It is assumed that ψ_k is a separable function of r and θ in the solution. The result for A_n is

$$A_n = \frac{R^{n\frac{N}{2}} - R^{-n\frac{N}{2}}}{R_a^{n\frac{N}{2}} - R_a^{-n\frac{N}{2}}}\cdot\frac{\sin\frac{n\pi}{2}}{n\frac{\pi}{2}}\cdot\frac{\sin n\frac{N}{2}\alpha}{n\frac{N}{2}\alpha}. \qquad (3.13)^3$$

---

1 II, 22, c, p 78.

2 See J. S. Needle, "A New Single-Cavity Resonator for a Multianode Magnetron", Technical Report No. 6, Electron Tube Laboratory, Dept. of Elec. Eng., Univ. of Michigan, Fig. 7.2a, January, 1951.

3 II, 22, c, p 80.

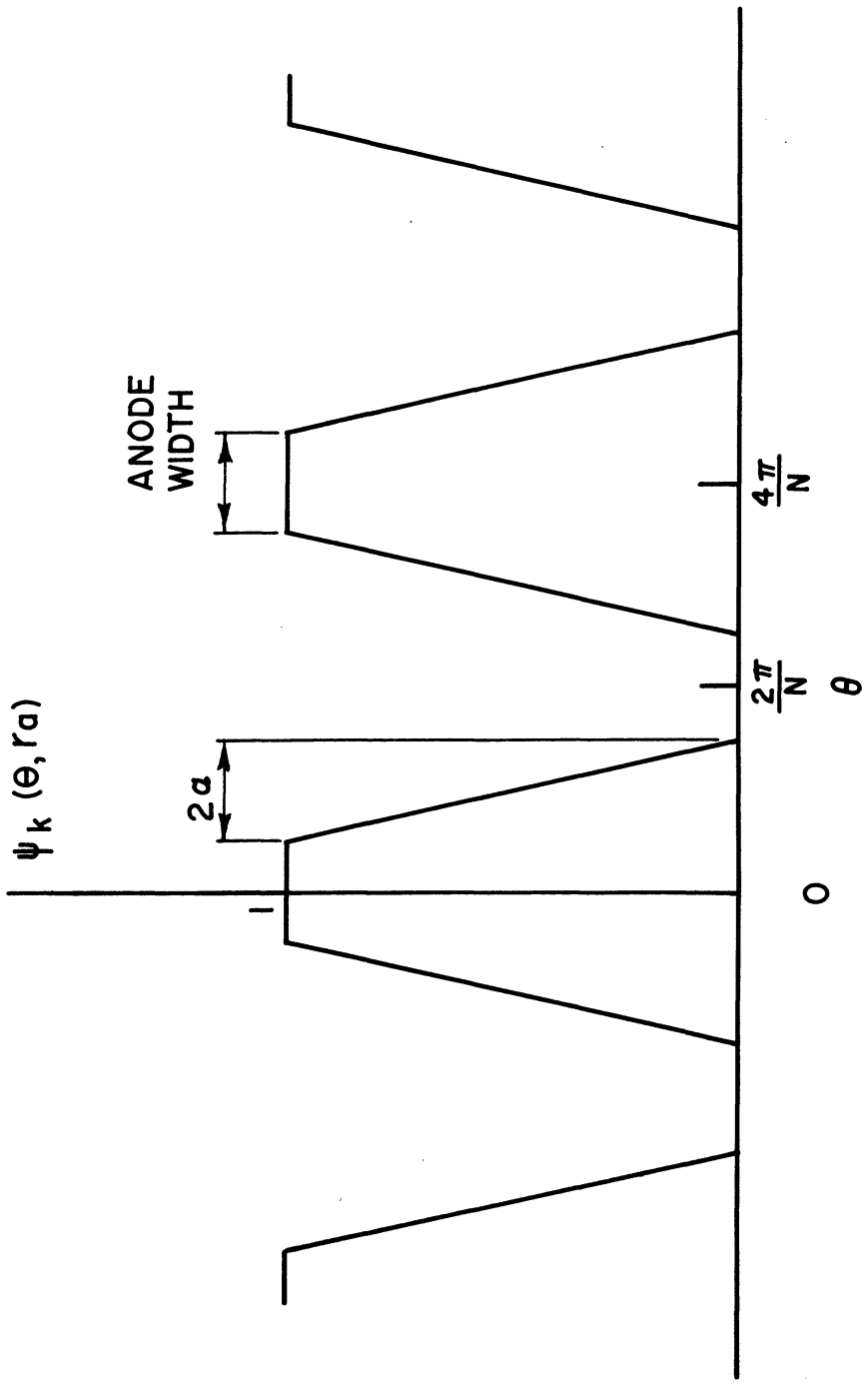

FIG. 3.3
ANGULAR VARIATION OF ψ_k AT ANODE RADIUS

where

$$R = \frac{r}{r_c}$$

$$R_a = \frac{r_a}{r_c} .$$

For the fundamental, given by Eq 3.12, n = 1. The value of $R^{\frac{N}{2}} - R^{-\frac{N}{2}}$ for several values of $\frac{N}{2}$ is plotted in Fig. 3.4. $\frac{\sin \alpha}{\alpha}$ is plotted in Fig. 3.5.

$$A_1 = \frac{R^{\frac{N}{2}} - R^{-\frac{N}{2}}}{R_a^{\frac{N}{2}} - R_a^{-\frac{N}{2}}} \frac{2}{\pi} \frac{\sin \frac{N}{2}\alpha}{\frac{N}{2}\alpha} . \qquad (3.14)$$

Inspection of this quantity shows that it is always less then unity.

Calculation of B_n and C_n. If it is assumed that the space-charge density distribution discussed in Section 2.6 exists in the interaction region, B_n and C_n can be readily calculated. Since the spokes are symmetrically placed the C_n's are zero. With reference to Fig. 3.2, the B_n's can be calculated as follows:

$$B_n = \frac{N}{2\pi} \int_{-\beta}^{\beta} \rho_s \cos n \frac{N}{2} \theta' \, d\theta' = \frac{2 \rho_s}{n\pi} \sin n \frac{N}{2} \beta , \qquad (3.15)$$

where ρ_s = the average charge density in the spokes. ρ_s is related to ρ, the average charge density within the interaction space, by

$$\rho_s = \frac{2\pi}{N\beta} \rho . \qquad (3.16)$$

The total charge in the spokes is

$$Q = \frac{N}{2} \rho_s r_c^2 (R_a^2 - R_n^2) \beta L . \qquad (3.17)$$

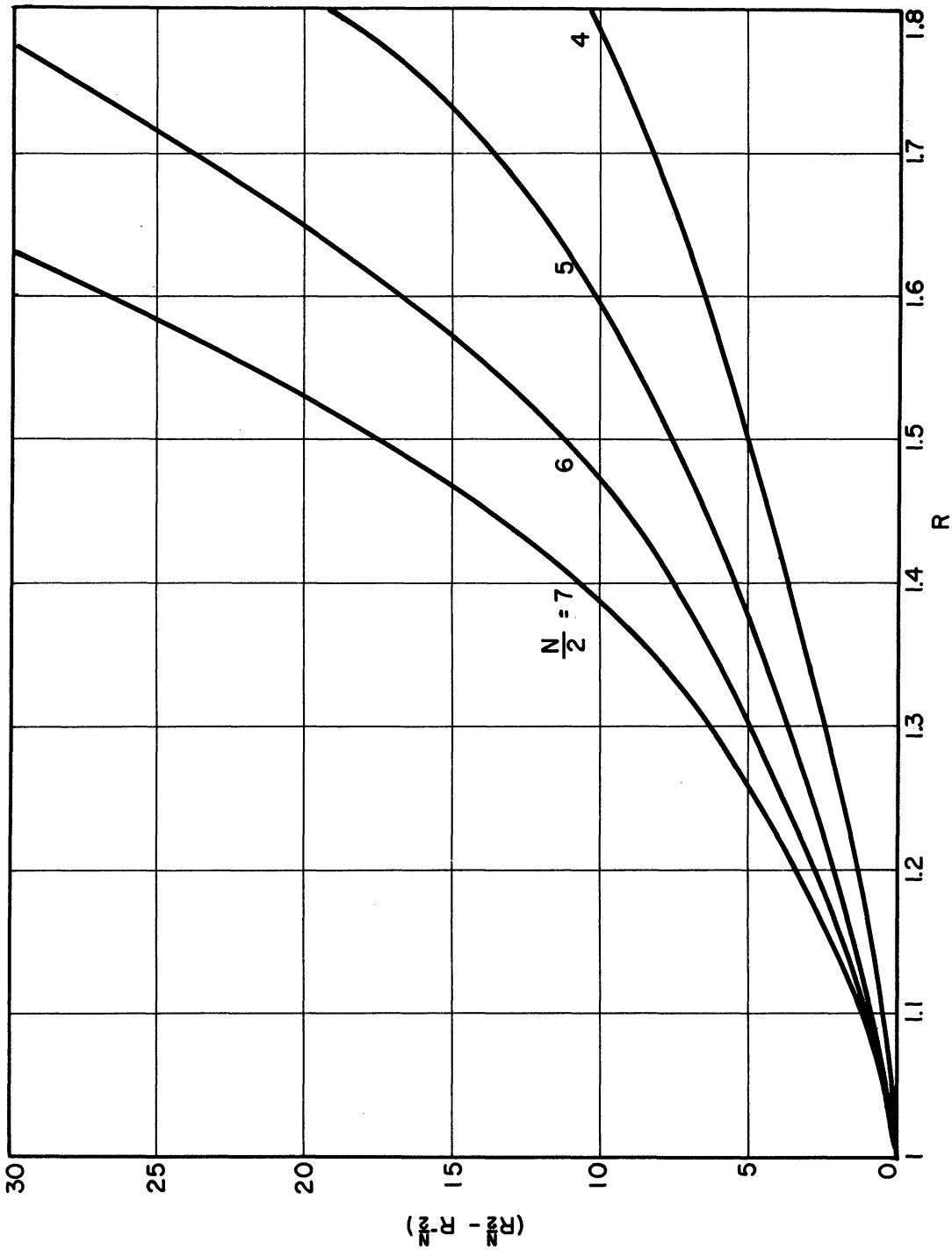

FIG. 3.4
FACTOR PRESENT IN EQUATION (3.13)

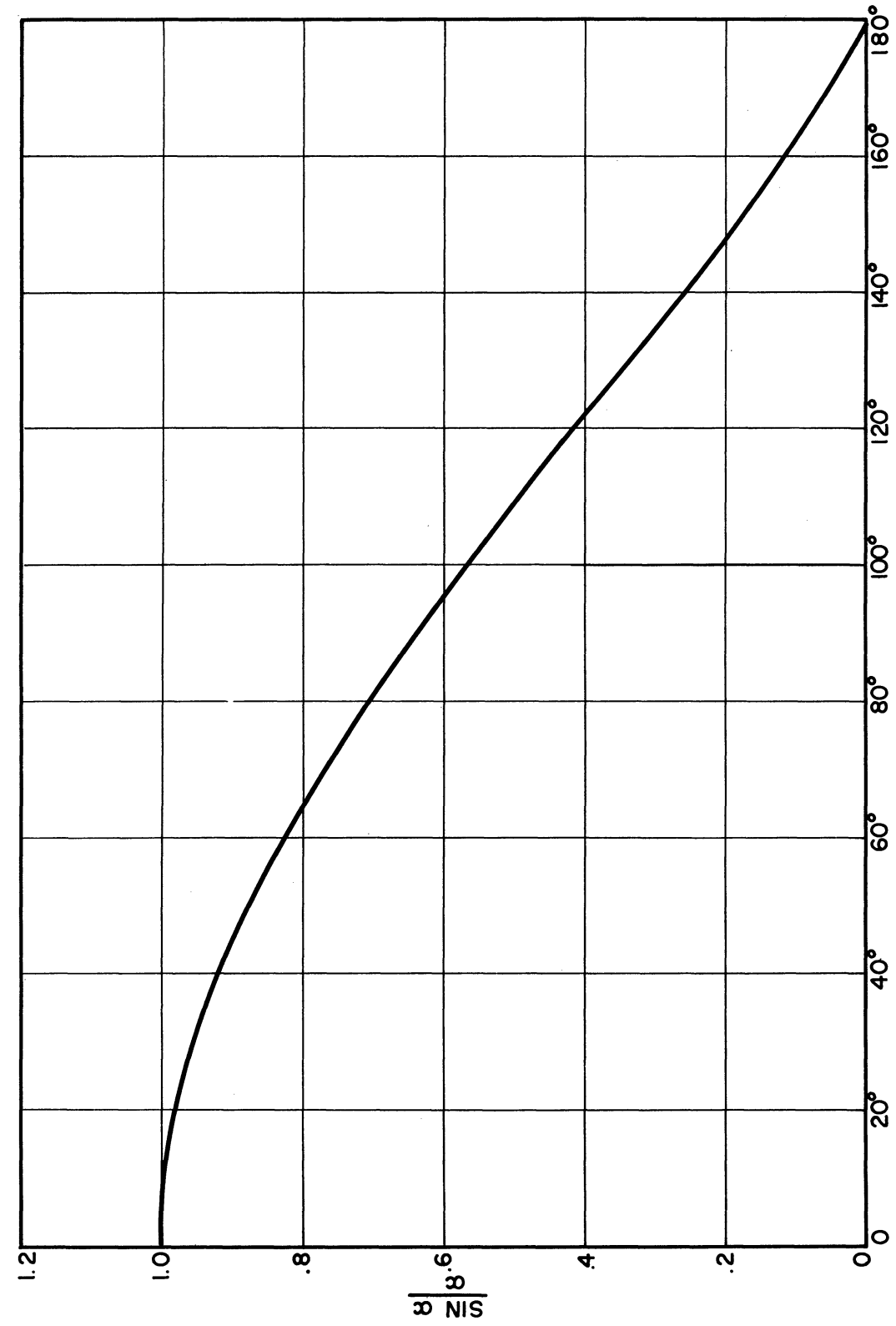

FIG. 3.5
FACTOR PRESENT IN EQUATIONS 3.13 & 3.20

We have, therefore,

$$\frac{B_n}{Q} = \frac{2}{\pi L\, r_c^2} \frac{1}{R_a^2 - R_n^2} \frac{\sin n \frac{N}{2} \beta}{n \frac{N}{2} \beta} . \qquad (3.18)$$

Final Expression for Fundamental Component of Induced Current.

The fundamental component of induced current is from 3.12, 3.14 and 3.18.

$$I_1 = 8Qf \frac{\sin \frac{N}{2} \alpha}{\frac{N}{2} \alpha} \frac{\sin \frac{N}{2} \beta}{\frac{N}{2} \beta} \int_{R_n}^{R_a} \frac{R^{\frac{N}{2}} - R^{-\frac{N}{2}}}{R_a^{\frac{N}{2}} - R_a^{-\frac{N}{2}}} \frac{R}{R_a^2 - R_n^2} dR .$$

But Q is given by 3.17. Thus, after integration

$$I_1 = 8L\, r_c^2\, f\, \rho_s \sin \frac{N}{2} \beta \frac{\sin \frac{N}{2} \alpha}{\frac{N}{2} \alpha} \frac{1}{R_a^{\frac{N}{2}} - R_a^{-\frac{N}{2}}}$$

$$\left[\frac{R_a^{2 + \frac{N}{2}}}{2 + \frac{N}{2}} - \frac{R_a^{2 - \frac{N}{2}}}{2 - \frac{N}{2}} - \frac{R_n^{2 + \frac{N}{2}}}{2 + \frac{N}{2}} + \frac{R_n^{2 - \frac{N}{2}}}{2 - \frac{N}{2}} \right] . \qquad (3.19)^1$$

In this expression the effect of the space-charge-density distribution and the effect of the electrode geometry are essentially separable. The space-charge distribution appears in the factor

$$\rho_s \sin \frac{N}{2} \beta$$

and the terms involving R_n in the remainder of the expression.

---

1 A more complete discussion of the derivation of this equation is given in reference III, 22, c, Section 11. The application of this result to the special case of a point charge and an approximate method useful in the treatment of odd-shaped spokes are also discussed in this reference.

There is little question as to the validity of the use of R_n as an inner boundary in the integration. Moreover, R_n is substantially constant for the ranges of frequencies generally encountered at constant magnetic field. On the other hand, the terms including ρ_s and β change substantially over a typical volt-ampere characteristic and bear further discussion. It is the variation in these terms which causes the characteristics of the magnetron space charge as an induced-current generator to differ from the characteristics of a constant-current generator.

Substituting for ρ_s from Eqs 3.16 and 2.58, we have

$$\rho_s \sin \frac{N}{2}\beta = \pi \rho_o \left[1 + \frac{4 \epsilon_o r_c^2}{\rho_o} \frac{\phi_a - \phi_{at}}{R_a^2 - R_n^2}\right] \frac{\sin \frac{N}{2}\beta}{\frac{N}{2}\beta}. \qquad (3.20)$$

The maximum width of a spoke (βN) is 180 electrical degrees. Thus the maximum expected value of $\frac{\beta N}{2}$ is 90°. The quantity $\frac{\sin \frac{N\beta}{2}}{\frac{N\beta}{2}}$ decreases as β increases such that, from Fig. 3.5,

$$1 > \frac{\sin \frac{N}{2}\beta}{\frac{N}{2}\beta} > \frac{2}{\pi}.$$

The expected range of the quantity in the parenthesis, as indicated by Fig. 2.12, is approximately from .9 to 1.3. This quantity increases as β increases tending to balance the effect of the variation in $\frac{\sin \frac{N}{2}\beta}{\frac{N}{2}\beta}$.

Note that $\frac{\beta N}{2} = \frac{\pi}{2} + \theta$ (Eq 2.47), so that

$$\frac{\sin \frac{\beta N}{2}}{\frac{\beta N}{2}} = \frac{\cos \theta}{\frac{\pi}{2} + \theta}.$$

This will be used in later development.

We now have a chain of relationships represented in Eqs 3.19, 3.20, 2.48, 2.49 and 2.50 which relate r-f potential and r-f current to the d-c potential, the electrode geometry and the circuit impedance. The magnetic field enters into the parameters ρ_o and ϕ_{at}. If electronic efficiency is estimated the d-c current can be estimated. In order to complete the analysis some discussion of the expected phase and admittance characteristics of the resonant circuit is necessary. This will be done in the next section.

3.3 Phase and Admittance Characteristics for the Magnetron Equivalent Circuit

In the discussion of the phase-focussing diagrams of Chapter 2 an obviously important characteristic of the behavior was found to be the relationship between the phase angle, θ, and the frequency. A second important characteristic is the relationship between frequency and the ratio of the induced r-f current to the r-f potential developed as a result of this current flowing through the circuit. In the last analysis the exact effect of changes in frequency and power level on the phase-focussing diagrams must be consistent with the properties of the circuit connected between the anode segments. It is necessary, therefore, to know the circuit phase and admittance characteristics before the effects of anode potential or anode current on frequency can be predicted.

A rigorous treatment of the microwave circuit in general requires the solution of Maxwell's equations or their equivalent in the form of transmission-line equations with the specified boundary conditions. In the case of magnetrons, in particular, it is usually possible to approximate the

circuit characteristics by a suitable network of inductances and capacitances arranged in an "equivalent circuit".

An essential feature of any magnetron seems to be the capacitance between the anode sets which is obviously present in any multianode set surrounding a cathode. (See, for example, Fig. 3.2.) The admittance connected to these anode sets, contained in the block labelled Y_T in Fig. 3.2, is invariably an inductive, or negative, susceptance and a conductance which absorbs the power generated by the magnetron space charge. The theory of phase focussing leads to the conclusion that this is a physically necessary condition, that is, the induced-current maximum must lag the r-f potential maximum if phase focussing is to occur. This was illustrated in the discussion pertaining to Figs. 2.8 and 2.9. This means that the phase angle θ in Eq 2.50,

$$\frac{I_1}{\phi_{r\text{-}f\ max}} = \left|Y_T\right| \angle\theta \,, \qquad (2.50)$$

is always negative. With this equation and the generalized equivalent circuit of Fig. 3.2 in mind the phase and admittance characteristics of representative equivalent circuits for the magnetron will be calculated.

A. Simple Parallel Resonant Circuit. Most conventional magnetron resonator structures are representable by the simple parallel resonant circuit of Fig. 3.6. This is particularly true of the type of c-w magnetron power tubes constructed in the University of Michigan Electron Tube Laboratory. These magnetrons consist of a single-cavity resonator, pill-box or coaxial in shape, loaded by a capacitance forming the multianode set. The anode set is justifiably considered a lumped capacitance since the dimensions are of the order of a tenth to an eighth of the free-space wavelength.

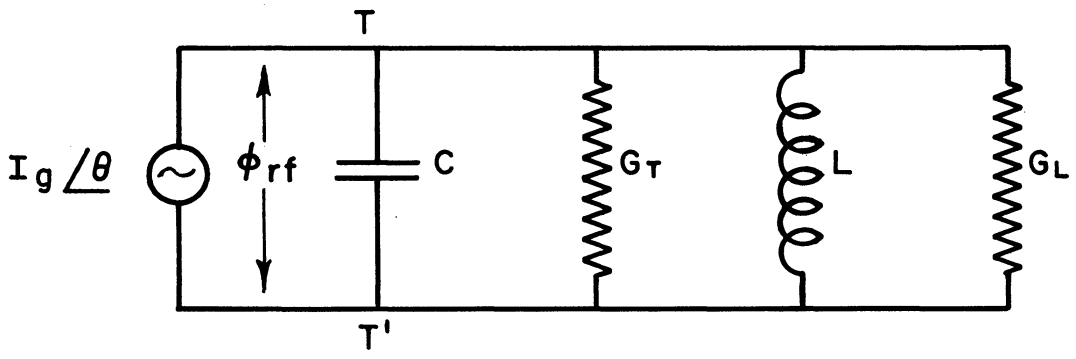

FIG. 3.6
EQUIVALENT CIRCUIT FOR OSCILLATING MAGNETRON

The frequency characteristic of the resonator considered as a short-circuited transmission line is closely approximated by the frequency characteristic of an inductance over the small range of frequencies covered by a resonance curve. It is convenient to represent the induced current, I_1, as a current generator with a phase angle referred to the r-f potential between circuit terminals. Thus

$$\frac{I_1}{\phi_{r\text{-}f\ max}} = |Y_T| \angle\theta = \frac{I_g \angle\theta}{\phi_{r\text{-}f}},$$

where I_g and $\phi_{r\text{-}f}$ are rms values. The admittance of the circuit of Fig. 3.6 can be shown to be

$$Y_T = |Y_T| \angle\theta \cong \frac{Y_{oc}}{Q_L}\sqrt{1 + 4\delta^2 Q_L^2}\ \angle\tan^{-1} 2\delta Q_L , \qquad (3.21)$$

where

$Y_{oc} = 2\pi f_o C = \sqrt{\frac{C}{L}}$ = characteristic admittance of circuit in mhos,

$2\pi f_o = \frac{1}{\sqrt{LC}}$ = angular resonance frequency in radians/sec,

$\delta = \frac{f - f_o}{f_o} = \frac{\lambda_o - \lambda}{\lambda_o}$ = fractional deviation of frequency from resonance frequency,

$Q_L = \frac{Y_{oc}}{G_T + G_L}$ = dimensionless quantity which is measure of sharpness of resonance of the circuit,

$Q_L = 2\pi \frac{\text{maximum energy stored in electric field}}{\text{energy dissipated in total conductance per cycle}}$.

The definition of Q_L must be handled with care in microwave resonators since the energy storage in the electric field is not in general taken care of by the energy stored in the lumped capacitance. A large fraction of the electrical energy storage may be in the transmission line which is represented by the inductance in Fig. 3.6. We have, for the phase and admittance characteristics of the simple parallel resonant circuit

$$\theta \cong \tan^{-1} 2\delta Q_L$$

$$|Y_T| \cong \frac{Y_{oc}}{Q_L}\sqrt{1 + 4\delta^2 Q_L^2} .$$

These are plotted in Fig. 3.7. The region of negative phase angle only is used, i.e., $f < f_o$.

The useful power is generated in the load conductance, G_L, and is given by

$$P_L = I_g \phi_{r-f} \cos\theta = \frac{I_g^2}{|Y_T|}\frac{G_L}{|Y_T|} ,$$

or

$$P_L = \frac{I_g^2}{\left(\frac{Y_{oc}}{Q_L}\right)^2 (1 + 4\delta^2 Q_L^2)} G_L . \qquad (3.22)$$

G_L is conveniently related to the experimentally measurable quantitity, Q_e, by

$$G_L = \frac{Y_{oc}}{Q_e} , \qquad (3.23)$$

where

$$Q_e = 2\pi \frac{\text{maximum energy stored in electric field}}{\text{energy dissipated in external load}} .$$

It is assumed that the load is not reactive in this definition. Q_e is determined from the measurable Q's, Q_L and Q_o through the relationship,

$$\frac{1}{Q_e} = \frac{1}{Q_L} - \frac{1}{Q_o} . \qquad (3.24)$$

$$Q_o = 2\pi \frac{\text{maximum energy stored in electric field}}{\text{energy dissipated in internal circuit losses}} ,$$

$$= Y_{oc}/G_T .$$

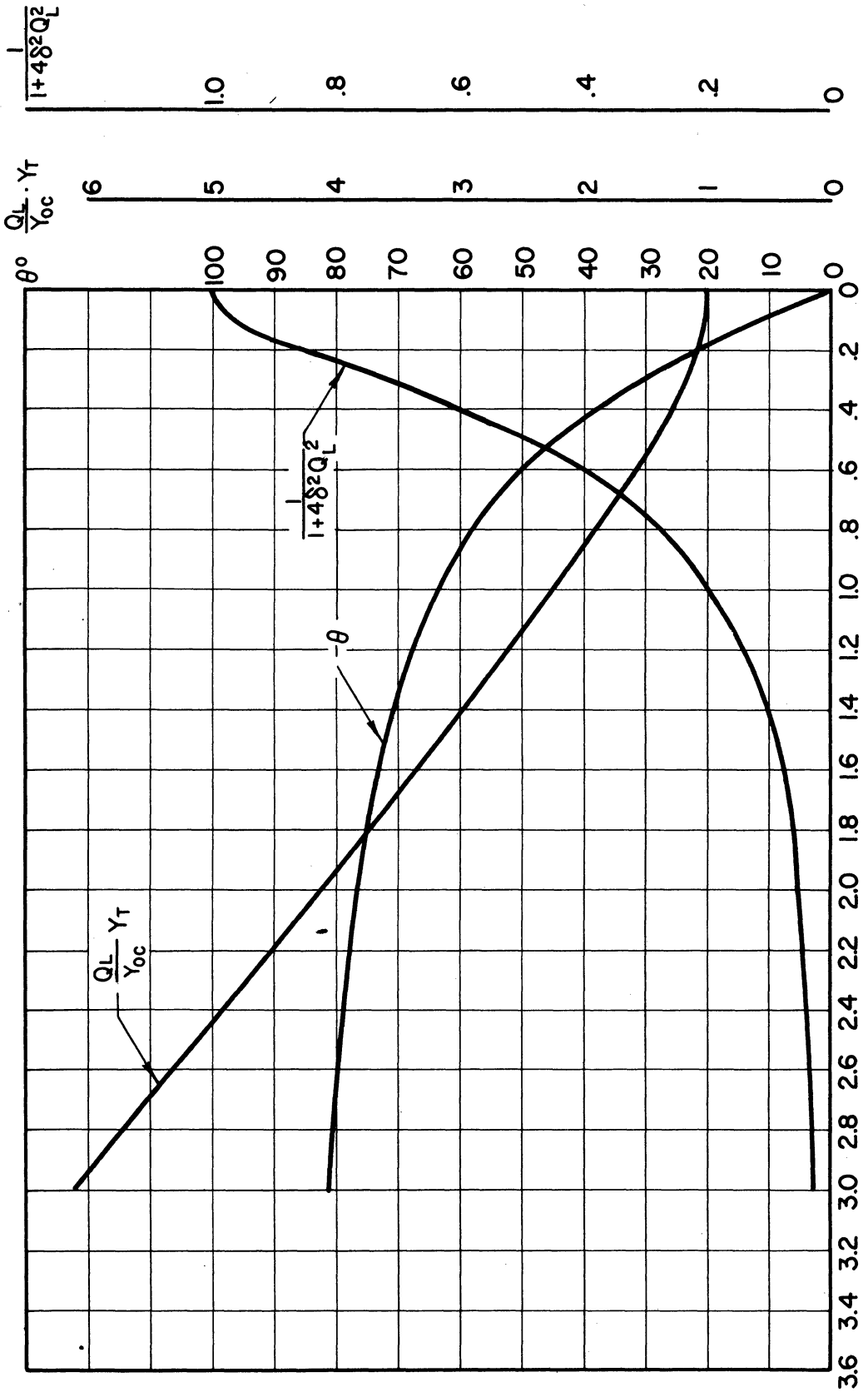

FIG. 3.7

PHASE AND ADMITTANCE CHARACTERISTICS FOR SINGLE PARALLEL RESONANT CIRCUIT

The power is related to the d-c anode current by

$$P_L = \eta \, \phi_a \, I_a \, , \tag{3.25}$$

where η is the overall efficiency.

$$\eta = \eta_e \, \eta_c$$

η_e = electronic efficiency

η_c = circuit efficiency

$$= \frac{Q_o - Q_L}{Q_o} \, .$$

We may write finally

$$P_L = \eta \, \phi_a \, I_a = \frac{I_g^2}{(Y_{oc}/Q_L)^2 \, (1 + 4\delta^2 \, Q_L^2)} \, \frac{Y_{oc}}{Q_e} \, . \tag{3.26}$$

This equation contains all measurable parameters except I_g. It, therefore, permits a calculation of I_g from experimental data if the assumptions leading to the equivalent circuit are correct. On the other hand, since

$$I_g = \frac{1}{\sqrt{2}} \, I_1 \tag{3.27}$$

and I_1 is expressed by Eq 3.19 with 3.20, it is also possible to calculate I_g for a set of phase-focussing diagrams which are consistent with the experimental observations. Thus a check on the theory is provided.

In general, I_g is related to frequency, the r-f potential, d-c potential and the phase angle. If the circuit is determined, the frequency, in turn, determines the phase angle. Whatever this dependence may be, the relationship between d-c current and frequency is strongly affected by the term

$$\frac{1}{1 + 4\delta^2 Q_L^2} .$$

This expression is plotted with the expressions for Y_T and θ in Fig. 3.7.

B. Double-Ended Non-Resonant Circuit. Another circuit of interest which has been studied in the University of Michigan laboratory is the "double-ended" circuit. A typical circuit in this category is shown in equivalent form in Fig. 3.8. The anode set is represented by the dotted capacitance. The circuit is assumed to be so far below resonance that this capacitance accepts a negligible amount of current. The load resistance R_L represents a matched transmission line connected directly to the terminals of the anode set. The other end of the circuit represented by R_T and X_T consists of a short-circuited transmission line. The resistance R_T represents the loss in this section and may purposefully be made large to obtain the desired phase or admittance characteristics.

The admittance seen from the terminals T - T' is given by

$$Y_T = \frac{1}{R_L} + \frac{1}{R_T + j X_T}$$

$$= \frac{1}{R_L} + \frac{R_T}{R_T^2 + X_T^2} - \frac{j X_T}{R_T^2 + X_T^2}$$

$$= \frac{1}{R_L} + \frac{1}{R_T} \frac{1}{1 + \frac{X_T^2}{R_T^2}} - j \frac{X_T}{R_T^2} \frac{1}{1 + \frac{X_T^2}{R_T^2}}$$

$$= \frac{1}{R_L} \frac{1}{1 + \frac{X_T^2}{R_T^2}} \left[1 + \frac{X_T^2}{R_T^2} + \frac{R_L}{R_T} - j \frac{R_L}{R_T} \frac{X_T}{R_T} \right]$$

$$Y_T R_L = \frac{1}{1 + \frac{X_T^2}{R_T^2}} \sqrt{\left[1 + \frac{X_T^2}{R_T^2} + \frac{R_L}{R_T} \right]^2 + \left[\frac{R_L}{R_T} \right]^2 \left[\frac{X_T}{R_T} \right]^2} \Big/ - \tan^{-1} \frac{R_L}{R_T} \frac{\frac{X_T}{R_T}}{1 + \frac{R_L}{R_T} + \frac{X_T^2}{R_T^2}}$$

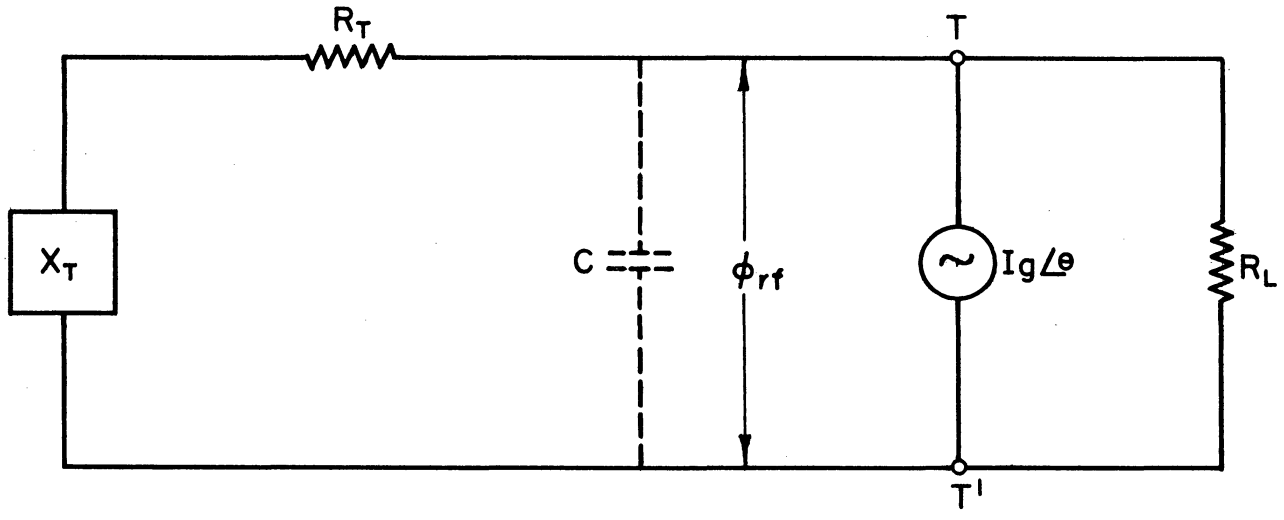

FIG. 3.8
EQUIVALENT CIRCUIT FOR DOUBLE ENDED OPERATION

The phase characteristic of this circuit is given by

$$\theta = - \tan^{-1} \frac{R_L}{R_T} \frac{\frac{X_T}{R_T}}{1 + \frac{R_L}{R_T} + \frac{X_T^2}{R_T^2}} , \tag{3.28}$$

$$|Y_T| \, R_L = \frac{1}{1 + \frac{X_T^2}{R_T^2}} \sqrt{\left(1 + \frac{X_T^2}{R_T^2} + \frac{R_L}{R_T}\right)^2 + \left(\frac{R_L}{R_T}\right)^2 \left(\frac{X_T}{R_T}\right)^2} . \tag{3.29}$$

For $R_T = 0$

$$\theta = - \tan^{-1} \frac{R_L}{X_T} , \tag{3.30}$$

$$|Y_T| \, R_L = \sqrt{1 + \left(\frac{R_L}{X_T}\right)^2} . \tag{3.31}$$

For $R_L = \infty$

$$\theta = - \tan^{-1} \frac{X_T}{R_T} , \tag{3.32}$$

$$|Y_T| \, R_T = \sqrt{1 + \left(\frac{X_T}{R_T}\right)^2} . \tag{3.33}$$

The maximum value for the phase angle can be determined by differentiating the argument of Eq 3.28 and setting the result equal to zero.

$$\frac{d}{d\left(\frac{X_T}{R_T}\right)} \frac{R_L}{R_T} \frac{\frac{X_T}{R_T}}{1 + \frac{R_L}{R_T} + \frac{X_T^2}{R_T^2}}$$

$$= \frac{\frac{R_L}{R_T}}{1 + \frac{R_L}{R_T} + \frac{X_T^2}{R_T^2}} - \frac{2 \frac{R_L}{R_T} \frac{X_T^2}{R_T^2}}{\left(1 + \frac{R_L}{R_T} + \frac{X_T^2}{R_T^2}\right)^2}$$

$$= 0 \text{ for maximum } \theta$$

$$\frac{R_L}{R_T} = \frac{X_T^2}{R_T^2} - 1 . \tag{3.34}$$

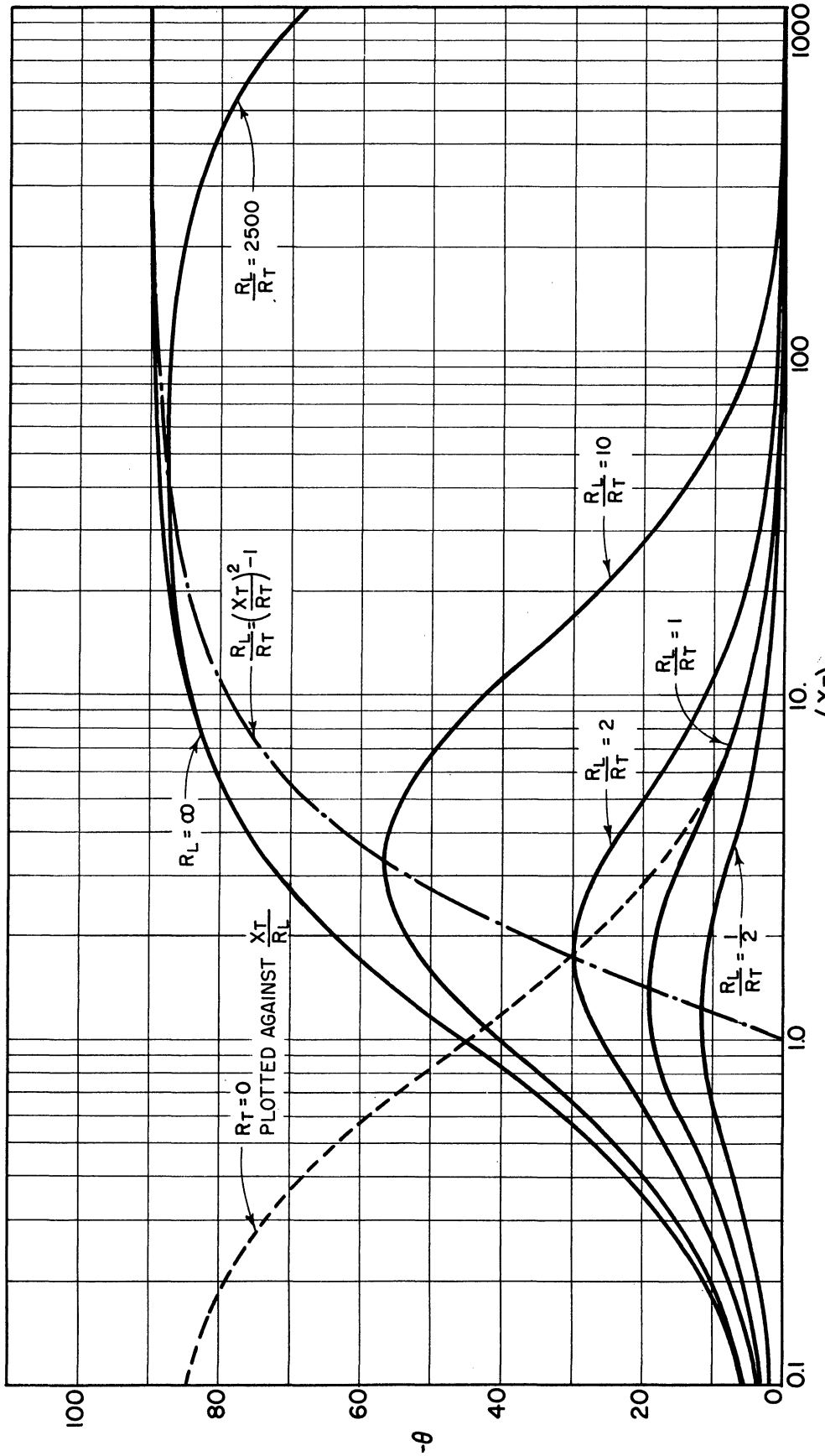

FIG. 3.9
PHASE CHARACTERISTICS FOR CIRCUIT OF FIG. 3.8

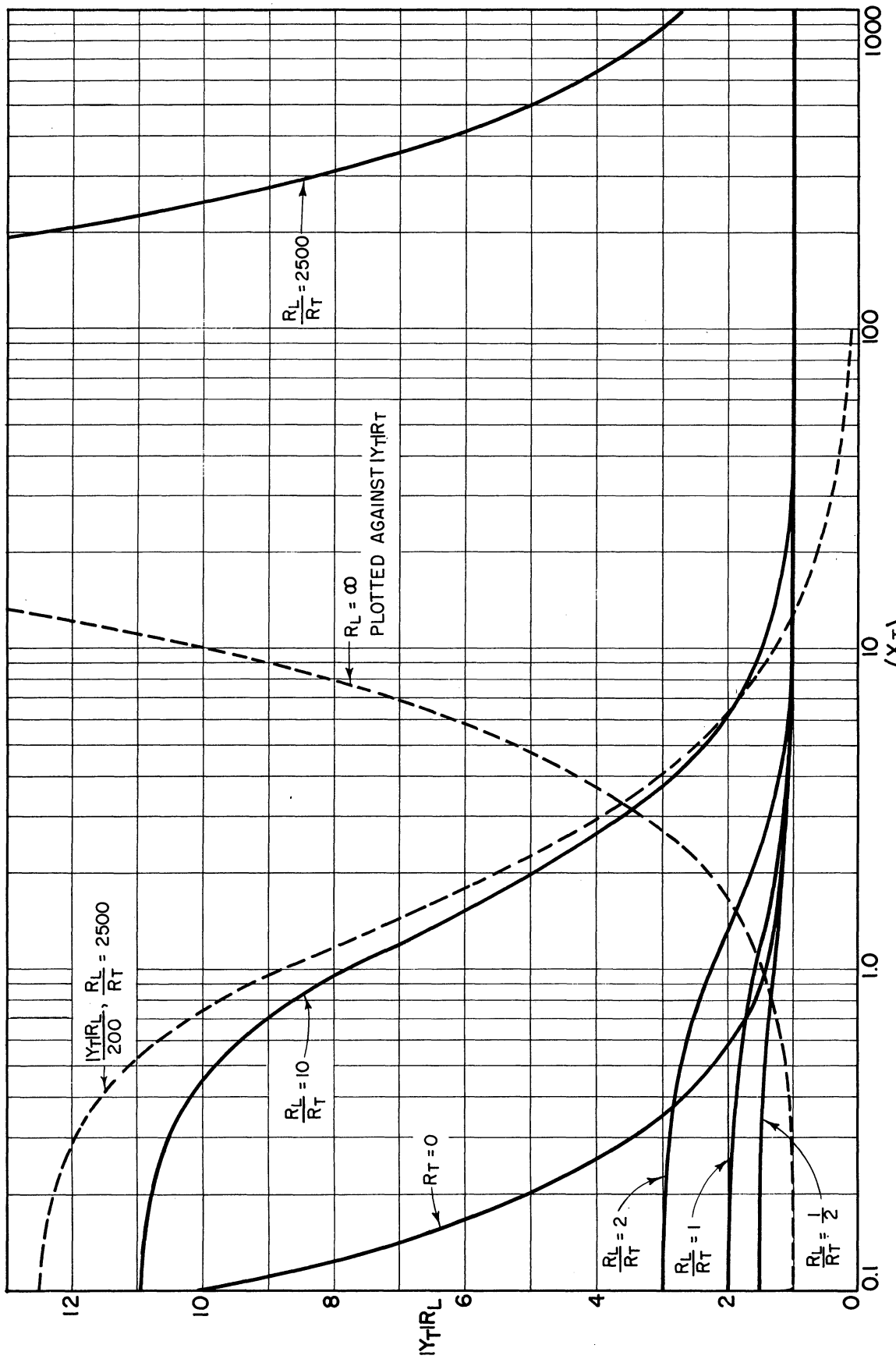

FIG. 3.10
ADMITTANCE CHARACTERISTICS FOR CIRCUIT OF FIG. 3.8

The maximum value of θ as a function of $\frac{R_L}{R_T}$ is given by

$$\theta_{max} = \tan^{-1} - \frac{\frac{R_L}{R_T}}{\sqrt{1 + \frac{R_L}{R_T}}} . \qquad (3.35)$$

The phase and admittance characteristics for representative values of $\frac{R_L}{R_T}$ are plotted in Fig. 3.9 and Fig. 3.10. For the special case of X_T, made up of an inductive reactance,

$$\frac{X_T}{R_T} = \frac{2\pi f L}{R_T} .$$

The quantity plotted on the abscissa is directly proportional to frequency. For the case of a short-circuited transmission line

$$\frac{X_T}{R_T} = \frac{Z_o}{R_T} \tan 2\pi \frac{\ell}{\lambda} .$$

ℓ = length of line, and

Z_o = characteristic impedance of the line.

C. Long-Line Effect. The number of variations in details of magnetron circuitry is very great and all variations are not the result of predetermined concepts. At microwave frequencies the effect of a cathode end-hat, supporting mechanisms for the tuning structure, etc., may be quite significant.[1] Substantial reflection in the output coupling or the line which carries power to the antenna also may completely alter the characteristics of the idealized circuit assumed in analyzing the magnetron. An effect which is increased in importance when very low-Q operation is desired is the "long-line effect".[2] When a transmission line a few wavelengths

---

[1] I, 6, d, p 533.

[2] I, 6, c, pp515-522.

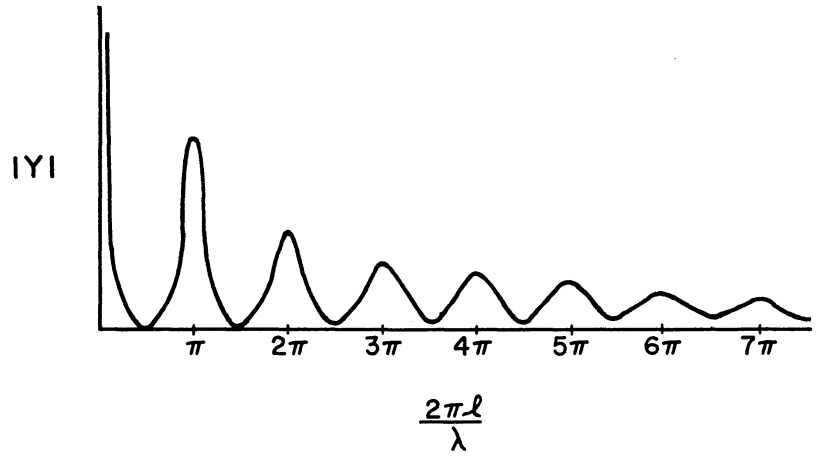

ABSOLUTE VALUE, ADMITTANCE OF SHORT CIRCUITED TRANSMISSION LINE

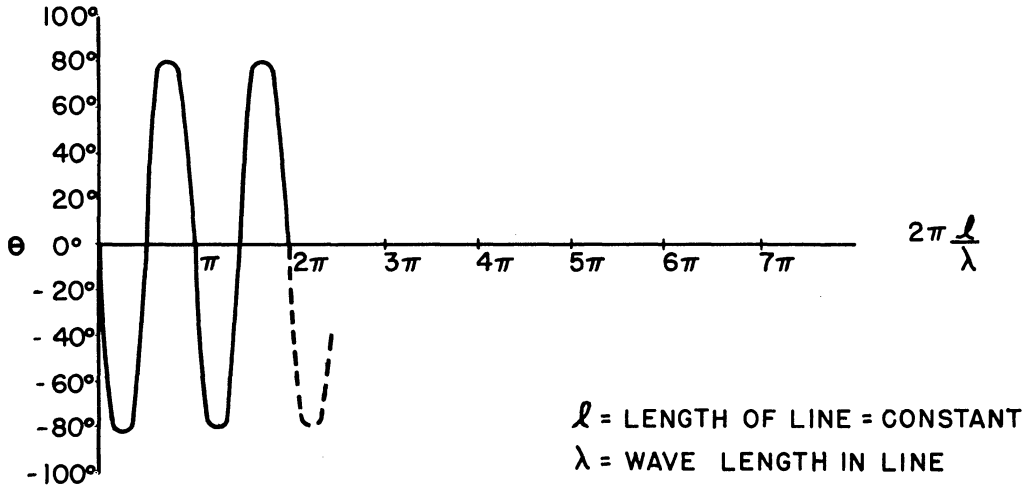

PHASE ANGLE OF ADMITTANCE OF SHORT CIRCUITED TRANSMISSION LINE

FIG. 3.11
TYPICAL PHASE AND ADMITTANCE CHARACTERISTICS
OF SHORT CIRCUITED TRANSMISSION LINE

long connects the magnetron to a load and the load is not perfectly matched to the transmission line, the admittance and phase characteristic will vary periodically with frequency. A complete cycle in this variation will occur each time the length of the line changes by one-half wavelength. Typical characteristics are shown in Fig. 3.11. For high-Q magnetron circuits the long-line effect is generally not serious unless very high standing-wave ratios exist in the line. However, for a circuit like that in Fig. 3.10 the variations in phase and admittance of the line would quite likely be more important than the variation in the circuit. In this case the load resistance, R_L, would be assumed not matched to the impedance of the line connecting it to the tube terminals. In practical application it is seldom possible to make this length of line arbitrarily short, since the tube is necessarily connected to an antenna or other useful load.

3.4 Admittance of the Electron Stream, Frequency Pushing and Voltage Tuning

Frequency pushing and voltage tuning have been defined in the introduction to this report (pages 2 and 3). As was stated in connection with this definition, the distinction is not always clear. However, with the aid of the material which has been presented, two sets of extreme conditions can be indicated which very closely predict the type of characteristics which have been defined as frequency-pushing characteristics and voltage-tuning characteristics.

When Eqs 3.20 and 2.47 are substituted into Eq 3.19, the rms r-f current generated by the magnetron can be written in the following form

$$I_g = \frac{I_1}{\sqrt{2}} = K_1 \left(1 + \frac{\phi_a - \phi_{at}}{\sqrt{2}\, K\, K_2}\right) \frac{\cos\theta}{\frac{\pi}{2} + \theta} \tag{3.36}$$

where

$$K_1 = \frac{8}{\sqrt{2}} \pi\, L\, r_c^2\, f\, \rho_o\, F\,(\alpha, N, R_a, R_n) \text{ amperes} \tag{3.37}$$

$$K_2 = \frac{\rho_o\, r_c^2\, (R_a^2 - R_n^2)}{4\sqrt{2}\, K\, \epsilon_o} \text{ volts} \tag{3.38}$$

$$F(\alpha,N,R_a,R_n) = \frac{\sin\frac{N}{2}\alpha}{\frac{N}{2}\alpha} \frac{1}{R_a^{\frac{N}{2}} - R_a^{-\frac{N}{2}}} \left[\frac{R_a^{2+\frac{N}{2}}}{2+\frac{N}{2}} - \frac{R_a^{2-\frac{N}{2}}}{2-\frac{N}{2}} - \frac{R_n^{2+\frac{N}{2}}}{2+\frac{N}{2}} + \frac{R_n^{2-\frac{N}{2}}}{2-\frac{N}{2}}\right], \tag{3.39}$$

$$\rho_o = -8\pi\, \epsilon_o \frac{m}{e} \frac{f}{N} \left(\frac{Be}{m} - \frac{4\pi f}{N}\right), \tag{3.40}$$

where $\frac{4\pi f}{N}$ has been substituted for ω_n in Eq 2.44.

R_n is determined from Eq 2.28.

$$K = \frac{\phi_f}{\phi_{r\text{-}f\ max}} \text{ (Eq 2.49)}$$

ϕ_f = the peak value of the fundamental travelling wave.

The absolute value of the admittance of the electron stream as it depends on the r-f potential can be obtained from division of Eq 3.36 by $\phi_{r\text{-}f}$.

$$|Y_e| = \frac{I_g}{\phi_{r\text{-}f}} = \frac{K_1}{\phi_{r\text{-}f}} \left(1 + \frac{\phi_a - \phi_{at}}{\sqrt{2}\, K\, K_2}\right) \frac{\cos\theta}{\frac{\pi}{2} + \theta}, \tag{3.41}$$

$$\text{for } \phi_a = \phi_{at}, \quad \theta = -45°, \quad \cos\theta = \frac{1}{\sqrt{2}}$$

$$|Y_e|_t = \frac{2\sqrt{2}}{\pi} \frac{K_1}{\phi_{r\text{-}f}} \text{ when } \phi_a = \phi_{at}. \tag{3.42}$$

The admittance of the electron stream is related to magnetron dimensions, frequency and magnetic field through the factor K_1. In the theory presented here some of the effects which r-f potential might have on the spoke formation are obviously neglected. This is illustrated by the case $\phi_a = \phi_{at}$. Reference to Fig. 2.8c shows that, if the assumptions leading to the evaluation of I_g are correct, I_g will not be dependent on the magnitude of the r-f potential at this particular operating point. This may be expressed, in other words, by stating that the r-f potential, for a particular set of operating conditions, is not determined until the circuit admittance characteristics are specified.

R-f potential, phase angle and d-c anode potential are related through the expression

$$\frac{\phi_a - \phi_{at}}{\sqrt{2}\, K\, \phi_{r\text{-}f}} = \cos 2\theta \qquad (3.43)$$

from Eqs 2.48 and 2.49.

$$\phi_{r\text{-}f} = \frac{\phi_a - \phi_{at}}{/2\, K \cos 2\theta} .$$

This ratio is indeterminate unless $\phi_a - \phi_{at}$ is known as a function of θ. In this case, for $\theta = -45°$, by L'Hospital's rule

$$\phi_{r\text{-}f} = - \frac{\frac{d(\phi_a - \phi_{at})}{d\theta}}{\sqrt{2}\, K\, 2 \sin 2\theta}\Bigg|_{\theta = -45°} ,$$

or

$$\phi_{r\text{-}f} = \frac{1}{2\sqrt{2}\, K} \frac{d(\phi_a - \phi_{at})}{d\theta}\Bigg|_{\theta = -45°} . \qquad (3.44)$$

θ is related to the spoke width by

$$\beta N = \pi + 2\theta .$$

Through the volt-ampere characteristic, $(\phi_a - \phi_{at})$ is related to d-c anode current. The d-c anode current in turn is expected to be roughly proportional to βN, the spoke width. Thus

$$\frac{d(\phi_a - \phi_{at})}{d\theta} = \frac{\partial(\phi_a - \phi_{at})}{\partial I_{d-c}} \frac{\partial I_{d-c}}{\partial(\beta N)} = -2 \frac{\partial(\phi_a - \phi_{at})}{\partial I_{d-c}} \frac{\partial I_{d-c}}{\partial \theta} .$$

Substituting in Eq 3.44

$$\phi_{r-f} = -\frac{1}{\sqrt{2}\,K} \frac{\partial(\phi_a - \phi_{at})}{\partial I_{d-c}} \frac{\partial I_{d-c}}{\partial \theta}\bigg|_{\theta = -45^\circ} . \qquad (3.45)$$

The significance of this relationship is in its expression of the possibility of a functional relationship between the r-f potential and the slope of the volt-ampere characteristic. It should not be given too much importance as a quantitative expression because not enough is known about the behavior of the derivatives involved. One can say that a high r-f voltage will be expected when the slope of the volt-ampere characteristic is high as compared to low r-f voltage when the slope of the volt-ampere characteristic is low. Also the two derivatives must be of opposite sign in order that the r-f potential have a positive value. Since $\frac{\partial(\phi_a - \phi_{at})}{\partial I_{d-c}}$ is usually positive, this means that θ must decrease as I_{d-c} increases.

When the magnetron is loaded by a particular circuit of which the phase and admittance characteristics are known, the phase angle and the r-f potential can be expressed as definite functions of frequency and magnitude of the induced current. It then becomes possible to express as functions of frequency the power measurable in the load and the anode potential. Eq 3.36 can be written

$$I_g = K_1 \left(1 + \frac{\phi_{r-f}}{K_2} \frac{\phi_a - \phi_{at}}{\phi_f}\right) \frac{\cos \theta}{\frac{\pi}{2} + \theta} .$$

Substituting

$$\phi_{r\text{-}f} = \frac{I_g}{|Y_T|},$$

$$\frac{\phi_a - \phi_{at}}{\phi_f} = \cos 2\theta,$$

and solving for I_g, we have

$$I_g = \frac{K_1}{\frac{\frac{\pi}{2} + \theta}{\cos \theta} - \frac{K_1}{K_2} \frac{\cos 2\theta}{|Y_T|}}. \tag{3.46}$$

The power in the load is given by

$$P_L = \phi_{r\text{-}f}^2 G_L = \frac{I_g^2}{|Y_T|^2} G_L$$

$$P_L = \frac{G_L}{|Y_T|^2} \left(\frac{K_1}{\frac{\frac{\pi}{2} + \theta}{\cos \theta} - \frac{K_1}{K_2} \frac{\cos 2\theta}{|Y_T|}} \right)^2, \tag{3.47}$$

if G_L is the load conductance as transformed to the terminals of the magnetron anode set.

The d-c anode potential is given by

$$\phi_a - \phi_{at} = K\sqrt{2}\, \phi_{r\text{-}f} \cos 2\theta = K\sqrt{2} \frac{I_g}{|Y_T|} \cos 2\theta$$

$$\phi_a - \phi_{at} = \frac{K\sqrt{2}}{|Y_T|} \frac{K_1}{\frac{\frac{\pi}{2} + \theta}{\cos \theta} - \frac{K_1}{K_2} \frac{\cos 2\theta}{|Y_T|}} \cos 2\theta. \tag{3.48}$$

A. Frequency Pushing. For the particular case of the simple parallel resonant circuit the phase and admittance characteristics have been calculated in the last section. The quantity $\frac{1}{|Y_T|^2}$ is proportional to

$\frac{1}{1 + 4\delta^2 Q_L^2}$ which was plotted in Fig. 3.7. If the magnetron were truly a constant-current generator, as is sometimes assumed, a pushing curve, giving power as a function of frequency, would have the form of $\frac{1}{|Y_T|^2}$. In order to obtain some idea of the modification of this curve due to the factor within the brackets, it is convenient to make the substitution

$$|Y_T| = \frac{Y_{oc}}{Q_L} \frac{1}{\cos \theta}$$

in this expression. With this substitution, we have

$$\frac{I_g}{K_1} \cong \frac{1}{\frac{\frac{\pi}{2} + \theta}{\cos \theta} - A \cos \theta \cos 2\theta}, \qquad (3.49)^1$$

$$\text{where } A = \frac{K_1}{K_2} \frac{Q_L}{Y_{oc}}. \qquad (3.49a)$$

Note that

$$\frac{K_1}{K_2} = \frac{32\pi K \varepsilon_o F(\alpha, N, R_a, R_n)}{R_a^2 - R_n^2} L f \text{ ohms} \qquad (3.49b)$$

is independent of ρ_o. $\frac{K_2}{K_1}$ for typical magnetrons is of the order of 500 to 1500 ohms.

When the Q_L of the circuit is reasonably high (i.e., 100), the phase angle, θ, varies much more rapidly with frequency than K_1 or K_2. K_1 and K_2 can, therefore, be considered constant in this expression. The ratio $\frac{I_g}{K_1}$ for representative values of A is plotted against δQ_L in Fig. 3.12. The auxiliary equation

$$2 \delta Q_L \cong \tan \theta \qquad (3.50)$$

is used.

---

[1] The reader is reminded that θ is conventionally negative when it represents a lagging phase angle so that $\left(\frac{\pi}{2} + \theta\right) < \frac{\pi}{2}$.

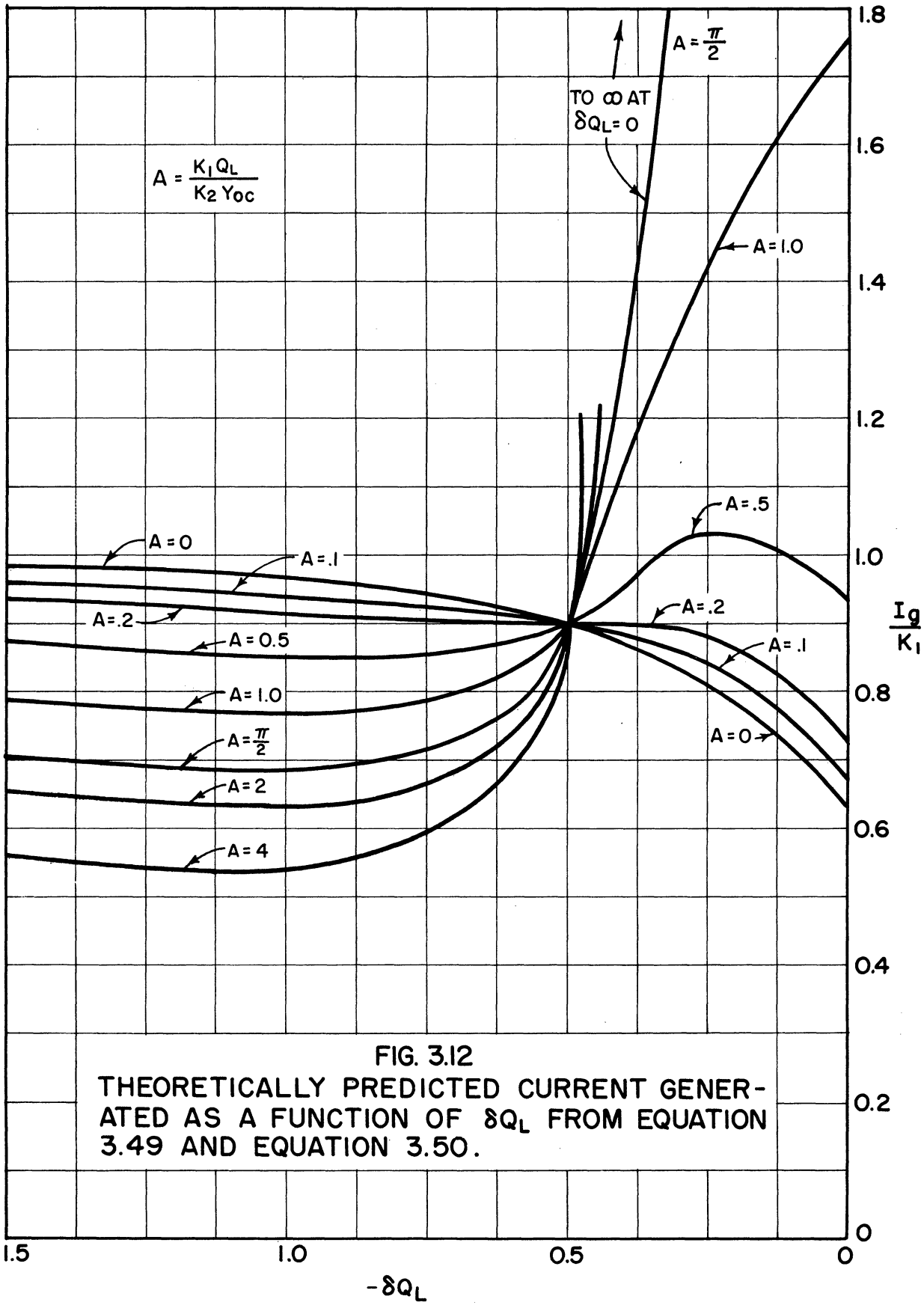

FIG. 3.12
THEORETICALLY PREDICTED CURRENT GENERATED AS A FUNCTION OF δQ_L FROM EQUATION 3.49 AND EQUATION 3.50.

Curves of frequency and anode potential as a function of power, as predicted by this theory, are plotted in Fig. 3.13, 3.14 and 3.15 for representative values of the parameter A. This parameter can be varied by changing various parameters in the magnetron design. The way in which these parameters were varied is illustrated by the curves of Fig. 3.16. The curves in each of the Figs. 3.13, 3.14 and 3.15 are plotted so that the relative magnitudes on the two sets of curves in each figure are quantitatively correct in terms of the power, potential or frequency scales. The equations used in plotting the curves are

$$\frac{P_L}{G_L K_2^2} \cong A^2 \cos^2\theta \left(\frac{I_g}{K_1}\right)^2 \qquad (3.51)$$

and

$$\frac{\phi_a - \phi_{at}}{\sqrt{2}\, K K_2} \cong A \frac{I_g}{K_1} \cos\theta \cos 2\theta \,, \qquad (3.52)$$

with Eq 3.50. If it is assumed that a direct proportionality exists between power and d-c anode current these curves give the expected form of frequency-pushing characteristics and volt-ampere characteristics.

The curves of Fig. 3.13 compare characteristics for two values of Q_L.[1] A and the conductance, G_L, are kept constant by changing Y_{oc} in proportion to Q_L. This is illustrated by curves 1 and 2 in Fig. 3.16. Note that the volt-power characteristic is the same for either case but the pushing characteristic shows a larger change in frequency for a given change in power for the case of the lower Q_L.

The curves of Fig. 3.14 illustrate the effect of changing the load conductance. The Q_L is maintained constant, in this case, by changing

---

[1] It is assumed in plotting these curves that $Q_L \cong \frac{Y_{oc}}{G_L}$, i.e., G_T is very small or internal circuit losses are negligible.

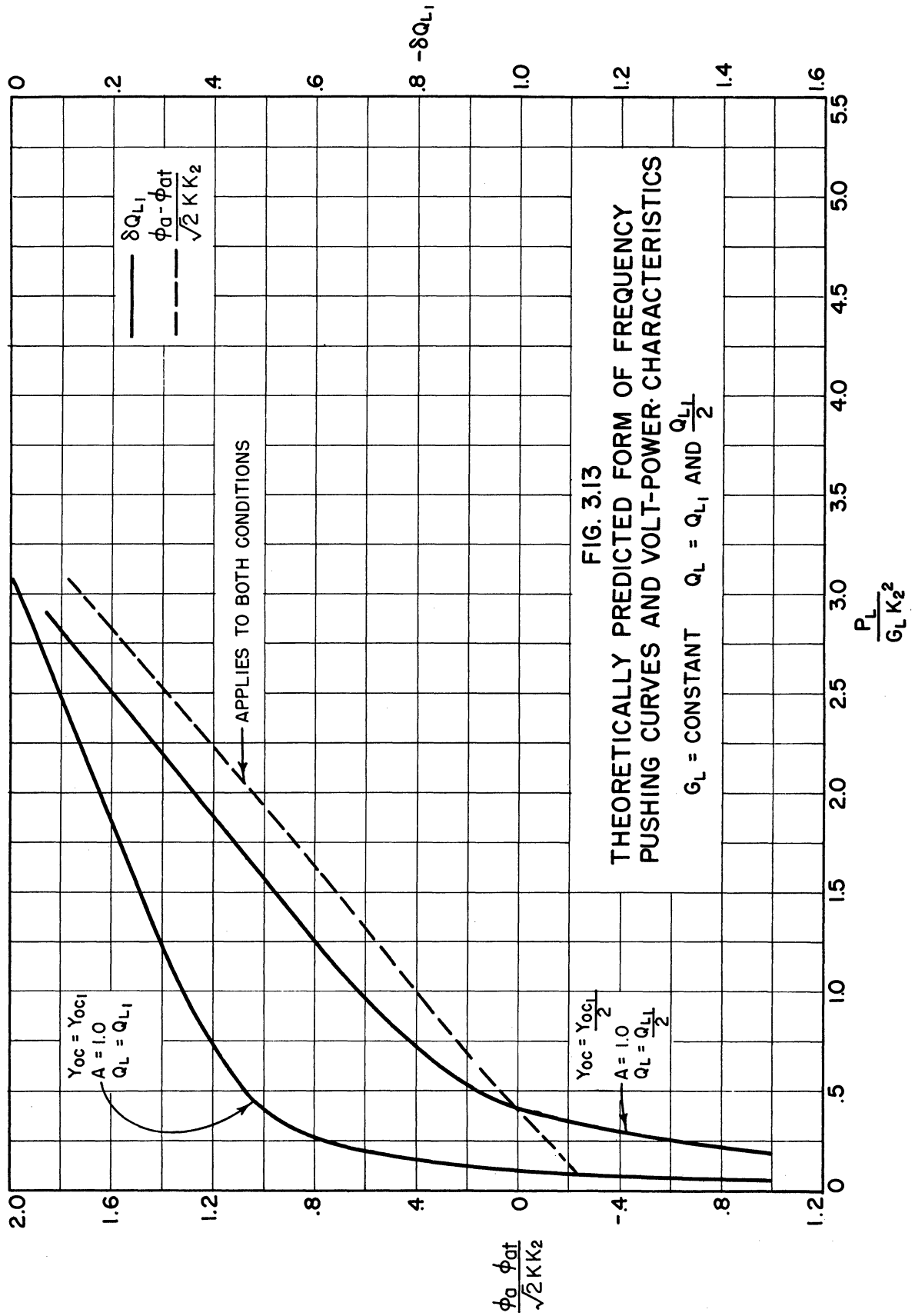

FIG. 3.13
THEORETICALLY PREDICTED FORM OF FREQUENCY PUSHING CURVES AND VOLT-POWER CHARACTERISTICS
G_L = CONSTANT $Q_L = Q_{L1}$ AND $\frac{Q_{L1}}{2}$

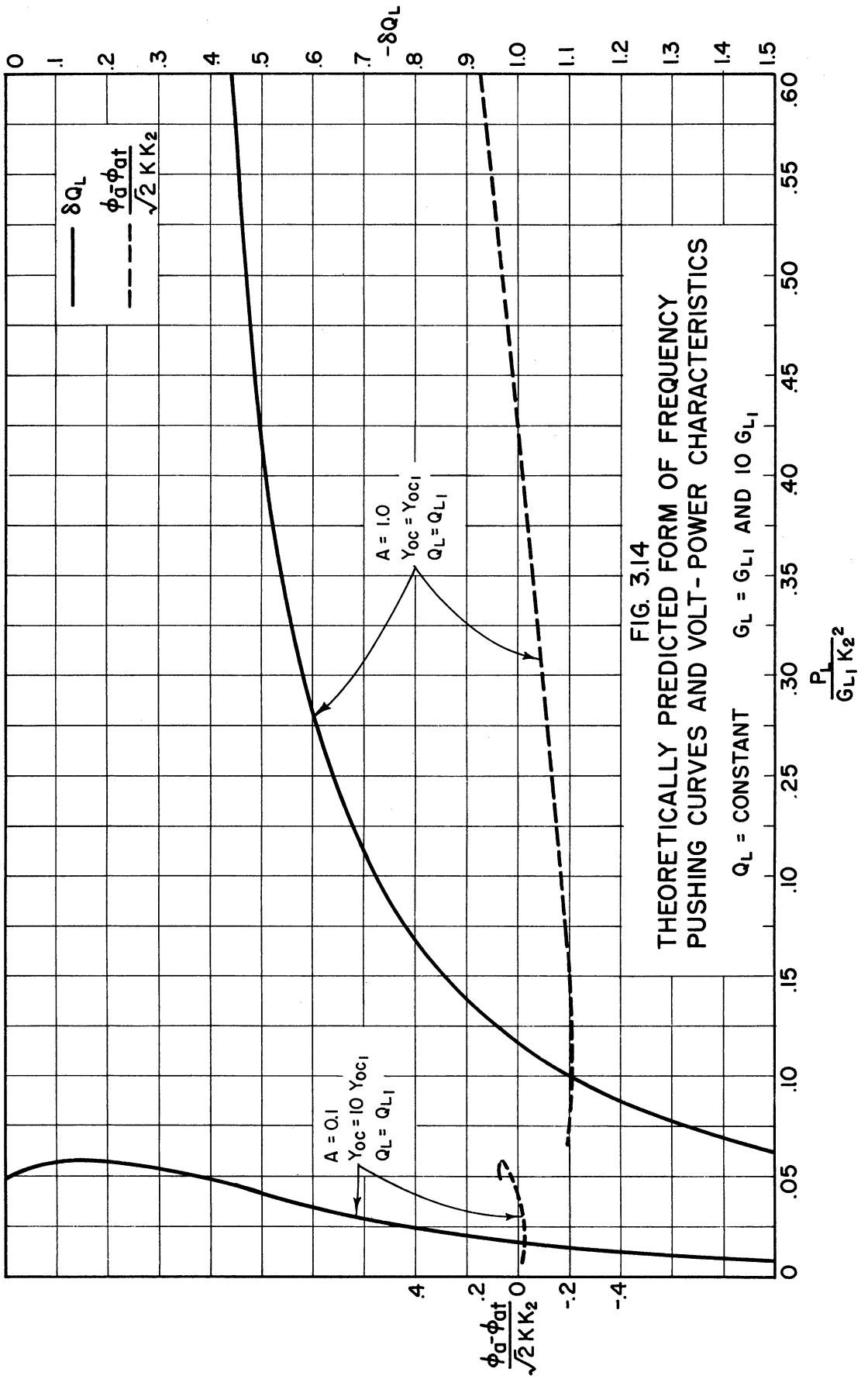

FIG. 3.14
THEORETICALLY PREDICTED FORM OF FREQUENCY PUSHING CURVES AND VOLT-POWER CHARACTERISTICS

Q_L = CONSTANT $G_L = G_{L1}$ AND $10\ G_{L1}$

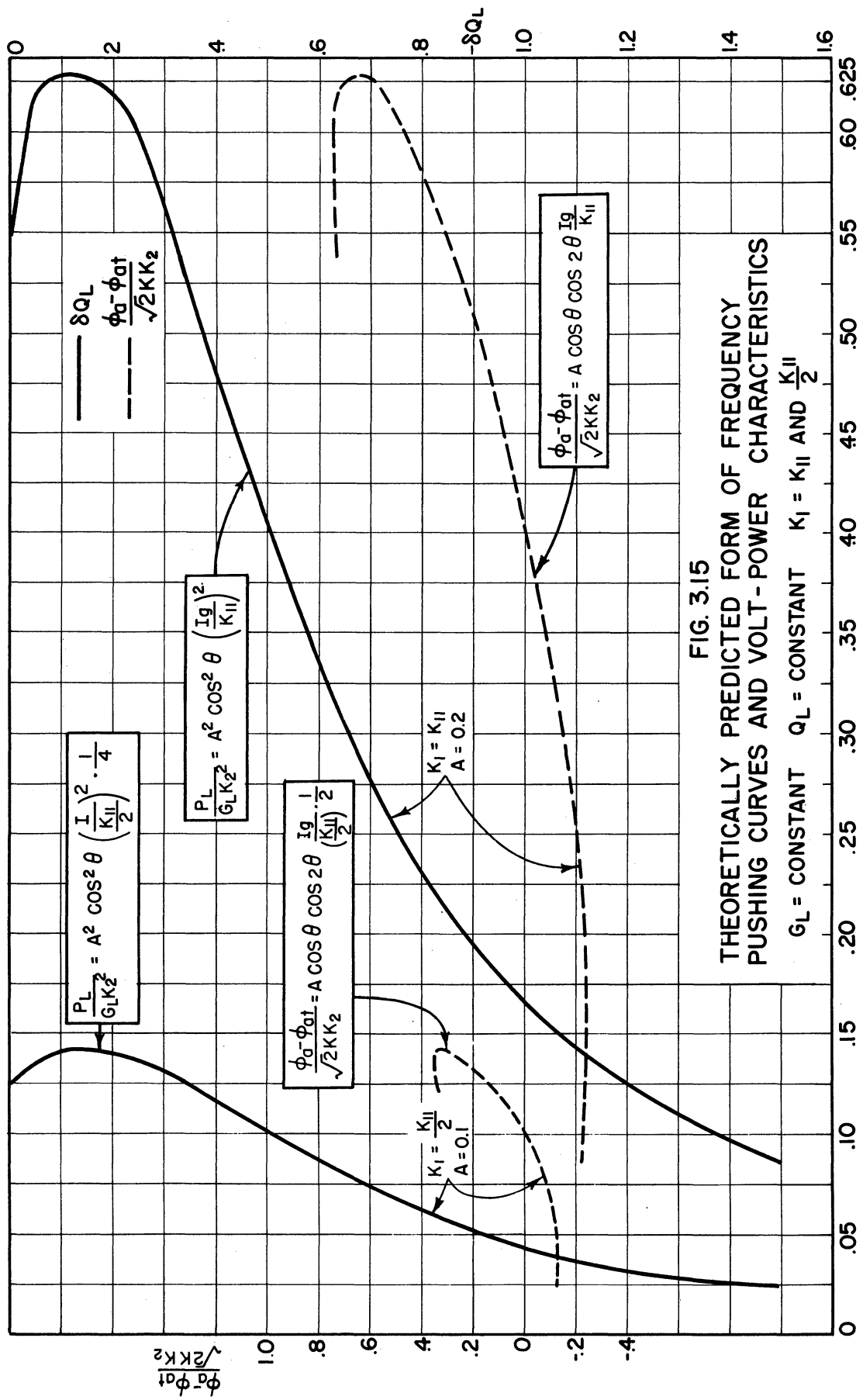

FIG. 3.15
THEORETICALLY PREDICTED FORM OF FREQUENCY PUSHING CURVES AND VOLT-POWER CHARACTERISTICS
G_L = CONSTANT Q_L = CONSTANT $K_I = K_{II}$ AND $\frac{K_{II}}{2}$

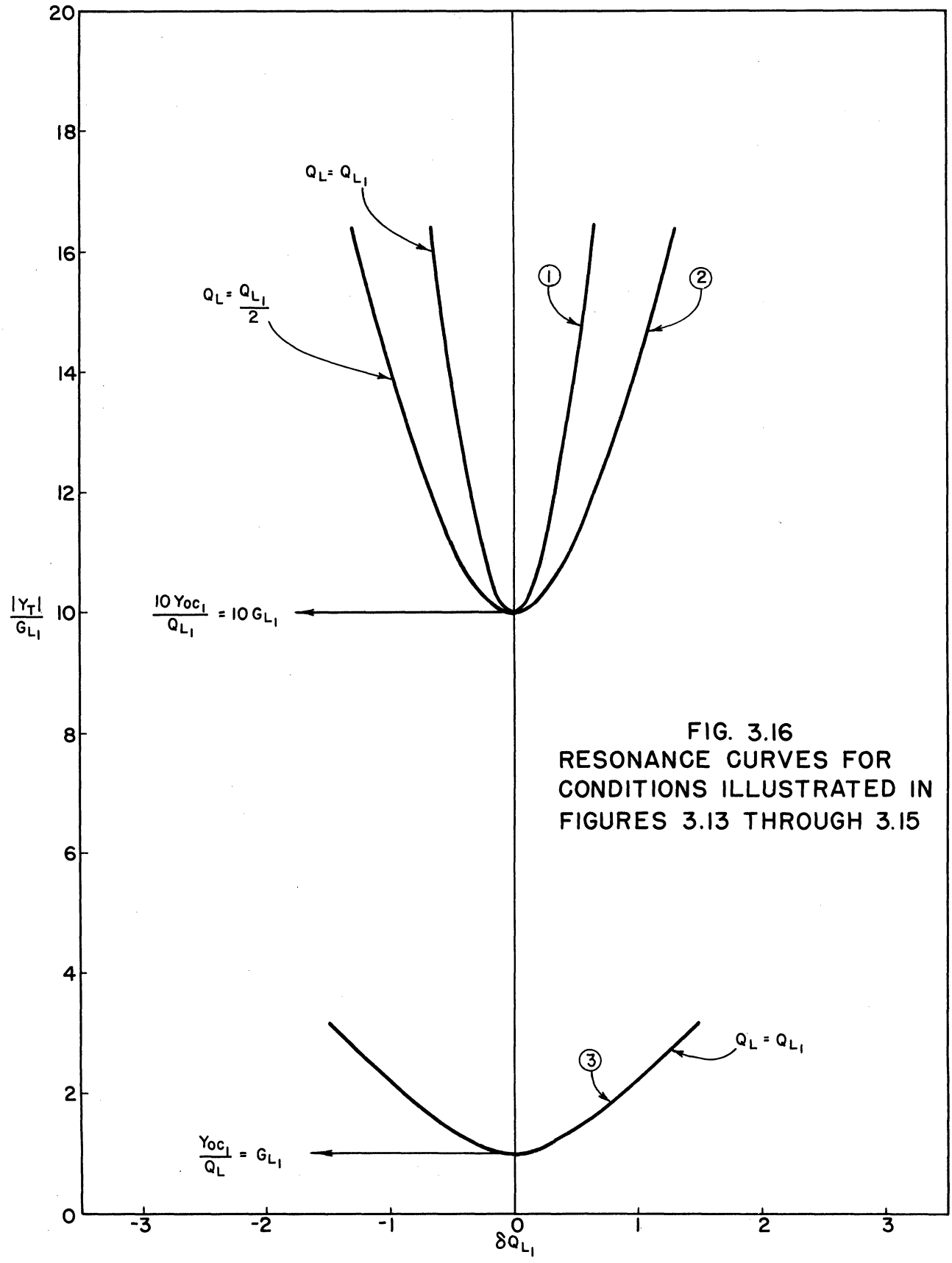

FIG. 3.16
RESONANCE CURVES FOR CONDITIONS ILLUSTRATED IN FIGURES 3.13 THROUGH 3.15

Y_{oc} (or energy storage) in the same proportion as G_L (or energy loss). A is decreased from 1.0 to 0.1 by this change. Curves 1 and 3 of Fig. 3.16 apply to this case. The total frequency shift over the volt-power characteristic is approximately the same for the two cases but the change in frequency for a given change in power is increased by roughly a factor of 10 when the conductance is increased by a factor of 10. The maximum relative power for A = 0.1 is .06 as compared to 3.1 for A = 1.0. (Obtained from the same curve plotted on a reduced scale in Fig. 3.13). This illustrates the effect on maximum-power boundary (or maximum-current boundary) to be expected from an increase in conductance associated with an increase in Y_{oc}.

In Fig. 3.15 the effect of redesign of the magnetron interaction space without a change in the circuit is illustrated. The constant K_1 is assumed to be changed by a factor of 2 such that A takes on the values A = 0.1 and A = 0.2. Both sets of curves are assumed to apply to the same resonance curve, i.e., curve number 3 in Fig. 3.16. For the case of A = 0.1 the current generating capacity of the magnetron (proportional to K_1) is reduced to half of the capacity for A = 0.2. The maximum relative power which can be produced is correspondingly reduced from 0.630 to 0.141. The slope of the volt-power characteristic is increased and the pushing for a given change in power is increased. This change in K_1 could be brought about, for example, by cutting the length of the cathode in half. If r_c^2 were reduced to 1/2, K_2 would also be changed and the curves would no longer be applicable without adjustment of the scales.

This discussion illustrates the effects which may be expected for practical changes in the magnetron parameters. Comparison with

experimentally observed results will be given in the next chapter. We will find that, although an exact quantitative check between theory and experiment is not obtained, the direction which parameters should be changed to achieve a particular result is correctly indicated.

Before leaving this discussion, it should be repeated and emphasized that the formulae used in plotting the curves of Fig. 3.12 through 3.16 are based on the assumption of space-charge-limited high-Q operation.

The phase-focussing diagrams given in Fig. 2.10, applying to the volt-ampere characteristics of Fig. 2.11, are also qualitatively applicable to the characteristics predicted here, particularly the curves for A = 1.0 in Fig. 3.13.

B. Voltage Tuning. The behavior of the magnetron under temperature-limited conditions with a non-resonant load cannot be discussed in the same terms that have been applied to the space-charge-limited operation into a resonant load. It is possible in particular instances to apply the relationship for power and anode potential of Eqs 3.47 and 3.48 to circuits other than the simple parallel resonant circuit but the calculations become very involved since K_1 and G_L are no longer frequency independent. A circuit like that in Fig. 3.8 would be expected to give frequency and power characteristics approaching those defined as voltage-tuning characteristics.

Let us examine qualitatively, for example, the region between $\frac{X_T}{R_T} = 1$ and $\frac{X_T}{R_T} = 3$ on the curves for $\frac{R_L}{R_T} = 10$ in Fig. 3.9 and 3.10. If X_T were proportional to frequency, as in the case for X_T, an inductive reactance, this would represent the coverage of a 3 to 1 frequency range. In

this range the phase angle varies over a relatively small range between $\theta = -40°$ and $\theta = -56°$. In this range of angle the induced current given by Eq 3.46 is not strongly affected by the change in angle. The circuit admittance, however, is changing from $|Y_T| R_L = 7.8$ to $|Y_T| R_L = 3.6$, by somewhat less than 3 to 1. The constant, K_1, being proportional to frequency, is increasing by a factor of 3 to 1. The ratio $\frac{K_1}{|Y_T|}$ which appears in the denominator, will increase a factor of the order of 8 or 9. The change in this factor and the factor K_1 increasing in the numerator will tend to make I_g increase by a factor of the order of 3 to 1 to 10 to 1 with frequency. The anode potential, although proportional to $\frac{I_g}{K_1}$, will not depart very much from the threshold potential while θ is near $-45°$. However, the current appears as a square in the expression of 3.47 for the power multiplied by

$$\frac{G_L}{|Y_T|^2} = \frac{1}{|Y_T|} \frac{1}{\cos \theta}$$

which also increases with frequency. Thus the power will be expected to rise sharply with increasing frequency.

The threshold potential, ϕ_{at}, is related to frequency through the threshold equation

$$\phi_{at} = \frac{\pi B}{n} f (r_a^2 - r_c^2) - 2\pi^2 \frac{m}{e} \frac{f^2}{n^2} r_a^2 . \quad (3.53, \text{ also } 2.42)$$

For large B, $\phi_{at} \propto f$. We may draw the conclusion, therefore, that, if $\phi_a - \phi_{at}$ does not become very large, the frequency will be approximately proportional to the anode potential

$$\phi_a \cong \phi_{at} . \quad (3.54)$$

We have approximately achieved one of the characteristics desired of voltage-tunable operation, frequency proportional to anode potential, but not the other, power output independent of frequency. A set of curves which have the characteristics suggested by this discussion is reproduced from data taken in the General Electric Laboratories in Fig. 4.41 of Section 4.3. A phase-focussing diagram is given in Fig. 3.17.

This discussion has been presented to illustrate the technique of making qualitative analyses of the effect of known phase-and-admittance characteristics on magnetron operation. Very similar results might be expected from a low-Q resonant circuit. The major difference would be in the behavior of the phase angle. This angle would be decreasing with frequency rather than increasing with frequency, as it is in Fig. 3.9.

In order to obtain the characteristic of power output independent of frequency it is necessary to resort to temperature-limited operation. In this case the assumptions leading to Eq 3.46 for the current generated are no longer valid. It will be assumed that the r-f potential is great enough to form well-defined spokes as suggested in the discussion of phase focussing under temperature-limited conditions in connection with Figs. 2.14 and 2.15. Under these conditions the general relationship for the induced current generated, 3.19, is applicable. It is not necessarily valid, however, to assume that the space-charge density in the spokes is determined by the relationship in Eq 3.20 which results from the discussion of Section 2.6. The actual value of this density under temperature-limited conditions has not been quantitatively determined. However, an estimate of the behavior of the density as anode potential is raised and frequency is increased can be made as follows.

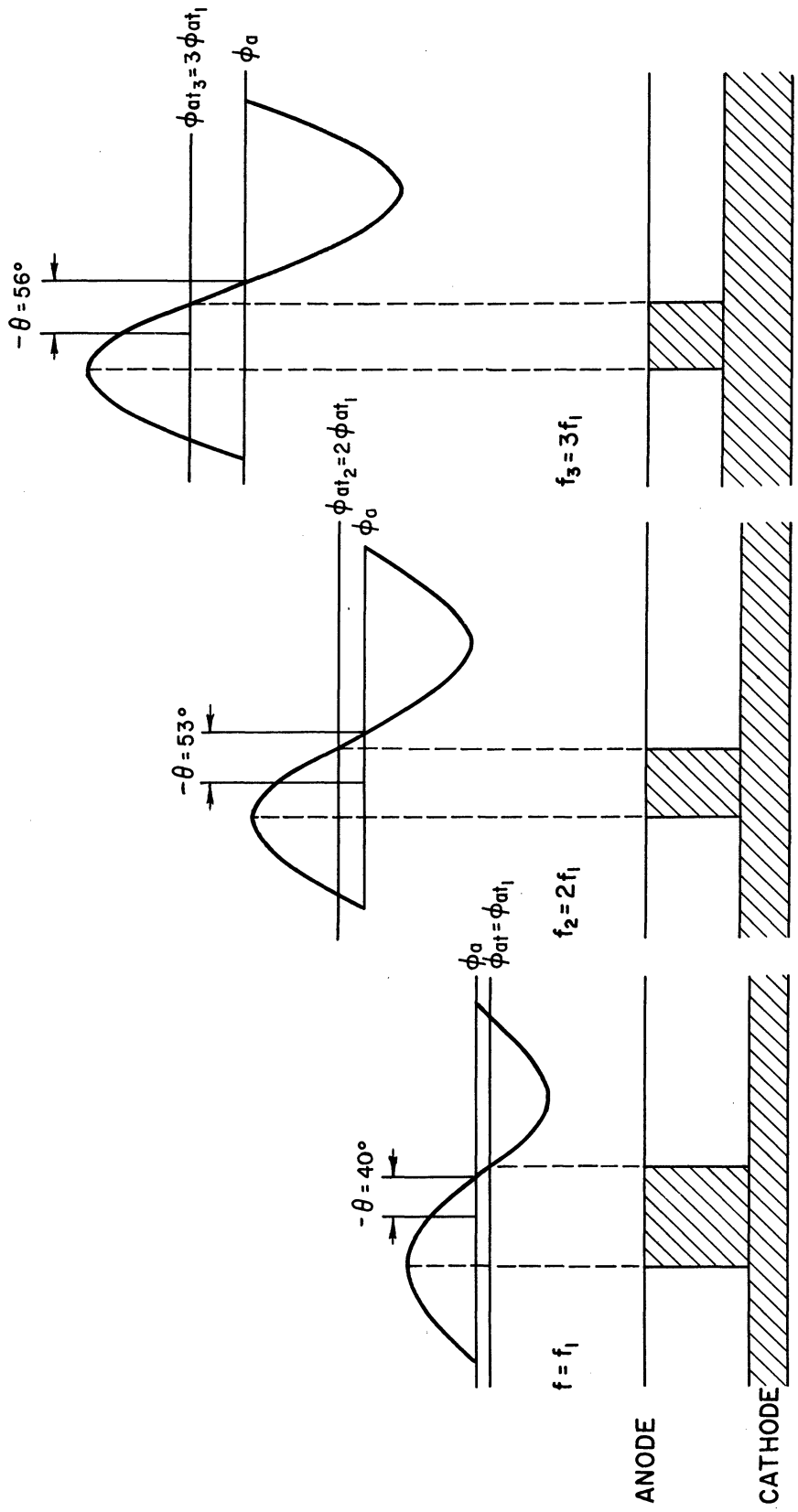

FIG. 3.17
APPROXIMATE PHASE FOCUSSING DIAGRAMS EXPECTED FOR OPERATION OVER A 3 TO 1 FREQUENCY RANGE WITH CIRCUIT OF FIGURE 3.8
(FREQUENCY f_1 CORRESPONDS TO $\frac{X_T}{R_T} = 1.$)

When temperature-limited conditions prevail at the cathode the total d-c current cannot increase beyond a specified value as the anode potential is raised. Assuming that the d-c current has reached this value a particular phase-focussing diagram will apply (i.e., that of Fig. 2.14c). The induced current will be given by Eq 3.19.

$$I_g = \frac{I_1}{\sqrt{2}} = 8 L r_c^2 f \rho_s \sin \frac{N}{2} \beta F (\alpha, N, R_a, R_n) , \qquad (3.55)$$

where ρ_s is undetermined. The current density through the spoke to the anode will be proportional to the temperature-limited d-c anode current

$$(\rho_s v)_n = C_1 I_T , \qquad (3.56)$$

I_T = temperature-limited current

C_1 = a constant

$(\rho_s v)_n$ = arrival current at the anode.

The total amount of charge collected per second is limited to I_T. An increase in anode potential, then, must increase the arrival velocity of the electrons. We may expect, therefore, that

$$v = C_2 \phi_a . \qquad (3.57)$$

Combining this relationship with Eq 3.56, we have

$$\rho_s = \frac{C_1}{C_2} \frac{I_T}{\phi_a} . \qquad (3.58)$$

We are assuming, a priori, that the circuit conditions are such as to encourage voltage-tunable operation. We may write

$$f \cong C_3 \phi_a \,. \tag{3.59}$$

Combining these conditions into Eq 3.55 we have finally

$$I_g = 8 L r_c^2 \frac{C_3 \cdot C_1}{C_2} I_T \sin \frac{N}{2} \beta F (\alpha, N, R_a, R_n) \,. \tag{3.60}$$

The resulting current depends on frequency through the variation of R_n in the function F (α, N, R_a, R_n). F varies extremely slowly with frequency. Note also that I_g is directly proportional to I_T.

The constant, $\frac{C_3 C_1}{C_2}$, has not been evaluated, however, the assumption of a constant-current generator is sufficient to predict the shape of the power-vs-frequency curve if the circuit characteristics are known. The general relationship

$$P_L = \frac{I_g^2}{|Y_T|} \cos \theta = \frac{I_g^2}{|Y_T|^2} G_L \tag{3.61}$$

can be used.

The voltage-tuning curve can be predicted using Eq 3.53 and the expression relating anode potential to the threshold potential

$$\frac{\phi_a - \phi_{at}}{\sqrt{2}\, K\, \phi_{r-f}} = \cos 2\theta \,.$$

Also

$$\phi_{r-f} = \frac{I_g}{|Y_T|} \,.$$

Finally

$$\phi_a = \sqrt{2}\, K \cos 2\theta \frac{I_g}{|Y_T|} + \frac{\pi B}{n} r_c^2 f (R_a^2 - R_c^2) - 2\pi^2 \frac{m}{e} \frac{r_c^2}{n^2} R_a^2 f^2 \,. \tag{3.62}$$

Eq 3.62 is, of course, quite general and presents a strictly linear relationship between anode potential and frequency only for the conditions that

(1) I_g, θ, $|Y_T|$ are not frequency dependent, and

(2) the f^2 term is negligible, i.e., for relatively large magnetic fields.

The first condition also makes the power, given by Eq 3.61, a constant. These conditions were assumed in constructing the phase-focussing diagrams of Fig. 2.16. These ideal conditions are illustrated in Fig. 3.18.

A lagging phase angle, of the order of -20° to -50° is desirable to achieve good phase focussing. A circuit which has this characteristic, as well as a constant admittance, over a wide frequency range is difficult to achieve. In Fig. 3.19 the power and frequency characteristics of the circuit given in Fig. 3.8 are plotted. This circuit is quite easily constructed and approaches the desired characteristics.

C. Effects of Arrival Current. In the analysis which has been presented the effect of motion of electrons toward the anode on the r-f current generated has been assumed negligible. This assumption is justifiable for small anode currents, but for large currents, particularly in pulsed radar magnetrons, the induced current due to the radial motion may become appreciable. Our only purpose here is to indicate the effect this current would have on the preceding analysis of frequency pushing. In voltage-tunable operation the d-c current is usually so small that the radial motion need not be considered. Consider the diagrams of Fig. 2.8 and 2.9. In Figs. 2.8b and 2.9b the current into the circuit due to the

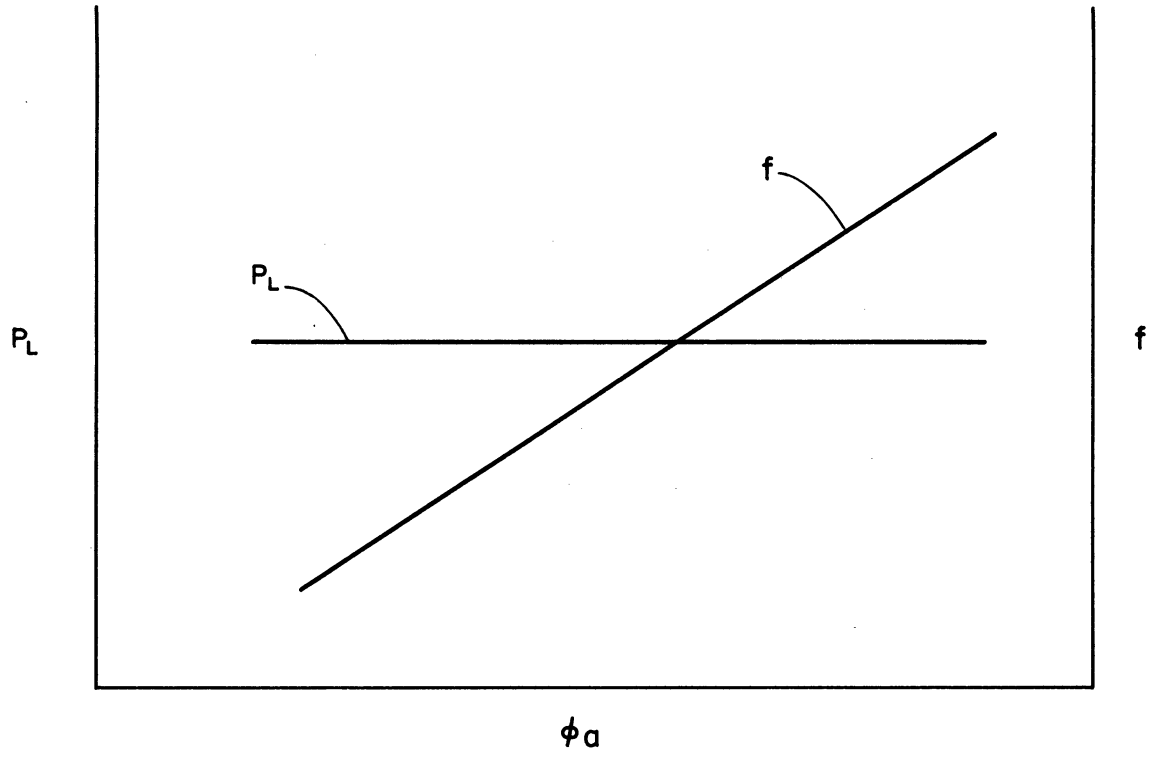

FIG. 3.18
IDEAL VOLTAGE TUNING CHARACTERISTICS

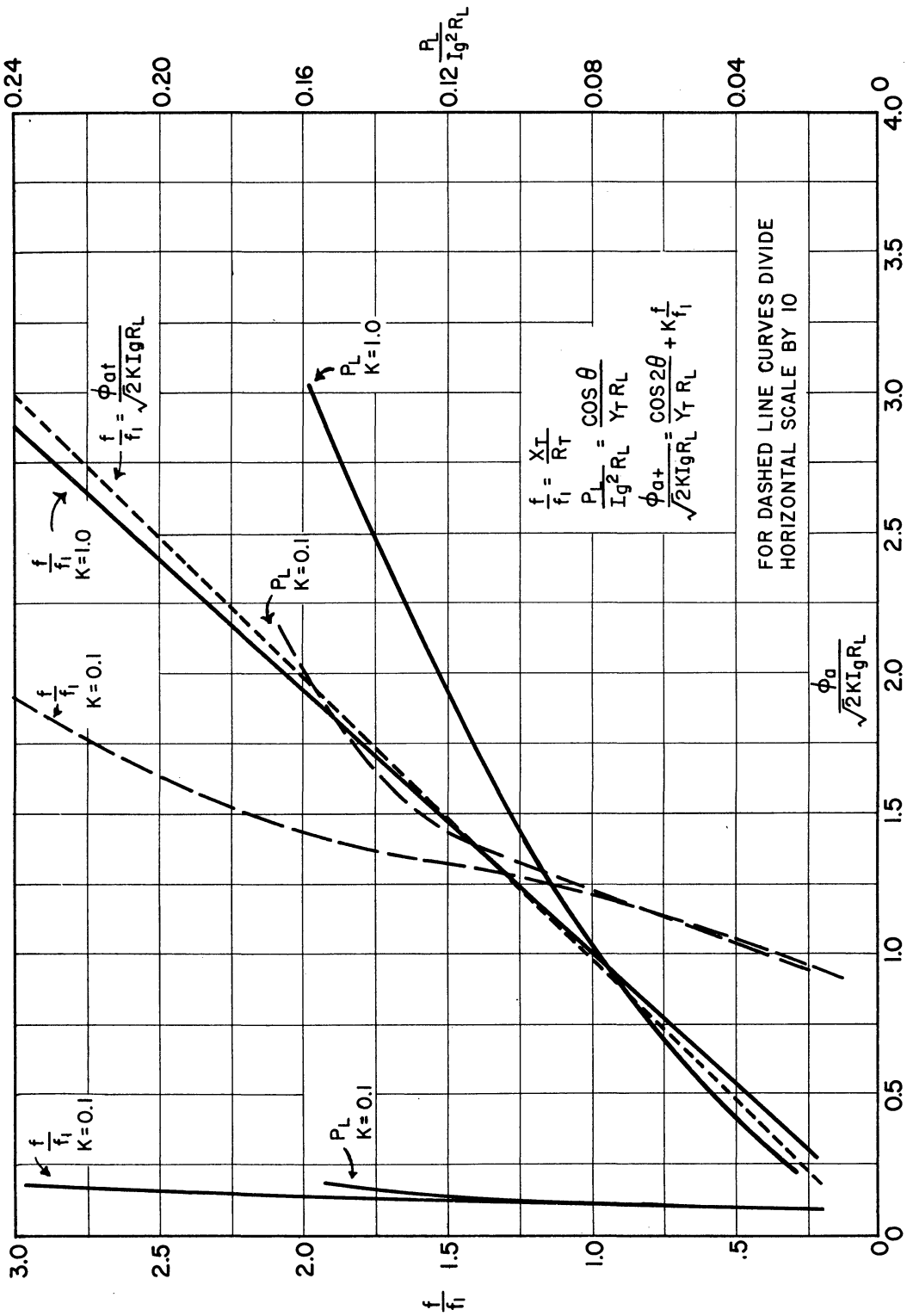

FIG. 3.19
THEORETICALLY PREDICTED VOLTAGE TUNING CHARACTERISTICS FOR CIRCUIT OF FIGURE 3.8

motion of the spokes parallel to the cathode is lagging the r-f voltage by an angle between -45° and -90°. The current due to motion of the electrons toward the anode, on the other hand, is leading the r-f voltage by less than 45°. As the phase of the spoke is advanced, this leading angle becomes greater while the lagging angle becomes smaller. The magnitude of the effect also increases as the phase angle becomes greater, so that, if it becomes appreciable it may be expected to do so as the condition of Fig. 2.8d is approached. The expected result would be a reversal in the pushing characteristic. Mr. J. F. Hull of Evans Signal Laboratory has recently suggested to the author that this effect, which he calls "anti-pushing", may be important in some magnetrons which he has observed. Mr. Hull has developed a method for approximating the magnitude of the contribution of arrival current to the total r-f current which indicates that, in pulsed magnetrons, arrival current should not be neglected.

4. EXPERIMENTAL RESULTS

The theory which has been presented is applicable, in principle, to almost any complete set of data on an oscillating magnetron. The criteria for completeness, however, are rather severe and not customarily satisfied. Also, for the purpose of the present treatment, it is more important that representative sets of data be presented than it is that numerous similar sets of data be presented. The discussion of experimental results will be limited, therefore, to a few sets of data, subject to quantitative analysis, which approach satisfaction of the criteria of completeness and to other sets of data which, although reasonably complete, display a degree of complexity which permits only semiquantitative analysis. Other data will be presented which illustrate qualitatively some of the points suggested by the theory, although not complete enough for quantitative discussion.

The author and others have presented detailed discussion of frequency characteristics of the preoscillating magnetron and the nonoscillating magnetic diode in other papers.[1] However, since effects of synchronism on resonance in the preoscillating magnetron are a direct result of phase focussing of the electrons into spokes, experimental

---

[1] III, 1, a, b; 7, a, b; 11; 22, a; and Brewer, G. R.,"The Propagation of Electromagnetic Waves in the Magnetron-Type Space Charge," Technical Report No. 8, Electron Tube Laboratory, Dept. of Elect. Eng., University of Michigan, July 1951. (Also Doctoral Thesis.)

evidence of this effect will be presented here along with results of frequency pushing and voltage-tuning measurements in the oscillating magnetron.

4.1 Measurements on the Preoscillating Magnetron

Complete measurements on a preoscillating magnetron include measurement of Q, resonance frequency, and impedance for various anode potentials up to the point of oscillation. The cathode temperature and magnetic field are, of course, properly adjusted so that oscillation can occur when the anode potential reaches the appropriate value. The presence of the electronic space charge in the magnetron is sufficient to cause a shift in the resonance frequency of the magnetron resonator. This shift may be either an increase or decrease in frequency depending on the magnetic field.[1] As the synchronism potential is reached the formation of spokes of space charge by the r-f voltage which is being used as a test signal is sufficient to overshadow the "passive" effects which are due only to the presence of the electrons and not related to their motion.

In order to study this effect experimentally over a wide range of magnetic fields the experimental setup of Fig. 4.1 has been used. This arrangement could not be used for the measurement of Q but facilitated rapid measurement of resonance frequency.[2]

A frequency-modulated signal from a klystron signal source is fed through lossy cable into the output pipe of the magnetron. The

---

[1] III, 22, a.

[2] For Q measurements and "passive" effects of the space charge on frequency see the reference just cited.

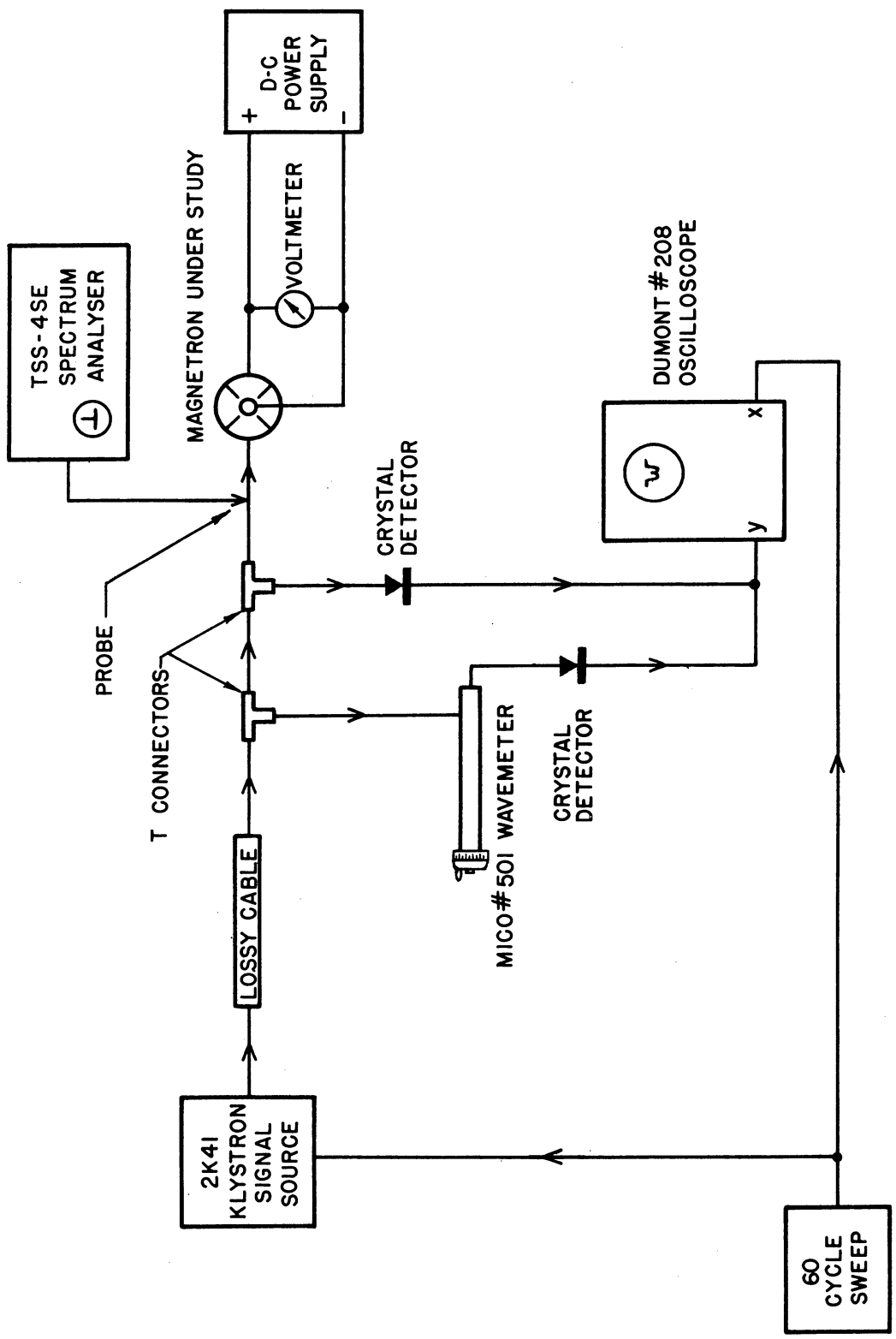

FIG. 4.1
EXPERIMENTAL ARRANGEMENT USED IN STUDY OF PREOSCILLATING MAGNETRON

lossy cable prevents changes in power reflected from the frequency-sensitive load from reacting on the signal source. Two "T" sections in the cable, leading to the magnetron test line, sample relatively large amounts of power. At frequencies away from the resonance of the magnetron cavity most of the power is reflected into the "T" sections. On resonance a substantial fraction of the power is absorbed by the magnetron. This absorption is indicated by a dip in the sweep pattern presented on the oscilloscope screen. The pip due to power transmitted through the wavemeter is superimposed on this pattern to check the frequency of the resonance. As the anode potential is raised the absorption dip moves due to the change in resonance frequency caused by the presence of the space charge. The wavemeter pip is quite readily matched to this change making extremely small changes observable.

A spectrum analyzer coupled by a probe into the test line and pretuned to the frequency of oscillation of the magnetron serves as a sensitive indication of the beginning of oscillation. Frequency of oscillation is then measured by the wavemeter.

Resonance frequency measurements were made for several anode potentials and several magnetic fields on the magnetron. Pushing data were not recorded for most of the measurements since the major purpose of the experiment was to get data on the preoscillating magnetron. However, in Fig. 4.2, preoscillating data for three magnetic fields is shown with pushing data in order to illustrate the relationship between the two types of data. In these graphs anode potential, ϕ_a, is plotted against δ_o where δ_o is given by

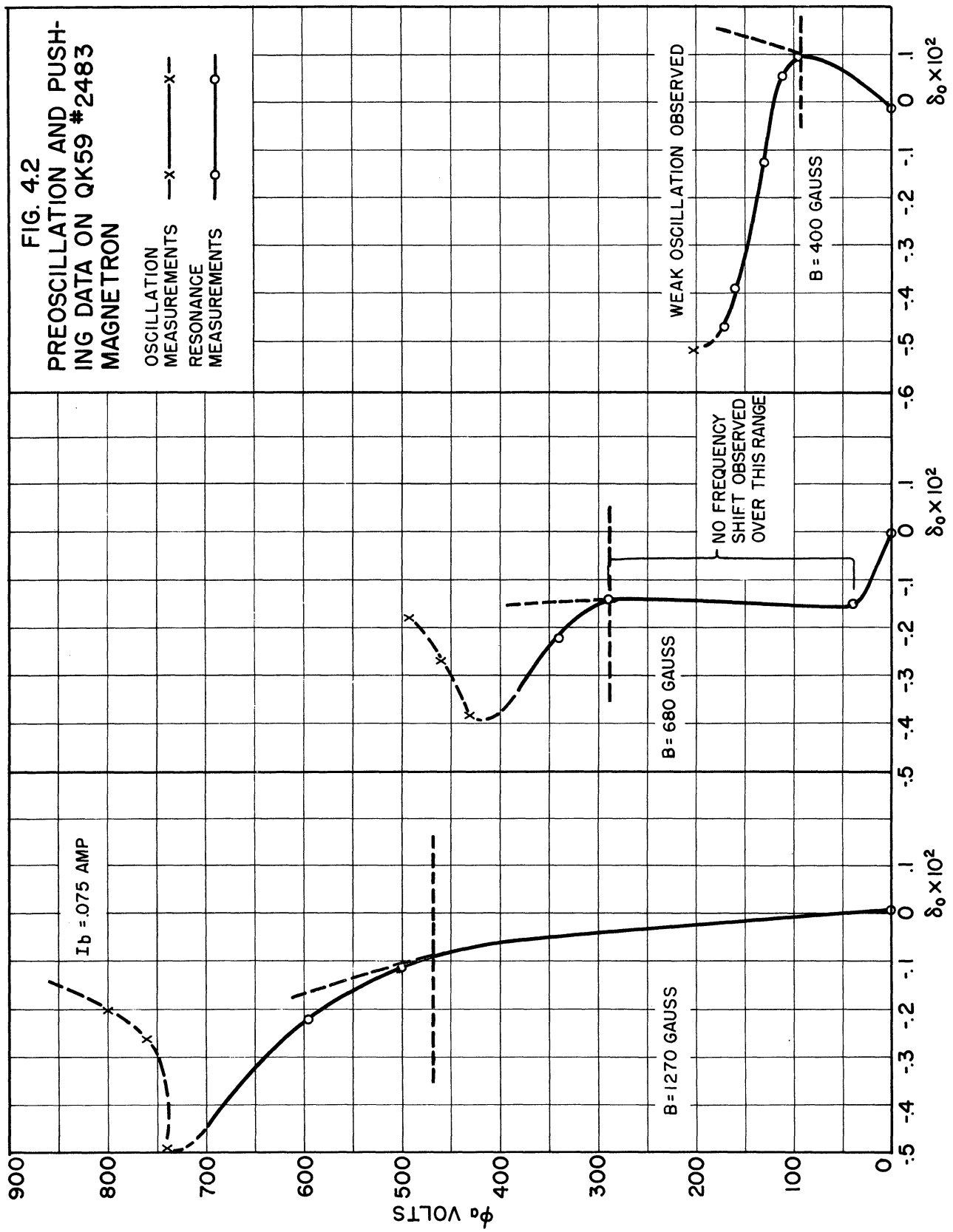
FIG. 4.2
PREOSCILLATION AND PUSHING DATA ON QK59 #2483 MAGNETRON
OSCILLATION MEASUREMENTS
RESONANCE MEASUREMENTS
Ib = .075 AMP
B = 1270 GAUSS
B = 680 GAUSS
NO FREQUENCY SHIFT OBSERVED OVER THIS RANGE
WEAK OSCILLATION OBSERVED
B = 400 GAUSS
φa VOLTS
δo × 10²

$$\delta_o = \frac{f_o - f_{oo}}{f_{oo}} = \frac{\lambda_{oo} - \lambda_o}{\lambda_{oo}}$$

f_o = resonance frequency with space charge present

λ_o = resonance wavelength with space charge present

f_{oo} = resonance frequency at $\phi_a = 0$

λ_{oo} = resonance wavelength at $\phi_a = 0$

At anode potentials below the value indicated by the dotted line parallel to the δ_o axis the frequency shift is attributed to the effect of mere presence of the space charge on the effective dielectric constant in the interaction space. The increasing rate of decrease in resonance frequency which occurs above this line and before oscillation is observed is not explained on the basis of this theory and is attributed to effects of synchronism. It is expected therefore that the marked change in slope of the curve should occur near and above the synchronism anode potential given by Eq 2.36. Points of oscillation are indicated by the (x) marks on the dashed-line curve. Further increase of anode potential beyond the potential for which oscillation begins causes the phase angle θ between the spokes and the r-f potential zero to decrease as predicted in the discussion of phase focussing. This causes the direction of frequency shift to reverse and follow the trend predicted by Eqs 3.47 and 3.48 toward the resonance frequency of the magnetron without the presence of the space charge.

The anode potential for which oscillations begin should be near the threshold potential given by Eq 2.42.

Data for several magnetic fields are given in Figs. 4.3a and 4.3b. The points of beginning oscillation are plotted against magnetic field in this presentation. The resonance frequency curves are connected

to the points of beginning oscillation, and plotted against a shifting scale on the lower abscissa. Thus the method of obtaining the points corresponding to an increasing rate of decrease in frequency is indicated for each set of data. Squares corresponding to this critical point are then plotted against the upper magnetic field scale. The results of this construction are summarized in Fig. 4.4. The theoretical threshold, synchronism, and cutoff potentials for this magnetron are plotted for comparison with the observed data.

The points of observed oscillation correspond to the first distinguishable single frequency signal. This signal was not of infinitesimal amplitude, but the r-f potential is not known because no power measurements were made in this experiment. Actually, noisy operation was observed at potentials well below these points in most cases, but the potential at which it was first observable was not clearly defined. These points of oscillation bear a definite relationship to the theoretical threshold potential curve, forming a curve of approximately the same slope but not coincident with it. Note that oscillation was observed at three points above the cutoff potential. In one set of data ($B = 310$ gauss) no oscillation or effects of synchronism were observed. (See data in Table 4.3.)

The spread of the points indicating the observable effect of synchronism is rather large and the accuracy of their determination not great, as the reader can see from examination of Fig. 4.3. However, one would not expect the effect of synchronism to become very noticeable until the synchronism potential was exceeded by an appreciable amount so that fairly definite focussing of the spokes could occur. At lower

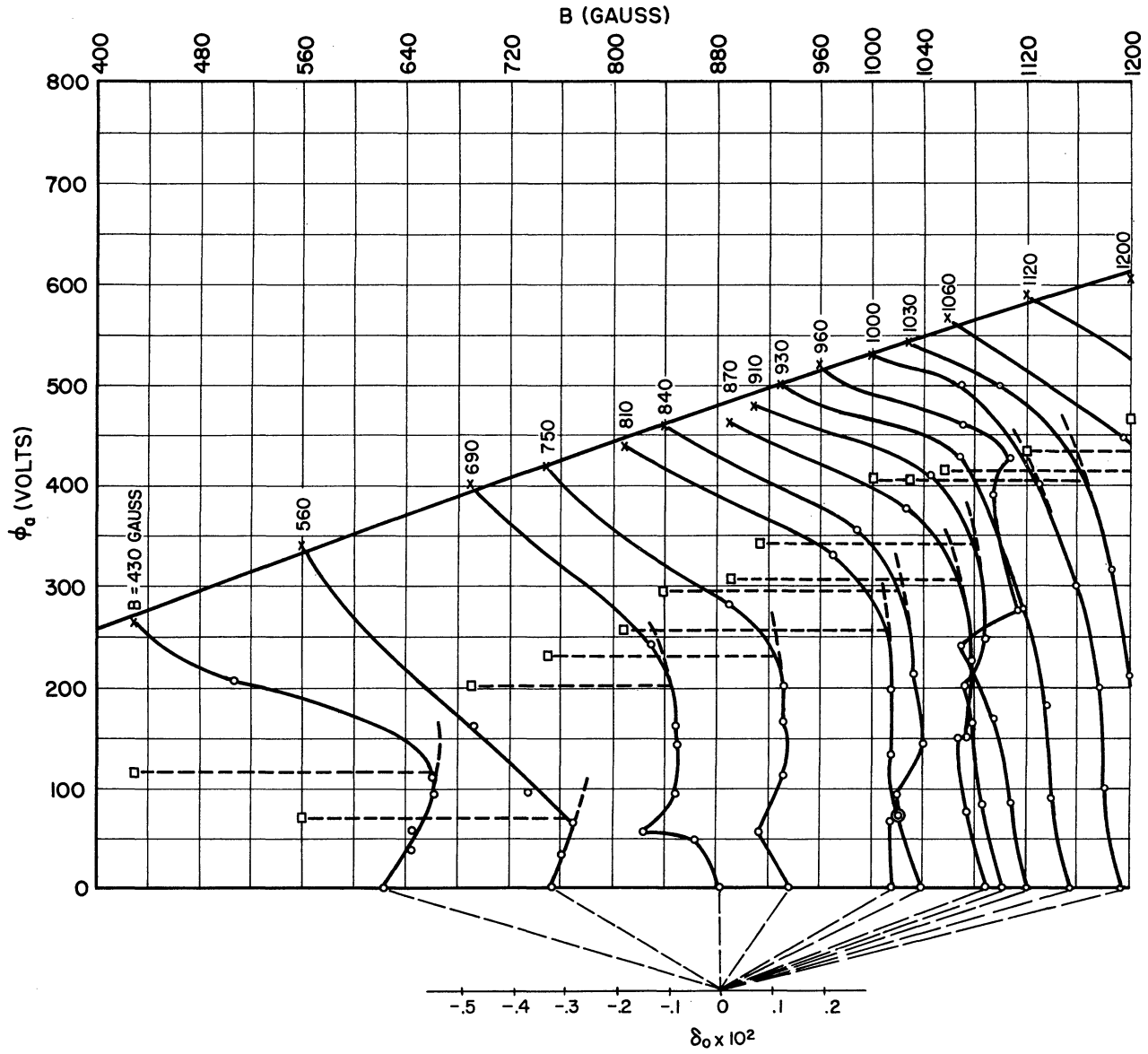

FIG. 4.3a

COMPLETE EXPERIMENTAL PRE-OSCILLATION DATA ON QK 59 #2483 MAGNETRON. METHOD OF OBTAINING POINTS IN FIGURE 4.4 IS INDICATED.

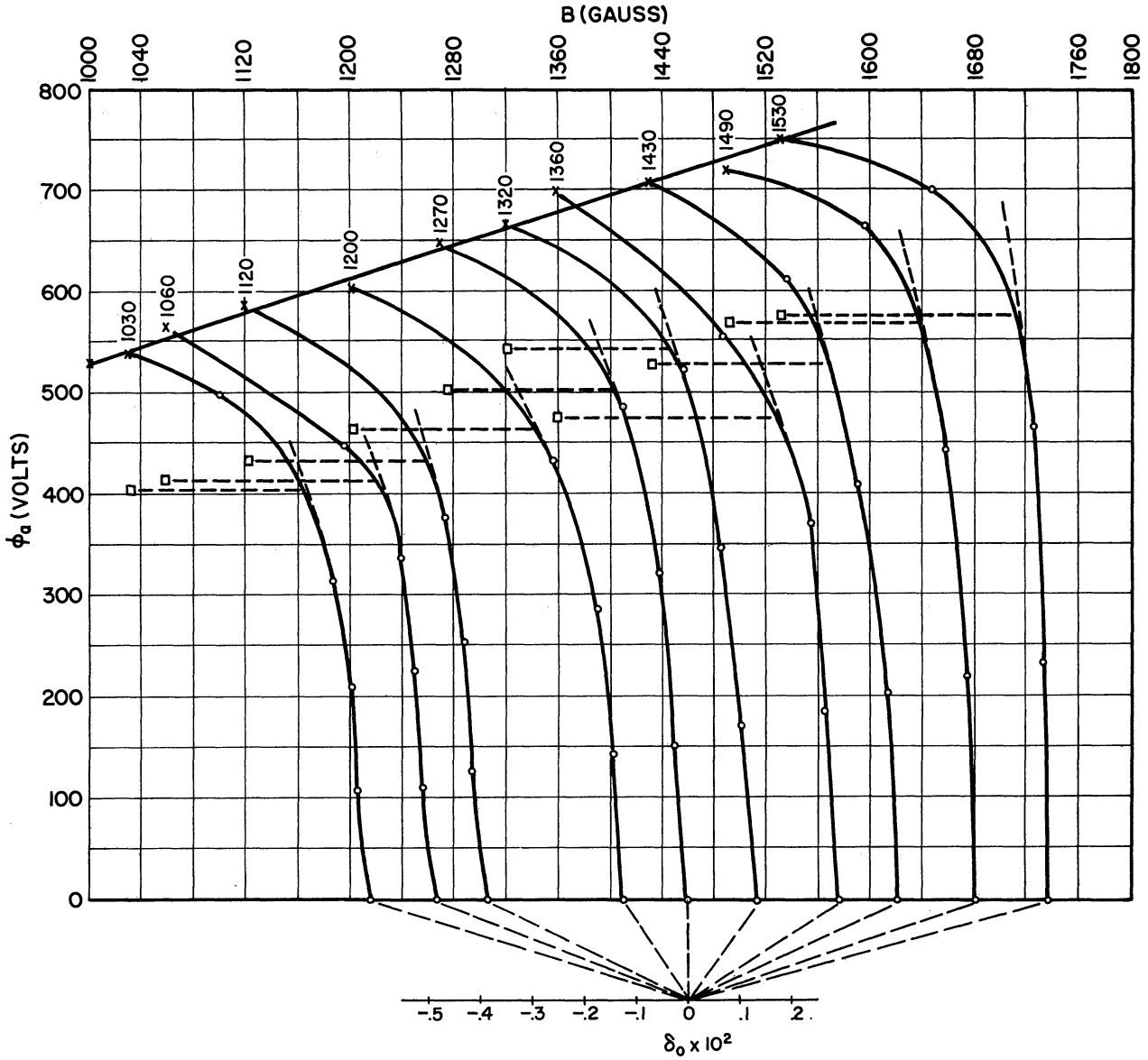

FIG. 4.3b

THRESHOLD POTENTIAL } PLOTTED AGAINST B SCALE

SYNCHRONISM POTENTIAL }

RELATIVE RESONANCE FREQUENCY PLOTTED AGAINST POTENTIAL

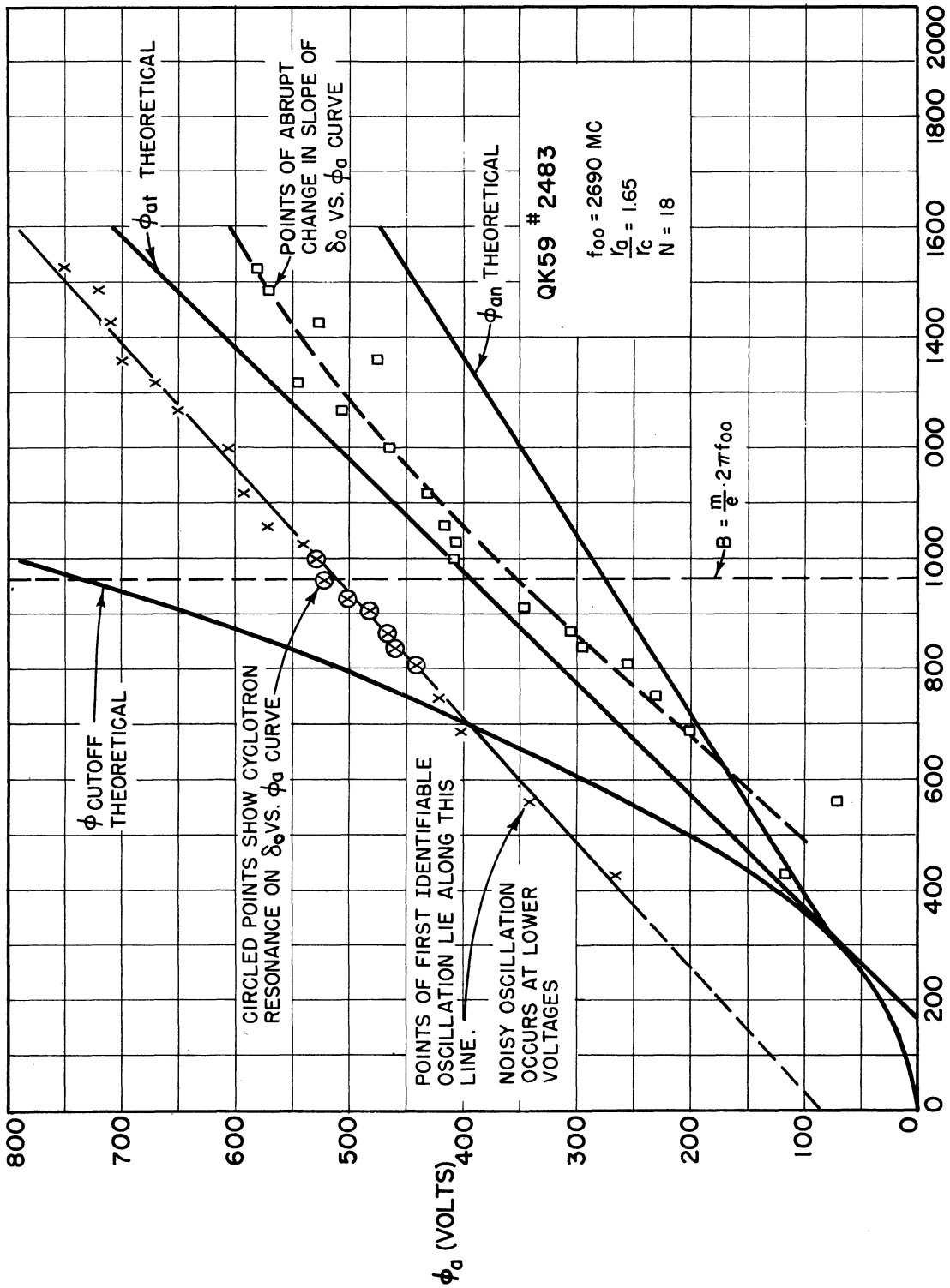

FIG. 4.4
SUMMARY OF DATA ON QK59 #2483 MAGNETRON OBTAINED FROM FIG. 4.3

magnetic fields, where the synchronism radius is approaching the anode radius (for $B = B_o$, $\phi = \phi_o$) these points approach coincidence with the theoretical synchronism potential curve (ϕ_{an}). These points, therefore, are a reasonably good indication of the effect to be expected of synchronism. No other data of this type exist in the author's experience.

The large discrepancy between the points indicating observable oscillation and the threshold potential curve is difficult to explain unless a fairly large r-f potential exists in the magnetron and the magnetron is loaded by a fairly high impedance. Under these conditions a large difference between threshold potential and anode potential could exist with small power output. An experimental setup at microwave frequencies which would provide information necessary to calculate the r-f potential and impedance in addition to the information provided by the apparatus shown in Fig. 4.1 would be extraordinarily complicated, and probably of questionable accuracy.

The most significant probable source of error in the accumulation of data used for the curves in Fig. 4.4 would be in the determination of the magnetic field or in the dimensions of the magnetron. The magnetic field for the entire set of measurements could be in error by 75 to 100 gauss due to the residual magnetism which may add or subtract from the calibration curve. This curve is given in Fig. 4.5. This amount of error would not explain the discrepancy in the observable oscillation and threshold potential curves. Also, it is doubtful that the error exists since the observance of no oscillation at 310 gauss and oscillation at 430 gauss (and 400 gauss in Fig. 4.2) is a reasonably good check on the value of $B_o = 336$ gauss. Moreover, the disturbance

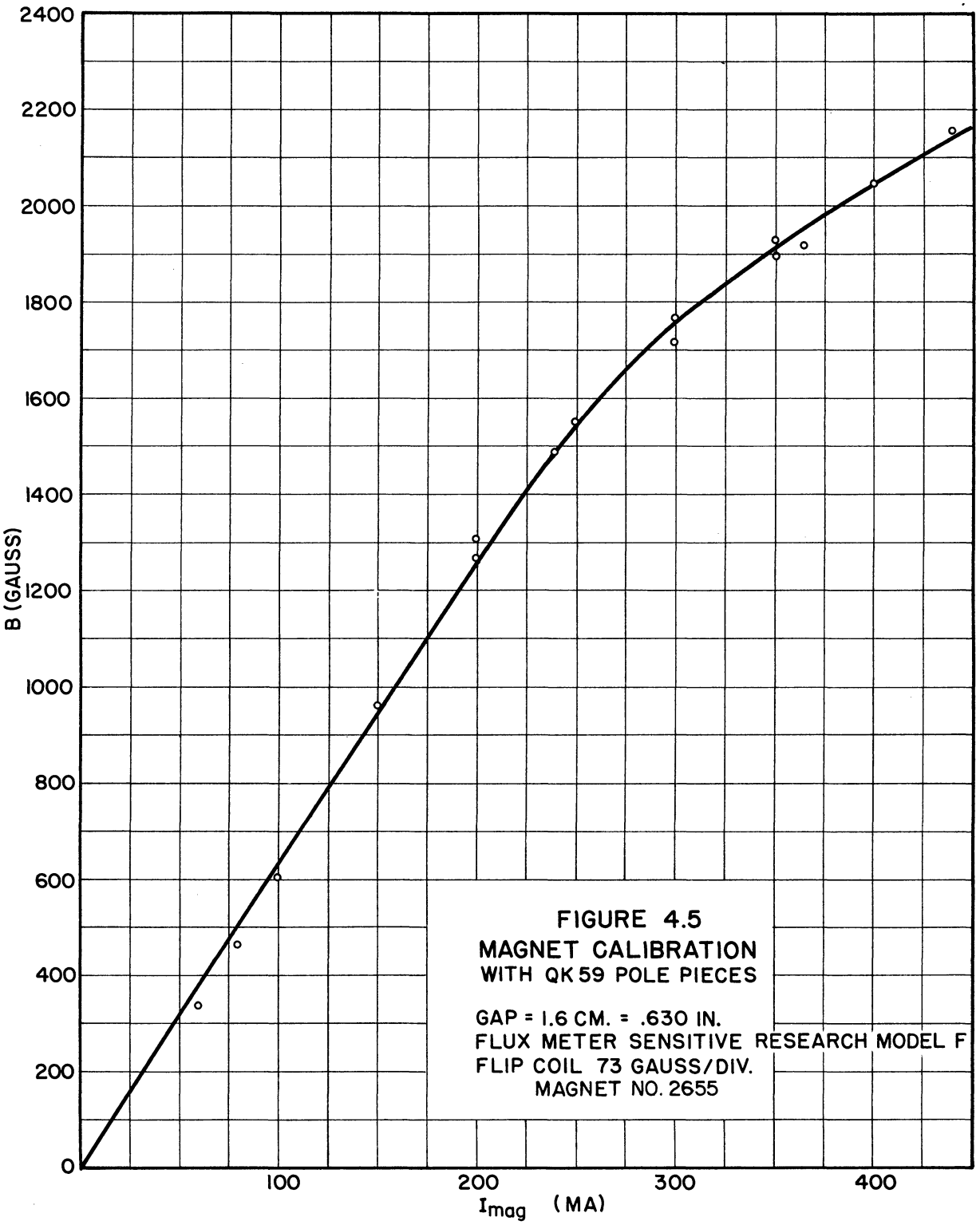

FIGURE 4.5
MAGNET CALIBRATION
WITH QK 59 POLE PIECES

GAP = 1.6 CM. = .630 IN.
FLUX METER SENSITIVE RESEARCH MODEL F
FLIP COIL 73 GAUSS/DIV.
MAGNET NO. 2655

in the resonance wavelength curves for magnetic fields between 870 and 1,000 gauss which is attributed to the cyclotron resonance is a reasonably good check on the cyclotron field B_c = 955 gauss. This disturbance is observable in the curves of Figs. 4.3a and 4.3b.

The magnetron dimensions may be in error since the Raytheon QK59 tube used was not constructed in the Michigan laboratory, and data was taken from tube specifications. In particular, the ratio r_a/r_c may be in error by 10 or 20%. Another tube which was taken apart had a cathode larger in this proportion.

The complete discussion of the curves in Fig. 4.2 is beyond the scope of this report. The same set of data has been discussed previously by the author with particular reference to the behavior of the curves at potentials less than the synchronism potential.[1] The reader will note the variation in this behavior from definitely increasing frequency at low magnetic fields to decreasing frequency at high magnetic fields as the anode potential is increased.

The data on the QK59 magnetron used in these tests are given in Table 4.1. Data for the curves of Fig. 4.2 are given in Table 4.2, and for the curves of Fig. 4.3 in Table 4.3.

Table 4.1

Data on Raytheon QK59 Magnetron

r_a	r_c	r_a/r_c	N	ϕ_o	B_o	Magnet Gap
.290 cm	.176 cm	1.65	18	83.5 volts	336 gauss	1.60 cm

---

[1] III, 22, a.

Table 4.2

Preoscillation and Pushing Data on QK59 No. 2483 Magnetron

I_{magnet} .2 amp.		B(gauss) 1270	I_{magnet} .12 amp.		B(gauss) 680
ϕ_a(volts)	λ_o(cm)	$\delta_o \times 10^2$	ϕ_a(volts)	λ_o(cm)	$\delta_o \times 10^2$
0	11.155	+.01	0	11.156	0
500	11.168	-.11	40	11.173	-.15
595	11.180	-.22	290	11.172	-.14
740	11.210	-.49 osc	340	11.180	-.22
760	11.185	-.26 osc	430	11.198	-.38 osc
800	11.178	-.20 osc I_b = .075 amp.	460	11.186	-.27 osc

I_{magnet} .065 amp.		B(gauss) 400	
ϕ_a(volts)	λ_o(cm)	$\delta_o \times 10^2$	
0	11.157	-.01	
95	11.145	+.098	
110	11.150	+.054	
130	11.170	-.125	questionable point
160	11.200	-.395	
170	11.208	-.470	
200	11.214	-.520	osc, very weak

Table 4.3

Preoscillation Data on QK59 No. 2483 Magnetron

(ϕ_a given in volts, λ_o in centimeters, starred points indicate clean oscillation observed.)

I_{mag} = 50 ma
B = 310 gauss

ϕ_a	λ_o	$\delta_o \times 10^2$
0	11.155	+.01
29	11.153	+.028
48	11.151	+.045
115	11.149	+.063
No oscillation observed		

I_{mag} = 70 ma
B = 430 gauss

ϕ_a	λ_o	$\delta_o \times 10^2$
0	11.155	+.01
37	11.150	+.054
55.5	11.150	+.054
92.5	11.145	+.098
110	11.140	+.099
205	11.188	-.29
265*	11.210	-.48

I_{mag} = 90 ma
B = 560 gauss

ϕ_a	λ_o	$\delta_o \times 10^2$
0	11.155	+.01
31.5	11.152	+.036
63	11.150	+.054
?94	11.160	-.036
160	11.172	-.14
340*	11.209	-.475

I_{mag} = 110 ma
B = 690 gauss

ϕ_a	λ_o	$\delta_o \times 10^2$
0	11.155	+.01
47.5	11.160	-.036
55	11.172	-.14
95	11.164	-.072
142	11.164	-.072
160	11.164	-.072
240	11.170	-.125
400*	11.210	-.48

I_{mag} = 120 ma
B = 750 gauss

ϕ_a	λ_o	$\delta_o \times 10^2$
0	11.155	+.01
56	11.163	-.063
112	11.158	-.018
168	11.158	-.018
200	11.158	-.018
280	11.170	-.125
420*	11.210	-.48

I_{mag} = 130 ma
B = 810 gauss

ϕ_a	λ_o	$\delta_o \times 10^2$
0	11.157	-.01
66	11.157	-.01
70	11.155	+.01
132	11.157	-.01
198	11.157	-.01
330	11.170	-.125
440*	11.214	-.52

I_{mag} = 135 ma
B == 840 gauss

ϕ_a	λ_o	$\delta_o \times 10^2$
0	11.156	0
71	11.161	-.045
120	11.161	-.045
142	11.156	0
213	11.158	-.018
355	11.170	-.125
460*	11.212	-.50

I_{mag} = 140 ma
B = 870 gauss

ϕ_a	λ_o	$\delta_o \times 10^2$
0	11.156	0
75	11.160	-.036
150	11.161	-.045
150	11.160	-.036
225	11.159	-.027
375	11.174	-.160
465*	11.212	-.50

Table 4.3

(Continued)

I_{mag} = 145 ma
B = 910 gauss

ϕ_a	λ_o	$\delta_o \times 10^2$
0	11.155	+.01
83	11.160	-.032
166	11.162	-.054
200	11.163	-.063
249	11.159	-.027
415	11.171	-.135
480*	11.210	-.48

I_{mag} = 150 ma
B = 930 gauss

ϕ_a	λ_o	$\delta_o \times 10^2$
0	11.156	0
86	11.159	-.027
172	11.162	-.054
240	11.170	-.125
275	11.158	-.018
430	11.170	-.125
500*	11.210	-.48

I_{mag} = 155 ma
B = 960 gauss

ϕ_a	λ_o	$\delta_o \times 10^2$
0	11.155	+.01
92	11.159	-.027
184	11.160	-.036
276	11.166	-.09
390	11.172	-.14
425	11.168	-.11
460	11.179	-.20
520*	11.210	-.48

I_{mag} = 160 ma
B = 1000 gauss

ϕ_a	λ_o	$\delta_o \times 10^2$
0	11.155	+.01
100	11.159	-.027
200	11.160	-.036
300	11.165	-.08
400	11.173	-.15
500†	11.190	-.30
530*	11.214	-.52

†noise observed

I_{mag} = 165 ma
B = 1030 gauss

ϕ_a	λ_o	$\delta_o \times 10^2$
0	11.156	0
106	11.160	-.036
212	11.162	-.054
318	11.165	-.080
530†	11.190	-.30
540*	11.209	-.475

†noise observed

I_{mag} = 170 ma
B = 1060 gauss

ϕ_a	λ_o	$\delta_o \times 10^2$
0	11.157	-.01
112	11.160	-.036
224	11.162	-.054
337	11.165	-.08
448	11.177	-.19
561	Noise observed	
570*	11.215	-.53

I_{mag} = 180 ma
B = 1120 gauss

ϕ_a	λ_o	$\delta_o \times 10^2$
0	11.156	0
126	11.159	-.027
254	11.161	-.045
378	11.165	-.08
590*	11.208	-.465

I_{mag} = 190 ma
B = 1200 gauss

ϕ_a	λ_o	$\delta_o \times 10^2$
0	11.156	0
144	11.159	-.027
288	11.162	-.054
432	11.172	-.14
605*	11.215	-.53

Table 4.3

(Continued)

I_{mag} = 200 ma
B = 1270 gauss

ϕ_a	λ_o	$\delta_o \times 10^2$
0	11.156	0
162	11.159	-.027
324	11.162	-.054
486	11.170	-.125
650*	11.209	-.475

I_{mag} = 210 ma
B = 1320 gauss

ϕ_a	λ_o	$\delta_o \times 10^2$
0	11.156	0
174	11.159	-.027
348	11.163	-.063
522	11.172	-.14
670*	11.210	-.48

I_{mag} = 220 ma
B = 1360 gauss

ϕ_a	λ_o	$\delta_o \times 10^2$
0	11.155	+.01
185	11.158	-.018
370	11.161	-.045
555	11.179	-.21
700*	11.215	-.53

I_{mag} = 230 ma
B = 1430 gauss

ϕ_a	λ_o	$\delta_o \times 10^2$
0	11.156	0
205	11.158	-.018
410	11.164	-.072
615	11.180	-.22
710*	11.209	-.475

I_{mag} = 240 ma
B = 1490 gauss

ϕ_a	λ_o	$\delta_o \times 10^2$
0	11.156	0
222	11.158	-.018
444	11.162	-.054
666	11.179	-.21
720*	11.210	-.48

I_{mag} = 250 ma
B = 1530 gauss

ϕ_a	λ_o	$\delta_o \times 10^2$
0	11.157	-.01
234	11.159	-.018
468	11.160	-.036
702	11.182	-.23
750*	11.215	-.53

4.2 Frequency-Pushing Measurements

The comparison of experimental results of pushing measurements with the theoretical analysis which has been presented is complicated by the complexity of the magnetron resonator structures which actually exist. It becomes necessary either to provide complete analysis of circuits other than the simple resonant circuit of Fig. 3.6 or to estimate by approximation the results to be expected on the basis of the analysis of the simple resonant circuit. The latter method is chosen here.

Data will be presented on three magnetrons designed and constructed in the University of Michigan laboratory. In all of these magnetrons the means for analysis of the resonator have been worked out with detail which permits calculation of the circuit parameters involved. However, the actual r-f circuit is complicated by the introduction of the cathode. The understanding of the effect of the cathode is shown to be quite important to the understanding of the space-charge behavior. It has, however, not been studied in the detail that has been given to the simple resonator.

Mr. W. C. Brown and Mr. E. Dench of Raytheon Mfg. Co. have made available to the author the results of a series of measurements on approximately 50 magnetrons of the RK5609-QK217 type. Several types of data were taken which illustrate several principles of magnetron behavior. These data are of interest to this study, particularly in that they illustrate the effects of cathode emission. Data on one of the magnetrons are presented here with some discussion. In most cases the data are not sufficiently complete to apply the method of analysis of Chapter 2 and Chapter 3.

Before presenting the experimental results, a general discussion of the type of data necessary, the methods used, and the accuracy expected will be given.

A. Methods of Measurement. The following data are necessary in order to provide experimental information which is sufficiently complete to allow interpretation of frequency pushing in the oscillating magnetron:

Dependent Variable

1. Frequency
2. Power
3. Anode potential

Readily Variable Parameters

4. Anode current
5. Magnetic field

Not-So-Readily-Variable Parameters

6. Q
7. Load conductance at anode terminals
8. Resonance frequency of the anode sets and attached resonator
9. Resonance frequency of the entire system
10. Complete interaction space dimensions

The accuracy of the instrumentation used in obtaining these data varies with the quantity being measured. The following is an estimation of the limitations in the techniques used in obtaining the data of this section.

Frequency was determined by a Mico No. 501 wavemeter. With reasonable care these wavemeters can be set and read to $\pm$ .002 cm. At

15-cm wavelength (2000 megacycles) this represents an expected error of ± .013% or ± .26 mc.

Power was determined by coupling the magnetron output through a 1-5/8-inch, 50-ohm coaxial line to a calorimetric water load. A water flow of .37 liters per minute was maintained using a Schuette Koerting Type P046-11-091 flowmeter. Periodic checks of the calibration of this instrument show no variation. Temperature differential was measured by a Foxboro differential thermometer having a 20° C full scale divided into 0.2° C divisions on a 270 angular degree dial (Serial No. 454988). The power calibration at this water flow is 25 watts/degree. Estimating the accuracy of flow determination at ± .01 liters/minute and the temperature determination at ± .05°, the expected error at the 100 watt level is ± 3.75% or ± 3.75 watts. The time constant of the calorimetric system is rather long, which also may have been a source of error in some measurements made before equilibrium was reached.

Anode potential and anode current were measured with panel meters on the laboratory supply. Potentials were read to ± 10 volts. At 2000 volts this means an expected error of ± .5%, which is within the accuracy of the instrument. Anode currents were measured with similar accuracy.

The magnetic field in the interaction space is assumed to be that given by a magnet current calibration curve made with pole pieces identical with those in the magnetron. Two fluxmeters have been used, one a Sensitive Research Model F flip coil type, the other a Rawson rotating coil type. This latter meter has been used with some success in the exploration of fields in the magnetron interaction space. It

is concluded from these measurements that the calibrations using the flip coil type of meter, which gives average flux, may be in error by approximately 5% because of the variation in flux density across the tube axis.[1] In general the flip coil method gives gauss readings about 5% low. The effects of hysteresis are also to be considered. A series of measurements on the magnet used in these experiments with the pole pieces for the Model 3 magnetron (see calibration curve of Fig. 4.26) at .5 amperes magnet current showed a maximum spread of 1830 to 1790 gauss. The magnet was turned on and off and current reversed with no attempt to control hysteresis.

Measurement of Q involves the use of a signal generator to feed power into the magnetron, a wavemeter to measure frequency, and a detector which measures the position of the minimum on the standing wave which results in the line and the ratio of the maximum to the minimum. The detector consisted of a probe in the line which fed into a TSS4SE spectrum analyzer through an attenuator calibrated in db. The signal appearing on the spectrum analyzer screen was kept at a constant level by use of the attenuator. Attenuator readings then gave SWR in db. This was converted to voltage standing wave ratio (VSWR) for plotting purposes. Accuracy of Q determination depends almost entirely on the determination of the minimum of the VSWR curve. Various methods of plotting the data exist.[2] Comparison of these methods and checking of

---

1 Measurements by S. R. Ruthberg, Quarterly Report No. 2, Electron Tube Laboratory, Dept. of Electrical Engineering, University of Michigan, June 1951.

2 The method used here is that discussed by L. Malter and G. R. Brewer in "Microwave Q Measurements in the Presence of Series Losses," Journal Appl. Phys., Vol. 20, No. 10, pp. 918-925, October 1949.

measurements indicate that Q may be determined, with reasonable care, within 10%. Extreme care and ideal conditions will, of course, give better accuracy.

B. Measurements on Michigan Magnetrons Model 7A No. 33 and Model 7D No. 42. Assembly drawings of the Model 7A magnetron and the Model 7D magnetron are given in Figs. 4.6 and 4.7. The resonator structure of these magnetrons[1] consists of a one-half wave coaxial line loaded capacitively by vanes, connected through slots between bars in the inner conductor. The tips of the vanes and the bars form the anode sets for the magnetron interaction space. Loading is accomplished by a "T" connection into the coaxial cavity. The position of this "T" connection is the major difference between the Model 7A and the Model 7D magnetrons. The Model 7D output "T" has approximately twice the mutual flux linkage with the coaxial cavity as the Model 7A. The Model 7A has an extra coupling loop which was designed to couple into a higher frequency vane mode. This loop does not affect the mode under study in these experiments.

A characteristic of the type of resonator and anode structure used in the Model 7 is a rather strong coupling to the coaxial line formed by the cathode stem and the magnet pole piece. In order to prevent loss of power through this coaxial line, it is made very low impedance (about 4 ohms) and one-quarter wavelength. The impedance presented to the line at the cathode terminals is relatively high, so that the impedance

---

[1] This type of magnetron resonator was given detailed discussion by J. S. Needle and G. Hok in "A New Single Cavity Resonator for a Multi-anode Magnetron," Technical Report No. 6, Electron Tube Laboratory, Dept. of Electrical Engineering, University of Michigan, January 8, 1951.

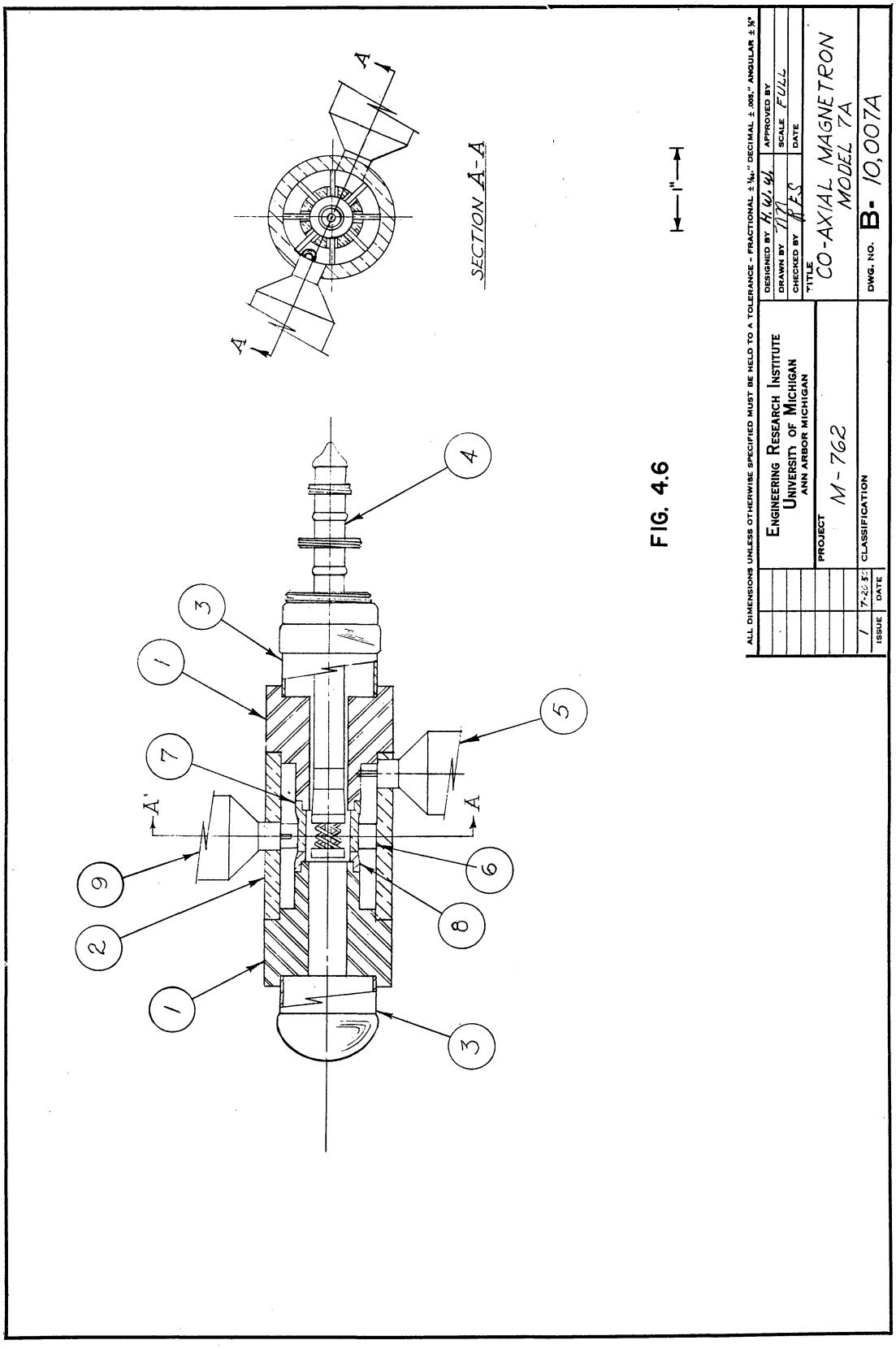
A
A
SECTION A-A
1"
4
3
1
7
A'
A
5
9
6
2
8
1
3
ALL DIMENSIONS UNLESS OTHERWISE SPECIFIED MUST BE HELD TO A TOLERANCE - FRACTIONAL ± 1/64" DECIMAL ± .005" ANGULAR ± 5°
ENGINEERING RESEARCH INSTITUTE
UNIVERSITY OF MICHIGAN
ANN ARBOR MICHIGAN
PROJECT
M-762
DESIGNED BY H.W.W.
DRAWN BY
CHECKED BY
APPROVED BY
SCALE FULL
DATE
TITLE
CO-AXIAL MAGNETRON
MODEL 7A
ISSUE
DATE
CLASSIFICATION
DWG. NO. B- 10,007A
DWG. NO. B

FIG. 4.6

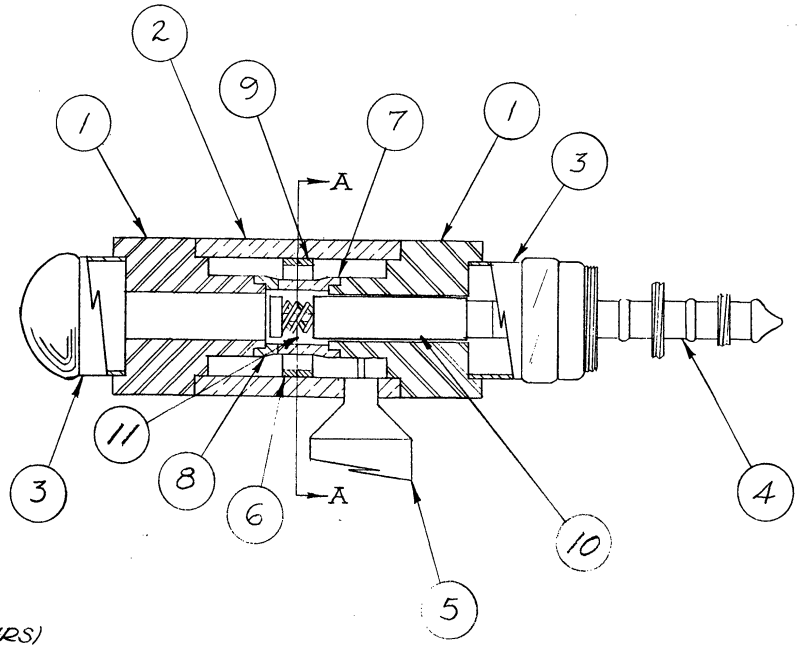

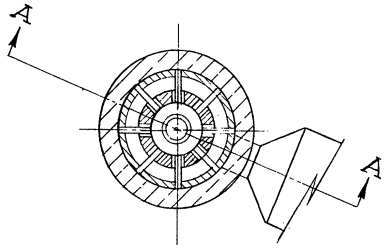

SECTION A-A

1 - POLE PIECE (HRS)
2 - CAVITY SHELL (CU)
4 - CATHODE CONNECTIONS
5 - OUTPUT PIPE
6 - FILLER RING (FOR MODE SEPARATION)
7 - CAVITY CENTER CONDUCTOR
10 - CATHODE LINE BY-PASS
11 - INTERACTION SPACE

FIG. 4.7

1"

ALL DIMENSIONS UNLESS OTHERWISE SPECIFIED MUST BE HELD TO A TOLERANCE - FRACTIONAL ± 1/64," DECIMAL ± .005," ANGULAR ± 1/2°

ENGINEERING RESEARCH INSTITUTE UNIVERSITY OF MICHIGAN ANN ARBOR MICHIGAN		DESIGNED BY H.W.W.	APPROVED BY
		DRAWN BY T.T.	SCALE FULL
		CHECKED BY T. R.B.	DATE 10-24-50
PROJECT M-762		TITLE CO-AXIAL MAGNETRON MODEL 7D	
CLASSIFICATION		DWG. NO. B- 10,007D	
ISSUE	DATE		

presented to the interaction space is very low compared to the anode resonator impedance. This effectively forms a bypass between the bar anodes and the cathode surface. The cathode is thus unbalanced relative to the two anode sets. This can be shown to be unimportant to the analysis of the space-charge behavior. However, it will be found important in the analysis of the circuit since the resonance frequency of the magnetron is shifted by the presence of the cathode, and the energy storage in the cathode bypass causes circulating currents along the cathode stem rather than in the coaxial cavity which contains the output coupling.

Insofar as the interaction space is concerned the Model 7A and Model 7D are supposed to be identical. In other words, the constants K_1 and K_2 of Eqs 3.46, 3.47, and 3.48 are the same for the two tubes. Any difference in their characteristics must, therefore, be caused by differences in the resonant circuit and loading. In order to facilitate comparison of the two sets of data, the frequency, power, and anode potential for the two tubes and the various magnetic fields are plotted side by side to the same scale in Figs. 4.9 to 4.16. A magnet calibration is given in Fig. 4.8. In Fig. 4.17 the lowest measured anode potentials for which oscillation is sustained, taken from the two sets of data, are plotted for comparison with the theoretical threshold potential. In Figs. 4.18 and 4.19 power output is plotted as a function of frequency for the Model 7A No. 33 magnetron. In Fig. 4.20 similar curves for the Model 7D No. 42 magnetron are plotted for three high magnetic fields. The anomalous behavior of both tubes at magnetic fields less than 1200 gauss is attributed to a cyclotron resonance in the electron

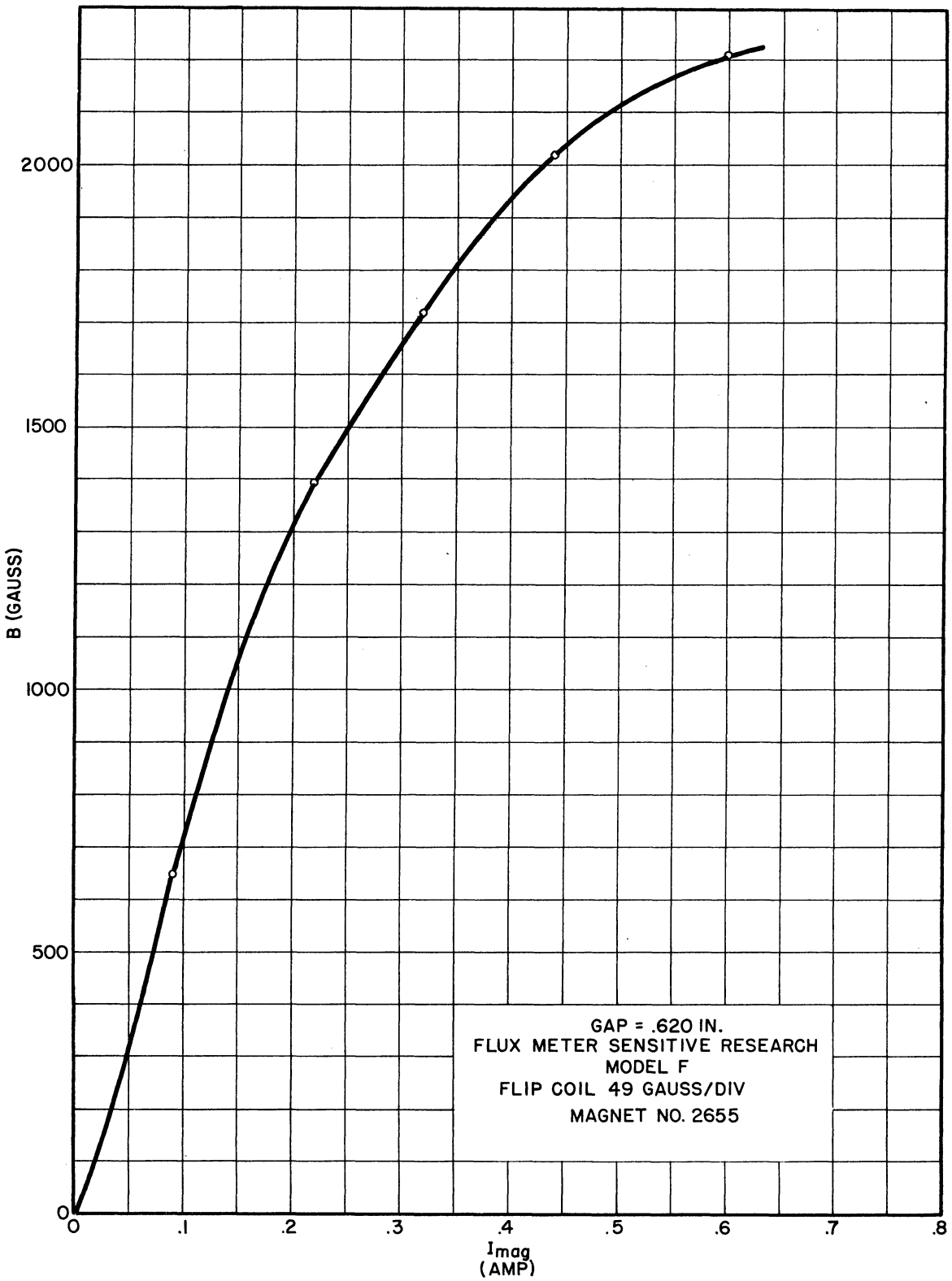

FIG. 4.8 MAGNET CALIBRATION MOD. 7 POLE PIECES

stream. The cyclotron field for this magnetron is 760 gauss. No attempt will be made at complete interpretation of this phenomenom in this discussion. It is related to the presence of the unbalanced radial fields caused by cathode unbalance. Attention will be concentrated on the more normal behavior at fields above 1200 gauss.

In order to apply the methods of analysis, developed in the last chapter, to the Model 7 magnetrons, the variables defined there must be determined. This has been done and the results are tabulated in Table 4.5. The data used in these calculations is given in Table 4.4. Values of the variables are listed for four different magnetic fields in order to illustrate the range of variation.

The constant $K = \frac{\phi_f}{\phi_{r\text{-}f\ max}}$ is determined as follows: The r-f potential distribution at the anode radius for maximum difference in potential is assumed to have a trapezoidal form like that of ψ_K in Fig. 3.3. Bars, vanes, and gaps between the bars and vanes all have the same angular width. The fundamental frequency component of a symmetrical trapezoid is given by

$$\frac{\phi_1}{\phi_{r\text{-}f}} = \sqrt{2}\,\frac{4}{\pi} \,. \qquad (1)$$

This wave is split into two travelling waves, one travelling with the electrons and one travelling in the opposite direction. Thus,

$$K = \frac{2\sqrt{2}}{\pi} = 0.9 \,.$$

---

1 Reference Data for Radio Engineers, Federal Telephone and Radio Corporation, 1946, p. 282.

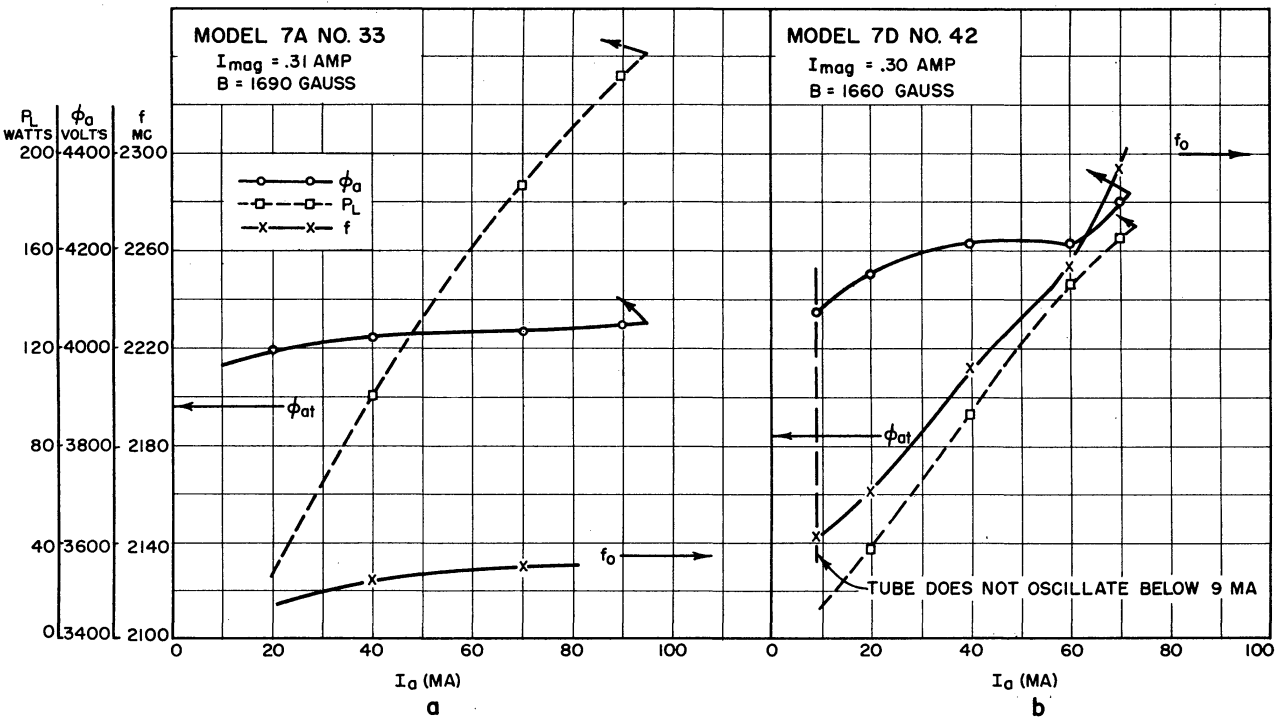

FIG. 4.9
PERFORMANCE DATA FOR MODEL 7 MAGNETRONS
B = 1690 GAUSS

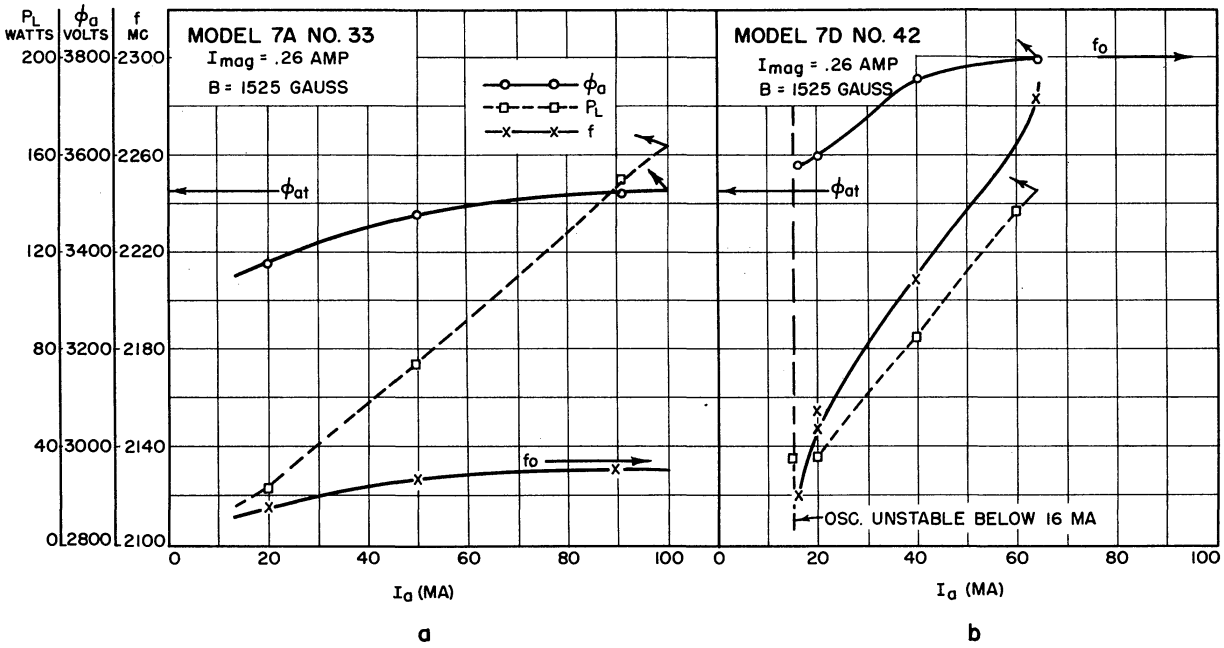

FIG. 4.10
PERFORMANCE DATA FOR MODEL 7 MAGNETRONS
B = 1525 GAUSS

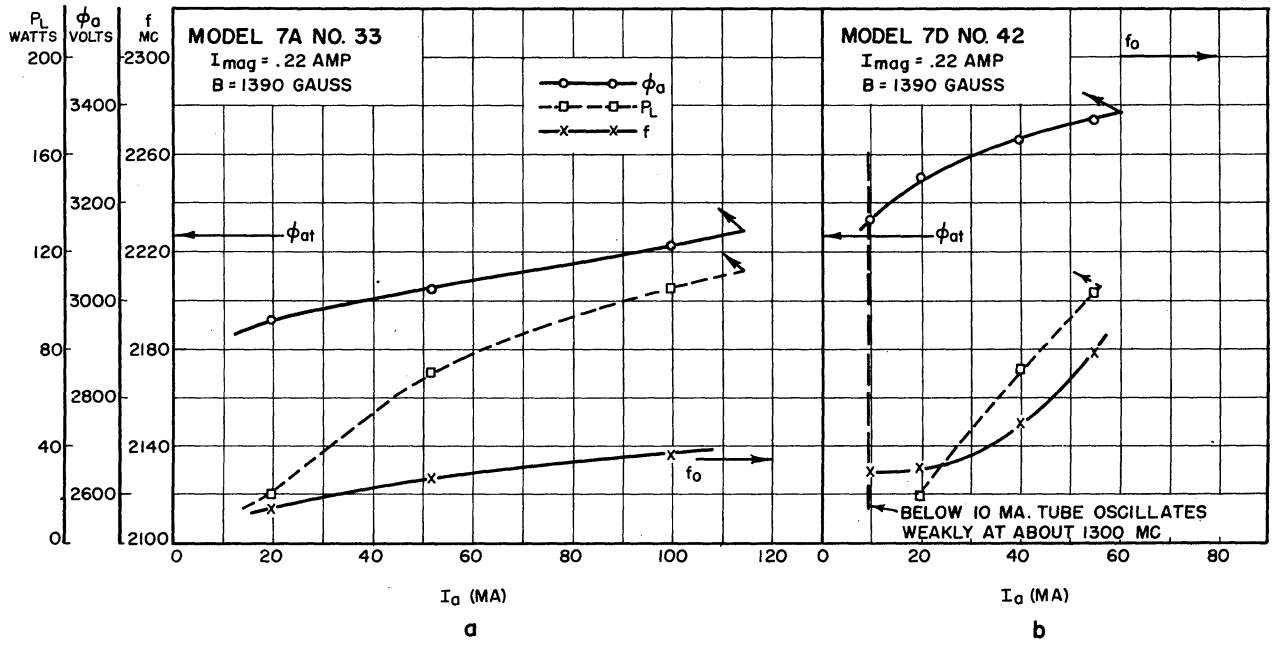

FIG. 4.11
PERFORMANCE DATA FOR MODEL 7 MAGNETRONS
B = 1390 GAUSS

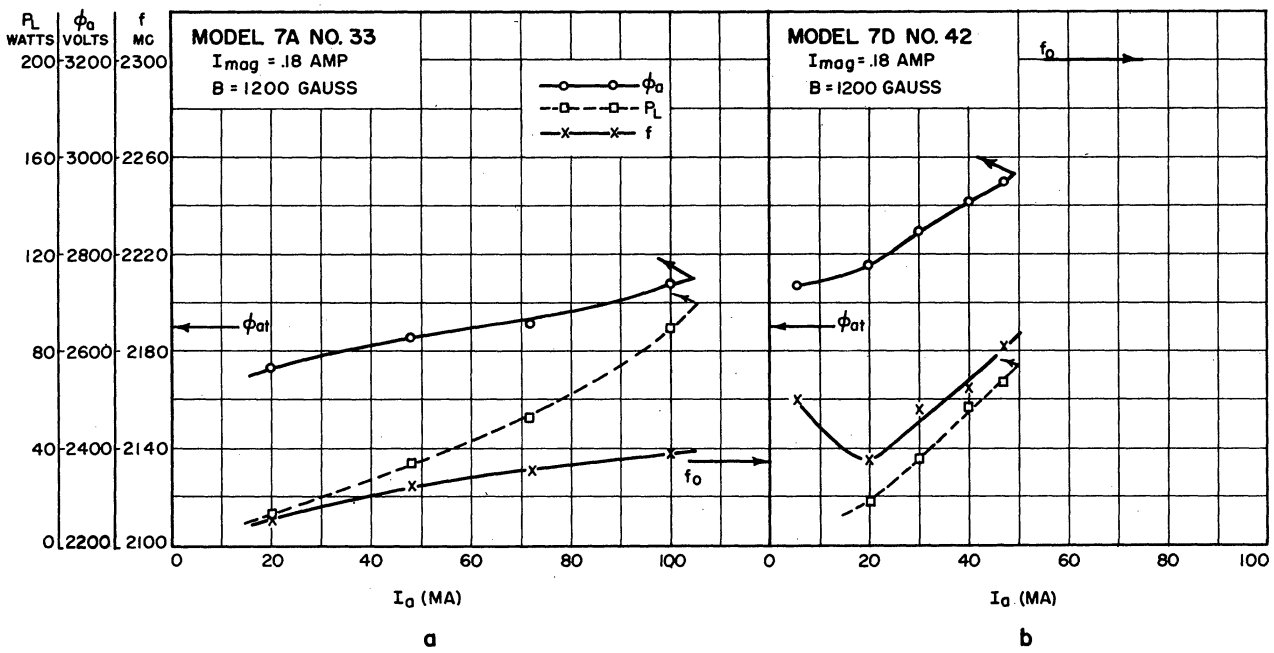

FIG. 4.12
PERFORMANCE DATA FOR MODEL 7 MAGNETRONS
B = 1200 GAUSS

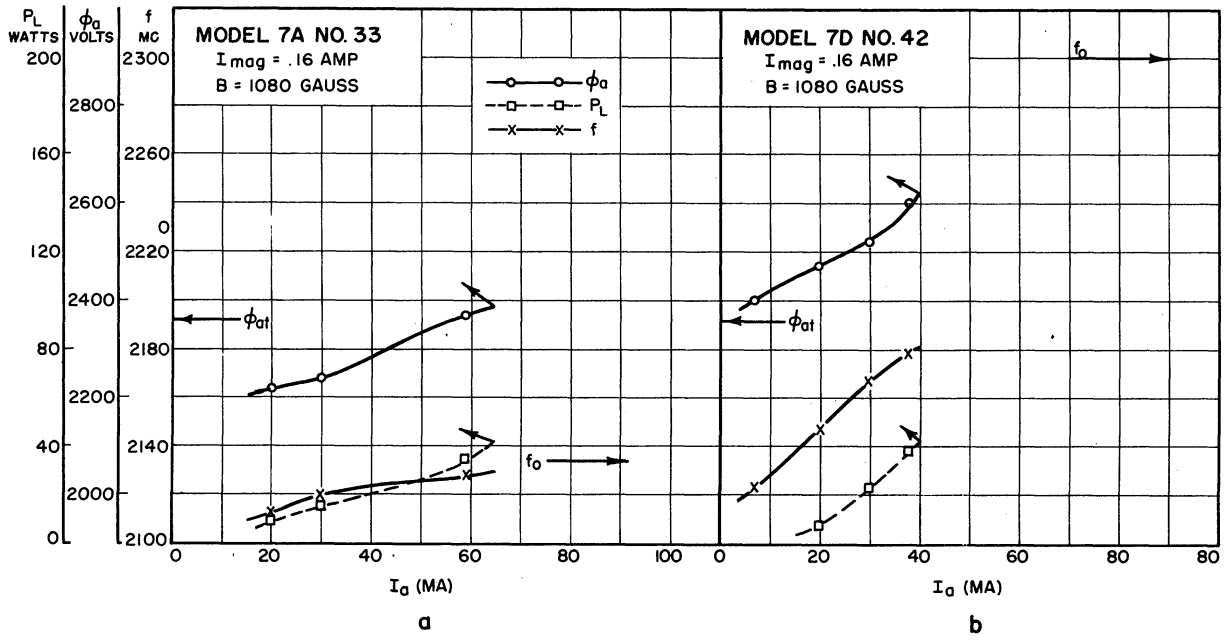

FIG. 4.13
PERFORMANCE DATA FOR MODEL 7 MAGNETRONS
B = 1080 GAUSS

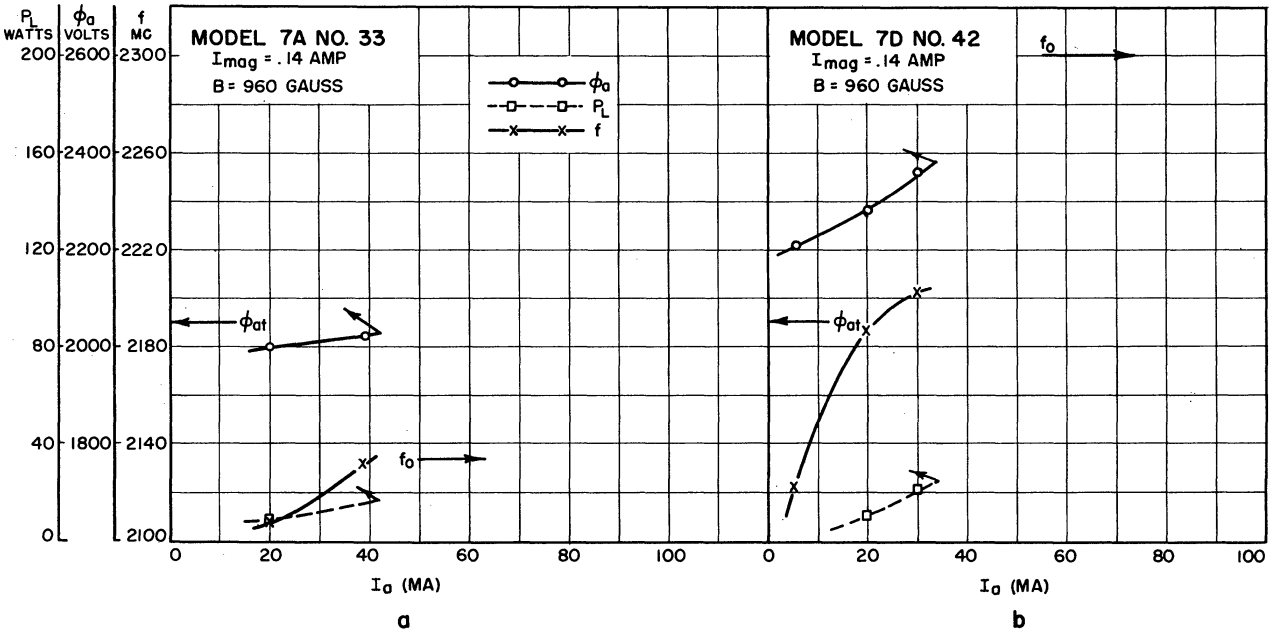

FIG. 4.14
PERFORMANCE DATA FOR MODEL 7 MAGNETRONS
B = 960 GAUSS

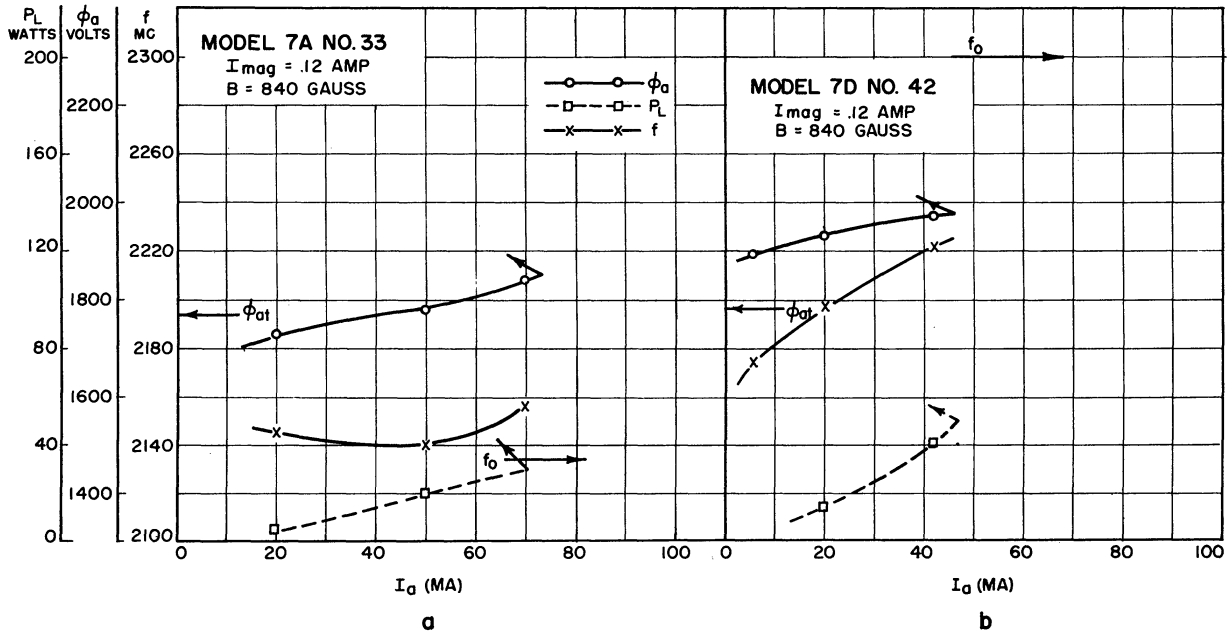

FIG. 4.15
PERFORMANCE DATA FOR MODEL 7 MAGNETRONS
B = 840 GAUSS

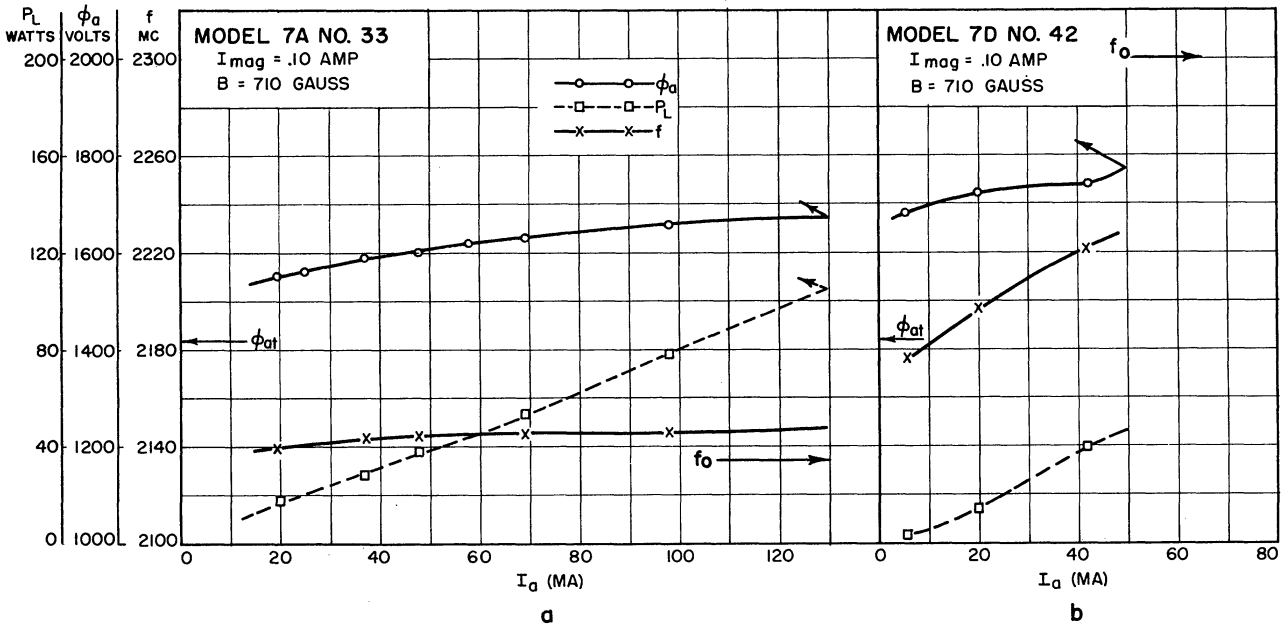

FIG. 4.16
PERFORMANCE DATA FOR MODEL 7 MAGNETRONS
B = 710 GAUSS

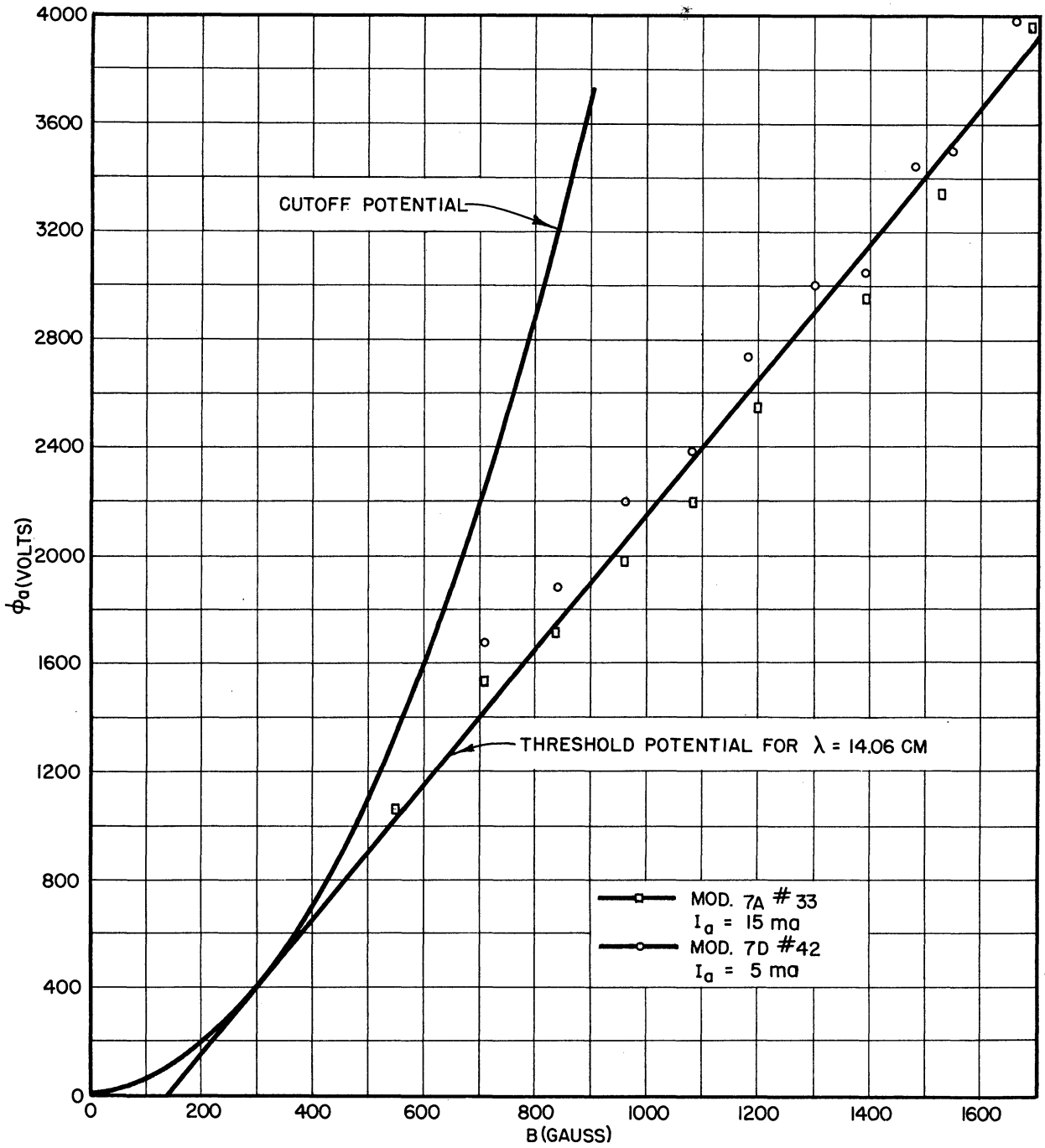

FIG. 4.17
STARTING POTENTIAL COMPARED WITH THRESHOLD POTENTIAL
FOR MOD. 7A NO. 33 AND MOD. 7D NO. 42 MAGNETRON

Table 4.4

Data on Interaction Geometry of Model 7A and Model 7D Magnetrons

r_a cm	r_c cm	R_a -	L cm	N -	α Degrees	$\frac{N}{2}\alpha$ Degrees	K —	f mc
.665	.381	1.75	.763	16	5.625°	45°	.9	2110 to 2136 mc normal operation 2140 to 2160 mc abnormal operation

Table 4.5

Calculated Variables for the Model 7 Magnetron, f = 2120 mc

Variable	B	ρ_o	R_n	F	K_1	K_2	$\frac{K_2}{K_1}$	A
Units	Webers/m^2	Coulombs/m^3	-	-	Amperes	Volts	Ohms	Q_L/Y_{oc} = 1835 ohms
Equation Used	-	3.40	2.28	3.39	3.37	3.38	3.49b	3.49a
	.1200	3.42×10^{-3}	1.080	.273	3.90	2080	534	3.44
	.1390	3.81×10^{-3}	1.075	.272	4.32	2330	540	3.40
	.1525	4.21×10^{-3}	1.065	.272	4.79	2600	543	3.38
	.1690	4.70×10^{-3}	1.060	.272	5.32	2940	554	3.32

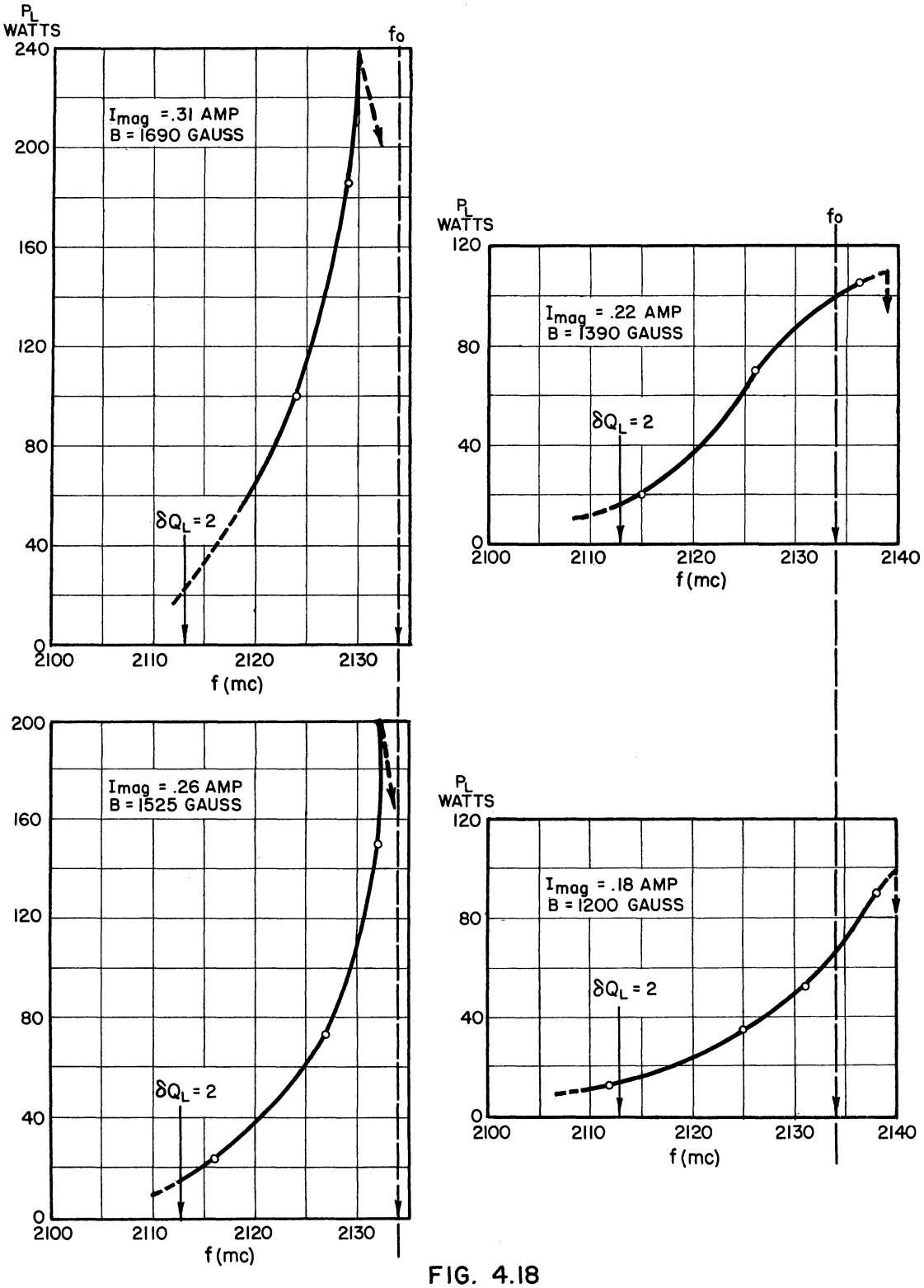

FIG. 4.18

FREQUENCY-POWER CURVES FOR MODEL 7A NO. 33, NORMAL OPERATION

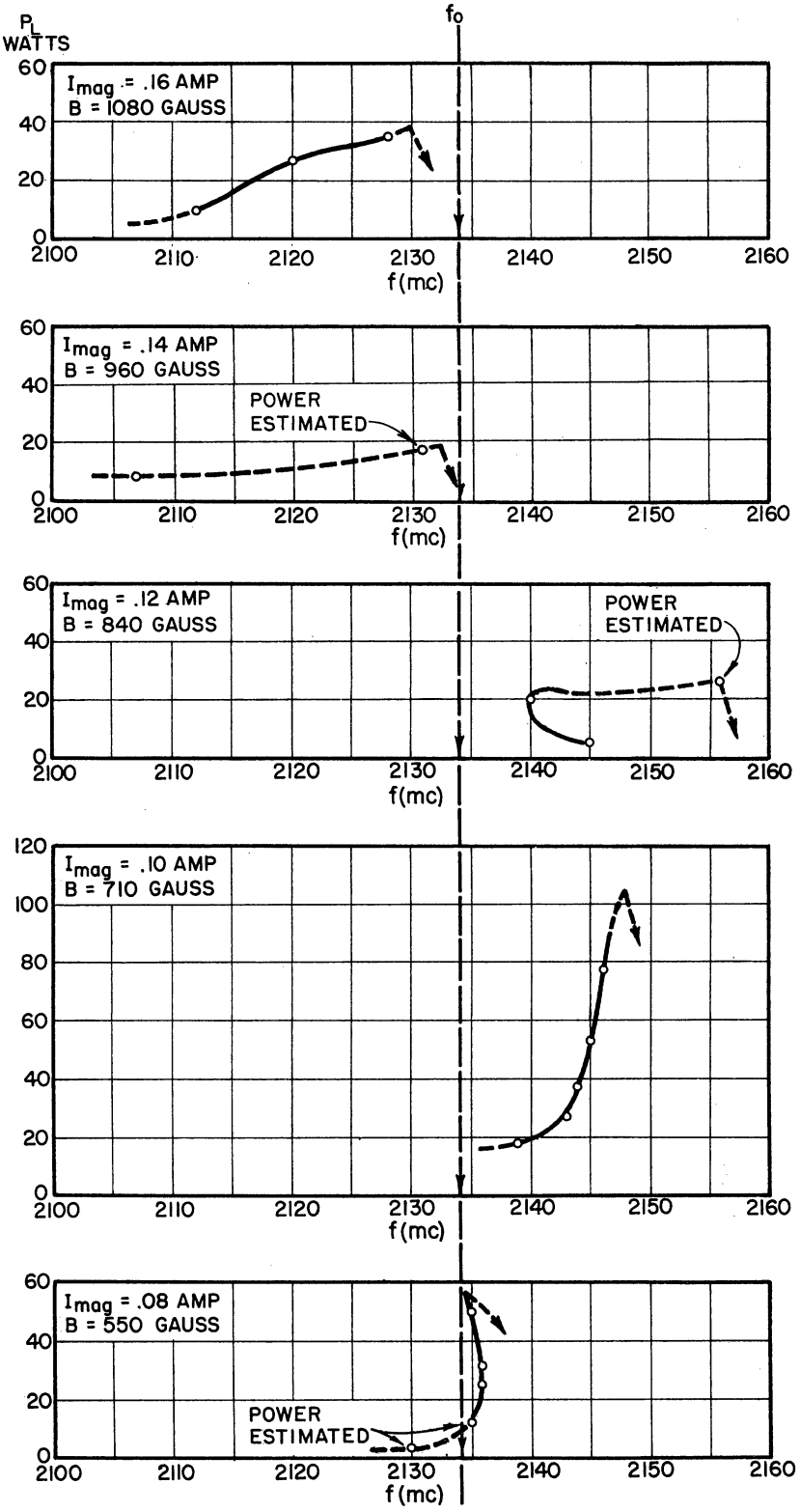

FIG. 4.19

FREQUENCY-POWER CURVES FOR MODEL 7A NO. 33, ABNORMAL OPERATION

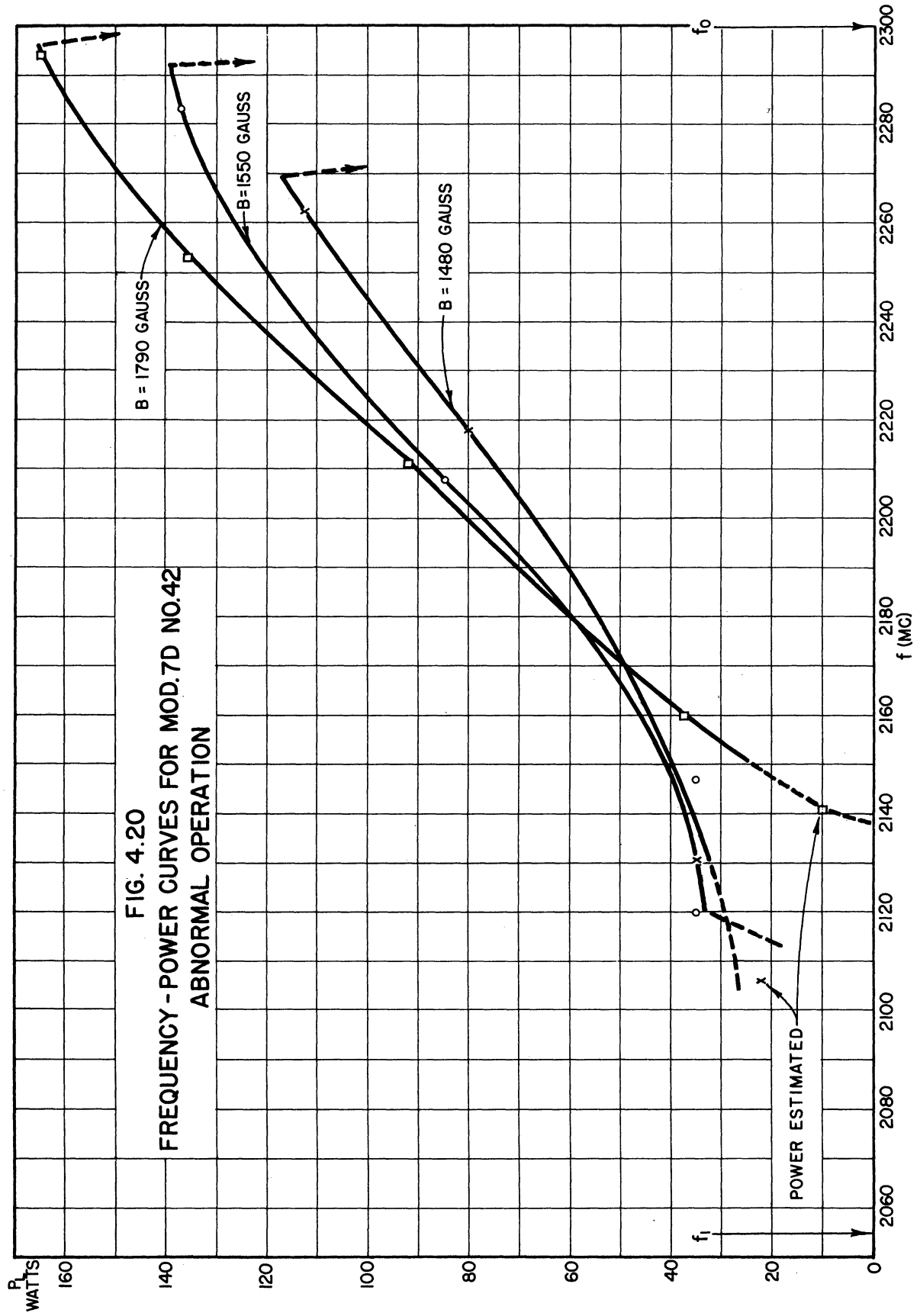

FIG. 4.20
FREQUENCY - POWER CURVES FOR MOD.7D NO.42
ABNORMAL OPERATION

Calculation of the current generated and power output as a function of frequency requires knowledge of the resonant circuit properties. These properties are somewhat in question but, nevertheless, the calculation will be made for the Model 7A No. 33 magnetron and the results compared with the observed experimental data.

In Fig. 4.21 two resonance curves resulting from Q measurements are plotted for the Model 7A No. 33 magnetron. Note that the resonance frequency is shifted and the Q lowered by insertion of the cathode. Also, the resonance curve is changed in shape indicating a complex resonance. These facts are interpreted with the help of Fig. 4.22.

In this diagram the cathode is introduced into the picture as a third electrode and the circuits between each anode set and the cathode represented by Z_{c1} and Z_{c2}. In the Model 7 magnetron geometry the set of anodes formed by the bars is essentially bypassed to the cathode by the transmission line formed by the cathode stem and the pole piece. This may be expressed by labeling

Anode Set No. 1 - Bar Anodes
Anode Set No. 2 - Vane Anodes

$$Z_{c1} \ll Z_{c2}$$

As long as the ψ function used in the induced current calculations is exactly the same for each anode set the current

$$I_c = 0 ,$$

and

$$I_{c1} = I_{c2} .$$

If the ψ functions are not alike for the two anode sets the current I_c will not be zero, but may be thought of as the difference in current

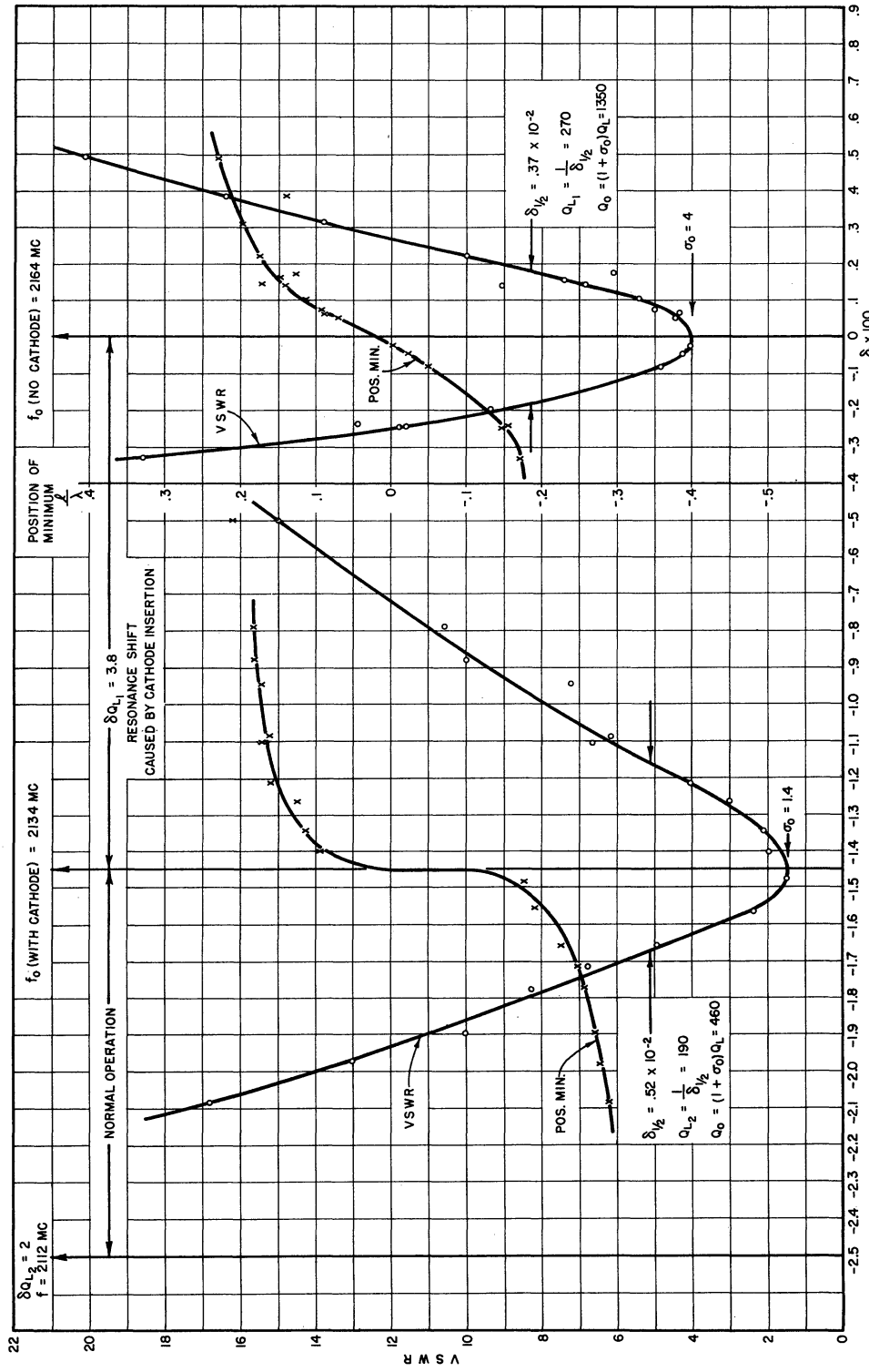

FIG. 4.21
RESONANCE CURVES FOR MODEL 7A NO. 33 MAGNETRON

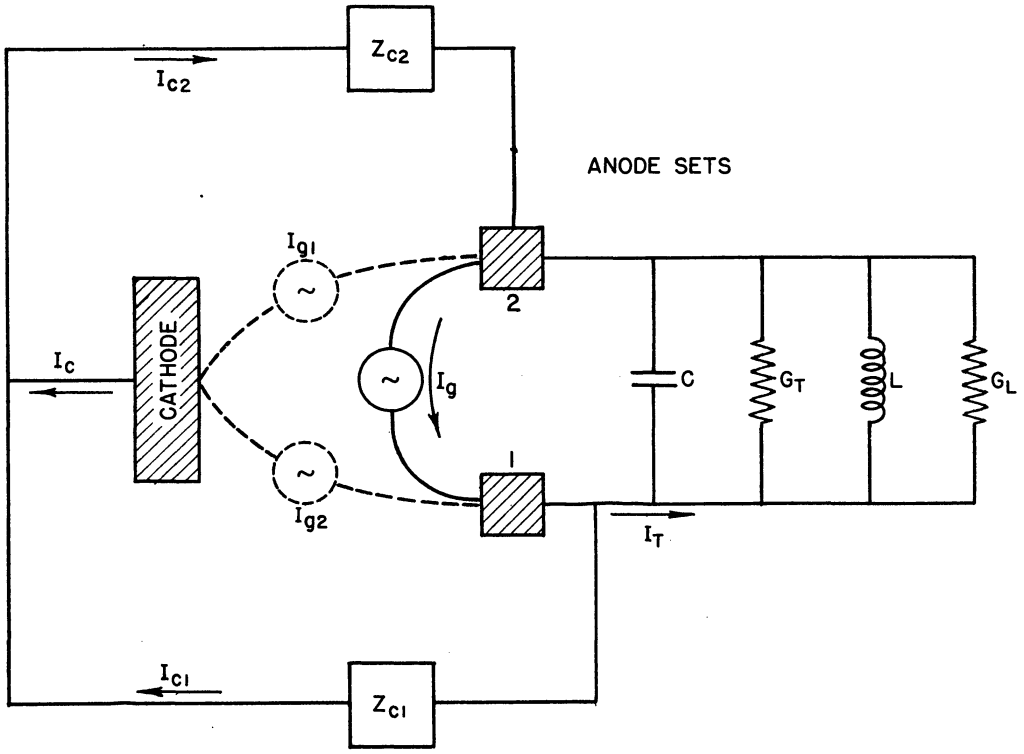

FIG. 4.22
EQUIVALENT CIRCUIT FOR MAGNETRON INCLUDING THE CATHODE CIRCUIT

which results from the connection of two dissimilar generators, I_{g1} and I_{g2} between anode sets 1 and 2 and the cathode. These are shown dotted in Fig. 4.22. This could occur in the Model 7 since the two anode sets are not quite alike.

The point of major importance to the analysis of results on the Model 7 magnetron is that the charge stored by current flow into Z_{c1} and Z_{c2} does not contribute appreciably to the circulating current in the tank circuit, but does contribute to the circulating current in the line formed by the cathode stem. This means that although the current I_T, which flows into the tank circuit, may not be greatly different in magnitude from I_g without the cathode, the phase angle of I_T relative to the r-f potential across the tank circuit will be determined by the phase characteristic of the resonator without cathode. It is concluded that, in the application of Eq 3.51 to the determination of the power, the angle θ which is used should be the angle determined by the circuit without the cathode,

$$\tan \theta_1 = 2 \delta_1 Q_{L1} .$$

On the other hand, the angle θ used in calculation of I_g/K_1 from Eq 3.49 will be given by

$$\tan \theta_2 = 2 \delta_2 Q_{L2} .$$

The load conductance as presented to the anode terminals has been calculated[1] for the Model 7 geometry with the assumption of a 50-ohm line coupled to the magnetron output. This value will be assumed to apply

---

[1] Needle, J. S., and Hok, G., op. cit. page 18.

in the determination of the constant A, i.e.,

$$\frac{Q_{L2}}{Y_{oc}} \cong G_L \ .$$

The calculated value is

$$R_L = \frac{1}{G_L} = 1835 \text{ ohms}$$

as is indicated in the (A) column of Table 4.5. The power in the load is given by

$$\frac{P_L}{G_L K_2^2} \cong A \cos^2 \theta_1 \left(\frac{I_g}{K_1}\right)^2$$

where

$$\frac{I_g}{K_1} \cong \frac{1}{\frac{\frac{\pi}{2} + \theta_2}{\cos \theta_2} - A \cos \theta_2 \cos 2\theta_2}$$

$\frac{I_g}{K_1}$ may be estimated from Fig. 3.12.

In Fig. 4.23 the curves predicted by these formulae are plotted for B = 1525 gauss for comparison with the experimental points. Further comparison of experimental results with theory does not seem worthwhile since a careful comparison cannot be made without extension of the theory to take into account the complexities of the particular magnetron under study. The significant conclusions to be drawn from this comparison are the following:

a. The magnetron operates over the approximate range of frequencies predicted by the theory.

b. The shape of the pushing curve is approximately correct.

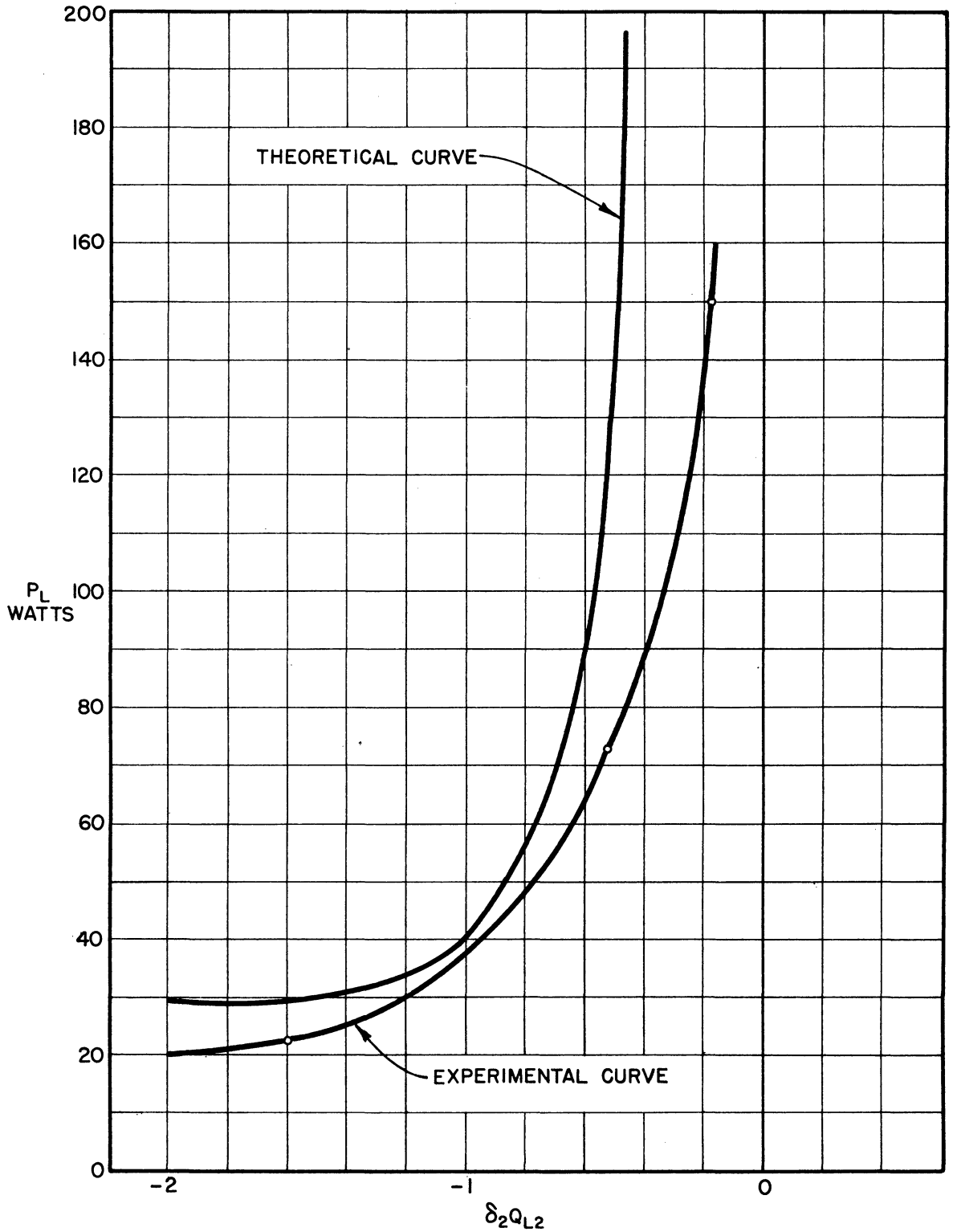

FIG. 4.23
COMPARISON OF THEORETICAL PUSHING CURVE
WITH EXPERIMENTAL RESULTS
MODEL 7A NO. 33 MAGNETRON B = 1525 GAUSS

c. The predicted power levels are of the right order of magnitude for $|\theta_2| > |45°|$. For $|\theta_2| < |45°|$ the predicted power approaches infinity. This, of course, requires infinite anode potential and induced current, which is not possible, so that the magnetron should cease oscillating before resonance ($\delta_2 Q_{L2} = 0$) is reached. For B = 1690 gauss and 1525 gauss oscillation ceases before resonance is reached. For the other curves this is not the case.

d. Anode potentials are consistently below the threshold potential with the exception of the cases for 1690 gauss and 710 gauss. This is as predicted for phase angles greater than 45°. The value of the anode potential should be determinable from the expression of 3.48 or from the expression

$$\frac{\phi_a - \phi_{at}}{K\sqrt{2}\,\phi_{r\text{-}f}} = \cos 2\theta \ .$$

From Fig. 4.10 or Fig. 4.17

$$\phi_a - \phi_{at} = -100 \text{ volts at } 20 \text{ ma.}$$

We also have

$$\delta_2 Q_{L2} = 1.6 \ ,$$

$$\therefore \ \theta = -73° \ ,$$

$$\cos 2\theta = -0.83 \ ,$$

$$K = 0.9 \ ,$$

and

$$\phi_{r\text{-}f} = 95 \text{ volts.}$$

The power in the load is given by

$$P_L = \frac{\phi_{r\text{-}f}^2}{R_L} \ .$$

For 20 watts at 95 volts

$$R_L = 450 \text{ ohms} ,$$

as opposed to 1835 ohms used in the previous calculations. This comparison is interesting but should not be taken too seriously since an error in magnet calibration of 50 gauss will, in this particular case, change $\phi_a - \phi_{at}$ by 125 volts. Thus, if

$$\phi_a - \phi_{at} = 225 \text{ volts} ,$$

$$\phi_{r-f} = 214 \text{ volts} ,$$

and

$$R_L = 2300 \text{ ohms} .$$

As was pointed out in connection with the discussion of the magnet calibration, this amount of error is quite feasible.

Data on the Model 7D No. 42 can be compared qualitatively with the data on the Model 7A No. 33. Resonance curves from Q measurements are given in Fig. 4.24. It is apparent that a second resonant system, possibly associated with the cathode stem, is storing energy with a higher Q than the resonant system of the coaxial cavity at this loading. This effectively makes a broad resonance, due to the two circuits coupled together, at 13 cm. The upper dotted resonance curve is plotted for comparison with the 13-cm minimum and corresponds to a Q_L of 10 (undercoupled). The frequency-power curves of Fig. 4.20 show operation over the range indicated on the graph. This range is roughly that to be expected with a circuit having a Q_L of 10. The frequencies f_o and f_1 are indicated on the graphs of Fig. 4.20. Oscillation at the frequency of

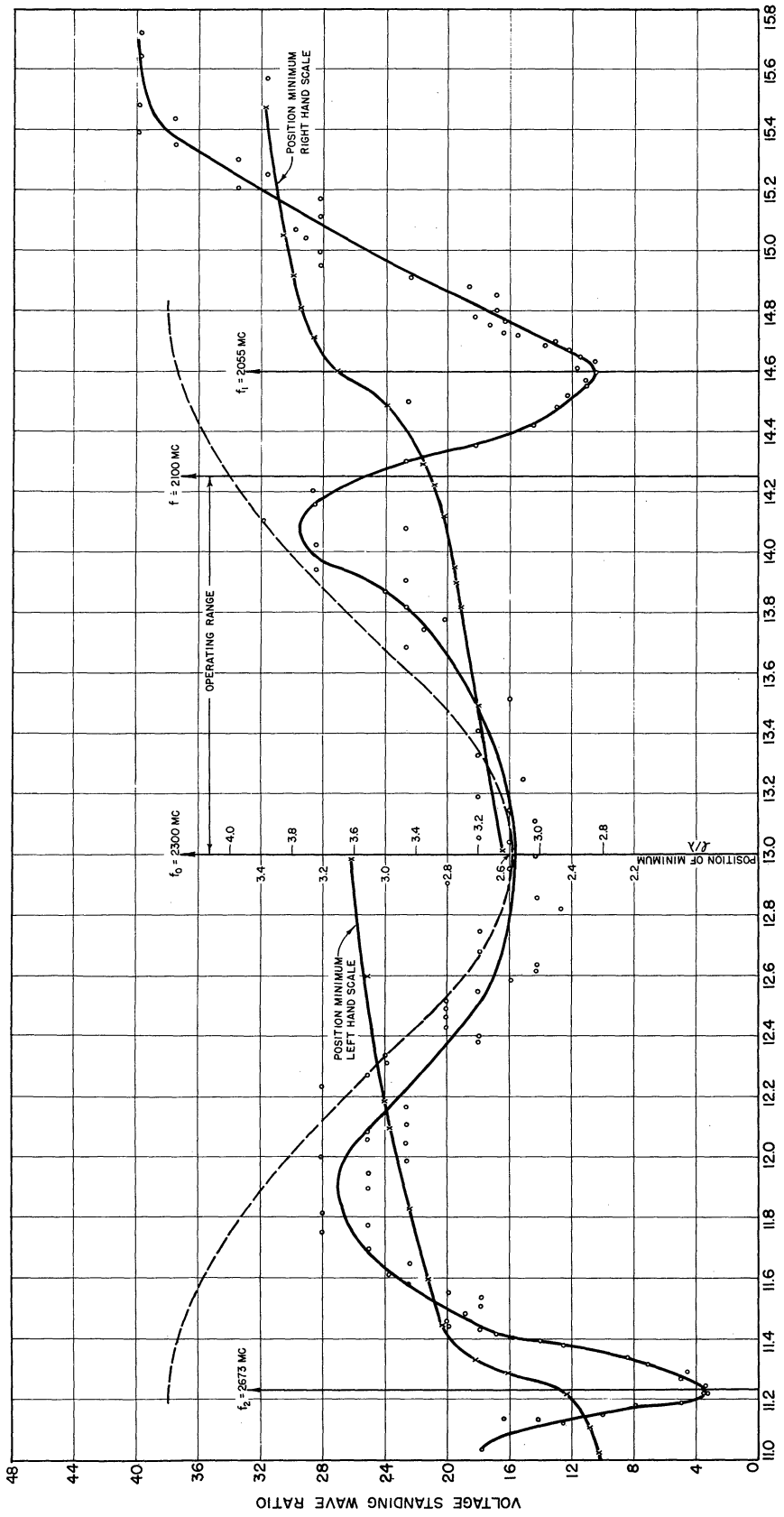

FIGURE 4.24 RESONANCE CURVE, MODEL 7D NO. 42 MAGNETRON

the second resonance, f_2 = 2670 mc, was also observed in pulsed operation. Operation at low anode currents was very erratic as is indicated on some of the performance data graphs.

C. Measurements on Michigan Magnetron Model 3 No. 8.[1]

Another magnetron for which fairly complete data exist is of the interdigital type. An assembly drawing of this tube is shown in Fig. 4.25. The cathode stem of this tube is also intimately coupled to the resonator and has a pronounced effect on the operation. The Model 3 tube is tunable, so that the exact resonance frequency without the cathode was not known for the conditions of this experiment. The resonant circuit consists of a pillbox type resonator capacitively loaded by "digits" or "fingers" alternately connected to top and bottom of the pillbox. Loading is accomplished by a loop coupling into the coaxial output.

Calibration of the magnet with the Model 3 pole pieces is given in Fig. 4.26. A resonance curve is given in Fig. 4.27. This resonance has a double minimum with the minima much more closely spaced than those observed in the Model 7 data. Q is calculated to be about 60 for the smooth dotted curve. Performance data are given in Figs. 4.28 and 4.29. Comparison of observed anode potentials with the threshold potential at two currents is given in Fig. 4.30. Data on the Model 3 magnetron interaction space is given in Table 4.6. The variables used in induced current calculations are given in Table 4.7.

---

[1] Analysis of this type of magnetron and the Model 3 design in particular are given detailed treatment by H. W. Welch, Jr., and G. R. Brewer in "Operation of Interdigital Magnetrons in the Zero Order Mode," Tech. Report No. 2, Electron Tube Lab., Dept. of Elec. Eng., Univ. of Mich., May 1949. Also see Hull, J. F., and Randalls, A. W., "High Power Interdigital Magnetrons," Proc. IRE, Vol. 36, No. 11, Nov. 1948, pp. 1357-1363.

DWG. NO. B-10,003

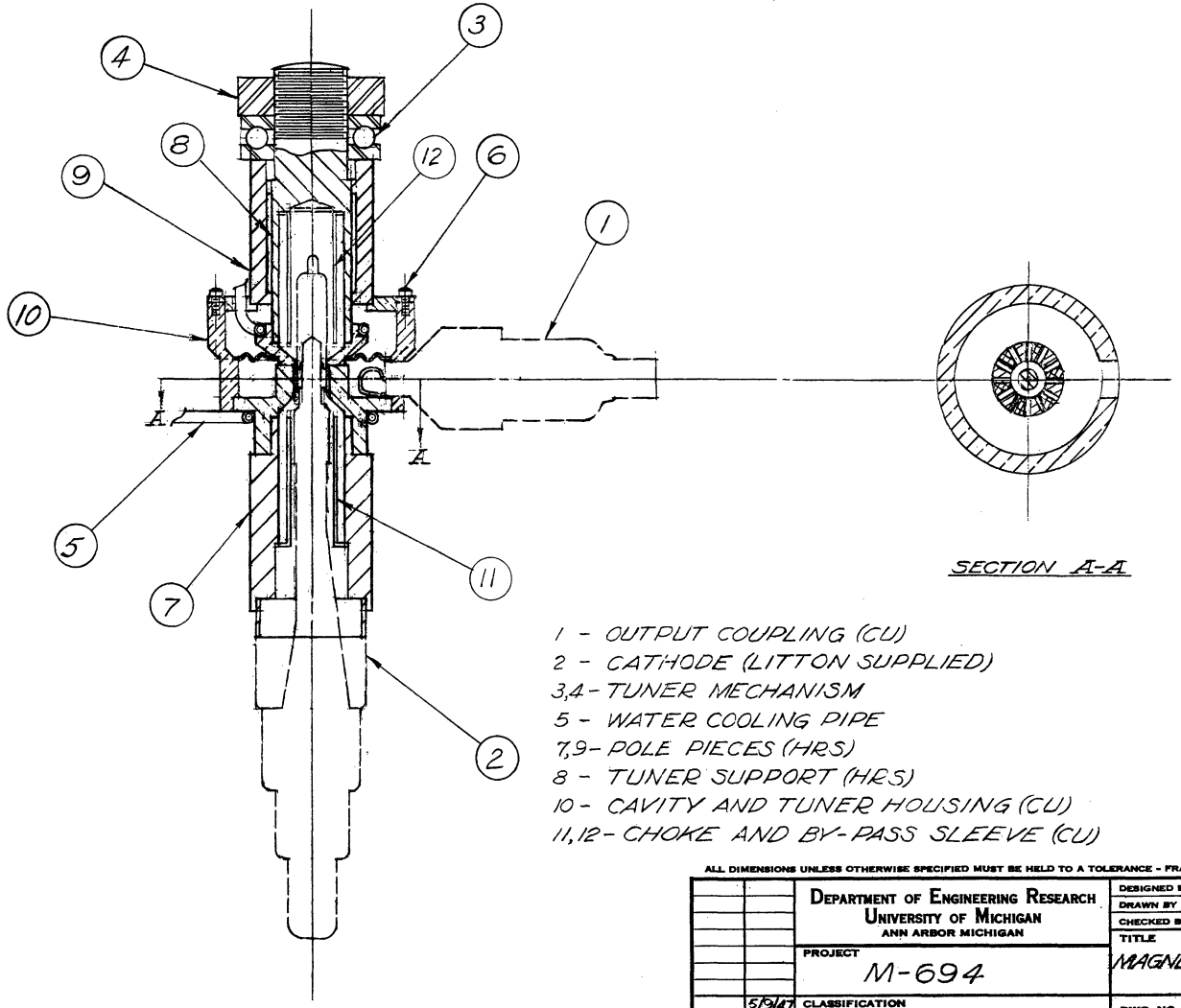

SECTION A-A

1 - OUTPUT COUPLING (CU)
2 - CATHODE (LITTON SUPPLIED)
3,4 - TUNER MECHANISM
5 - WATER COOLING PIPE
7,9 - POLE PIECES (HRS)
8 - TUNER SUPPORT (HRS)
10 - CAVITY AND TUNER HOUSING (CU)
11,12 - CHOKE AND BY-PASS SLEEVE (CU)

1"

FIG. 4.25

ALL DIMENSIONS UNLESS OTHERWISE SPECIFIED MUST BE HELD TO A TOLERANCE - FRACTIONAL ± 1/64," DECIMAL ± .005," ANGULAR ± 30'

		DEPARTMENT OF ENGINEERING RESEARCH UNIVERSITY OF MICHIGAN ANN ARBOR MICHIGAN	DESIGNED BY H. W. W. / APPROVED BY H W W
			DRAWN BY J M / SCALE FULL SIZE
			CHECKED BY H W W / DATE 5/9/47
		PROJECT M-694	TITLE MAGNETRON ASSEMBLY MODEL 3
	5/9/47	CLASSIFICATION	DWG. NO. B-10,003
ISSUE	DATE		

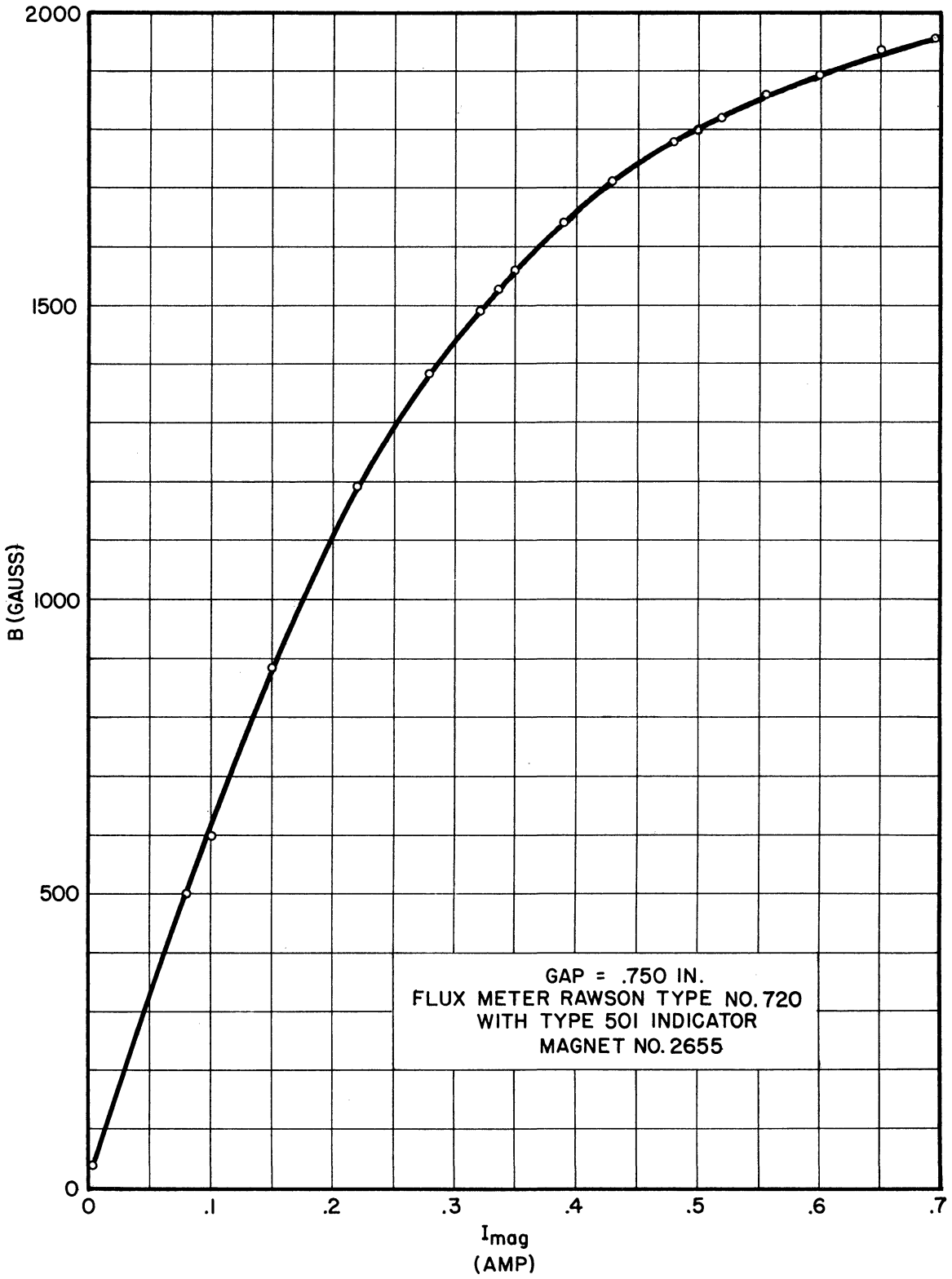

FIG. 4.26

MAGNET CALIBRATION MOD. 3 POLE PIECES

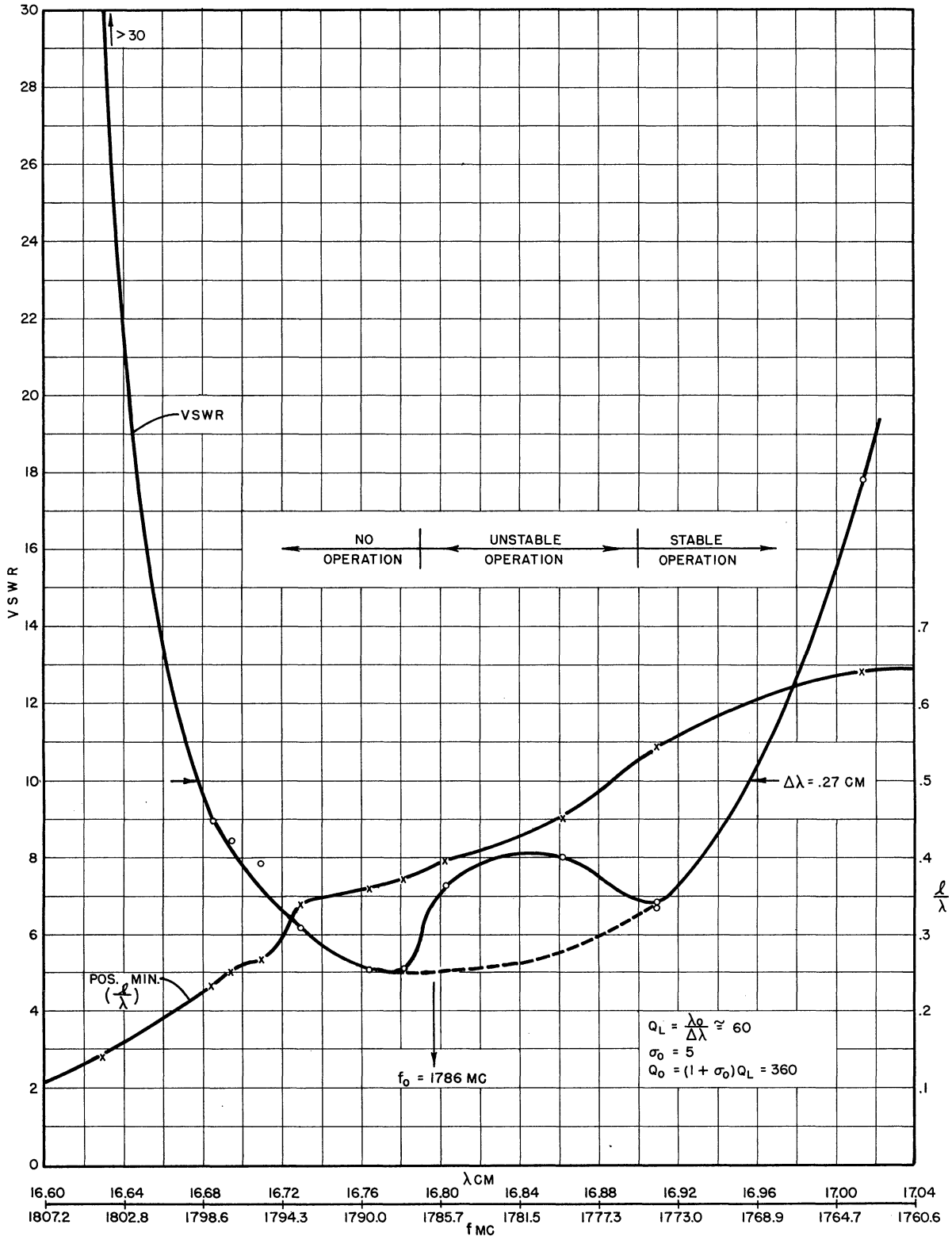

FIG. 4.27
RESONANCE CURVE FOR MODEL 3 NO. 8 MAGNETRON

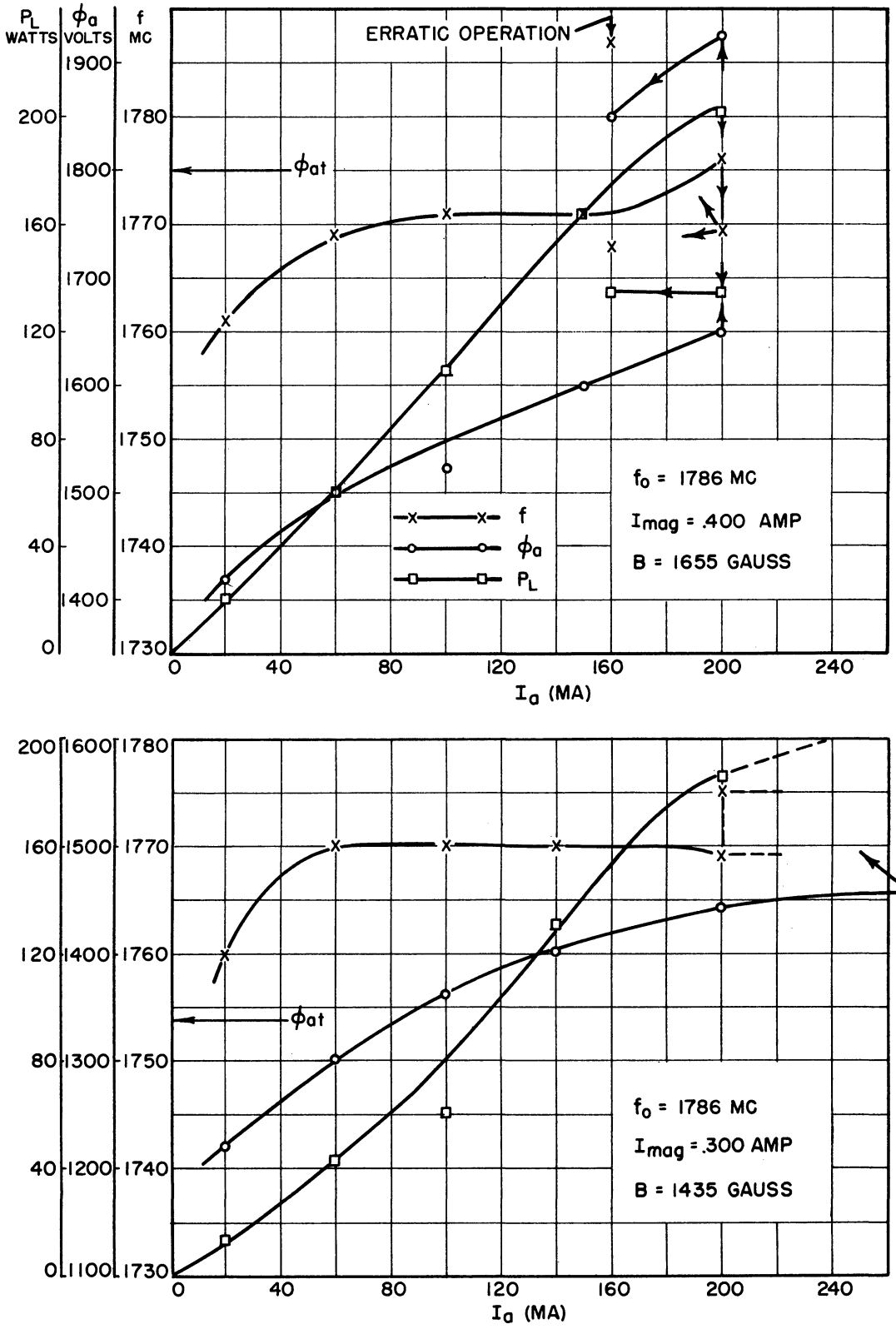

FIG. 4.28 PERFORMANCE DATA FOR MODEL 3 MAGNETRON FILAMENT 6.5 VOLTS, 19 AMP

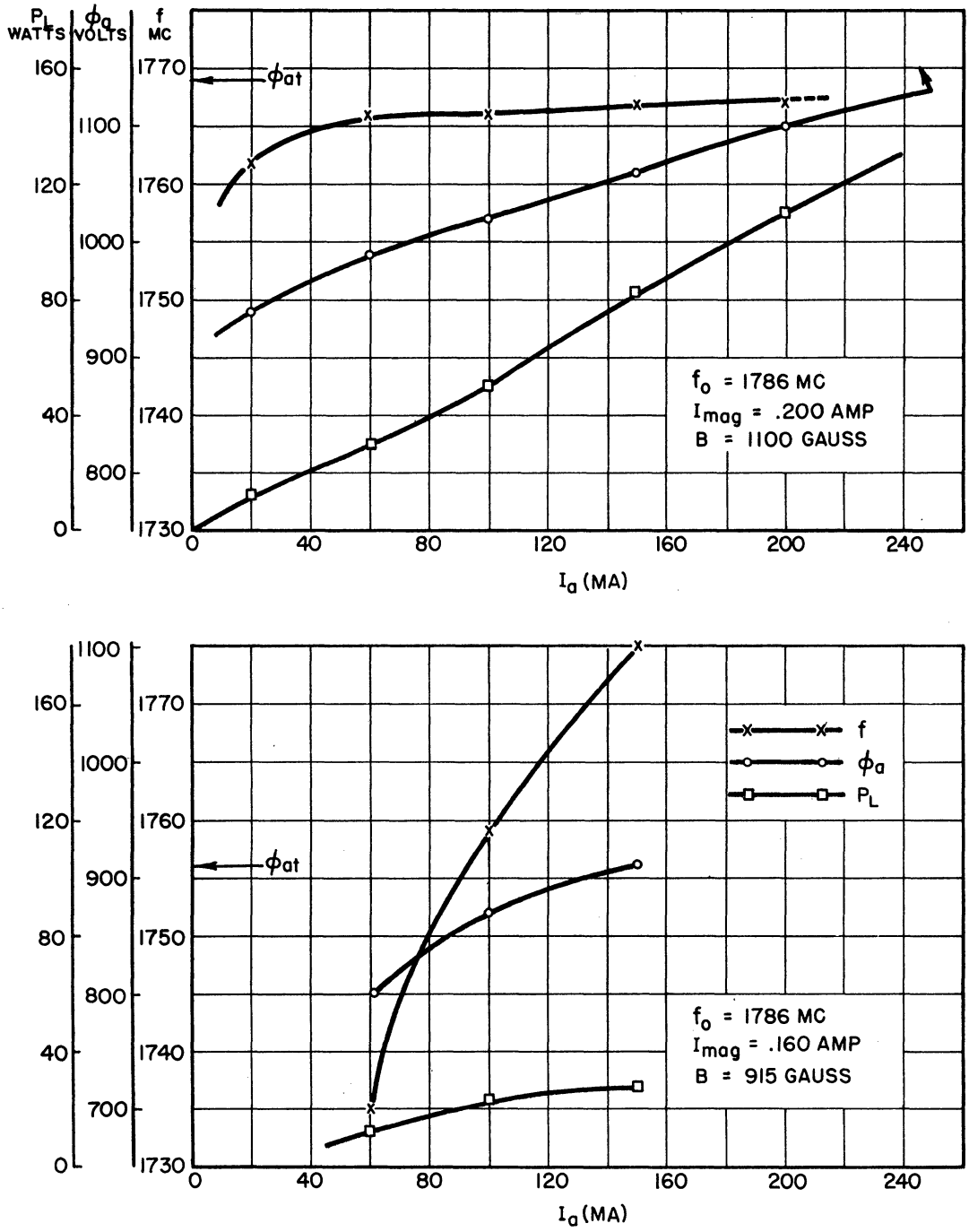

FIG. 4.29
PERFORMANCE DATA FOR MODEL 3 MAGNETRON
FILAMENT 6.5 VOLTS, 19 AMP

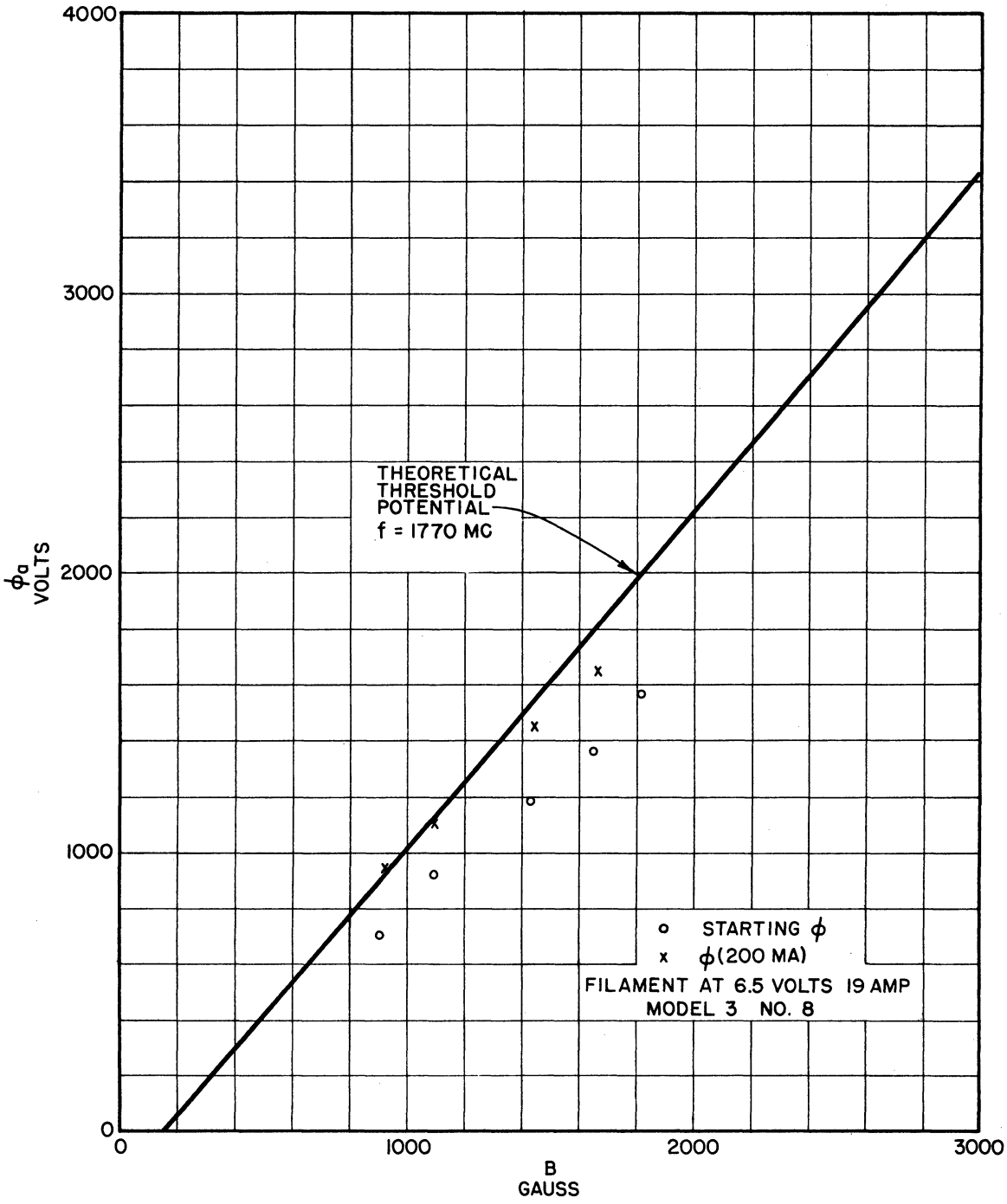

FIG. 4.30

COMPARISON OF OBSERVED OPERATING ANODE POTENTIAL WITH THRESHOLD POTENTIAL FOR MODEL 3 MAGNETRON

Table 4.6

Data on Interaction Geometry of Model 3 Magnetron

r_a cm	r_c cm	R_a -	L cm	N -	α Degrees	$\frac{N}{2}\alpha$ Degrees	K -	f mc
.45	.27	1.66	.66	12	7.5	45	.9	1760-1775

Table 4.7

Calculated Variables for the Model 3 Magnetron

Variable	B	ρ_o	R_n	F	K_1	K_2	$\frac{K_2}{K_1}$	A
Units	Webers/m^2	Coulombs/m^3	-	-	Amperes	Volts	Ohms	Q_L/Y_{oc} = 1100 ohms
Equation Used	-	3.40	2.28	3.39	3.37	3.38	3.49b	3.49a
	.0915	2.65×10^{-3}	1.14	.286	1.15	627	545	2.02
	.1100	3.25×10^{-3}	1.11	.288	1.42	806	570	1.93
	.1435	4.36×10^{-3}	1.08	.290	1.92	1130	590	1.80
	.1655	5.09×10^{-3}	1.075	.290	2.24	1320	590	1.80
	.1800	5.55×10^{-3}	1.07	.290	2.44	1440	590	1.80

The impedance between the Model 3 cathode stem and the anode block is maintained high by a resonant short-circuited quarter-wave line in series with an open-circuited quarter-wave bypass. In the Model 7 magnetron this impedance was kept low by using only the bypass. Another Model 7 tube, the Model 7C No. 41 magnetron incorporated in the cathode stem an arrangement similar to that in the Model 3.[1] This tube was inoperable on c-w tests because of poor performance of an oxide-coated cathode. All other tubes discussed here use thoriated tungsten cathodes. In pulsed operation the Model 7C No. 41 did operate at near the resonance frequency of the coaxial resonator and showed high mode boundaries under some loading conditions.

Quantitative comparison, on the power scale, of Model 3 data with theory is not possible since the resonance frequency without the cathode is not known. However, the form of the pushing curve and the range of frequency expected can be approximated by assuming a simple resonant circuit and comparing the predicted and experimental curves on an adjusted scale.

For the Model 3 magnetron

$$Y_{oc} \cong 2\pi f C_A$$

where C_A is the capacitance between anode sets. C_A has been calculated to be[2]

---

1 Needle, J. S., and Hok, G., loc. cit.

2 Welch, H. W., and Brewer, G. R., loc. cit.

$$C_A = 4.9\ \mu\mu f ,$$

$$Y_{oc} = .055 \text{ mhos} .$$

For $Q_L = 60$

$$\frac{Q_L}{Y_{oc}} = 1100 \text{ ohms} .$$

This value is used in the calculation of A in Table 4.7. The power is calculated using Eq 3.51 and compared with the experimental points in Fig. 4.31 for B = 1655 gauss. The following conclusions are made from this comparison:

a. The magnetron operates over the approximate range of frequencies predicted by the theory. Oscillation ceases at between -35° and -40° off resonance ($\delta Q_L = -.35$ to $-.42$).

b. The shape of the predicted pushing curve is approximately correct.

c. The predicted power levels are a factor of > 10 high. This means that the current predicted is a factor of > 3 high. This discrepancy is possibly caused by the neglect of the effects of the cathode line on the phase characteristic of the circuit. The factor, $\cos^2 \theta$, which is contained in the expression for power, changes by a factor of approximately 10 between $\theta = -72°$ and $\theta = -84°$. This would correspond to a shift in frequency of 3.5% for $Q_L = 100$ or 62 mc at f = 1786 mc. Another possible source of discrepancy is in the assumed value of Q_L/Y_{oc}.

d. The anode potentials are consistently below the threshold potential as is expected for the phase angle $|\theta| > |45°|$. Values of the r-f potential, calculated with Eq 2.48, are too large by a factor of 4

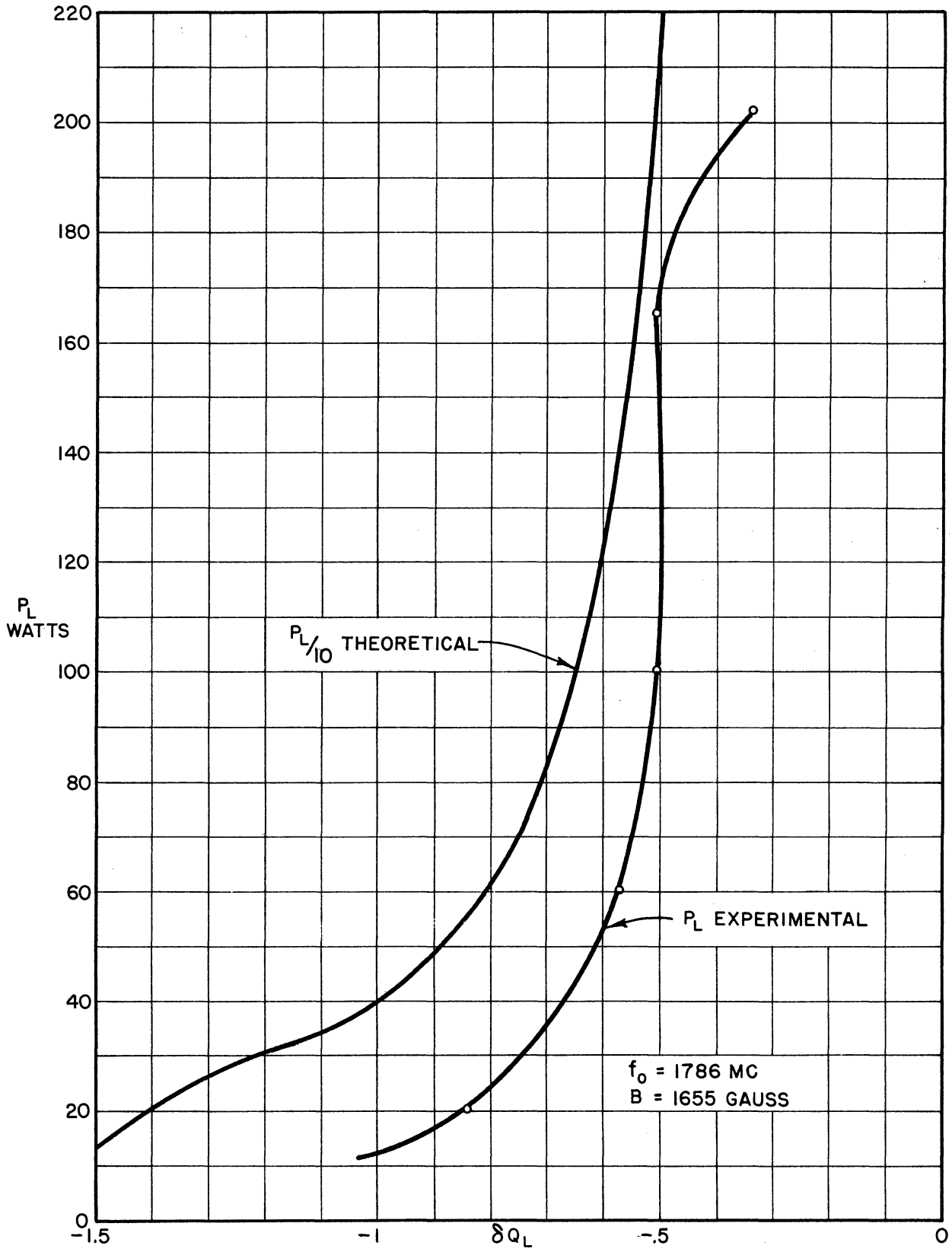

FIG. 4.31

COMPARISON OF EXPERIMENTAL PUSHING CURVE WITH THEORETICAL CURVE FOR MODEL 3 NO. 8 MAGNETRON. A SIMPLE RESONANT CIRCUIT IS ASSUMED.

or 5 if the value of Q_L/Y_{oc} = 1100 ohms is assumed approximately correct. Again it will be pointed out that a quantitative check of this value is very critically dependent on knowledge of the magnetic field.

D. Measurements Showing Effect of Cathode Emission on Performance Characteristics. Two sets of data are reproduced here with the purpose of indicating the effect of cathode power on operating characteristics. The Model 7A No. 33 magnetron and the Model 3 No. 8 magnetron were used in these tests. In Fig. 4.32 performance characteristics for the Model 7A No. 33 magnetron for full cathode and part cathode at rated current of I_f = 15.5 amperes are plotted for comparison. The cathode in this magnetron is a bifilar tungsten helix with a center tap making possible use of part of the cathode at the rated current. Note that the slope of the volt-ampere characteristic is strongly affected by reducing the cathode power. Presumably this is caused by the reduction of emission. The maximum power reached and the pushing are not affected greatly as is clearly shown in Fig. 4.33. The entire pushing curve is shifted about 6 megacycles toward higher frequencies by the reduction of emission. This shift is borne out by other measurements, including those in Fig. 4.34. Here similar data are presented for the Model 3 No. 8 magnetron. In this case the entire cathode was used for both sets of data, but the heater current reduced to reduce emission. Note that the filament voltage required to maintain 19 amperes increases rather sharply in the region of erratic operation. This indicates back-bombardment by the electrons, which increases the temperature and, consequently, the resistance of the filament. The slope of the volt-ampere characteristic did not change in this test.

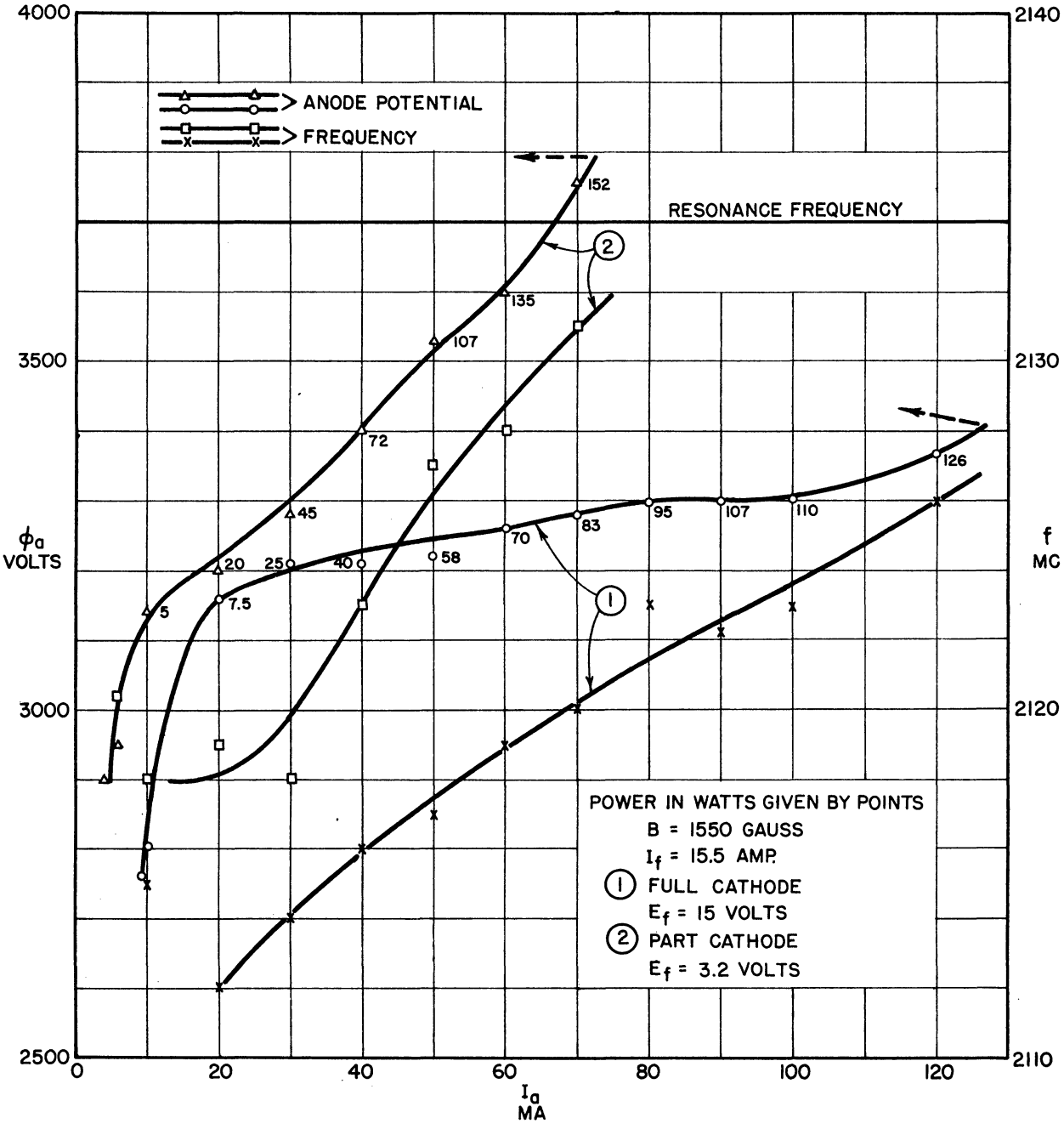

FIG. 4.32

PERFORMANCE DATA ON MODEL 7 NO. 33 MAGNETRON SHOWING THE EFFECT OF REDUCTION OF CATHODE POWER

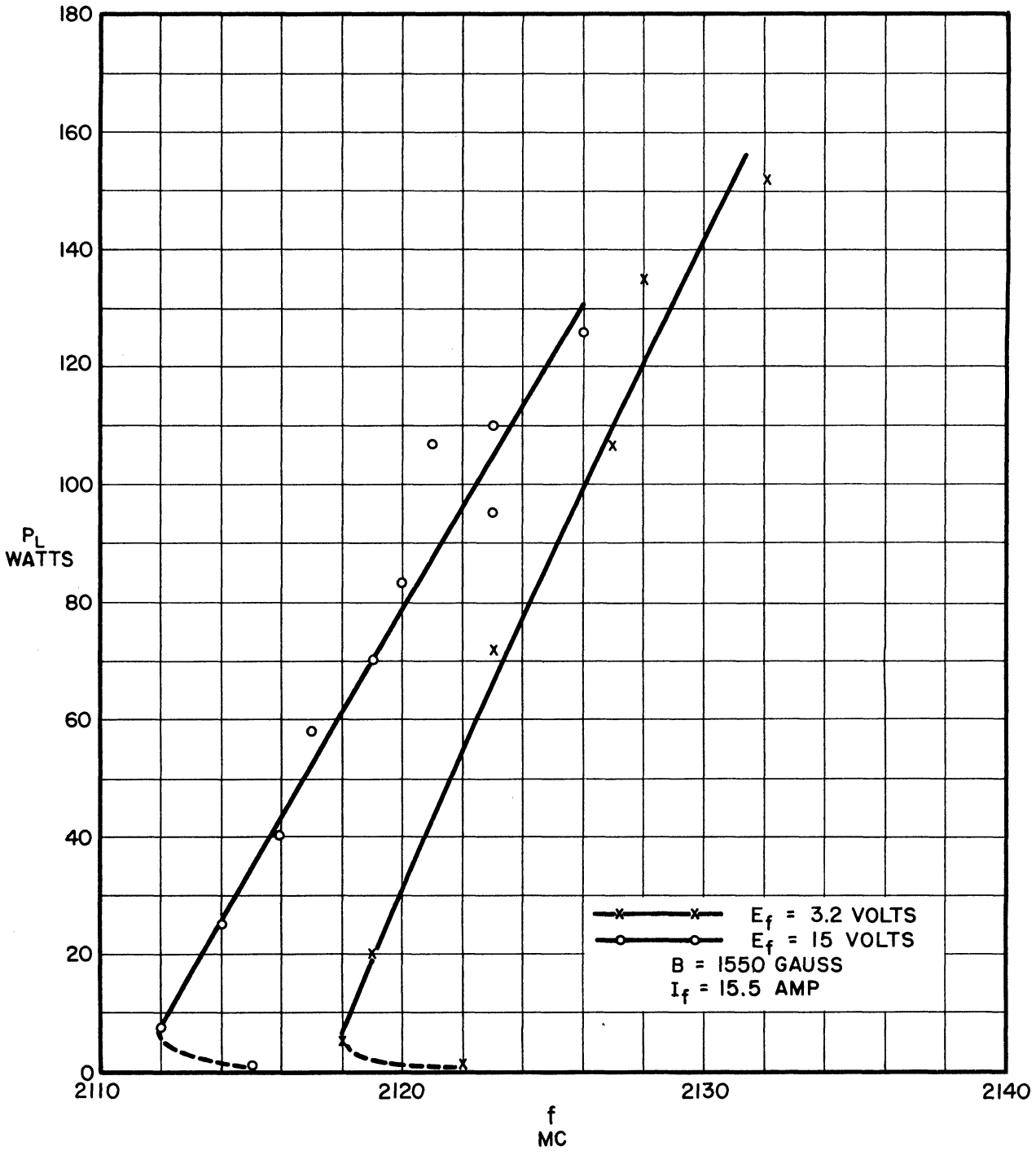

FIG. 4.33
FREQUENCY-POWER CURVES FOR TWO VALUES OF CATHODE POWER.
MODEL 7A NO. 33 MAGNETRON

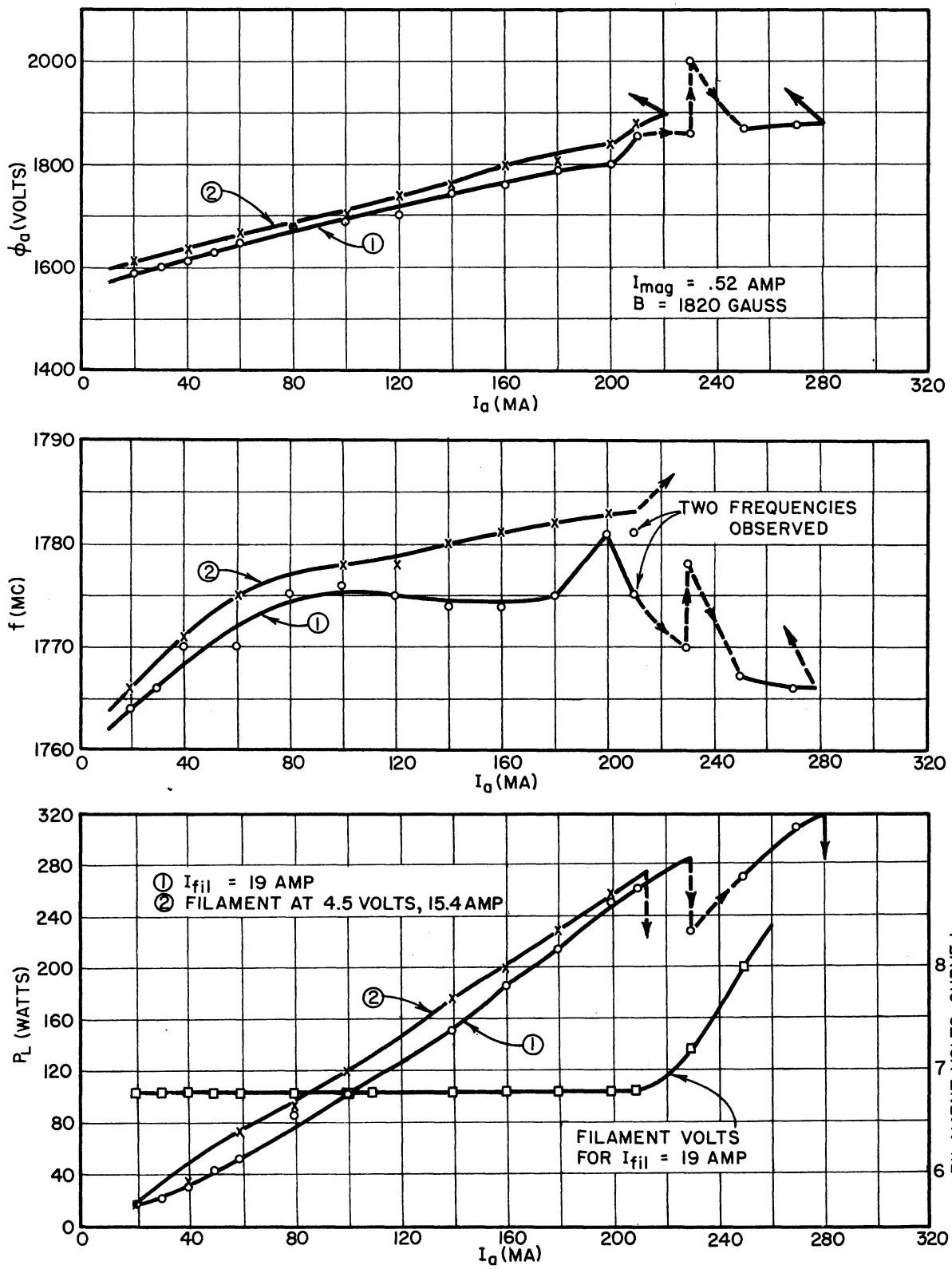

FIG. 4.34
PERFORMANCE DATA ON MODEL 3 NO. 8 MAGNETRON
SHOWING THE EFFECT OF REDUCTION OF CATHODE POWER

E. Measurements on Raytheon QK217 Magnetron RK5609 No. 16.

In an attempt to correlate various parameters of magnetron design with maximum current boundary, a number of production tubes have been studied in the Magnetron Development Laboratory at Raytheon Manufacturing Company. The results of these tests were made available to the author. Data of several types on one of the magnetrons studied will illustrate further the effect of temperature on magnetron operation. This magnetron is of the RK5609 type, Serial No. 16 in the test series. This magnetron is a 16-vane magnetron. The measured resonance characteristics were

$$Q_L = 269 ,$$

$$Q_o = 1020 ,$$

$$f_o = 2164 \text{ mc} .$$

The data are plotted in Figs. 4.35 to 4.41. The curves of Figs. 4.38, 4.39, and 4.40 are of particular interest. These curves appear to correlate the transition from space-charge-limited operation to temperature-limited operation with a transition from frequency pushing to something similar to voltage tuning. On the curves of Fig. 4.38, at low emission between 1440 and 1510 volts, the d-c current is constant and the frequency is varying comparatively rapidly. In Fig. 4.39 this region is moved up to 1480 to 1520 volts. In Fig. 4.40, at high emission, the region has disappeared. Making a quantitative comparison, at 1585-ma emission and 1475 volts,

$$\frac{\Delta f}{\Delta \phi_a} = .2 \times 10^{-2} \frac{\text{mc}}{\text{volt}} ,$$

and at 417-ma emission,

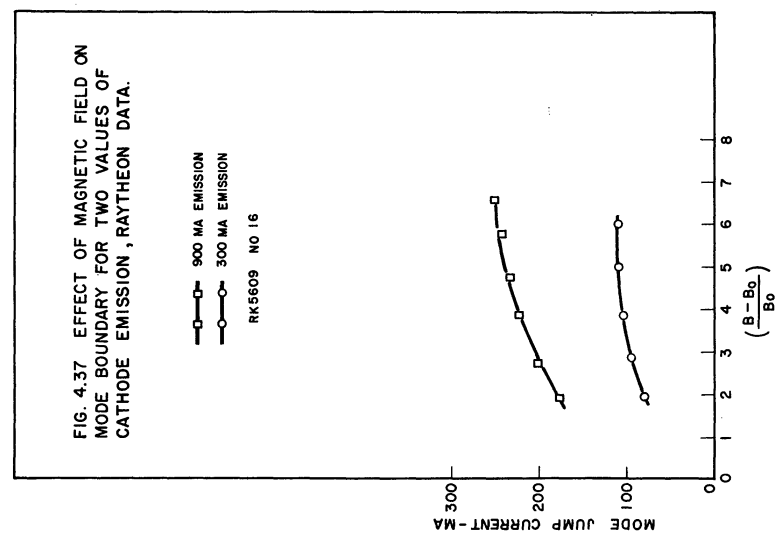
FIG. 4.37 EFFECT OF MAGNETIC FIELD ON MODE BOUNDARY FOR TWO VALUES OF CATHODE EMISSION, RAYTHEON DATA.
900 MA EMISSION
300 MA EMISSION
RK5609 NO 16
MODE JUMP CURRENT - MA
0
100
200
300
0 1 2 3 4 5 6 7 8
$\left(\frac{B-B_0}{B_0}\right)$

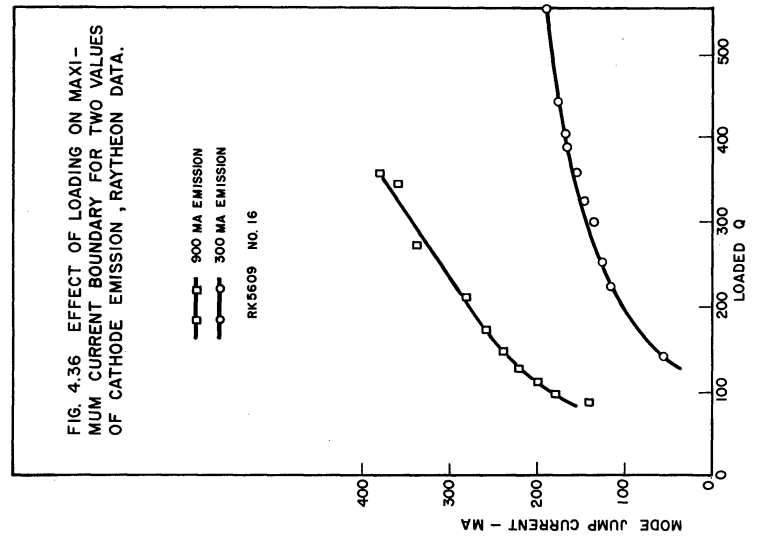
FIG. 4.36 EFFECT OF LOADING ON MAXIMUM CURRENT BOUNDARY FOR TWO VALUES OF CATHODE EMISSION, RAYTHEON DATA.
900 MA EMISSION
300 MA EMISSION
RK5609 NO. 16
MODE JUMP CURRENT - MA
0
100
200
300
400
0 100 200 300 400 500
LOADED Q

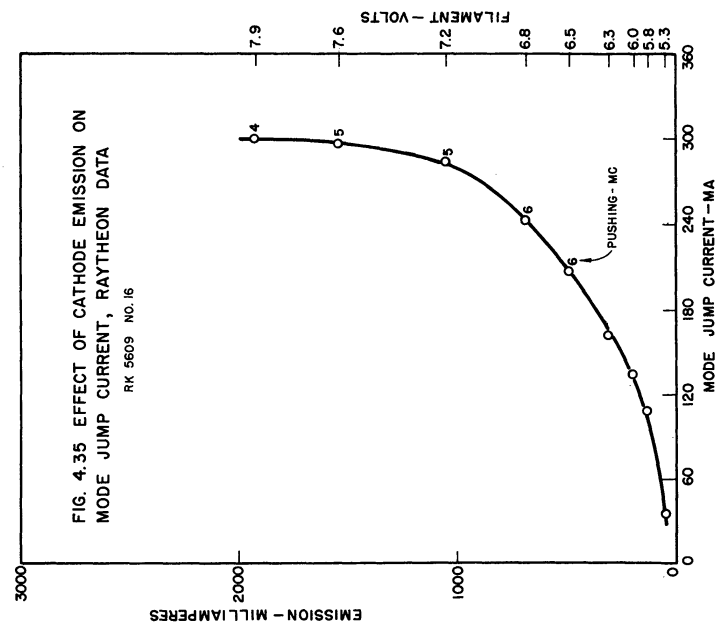
FIG. 4.35 EFFECT OF CATHODE EMISSION ON MODE JUMP CURRENT, RAYTHEON DATA
RK 5609 NO. 16
EMISSION - MILLIAMPERES
0
1000
2000
3000
FILAMENT - VOLTS
7.9
7.6
7.2
6.8
6.5
6.3
6.0
5.8
5.3
0 60 120 180 240 300 360
MODE JUMP CURRENT - MA
4
5
5
6
6
PUSHING - MC

$$\frac{\Delta f}{\Delta \phi_a} = 4 \times 10^{-2} \frac{mc}{volt} ,$$

or a factor of 20 increase in slope of the frequency voltage characteristic.

4.3 Voltage-Tuning Measurements

Almost all of the experimental suudy of voltage tunable magnetrons has been carried on by Wilbur and Peters, who first reported the effect, in the G. E. Research Laboratories[1] or by Needle in the University of Michigan Electron Tube Laboratory.[2] The work of the G. E. group is primarily at frequencies below 1000 mc, whereas the Michigan work has been at frequencies primarily between 1000 and 3000 megacycles. The author has worked in close cooperation with Dr. Needle in the study of voltage tuning. The analysis of the double-ended circuit and the study of the magnetron with temperature-limited d-c current have been stimulated by this contact.

The calculation of the frequency-vs.-anode-potential characteristic of a voltage-tunable magnetron is quite straightforward. If the conditions of operation indicated by the discussion of Section 3.4B are satisfied, the relationship between frequency and anode potential will be a linear one. These conditions are

(1) I_g, θ, $|Y_T|$ are not frequency dependent.

(2) $\phi_a >> \phi_o$ (or $B >> B_o$). This makes the f^2 term in Eq 3.62 negligible.

---

1 III, 23.

2 Needle, J. S., "The Insertion Magnetron," Technical Report No. 11, Electron Tube Laboratory, Dept. of Elec. Eng., Univ. of Michigan, August 1951 (also Doctoral Thesis).

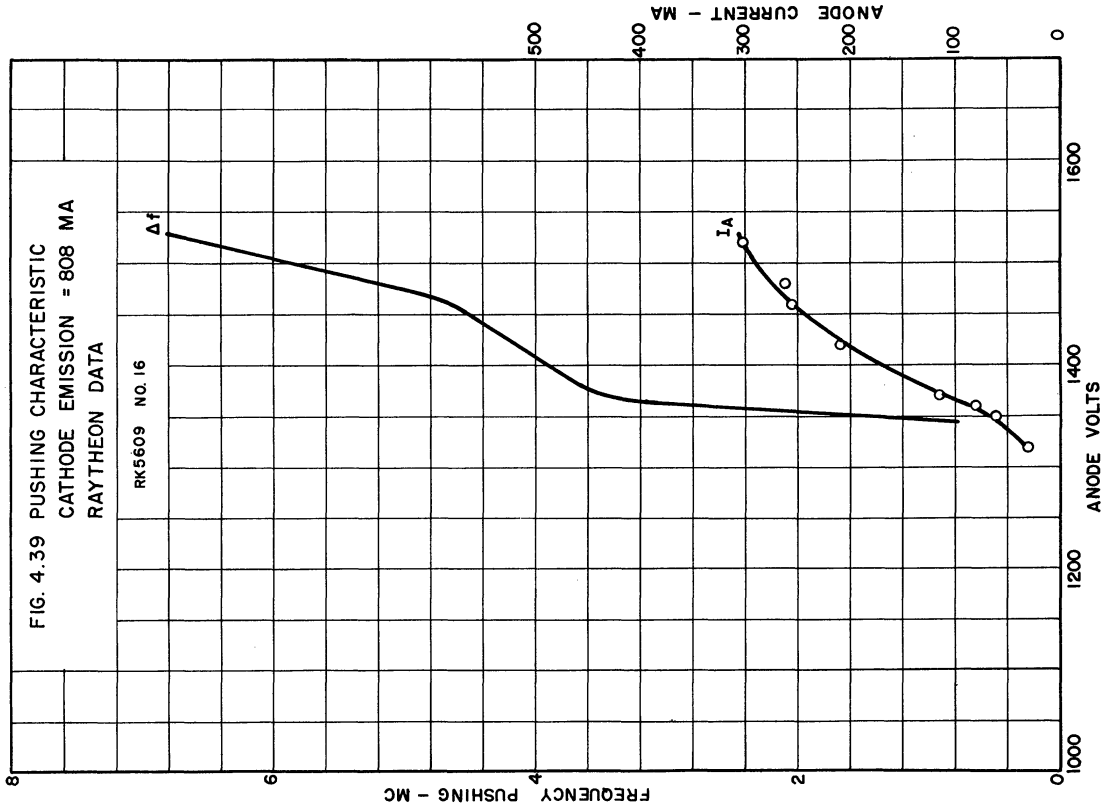
FIG. 4.39 PUSHING CHARACTERISTIC
CATHODE EMISSION = 808 MA
RAYTHEON DATA
RK5609 NO. 16
Δf
IA
FREQUENCY PUSHING - MC
ANODE CURRENT - MA
ANODE VOLTS
0
2
4
6
8
0
100
200
300
400
500
1000
1200
1400
1600

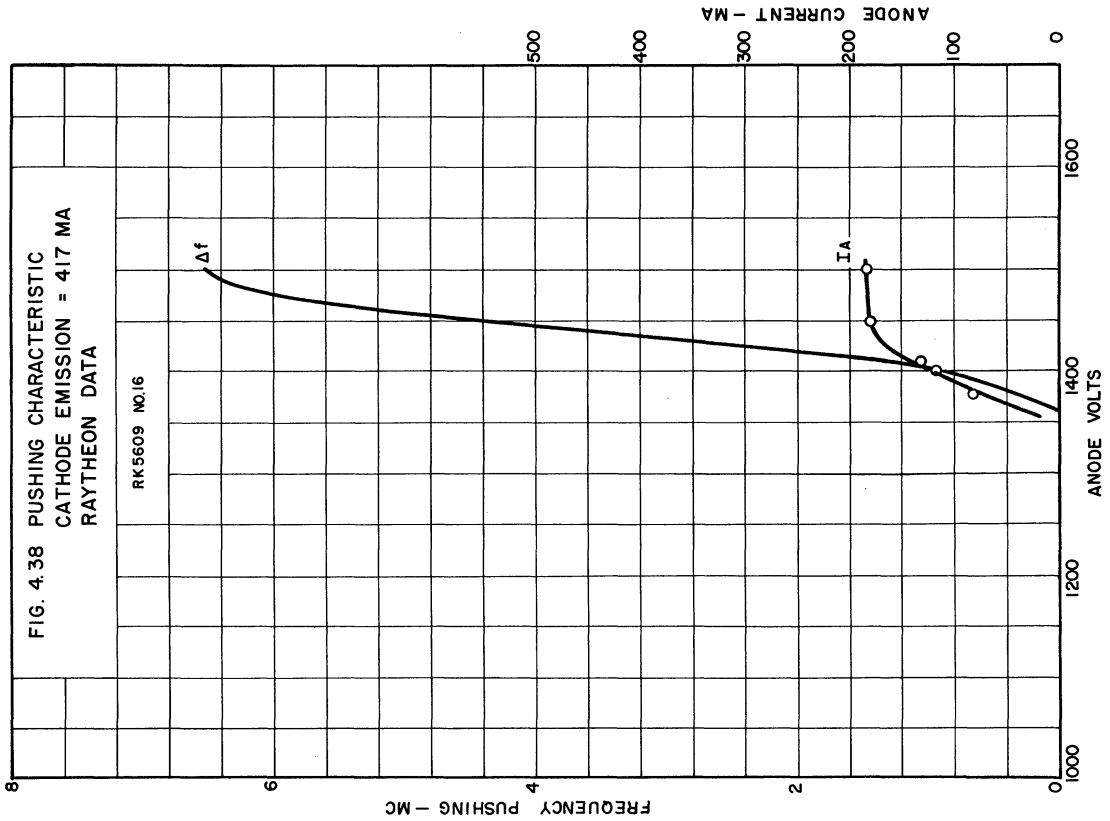
FIG. 4.38 PUSHING CHARACTERISTIC
CATHODE EMISSION = 417 MA
RAYTHEON DATA
RK5609 NO.16
Δf
IA
FREQUENCY PUSHING - MC
ANODE CURRENT - MA
ANODE VOLTS
0
2
4
6
8
0
100
200
300
400
500
1000
1200
1400
1600

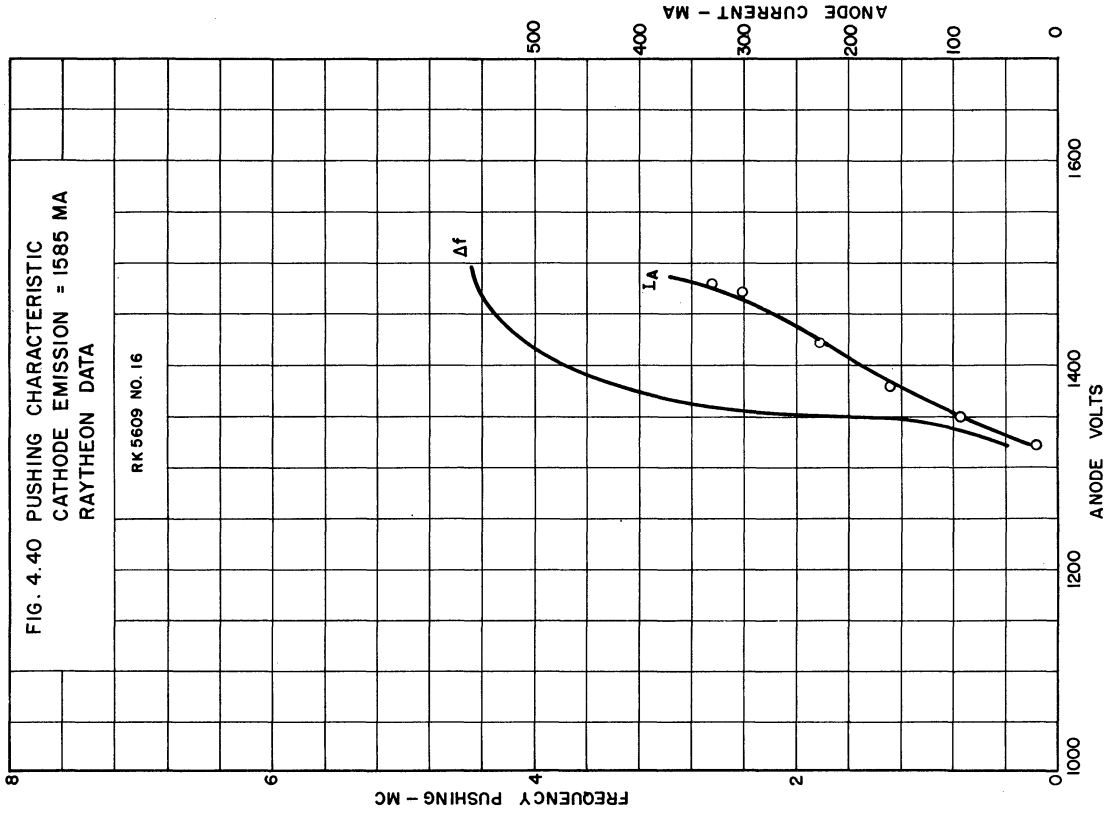
FIG. 4.40 PUSHING CHARACTERISTIC
CATHODE EMISSION = 1585 MA
RAYTHEON DATA
RK 5609 NO. 16
Δf
IA
FREQUENCY PUSHING - MC
ANODE CURRENT - MA
ANODE VOLTS
0
2
4
6
8
0
100
200
300
400
500
1000
1200
1400
1600

These conditions require special circuitry and limited anode current. If they do not exist, pure voltage tuning, by definition, does not exist. In short, the problem is not one of analyzing a voltage-tuning frequency characteristic, but in achieving it with reasonable power output and acceptable noise level. The latter is important because voltage-tunable magnetrons look promising as local oscillators for receivers or spectrum analyzers.

Although the frequency characteristic is predictable, the theory has not been developed to the point of calculating the power level to be expected under given conditions. The actual achievement of the ideal circuit is so difficult, in fact, that the power level does not remain constant in most of the experimental results.

In Fig. 4.41 a set of data is reproduced from the G. E. results[1] which compares qualitatively with the predicted curves of Fig. 3.20; i.e., a two to one change in anode potential produces approximately a two to one change in frequency and a ten to one increase in power. The power increases with frequency much more rapidly at voltages above 1500 volts than is indicated on the curves of Fig. 3.20, indicating that the circuit used has a resonance in the admittance characteristic.

In Fig. 4.42 data obtained at G. E. on a specially constructed miniature magnetron is reproduced with the computed threshold potential curve for comparison. This curve is given by Eq 3.62,

$$\phi_a = \sqrt{2}K \cos 2\theta \frac{I_g}{|Y_T|} + \frac{\pi B}{n} r_c^2 f(R_a^2 - R_c^2) - 2\pi^2 \frac{m}{e} \frac{r_c^2}{n^2} R_a^2 f^2 \qquad (3.62)$$

---

[1] III, 23, p. 82.

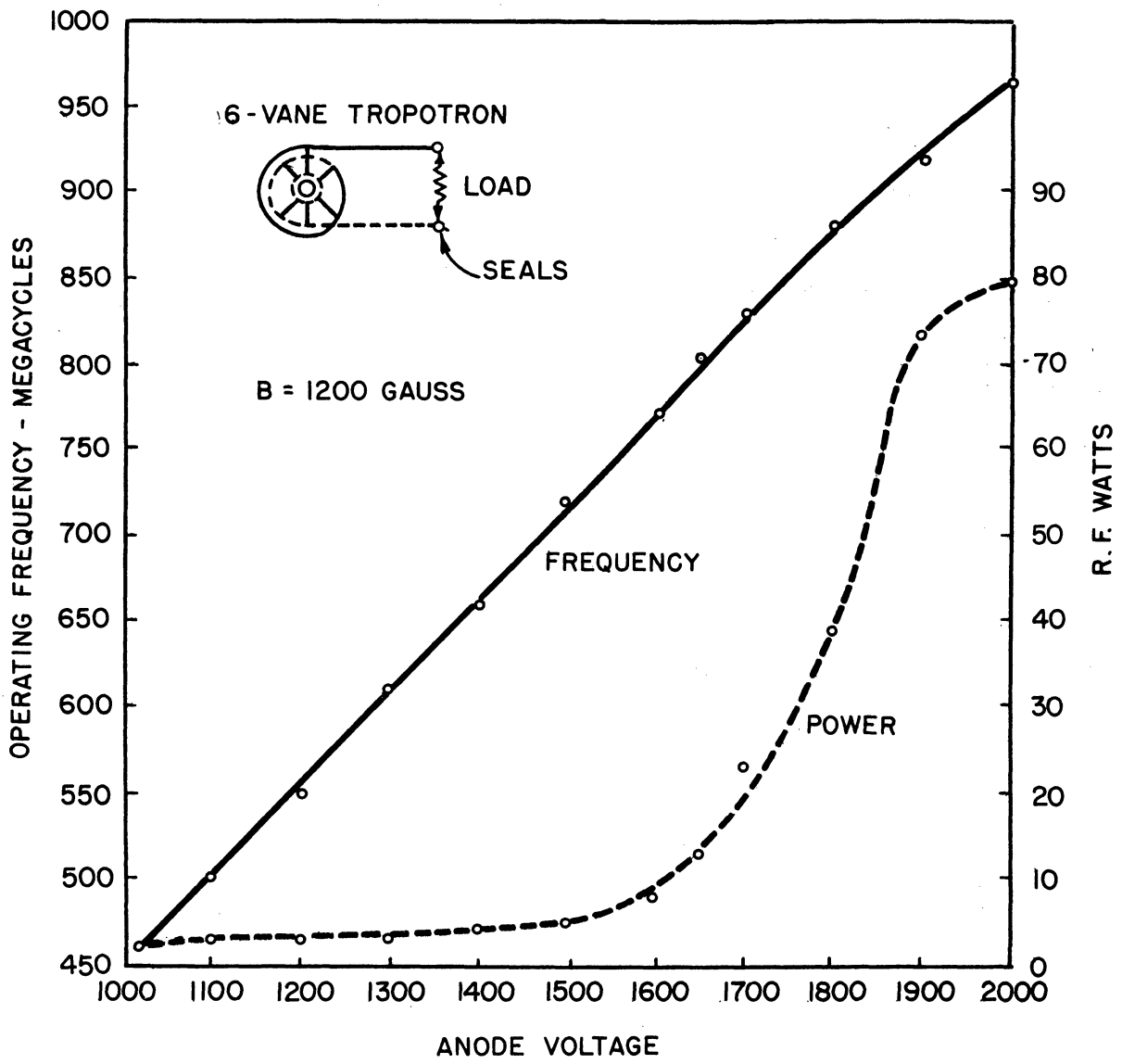

FIG. 4.41

ANODE VOLTAGE TUNING OF SIX-VANE MAGNETRON #43422

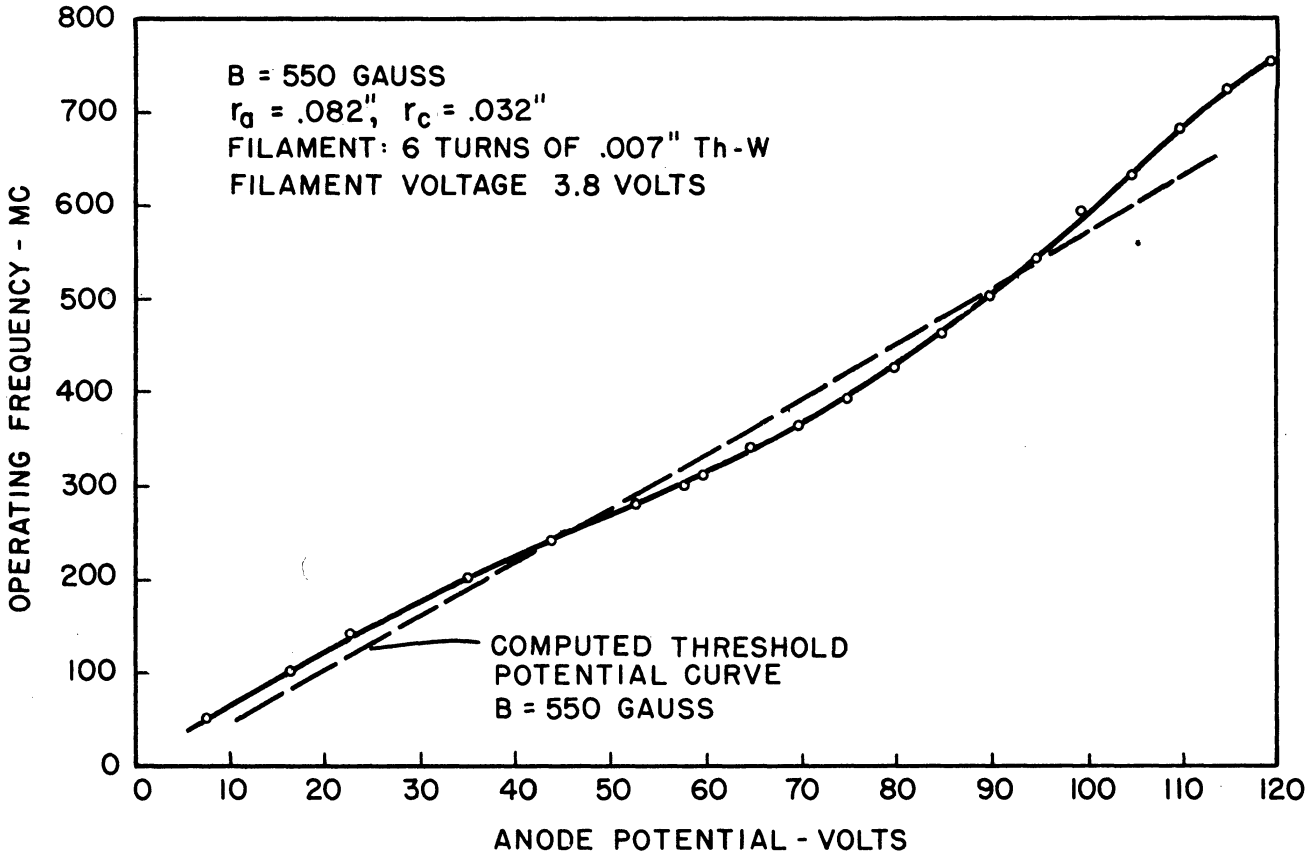

FIG. 4.42
VOLTAGE TUNING CHARACTERISTIC FOR SIX-VANE MINIATURE MAGNETRON. G. E. DATA.

In Fig. 4.43 results obtained by Needle in the Michigan laboratory are compared with the threshold-potential relationship. Needle suggests that the magnetic field may be in error causing the operating potential to be below the threshold potential. The measured value of the field was 1520 gauss, but the data compares more favorably with the curve for 1400 gauss. The results of the analysis of phase focussing will not explain this large a difference for the small power output which existed in this experiment (10 to 30 microwatts). Referring to Eq 3.62, the term

$$\sqrt{2}K \cos 2\theta \frac{I_g}{|Y_T|}$$

would have to exceed 50 to 100 volts to explain the discrepancy. This certainly is not the case at a few microwatts output in an almost purely resistive circuit.

The long-line effect, described briefly in Section 3.3C, is illustrated by Fig. 4.44. This plot is taken from an oscillogram and illustrates the increased stability which results from a reduction in cathode temperature.

The circuit used in obtaining the data of Fig. 4.43 and Fig. 4.44 is sketched in Fig. 4.45. An assembly drawing of the insertion magnetron is given in Fig. 4.46. This magnetron, with its associated external cavity, is seen to be similar to the Model 7 discussed in the last section, except for the method of loading: For voltage-tunable operation one end of the shorted coaxial line is coated with aquadag to lower the Q. This corresponds to increasing the resistance R_T in Fig. 3.8. The short circuit is removed from the other end of the cavity, and the power allowed to radiate directly into a coaxial line. This is represented by

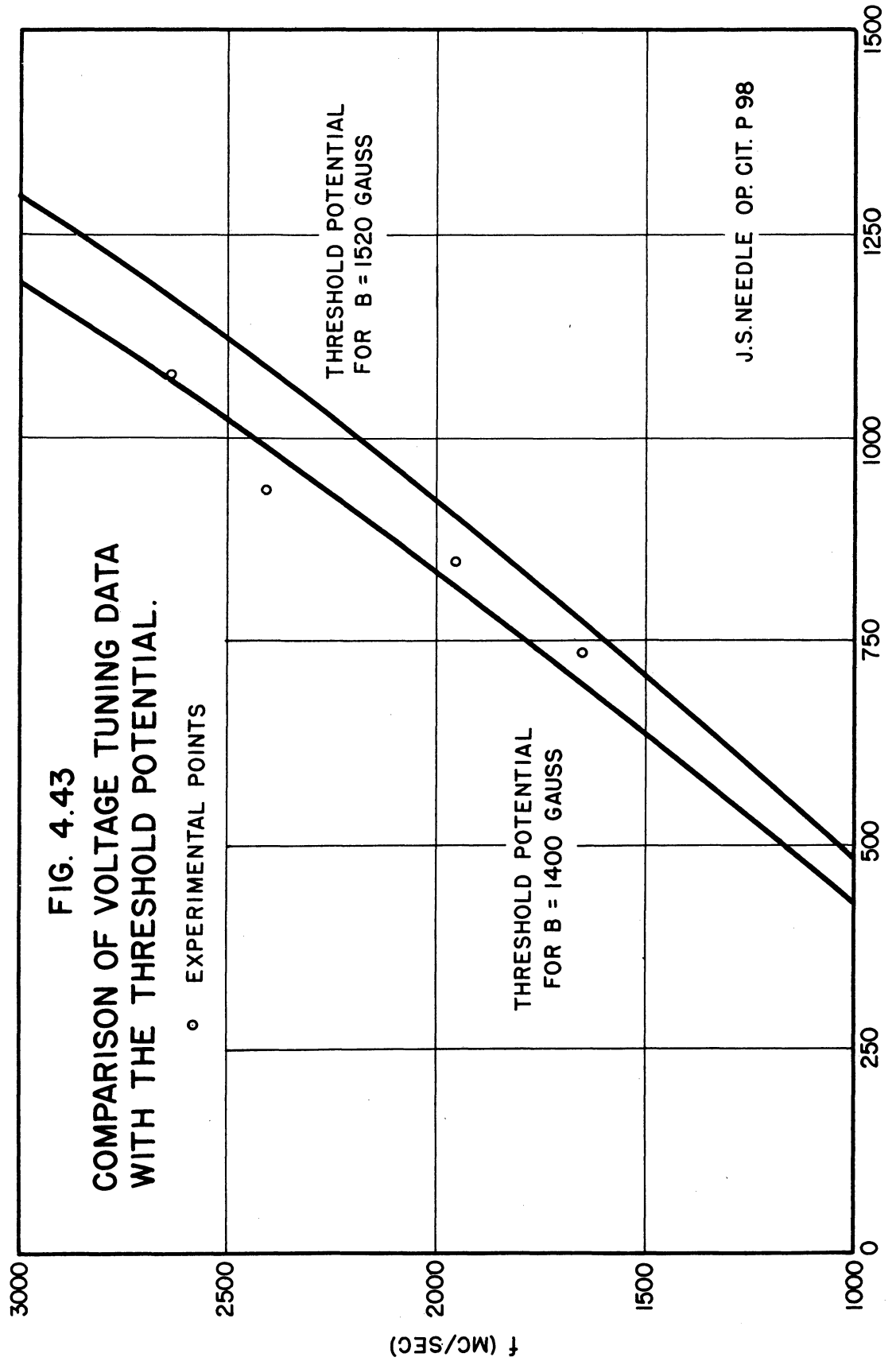
FIG. 4.43
COMPARISON OF VOLTAGE TUNING DATA WITH THE THRESHOLD POTENTIAL.
° EXPERIMENTAL POINTS
THRESHOLD POTENTIAL FOR B = 1520 GAUSS
THRESHOLD POTENTIAL FOR B = 1400 GAUSS
J.S.NEEDLE OP. CIT. P 98
f (MC/SEC)
3000
2500
2000
1500
1000
0
250
500
750
1000
1250
1500
ϕ_a (VOLTS)

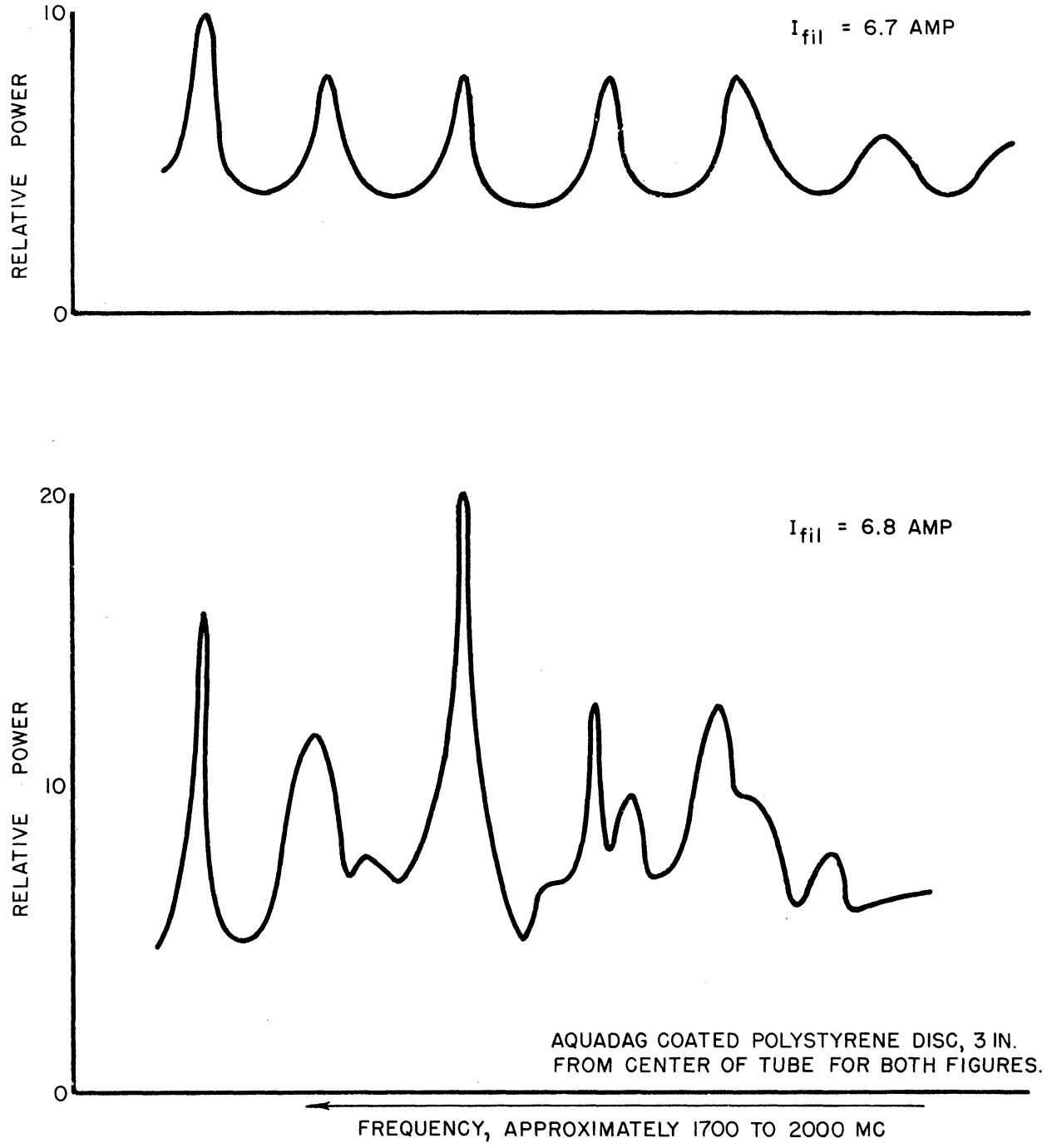

FIG. 4.44

DATA ON VOLTAGE TUNABLE MAGNETRON SHOWING LONG-LINE EFFECT

TAKEN FROM PHOTOGRAPH OF OSCILLOSCOPE SCREEN. J.S.NEEDLE

OP. CIT. P 104

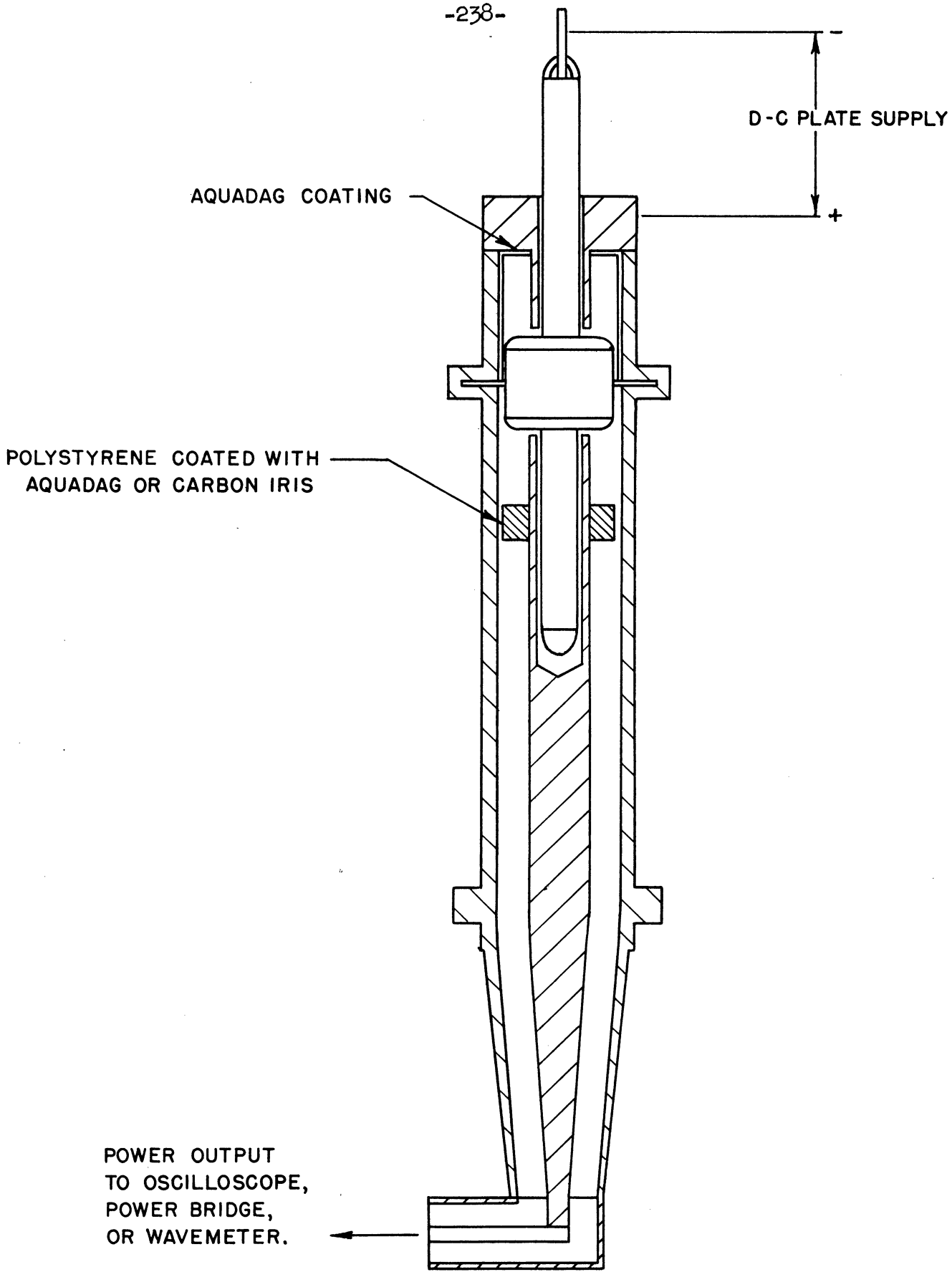

FIG. 4.45
SKETCH OF EXPERIMENTAL SET UP FOR
VOLTAGE TUNABLE OPERATION

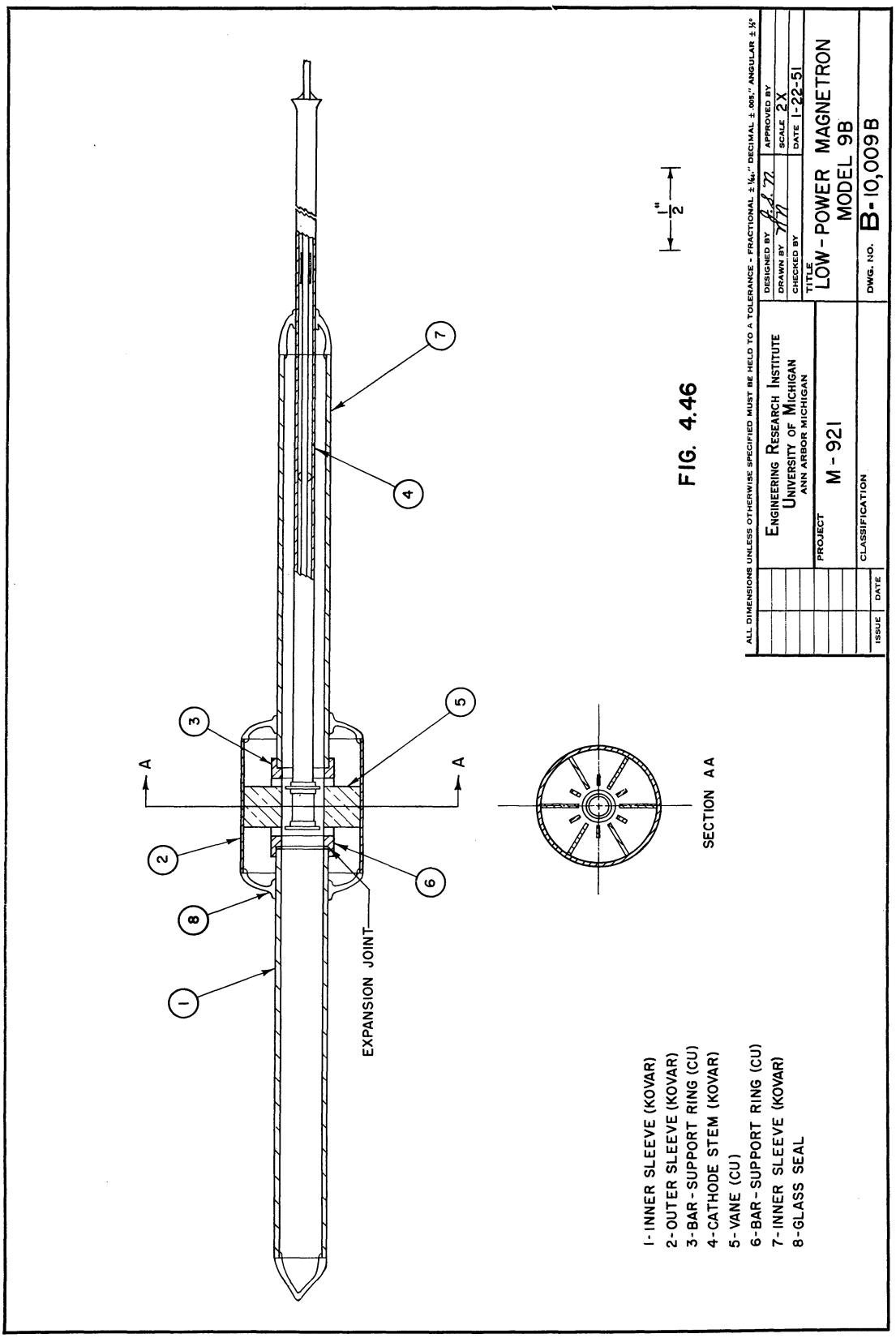
1-INNER SLEEVE (KOVAR)
2-OUTER SLEEVE (KOVAR)
3-BAR-SUPPORT RING (CU)
4-CATHODE STEM (KOVAR)
5-VANE (CU)
6-BAR-SUPPORT RING (CU)
7-INNER SLEEVE (KOVAR)
8-GLASS SEAL
EXPANSION JOINT
SECTION AA
1"
2
ALL DIMENSIONS UNLESS OTHERWISE SPECIFIED MUST BE HELD TO A TOLERANCE - FRACTIONAL ± 1/64" DECIMAL ± .005" ANGULAR ± 1/2°
ENGINEERING RESEARCH INSTITUTE
UNIVERSITY OF MICHIGAN
ANN ARBOR MICHIGAN
DESIGNED BY
DRAWN BY
CHECKED BY
APPROVED BY
SCALE 2X
DATE 1-22-51
PROJECT M-921
TITLE LOW-POWER MAGNETRON MODEL 9B
CLASSIFICATION
DWG. NO. B-10,009B
ISSUE
DATE
DWG. NO. B-10,009 B

FIG. 4.46

R_L in Fig. 3.8. If the short-circuited length of line is made very short compared to a wavelength, the capacitance, C, can be neglected. Carbon- or aquadag-coated irises are placed in the line to increase the impedance as seen by the magnetron. Such steps are necessary to make the r-f fields in the interaction space great enough for effective focussing action. Batteries were used for the d-c plate supply to insure good regulation.

For the tests recorded in Fig. 4.44 a polystyrene iris was located about 7.5 centimeters from the tube in the coaxial line. For the data in Fig. 4.43 no irises were used.

This concludes the discussion of voltage-tuning experiments. For more extensive information the work of Wilbur, Peters, and Needle should be consulted.

5. CONCLUSIONS

A summary of the limitations inherent in the method of analysis which has been proposed, a review of the most important points in the theory, discussion of the practicability of the theory in its application to design problems or analysis of experimental results, and suggested topics for further study are presented in this section.

The major objective in this treatment is to provide an approximate simplified method of analysis which will describe the relationship between the phase angle of the r-f current produced by the magnetron relative to the r-f potential produced in the circuit, and relate this to the steady-state quantities measurable in the oscillating magnetron. The knowledge of this phase relationship with the knowledge of the phase characteristic of the circuit connected to the magnetron is sufficient to provide interpretation of the frequency characteristics of the oscillating magnetron. Similar conclusions could be reached by applying extensively the laborious methods of self-consistent field calculations, developed by Hartree and his group, which were discussed briefly in the introduction. The condition of optimum impedance has not been established. This impedance is frequently defined for self-excited power oscillators as the impedance of most effective energy transfer from the electron stream to the circuit. It is known from experimental studies that such an impedance exists for a magnetron. In the method of analysis described here it is assumed that the geometry of a spoke for a given phase angle does not change as the r-f potential is increased by changing the load

impedance. It is only required that the d-c anode potential can change. It is true that this would result in a change in the space-charge density in the spokes, which would probably result in a change in the d-c anode current with a consequent change in interaction efficiency. A fundamental condition for oscillator stability is that the power supplied by the flow of d-c current be sufficient to support the oscillation. This condition has not been established by the theory; it has been assumed to exist.

Probably the most serious limitation in the theory is in the accuracy of determination of the space-charge density in the spokes. The predicted density is probably too high since it is essentially based on the assumption that no radial motion of electrons exists. As soon as the electrons have some energy of radially directed motion in addition to the synchronism energy, the square law potential distribution must flatten out. Application of Poisson's equation would then indicate smaller densities than calculated.

The position of the spoke has been determined with two limiting assumptions. One, that the cycloidal-like excursions of the electron around its drift path toward the anode do not alter materially the shape of the spoke; two, that the phase position of the entire spoke is determined approximately by the phase position of electrons which reach the anode. The excursions of the electron would tend to make the spoke more diffuse than indicated in the phase-focussing diagrams. The second assumption is not as restricting as may be suspected since the induced current results primarily from the motion of electrons close to the anode.

This is a consequence of the rapidity with which the ψ function used in the calculations is attenuated as one moves away from the anode.

The most important single result in the theory is the expression

$$\frac{\phi_a - \phi_{at}}{K\sqrt{2}\,\phi_{r\text{-}f}} = \cos 2\theta \qquad (2.48)$$

which makes possible relation of the circuit phase angle to the operating potential of the magnetron for a given r-f potential. In order to complete the calculation it is necessary to evaluate the space-charge density in the spokes,

$$\frac{\beta N}{2\pi}\rho_s = \rho_o\left(1 + \frac{4\epsilon_o\,\phi_a - \phi_{at}}{\epsilon_o\, r_c^2\left(R_a^2 - R_n^2\right)}\right). \qquad (3.58)$$

With this evaluation the results of Eq 3.47 and Eq 3.48 determining the power and anode potential are perfectly general and applicable to any circuit.

$$P_L = \frac{GL}{|Y_T|^2}\left(\frac{K_1}{\frac{\frac{\pi}{2}+\theta}{\cos\theta} - \frac{K_1}{K_2}\frac{\cos 2\theta}{|Y_T|}}\right)^2 \qquad (3.47)$$

$$\phi_a - \phi_{at} = \frac{K\sqrt{2}}{|Y_T|}\,\frac{K_1}{\frac{\frac{\pi}{2}+\theta}{\cos\theta} - \frac{K_1}{K_2}\frac{\cos 2\theta}{|Y_T|}}\cos 2\theta\,. \qquad (3.48)$$

Eqs 3.49, 3.50, 3.51, and 3.52 apply only to the particular case of a simple resonant circuit. However, the phase characteristic of most high Q, resonant systems is closely approximated by the characteristic of the simple resonant circuit of Fig. 3.6.

The constant A defined in 3.49a could be more generally defined

$$A = \frac{K_1}{K_2}\frac{1}{|Y_T|}$$

since it is not always possible to represent Y_T by the form Y_{oc}/Q_L.

The constant $\frac{K_2}{K_1}$ has a small range of variation in conventional magnetrons, primarily because magnetron design is more or less standardized. The quantities $R_a^2 - R_n^2$ and Lf which appear in the relationship defining $\frac{K_2}{K_1}$ do not vary appreciably in conventional design.

The theory predicts that the normalized induced current, $\frac{I_g}{K_1}$, will become infinite at some phase angle less than 45° off resonance for $A > \frac{\pi}{2}$. This fact was not foreseen in the early stages of development of the theory and is not obvious in the consideration of the phase-focussing diagram. It implies infinite anode potential and r-f potential and, quite obviously, that the magnetron cease oscillating in the mode in question before the resonance frequency is reached. For $A \lesssim 1$ the magnetron should operate at all frequencies up to resonance.

The most significant statements in the discussion of the problem of voltage tuning are those leading to the criteria following Eq 3.62 and the conclusion that the induced current, I_g, is directly proportional to the temperature-limited d-c current, I_T, in Eq 3.60. It should be realized that other methods than temperature limitation for limiting anode current are conceivable.

In the analysis which has been presented the emphasis has been placed on the interpretation of space-charge behavior. In order to apply the analysis to a particular magnetron, the exact characteristics of the resonator must be known. In order to have a really firm comparison of the theory with experiment, tests should be made on a magnetron which is known to have the circuit characteristics assumed in the development of Eqs 3.51 and 3.52, or the theory of the circuit should be developed to determine exact dependence of $|Y_T|$ and θ on frequency.

Frequency pushing and voltage tuning can be distinquished by the general statements: Frequency pushing may be expected when the phase angle of the magnetron resonator varies rapidly with frequency. Voltage tuning may be expected when the phase angle of the circuit does not vary, or, varies slowly with frequency. Frequency pushing is characteristic of space-charge-limited operation when the current generated by the magnetron varies (generally increases) with frequency. Voltage tuning is characteristic of operation with limited d-c current when the magnetron acts as a constant-current generator.

The points of the theory which are well confirmed by the experimental results are the following:

(a) The magnetron oscillates at frequencies below resonance.

(b) At approximately one-tenth of the maximum power generated the magnetron will operate at approximately $f_o \times \frac{2}{Q_L}$ megacycles below resonance. The range of operation is from this point to between $\frac{f_o}{2Q_L}$ below resonance and f_o.

(c) The form of the pushing curve predicted by the theory is a good approximation of the observed form. This is significant since the form predicted, assuming a constant current generator, is not a good approximation. The characteristics of the current generator which are predicted, therefore, alter the resulting pushing curve in the right direction.

The power levels predicted by the theory are in question since the approximations made in considering the circuit are questionable. After consideration of the theoretical approach the conclusion is that the weakest point is in the calculation of the space-charge density. In order to

account for the disagreement between the experimental and theoretical curves for the Model 3 magnetron (Fig. 4.31), a reduction of the predicted density by a factor of 3 to 5 is necessary. This seems unlikely, and it is concluded that the explanation lies in the analysis of the characteristics of the circuit. The shape of the curves for $\frac{I_g}{K_1}$ in Fig. 3.12 is also sensitive to the variation of space-charge density with anode potential and should be considered subject to this limitation in the comparison with experimental results.

The general conclusion is that the theory offers a reasonably accurate approach to the prediction of frequency characteristics of magnetrons and that the theory is partially confirmed experimentally if a relative power scale is used rather than an absolute power scale. The very critical relationship between the quantity $\phi_a - \phi_{at}$ and magnetic field makes difficult the experimental confirmation of the relationship between anode potential and frequency (Eq 3.48). However, as in the case of the power-frequency characteristic, the form of the curve, i.e., the change in voltage expected between two given frequencies, can be determined.

There are several points of which further investigation seems worthwhile. In some cases the problems appear rather formidable, but there is certainly a possibility of some extension to the discussion which has been presented here.

a. The behavior of the temperature-limited magnetron is quite obviously significantly different from the space-charge-limited magnetron. This problem has been considered to some extent by Twiss[1] for the static

---

[1] II, 10.

magnetron. However, Twiss' work does not offer a complete interpretation, and the oscillating magnetron is still another problem.

b. The theory presented here applies primarily to the phase-focussing region external to the synchronism boundary. It appears to the author that an analytical approach to the problem in the "phase-sorting" region internal to the synchronism boundary is quite feasible. The reasons for this statement are: one, the r-f field variation on this boundary is, without question, small compared to the d-c field so that perturbation methods might be used; two, the ratio of synchronism boundary radius to the cathode radius is always small enough so that the approximation of the planar magnetron should be good. The result of such an analysis could be used as a boundary condition on the inner boundary of the phase-focussing region. This should make possible a more accurate definition of the spoke configuration.

c. More experimental evidence, using magnetrons simple enough in construction to make unquestionable the circuit phase and admittance characteristics, is needed to substantiate or disprove parts of the theory.

d. The change in d-c anode potential which is expected to result when the load admittance is changed, at constant phase angle, is observed in Rieke diagrams. Carefully recorded Rieke diagrams on magnetrons for which circuit characteristics are known would check this point quantitatively.

e. The theory could be extended to give more detailed analysis of several points, for example, effects of the load on slope of the volt ampere characteristic, the question of behavior at near the starting

potential, and the study of characteristics of particular circuits, especially those for voltage tunable operation.

f. It is apparently possible, in voltage tunable operation, with a non-resonant circuit, to approximate single frequency, (undistorted-sine-wave) operation. The reason for this is not clear. The more detailed analysis of the induced current problem shows that the fundamental frequency component of current is encouraged by the form of the ψ function in the interaction space. This bears further investigation.

BIBLIOGRAPHY

The references in the following list were all influential in one way or another to the development of the present report. There are other references which are undoubtedly important which the author did not have the opportunity to read. There are also other references which are not particularly related to the work presented herein. The references are arranged under four headings descriptive of their content. Footnote references in the text (with the page when necessary) are made to the numbers given below.

I. References to Survey or General Treatment of the Magnetron Problem

1. Boot, H. A. H. and Randall, J. T.

   (a) "The Cavity Magnetron," Pt. 3, Jour. Inst. Elec. Eng., London, Vol. 93, No. 5, pp. 928-938, 1946.

   (b) "Discussion," Pt. 3, Vol. 95, pp. 130-134, May 1948, and Pt. 3, Vol. 96, pp. 261-263, July 1949.

2. Collins, G. B., editor, Microwave Magnetrons, New York, McGraw-Hill, 1948, M. I. T. Radiation Laboratory Series, Vol. 6.

3. Doehler, O.

   (a) "Sur les Propriéties des tubes á champ magnétique constant," Pt. I, Annales de Radioélectricité, Vol. 3, pp. 29-39, January 1948.

   (b) "Les Oscillations de résonance dans le tube á champ magnetique constant," Pt. II, Annales de Radioélectricité, Vol. 3, pp. 169-183, July 1948.

Doehler, O. and Brossart, J.

(c) "Les Tubes á propagation d'onde á champ magnétique," Pt. III, Annales de Radioélectricité, Vol. 3, pp. 328-338, 1948.

Doehler, O., Brossart, J. and Mourier, G.

(d) "Les Tubes á propagation d'onde á champ magnétique," Pt. IV, Annales de Radioélectricité, Vol. 5, pp. 293-307, October 1950.

The first two articles of this series are of most interest in the magnetron problem. A translation of this series by G. R. Brewer has been issued as Technical Report No. 9 of the University of Michigan, Department of Electrical Engineering, Electron Tube Laboratory.

4. Fisk, J. B., Hagstrum, H. D., and Hartman, P. L., "The Magnetron as a Generator of Centimeter Waves," Bell System Technical Journal, Vol. 25, No. 2, April 1946.

5. Goudet, G., "Development recents de la technique du magnetron," L'Onde Électrique, Vol. 26, No. 227, pp. 49-59, February 1946.

6. Hok, Gunnar

(a) "The Microwave Magnetron," edited by L. Marton, Advances in Electronics, Vol. II, New York, Academic Press, 1950, pp. 219-249.

The following in Very High Frequency Techniques, Vol. I, by Radio Research Laboratory Staff, New York, McGraw-Hill, 1946.

Hok, Gunnar and Dow, W. G.

(b) "Principles of Magnetron Operation," Chapter 20, pp. 473-501.

(c) "Operating Characteristics of C-W Magnetrons," Chapter 21, pp. 502-525.

Hok, Gunnar, Welch, H. W., Jr.,and Dow, W. G.

(d) "Description, Characteristics, and Operation of Typical Cavity Magnetrons," Chapter 22, pp. 526-554.

7. Lüdi, F., "Zur Theorie des Magnetfeldgenerators für Mikrowellen," Helvetica Physica Acta, Vol. 19, No. 1, pp. 3-20, 1946.

8. Megaw, E. C. S.

(a) "The High Power Pulsed Magnetron. A Review of Early Developments," Pt. 3, Jour. Inst. Elec. Eng., London, Vol. 93, No. 5, pp. 977-984, 1946.

(b) "Discussion," Pt. 3, Vol. 95, pp. 130-134, May 1948.

9. Slater, J. C., Microwave Electronics, New York, VanNostrand, 1950, Chapter 13, "The Magnetron Oscillator," pp. 302-361.

10. Spangenberg, K., Vacuum Tubes, New York, McGraw-Hill, 1948, Chapter 18, "Magnetron Oscillators," pp. 621-667.

11. Voge, J., "Le Mecanisme interne du Magnetron," L'Onde Electrique, Vol. 26, pp. 345-354 and pp. 374-386, August and October 1946.

12. Willshaw, W. E., Rushforth, L., Stainsby, A. G., Latham, R., Balls, A. W. and King, A. H.

(a) "The High Power Pulsed Magnetron. Development and Design for Radar Applications," Pt. 3, Jour. Inst. Elec. Eng., London, Vol. 93, No. 5, pp. 985-1005, 1946.

(b) "Discussion," Pt. 3, Vol. 95, pp. 130-134, May 1948.

II. References to the Study of Space Charge in the Static Magnetron

1. Bethenod, J., "Sur la variation du courant d'espace dans un magnetron sous l'action du champ magnetique," Academie des Sciences, Comptes Rendus, Vol. 209, pp. 832-834, 1939.

2. Brillouin, L. (References (a) and (b) summarize Brillouin's most important work.)

(a) "Electronic Theory of the Plane Magnetron," Advances in Electronics, New York, Academic Press, 1951, Vol. 3, p. 85. Note: This paper is based on work done for the Office of Scientific Research and Development under contract OEMsr-1007 with Columbia University (1944).

Brillouin, L. and Bloch, F.

(b) "Electronic Theory of the Cylindrical Magnetron," Advances in Electronics, New York, Academic Press, 1951. Vol. 3, p. 145. Note: This paper is based on work done by the authors for the Office of Scientific Research and Development under contracts with Columbia University (L. B.) and Harvard University (F. B.).

(c) "Theory of the Magnetron, I," Phys. Rev., Vol. 60, pp. 385-396, Sept. 1, 1951.

(d) "Theory of the Magnetron, II," Phys. Rev., Vol. 62, pp. 166-177, August 1 and 15, 1942.

(e) "Theory of the Magnetron, III," Phys. Rev., Vol. 63, pp. 127-136, Feb. 1 and 15, 1943.

(f) "Theory of the Magnetron," Elec. Commun., Vol. 20, pp. 112-121.

(g) "Electron Trajectories in a Plane Single Anode Magnetron -- A General Result," Elec. Commun., Vol. 23, pp. 460-463, December 1946.

3. Doehler, O., Op. Cit., I, 3 (a).

4. Hahn, W. C. and Blewett, J. P., "Part II, Electron Paths in Magnetrons," Proc. I. R. E., Vol. 36, No. 1, pp. 74-76, January 1948. Part II of a paper in three parts on the tracing of electron trajectories using the differential analyzer.

5. Hull, A. W., "Effect of a Uniform Magnetic Field on the Motion of Electrons between Coaxial Cylinders," Phys. Rev., Vol. 18, pp. 31-61, July 1921.

6. Page, L. and Adams, N. I.

(a) "Space Charge in Plane Magnetron," Phys. Rev., Vol. 69, pp. 492-494, May 1-15, 1946.

(b) "Space Charge in Cylindrical Magnetron," Phys. Rev., Vol. 69, pp. 494-500, May 1-15, 1946.

7. Reverdin, D. L., "Electron Optical Exploration of Space Charge in a Cut-Off Magnetron," Journal of Applied Physics, Vol. 22, No. 3, p. 257, 1951.

8. Slater, J. C., Op. Cit., pp. 333-354.

9. Spangenberg, K. ., Op. Cit., pp. 631-651.

10. Twiss, R. Q., On the Steady State and Noise Properties of Linear and Cylindrical Magnetrons, Doctoral Thesis, M. I. T., 1949.

11. Walker, L. R., "The Interaction of the Electrons and the Electromagnetic Field," Chapter 6 of Microwave Magnetrons, cited I, 2, pp. 209-253. In particular pp. 243-253.

III. References to the Study of the Electronic Behavior of the Oscillating Travelling-Wave Magnetron and to the Effects of Magnetron Space Charge on Frequency

1. Blewett, J. P. and Ramo, S.

   (a) "High Frequency Behavior of a Space Charge Rotating in a Magnetic Field," Phys. Rev., Vol. 57, pp. 635-641, April 1940.

   (b) "Propagation of Electromagnetic Waves in a Space Charge Rotating in a Magnetic Field," Journal of Applied Physics, Vol. 12, p. 856, 1941.

2. Boot, H. A. H. and Randall, J. T., Op. Cit., I, 1, (a) and (b).

3. Brillouin, L., Op. Cit., II, 2, (a).

4. Dench, E., Damon, R., Smith, R. and White, W., "Study of Magnetron Performance with Emphasis on Factors Affecting Maximum-Current Boundary," (unpublished information provided by Mr. W. C. Brown and Mr. E. Dench of Raytheon Mfg. Co.).

5. Doehler, O., Op. Cit., I, 3, (b).

6. Dunsmuir, R., Milner, C. J., and Spayne, A. J., "Pinhole Radiography of Magnetrons," Nature, London, Vol. 161, pp. 244-245, February 14, 1948.

7. Fechner, P.

   (a) "Fréquences de résonance de la charge d'espace d'un magnetron," Comptes Rendus, Academie des Sciences, Vol. 230, pp. 1848-1849, May 22, 1950. (Paris)

   (b) "Mesure des fréquences de résonance de la charge d'espace d'un magnetron a cavités," Comptes Rendus, Academie des Sciences, Vol. 231, pp. 270-271, July 24, 1950. (Paris)

8. Fisk, J. B. and others, Op. Cit., I, 4, particularly Part I, pp. 167-264.

9. Hok, Gunnar and others, Op. Cit., I, 6, (a), (b), (c) and (d).

10. Hunter, L. P., "Energy Build-Up in Magnetrons," Journal of Applied Physics, Vol. 17, pp. 833-843, October 1946.

11. Lamb, W. E., Jr., and Phillips, M., "Space Charge Frequency Dependence of Magnetron Cavity," Journal of Applied Physics, Vol. 18, pp. 230-238, February 1947.

12. Lüdi, F.

(a) Op. Cit., I, 7.

(b) "Zur Theorie der geschlitzten Magnetfeldrohre," Helvetica Physica Acta, Vol. 16, pp. 59-82, 1943.

13. Posthumus, K., "Oscillations in a Split-Anode Magnetron, Mechanism of Generation," Wireless Engineer, Vol. 12, pp. 126-132, 1935.

14. Rieke, F. F.

(a) "The Space Charge as a Circuit Element," in M. I. T. Radiation Laboratory Series, Vol. 6, Microwave Magnetrons, New York, McGraw-Hill, 1948, Chapter 7, pp. 228-338.

(b) "Transient Behavior," Microwave Magnetrons, cited above, Chapter 8, pp. 339-387.

(c) "Noise," Microwave Magnetrons, cited above, Chapter 9, pp. 388-398.

15. Slater, J. C., Op. Cit., I, 9, pp. 354-367.

16. Spangenberg, K., Op. Cit., I, 10, pp. 636-642 and 651-674.

17. Turnbull, Otis, Duggan, and Welch, "Modulation Tests of the 6J21 Magnetron," Report No. 411-235, Radio Research Laboratory, Harvard University, October 29, 1945.

18. Voge, J., Op. Cit., I, 11.

19. Wagener, W. C., "Development of 1000 Watt Tunable Magnetron for S Band," O. S. R. D. Report No. 1357-1, Litton Engineering Laboratories, September 30, 1945.

20. Walker, L. R., Op. Cit., II, 11, pp. 253-288.

21. Weinner, P. K. and Rose, A., "The Motion of Electrons Subject to Forces Transverse to a Uniform Magnetic Field," Proc. I. R. E., Vol. 35, No. 11, p. 1273, November 1947.

22. Welch, H. W., Jr.

(a) "Effects of Space Charge on Frequency Characteristics of Magnetrons," Proc. I. R. E., Vol. 38, No. 12, pp. 1434-1449, December 1950.

Welch, H. W., Jr., and Dow, W. G.

(b) "Analysis of Synchronous Conditions in the Cylindrical Magnetron Space Charge," Journal of Applied Physics, Vol. 22, No. 4, pp. 433-438, April 1951.

Welch, H. W., Jr., Ruthberg, S., Batten, H. W., and Peterson, W.

(c) "Analysis of Dynamic Characteristics of the Magnetron Space Charge -- Preliminary Results," Technical Report No. 5, University of Michigan, Department of Electrical Engineering, Electron Tube Laboratory, January 1951.

23. Wilbur, D. A., Nelson, R. B., Peters, P. H., King, A. J., and Koller, L. R., C-W Magnetron Research, Final Report, Contract No. W-36-039 sc-32279, Research Laboratory, General Electric Company, April 1, 1950.

24. Willshaw, W. E., and others, Op. Cit., I, 12, (a) and (b).

25. Willshaw, W. E., and Robertshaw, R. G., "The Behavior of Multiple Circuit Magnetrons in the Neighborhood of the Critical Anode Voltage," Proc. Phys. Soc., Vol. 63, pp. 41-45, January 1, 1950.

IV. References to the Study of Related Space-Charge Problems not Specifically Connected with the Magnetron

1. Brillouin, L.

(a) "Waves and Electrons Travelling Together -- A Comparison between Travelling-Wave Tubes and Linear Accelerators," Phys. Rev., Vol. 74, pp. 90-92, July 1, 1948.

(b) "Influence of Space Charge on the Bunching of Electron Beams," Phys. Rev., Vol. 70, Nos. 3 and 4, pp. 187-196, August 1-15, 1946.

(c) "Electron Trajectories in a Plane Diode -- A General Result," Elec. Commun., Vol. 22, No. 3, p. 212, 1945.

(d) "Transit Time and Space Charge in a Plane Diode," Elec. Commun., Vol. 22, No. 22, p. 110, 1944.

2. Copeland, P. L., and Eggenberger, D. N., "The Electric Field at a Thermionic Cathode as a Function of Space Current," Phys. Rev., Vol. 80, p. 298, October 15, 1950.

3. Fay, S., and Shockley, "On the Theory of Space Charge Between Parallel Plane Electrodes," Bell System Technical Journal, Vol. 17, p. 49, 1948.

4. Gabor, D.

(a) "Energy Conversion in Electronic Devices," Jour. Inst. Elec. Eng., Vol. 91, pp. 128-145, June 1944.

(b) "Dynamics of Electron Beams -- Applications of Hamiltonian Dynamics to Electronic Problems," Proc. I. R. E., Vol. 33, No. 11, pp. 792-805, November 1945.

5. Garbuny, M., "Graphical Representation of Particle Trajectories in a Moving Reference System," Journal of Applied Physics, Vol. 21, pp. 1054-1056, October 1950.

6. Ivey, H. F., "Cathode Field in Diodes under Partial Space-Charge Conditions," Phys. Rev., Vol. 76, pp. 554-558, August 15, 1949.

7. Jen, C. K., "On the Induced Current and Energy Balance in Electronics," Proc. I. R. E., Vol. 29, pp. 345-348, June 1941.

8. Lüdi, F.

(a) "Zur Theorie der Laufzeitschwingungen," Helvetica Physica Acta, Vol. 13, p. 77, 1940.

(b) "Der Ultrakurzwellengenerator mit Phasenfocussierung (Klystron)," Helvetica Physica Acta, Vol. 13, p. 122, 1940.

(c) "II. Uber einen neuartigen Ultrakurzwellengenerator mit Phasenfocussierung," Helvetica Physica Acta, Vol. 13, p. 498, 1940.

9. Page, L., and Adams, N. I., Jr., "Diode Space Charge for Any Initial Velocity and Current," Phys. Rev., Vol. 76, pp. 381-388, August 1, 1949.

10. Ramo, S., "Currents Induced by Electron Motion," Proc. I. R. E., Vol. 27, pp. 584-585, September 1939.

11. Shockley, W., "Currents Induced by a Moving Charge," Journal of Applied Physics, Vol. 9, 635-636, 1938.

12. Wang, Chao-Chen, "Large-Signal High-Frequency Electronics of Thermionic Vacuum Tubes," Proc. I. R. E., Vol. 29, pp. 200-214, April 1941.

The following reports have been issued by the University of Michigan, Department of Electrical Engineering, Electron Tube Laboratory, since the above list was compiled.

Brewer, G. R., "The Propagation of Electromagnetic Waves in a Magnetron-Type Space Charge," Technical Report No. 8, July 1951.

Hok, Gunnar, "Space-Charge Equilibrium in a Magnetron: A Statistical Approach," Technical Report No. 10, July 13, 1951.

Needle, J. S., "The Insertion Magnetron: A New External-Cavity Magnetron for Low-Power Electronically-Tunable Operation in the 10 to 20-CM Wavelength Range," Technical Report No. 11, August 1951.

DISTRIBUTION LIST

22 copies - Director, Evans Signal Laboratory
Belmar, New Jersey
FOR - Chief, Thermionics Branch

12 copies - Chief, Bureau of Ships
Navy Department
Washington 25, D. C.
ATTENTION: Code 930A

12 copies - Director, Air Materiel Command
Wright Field
Dayton, Ohio
ATTENTION: Electron Tube Section

4 copies - Chief, Engineering and Technical Service
Office of the Chief Signal Officer
Washington 25, D. C.

2 copies - Mr. John Keto
Director, Aircraft Radiation Laboratory
Air Materiel Command
Wright Field
Dayton, Ohio

2 copies - H. W. Welch, Jr., Research Physicist
Electronic Defense Group
Engineering Research Institute
University of Michigan
Ann Arbor, Michigan

1 copy - Engineering Research Institute File
University of Michigan
Ann Arbor, Michigan

W. E. Quinsey, Assistant to the Director
Engineering Research Institute
University of Michigan
Ann Arbor, Michigan

W. G. Dow, Professor
Department of Electrical Engineering
University of Michigan
Ann Arbor, Michigan

Gunnar Hok, Research Engineer
Engineering Research Institute
University of Michigan
Ann Arbor, Michigan

J. R. Black, Research Engineer
Engineering Research Institute
University of Michigan
Ann Arbor, Michigan

J. S. Needle, Instructor
Department of Electrical Engineering
University of Michigan
Ann Arbor, Michigan

G. R. Brewer
Electron Tube Laboratory
Research and Development Laboratory
Hughes Aircraft Company
Culver City, California

Department of Electrical Engineering
University of Minnesota
Minneapolis, Minnesota
ATTENTION: Professor W. G. Shepherd

Westinghouse Engineering Laboratories
Bloomfield, New Jersey
ATTENTION: Dr. J. H. Findlay

Columbia Radiation Laboratory
Columbia University
Department of Physics
New York 27, New York

Electron Tube Laboratory
Department of Electrical Engineering
University of Illinois
Urbana, Illinois

Department of Electrical Engineering
Stanford University
Stanford, California
ATTENTION: Dr. Karl Spangenberg

National Bureau of Standards Library
Room 203, Northwest Building
Washington 25, D. C.

Radio Corporation of America
RCA Laboratories Division
Princeton, New Jersey
ATTENTION: Mr. J. S. Donal, Jr.

Department of Electrical Engineering
The Pennsylvania State College
State College, Pennsylvania
ATTENTION: Professor A. H. Waynick

Document Office - Room 20B-221
Research Laboratory of Electronics
Massachusetts Institute of Technology
Cambridge 39, Massachusetts
ATTENTION: John H. Hewitt

Bell Telephone Laboratories
Murray Hill, New Jersey
ATTENTION: S. Millman

Radio Corporation of America
RCA Victor Division
415 South 5th Street
Harrison, New Jersey
Building 55
ATTENTION: Hans K. Jenny

Magnetron Development Laboratory
Power Tube Division
Raytheon Manufacturing Company
Waltham 54, Massachusetts
ATTENTION: Edward C. Dench

Vacuum Tube Department
Federal Telecommunication Laboratories, Inc.
500 Washington Avenue
Nutley 10, New Jersey
ATTENTION: A. K. Wing, Jr.

Microwave Research Laboratory
University of California
Berkeley, California
ATTENTION: Professor L. C. Marshall

General Electric Research Laboratory
Schenectady, New York
ATTENTION: P. H. Peters

Cruft Laboratory
Harvard University
Cambridge, Massachusetts
ATTENTION: Professor E. L. Chaffee

Collins Radio Company
Cedar Rapids, Iowa
ATTENTION: Robert M. Mitchell

Research Laboratory of Electronics
Massachusetts Institute of Technology
Cambridge, Massachusetts
ATTENTION: Professor S. T. Martin

Department of Electrical Engineering
University of Kentucky
Lexington, Kentucky
ATTENTION: Professor H. Alexander Romanowitz

Department of Electrical Engineering
Yale University
New Haven, Connecticut
ATTENTION: Dr. H. J. Reich

Department of Physics
Cornell University
Ithaca, New York
ATTENTION: Dr. L. P. Smith

Mrs. Marjorie L. Cox, Librarian
G-16, Littauer Center
Harvard University
Cambridge 38, Massachusetts

Mr. R. E. Harrell, Librarian
West Engineering Library
University of Michigan
Ann Arbor, Michigan

Mr. C. L. Cuccia
RCA Laboratories Division
Radio Corporation of America
Princeton, New Jersey

Dr. O. S. Duffendack, Director
Phillips Laboratories, Inc.
Irvington-on-Hudson, New York

Air Force Cambridge Research Laboratories
Library of Radiophysics Directorate
230 Albany Street
Cambridge, Massachusetts

Air Force Cambridge Research Laboratories
Library of Geophysics Directorate
230 Albany Street
Cambridge, Massachusetts
ATTENTION: Dr. E. W. Beth

Raytheon Manufacturing Company
Research Division
Waltham 54, Massachusetts
ATTENTION: W. M. Gottschalk

General Electric Research Laboratory
Schenectady, New York
ATTENTION: Dr. A. W. Hull

Sanders Associates Inc.
135 Bacon Street
Waltham 54, Massachusetts
ATTENTION: Mr. James D. LeVan

Sperry Gyroscope Company
Library Division
Great Neck, Long Island, New York

Sylvania Electric Products, Inc.
70 Forsyth Street
Boston 15, Massachusetts
ATTENTION: Mr. Marshall C. Pease

Dr. D. L. Marton
Chief, Electron Physics Section
National Bureau of Standards
Washington 25, D. C.

National Research Council of Canada
Radio and Electrical Engineering Division
Ottawa, Canada